



HAL
open science

Electrochemical virtual sensor development for Lithium-ion batteries

Mian Mohammad Arsalan Asif

► **To cite this version:**

Mian Mohammad Arsalan Asif. Electrochemical virtual sensor development for Lithium-ion batteries. Automatic Control Engineering. INSA de Lyon, 2023. English. NNT : 2023ISAL0117 . tel-04689683

HAL Id: tel-04689683

<https://theses.hal.science/tel-04689683v1>

Submitted on 5 Sep 2024

HAL is a multi-disciplinary open access archive for the deposit and dissemination of scientific research documents, whether they are published or not. The documents may come from teaching and research institutions in France or abroad, or from public or private research centers.

L'archive ouverte pluridisciplinaire **HAL**, est destinée au dépôt et à la diffusion de documents scientifiques de niveau recherche, publiés ou non, émanant des établissements d'enseignement et de recherche français ou étrangers, des laboratoires publics ou privés.



N°d'ordre NNT : 2023ISAL0117

**THESE de DOCTORAT DE L'INSA LYON,
membre de l'Université de Lyon**

**Ecole Doctorale N° 160
ÉLECTRONIQUE, ÉLECTROTECHNIQUE, AUTOMATIQUE (EEA)**

**Spécialité/ discipline de doctorat :
AUTOMATIQUE**

Soutenue publiquement le 19/12/2023, par :
Mian Mohammad Arsalan ASIF

**Electrochemical Virtual Sensor
Development for Lithium-ion Batteries**

Devant le jury composé de :

| | | | |
|---|--|---|---|
| VAZQUEZ VALENZUELA, Rafael DI MEGLIO, Florent | Professeur Maître-Assistant de l'Institut Mines- Télécom HDR | Universidad de Sevilla Mines Paris PSL | Rapporteur Rapporteur |
| CADET, Catherine SENAME, Olivier BIDEAUX, Eric BRIBIESCA ARGOMEDO, Federico | Maître de Conférences HDR Professeur des Universités Grenoble Professeur des Universités Maître de Conférences | Grenoble INP – UJF INP – UGA INSA Lyon INSA Lyon | Examinatrice Examinateur, Président Directeur de thèse Co-directeur de thèse |

Département FEDORA – INSA Lyon - Ecoles Doctorales

| SIGLE | ECOLE DOCTORALE | NOM ET COORDONNEES DU RESPONSABLE |
|---------------------|--|--|
| ED 206 CHIMIE | CHIMIE DE LYON https://www.edchimie-lyon.fr Sec. : Renée EL MELHEM Bât. Blaise PASCAL, 3e étage secretariat@edchimie-lyon.fr | M. Stéphane DANIELE C2P2-CPE LYON-UMR 5265 Bâtiment F308, BP 2077 43 Boulevard du 11 novembre 1918 69616 Villeurbanne directeur@edchimie-lyon.fr |
| ED 341 E2M2 | ÉVOLUTION, ÉCOSYSTÈME, MICROBIOLOGIE, MODÉLISATION http://e2m2.universite-lyon.fr Sec. : Bénédicte LANZA Bât. Atrium, UCB Lyon 1 Tél : 04.72.44.83.62 secretariat.e2m2@univ-lyon1.fr | Mme Sandrine CHARLES Université Claude Bernard Lyon 1 UFR Biosciences Bâtiment Mendel 43, boulevard du 11 Novembre 1918 69622 Villeurbanne CEDEX e2m2.codir@listes.univ-lyon1.fr |
| ED 205 EDISS | INTERDISCIPLINAIRE SCIENCES-SANTÉ http://ediss.universite-lyon.fr Sec. : Bénédicte LANZA Bât. Atrium, UCB Lyon 1 Tél : 04.72.44.83.62 secretariat.ediss@univ-lyon1.fr | Mme Sylvie RICARD-BLUM Laboratoire ICBMS - UMR 5246 CNRS - Université Lyon 1 Bâtiment Raulin - 2ème étage Nord 43 Boulevard du 11 novembre 1918 69622 Villeurbanne Cedex Tél : +33(0)4 72 44 82 32 sylvie.ricard-blum@univ-lyon1.fr |
| ED 34 EDML | MATÉRIAUX DE LYON http://ed34.universite-lyon.fr Sec. : Yann DE ORDENANA Tél : 04.72.18.62.44 yann.de-ordenana@ec-lyon.fr | M. Stéphane BENAYOUN Ecole Centrale de Lyon Laboratoire LTDS 36 avenue Guy de Collongue 69134 Ecully CEDEX Tél : 04.72.18.64.37 stephane.benayoun@ec-lyon.fr |
| ED 160 EEA | ÉLECTRONIQUE, ÉLECTROTECHNIQUE, AUTOMATIQUE https://edeea.universite-lyon.fr Sec. : Philomène TRECOURT Bâtiment Direction INSA Lyon Tél : 04.72.43.71.70 secretariat.edeea@insa-lyon.fr | M. Philippe DELACHARTRE INSA LYON Laboratoire CREATIS Bâtiment Blaise Pascal, 7 avenue Jean Capelle 69621 Villeurbanne CEDEX Tél : 04.72.43.88.63 philippe.delachartre@insa-lyon.fr |
| ED 512 INFOMATHS | INFORMATIQUE ET MATHÉMATIQUES http://edinfomaths.universite-lyon.fr Sec. : Renée EL MELHEM Bât. Blaise PASCAL, 3e étage Tél : 04.72.43.80.46 infomaths@univ-lyon1.fr | M. Hamamache KHEDDOUCI Université Claude Bernard Lyon 1 Bât. Nautilus 43, Boulevard du 11 novembre 1918 69 622 Villeurbanne Cedex France Tél : 04.72.44.83.69 direction.infomaths@listes.univ-lyon1.fr |
| ED 162 MEGA | MÉCANIQUE, ÉNERGÉTIQUE, GÉNIE CIVIL, ACOUSTIQUE http://edmega.universite-lyon.fr Sec. : Philomène TRECOURT Tél : 04.72.43.71.70 Bâtiment Direction INSA Lyon mega@insa-lyon.fr | M. Jocelyn BONJOUR INSA Lyon Laboratoire CETHIL Bâtiment Sadi-Carnot 9, rue de la Physique 69621 Villeurbanne CEDEX jocelyn.bonjour@insa-lyon.fr |
| ED 483 ScSo | ScSo¹ https://edsciencesociales.universite-lyon.fr Sec. : Mélina FAVETON Tél : 04.78.69.77.79 melina.faveton@univ-lyon2.fr | M. Bruno MILLY (INSA : J.Y. TOUSSAINT) Univ. Lyon 2 Campus Berges du Rhône 18, quai Claude Bernard 69365 LYON CEDEX 07 Bureau BEL 319 bruno.milly@univ-lyon2.fr |

Contents

| | |
|--|-----------|
| Acknowledgments | 6 |
| List of Figures | 7 |
| List of Tables | 11 |
| Nomenclature | 12 |
| Résumé de la thèse | 13 |
| 1 Background | 35 |
| 1.1 Motivation | 37 |
| 1.2 INSTABAT Project | 38 |
| 1.3 Objectives of the PhD | 40 |
| 1.4 Challenges and Issues | 41 |
| 1.5 Summary of the PhD Thesis and Main Contributions | 42 |
| 1.6 Conclusion of the Chapter | 43 |
| 2 State of the art | 45 |
| 2.1 Battery Models | 48 |
| 2.1.1 Equivalent Circuit Models | 48 |
| 2.1.2 Machine Learning Models | 51 |
| 2.1.3 Electrochemical Models | 56 |
| Comparison of Electrochemical Battery Models | 56 |
| Pseudo-Two-Dimensional Model (P2D) | 56 |

| | | |
|-------|--|----|
| | Electrode Average Model (EAM) | 57 |
| | Porous Electrode with Polynomial Model (PPM) | 58 |
| | Single Particle Model (SPM) | 58 |
| | SPM with Electrolyte (SPMe) | 59 |
| 2.2 | State Estimation | 62 |
| 2.2.1 | Open-Loop Methods for state estimation | 62 |
| | Coulomb Counting Estimation | 63 |
| | OCV based method | 63 |
| | Towards Closed-Loop Approaches | 65 |
| 2.2.2 | Adaptive Filter-Based Methodologies for state estimation | 65 |
| | Recursive Least Squares | 66 |
| | Kalman filter-based | 66 |
| 2.2.3 | Adaptive AI-Based Methodologies | 68 |
| | Particle Swarm Optimization | 69 |
| | Genetic Algorithm based Estimation | 71 |
| | Fuzzy-based Neural Networks | 72 |
| | Artificial Neural Networks | 73 |
| 2.2.4 | Model-Based Methodologies for state estimation | 74 |
| | Electrical Circuit Models | 74 |
| | Electrochemical Models | 75 |
| 2.2.5 | Hybrid estimation techniques for state estimation | 77 |
| 2.3 | Lithium Ion Battery Degradation | 78 |
| 2.3.1 | Degradation Mechanisms of Lithium-Ion Batteries | 78 |
| | Primary Degradation Mechanisms and Their Implications | 80 |
| | Key Degradation Mechanisms | 80 |
| | Interplay Between Degradation Mechanisms | 81 |
| 2.3.2 | Operational Implications of Lithium Degradation | 83 |
| | Observable Consequences (Modes) | 83 |
| | Operational Effects | 83 |
| 2.4 | Conclusion of the Chapter | 84 |

| | | |
|----------|--|------------|
| 3 | Development and Analysis of the Multi-Particle Model with Electrolyte Dynamics | 86 |
| 3.1 | Doyle-Fuller-Newman Model | 88 |
| 3.2 | Single Particle Model with Electrolyte Dynamics (SPMe) | 92 |
| 3.3 | Derivation of the Multi-Particle Model with Electrolyte Dynamics (MPMe) | 94 |
| 3.4 | Simulation of the MPMe | 100 |
| 3.4.1 | Validation of the Model | 100 |
| 3.4.2 | Spatial Heterogeneity of Internal States | 104 |
| 3.4.3 | Lithium Conservation in the System | 108 |
| 3.4.4 | Simulation Analysis: Effects of Incorrect Lithium Amounts | 110 |
| | Deviation in Lithium Content within the Electrolyte Phase | 110 |
| | Deviation in Lithium Content within the Solid Phase | 110 |
| 3.5 | Integration of Temperature dependence in the Battery model parameters | 111 |
| 3.5.1 | Single Particle Model with Electrolyte and Thermal Dynamics | 111 |
| 3.5.2 | Thermal dependence of parameters | 112 |
| 3.5.3 | Effect of Temperature on battery behaviour | 113 |
| 3.6 | Conclusion of the Chapter | 116 |
| 4 | State Observers for the MPMe | 117 |
| 4.1 | State Observer for the Electrolyte Lithium Concentration | 120 |
| 4.1.1 | Assumptions | 121 |
| 4.1.2 | Model Simplification | 122 |
| 4.1.3 | Formulation of the Electrolyte Concentration Observer | 122 |
| 4.1.4 | Stability Analysis | 124 |
| 4.2 | State observer for the solid lithium concentration using voltage error injection | 129 |
| 4.2.1 | Assumptions | 129 |
| 4.2.2 | Observer Formulation | 129 |
| 4.2.3 | Stability Analysis | 131 |
| 4.3 | Validation of the observers with simulation results | 135 |
| 4.3.1 | Constant Discharge Scenario at 2C Current | 135 |

| | | |
|----------|--|------------|
| 4.3.2 | Electric Vehicle charge/discharge cycle | 139 |
| 4.4 | Conclusion of the Chapter | 144 |
| 5 | Advanced BMS Predictions: Leveraging the Observer for State Estima- tions | 146 |
| 5.1 | Battery Management System Predictions | 148 |
| 5.2 | State of Charge Estimation | 151 |
| 5.3 | State of Health Estimation | 153 |
| 5.3.1 | Lithium Plating Management | 154 |
| 5.4 | State of Power | 156 |
| 5.5 | Conclusion of the Chapter | 158 |
| 6 | Conclusion of the Thesis | 160 |
| 6.1 | Main Contributions of this PhD: | 161 |
| 6.2 | Future Perspectives | 162 |

Acknowledgments

First and foremost, all praise is due to God, the Most Gracious and the Most Merciful, for bestowing upon me perseverance, knowledge, and grace throughout my doctoral journey. I am humbled by His infinite blessings and the continuous guidance that has illuminated my path during challenging and prosperous times alike.

My heartfelt thanks go to my parents, whose unwavering support and sacrifices have been my pillar of strength throughout this endeavor. Your love and encouragement have been my constant motivation.

I am immensely grateful to my supervisor, Dr. Federico Bribiesca Argomedo, for his invaluable guidance, patience, and persistent help. I am very thankful to him for always believing in me. His insights and wisdom have been pivotal in shaping this research.

Special thanks to my thesis director, Professor Eric Bideaux, for his crucial advice, constructive criticism, and continuous encouragement throughout the course of this research. His support and wisdom have been indispensable in the realization of this work.

I would also like to extend my gratitude to my friends and colleagues at the Ampere Lab. Their camaraderie, collaborative spirit, and shared wisdom have enriched my doctoral journey and made it a memorable experience.

To everyone who has been a part of this journey, directly or indirectly, I extend my sincere thanks. Your contributions, in various forms, have been vital in the completion of this thesis.

List of Figures

| | | |
|-----|---|----|
| 1 | Le modèle de Thévenin, un exemple d'ECM, tiré de [1,2] | 17 |
| 2 | La structure générale des ANNs [3] | 18 |
| 3 | Le modèle P2D, un type d'EChM [4] | 19 |
| 4 | Total Voltage Comparisons for 2C constant charge | 21 |
| 5 | Error in Total Voltage Comparisons 2C constant charge | 21 |
| 6 | Hétérogénéité dans l'électrode négative (Charge constante à 4C) | 22 |
| 7 | Hétérogénéité dans l'électrode positive (Charge constante à 4C) | 22 |
| 8 | Lithium total dans la phase solide (charge constante à 4C) | 23 |
| 9 | Tension de la batterie pour différentes températures | 24 |
| 10 | Structure de l'observateur avec injection d'erreur de tension de [5] | 28 |
| 11 | Profil de courant du cycle UDDS de [5] | 30 |
| 12 | Tensions avec le cycle UDDS de [5] | 31 |
| 13 | $c_s^\pm(x, r, t^*)$ et $z^\pm(x, r, t)$ de [5] | 32 |
| 14 | Représentation schématique de l'algorithme BMS proposé de [6] | 33 |
| 15 | Estimation du SOC | 34 |
| 16 | Prédiction du SOP de [6]. | 34 |
| 2.1 | Battery Models | 48 |
| 2.2 | General structure of the general structure of Neural Networks [3] | 52 |
| 2.3 | Flow chart for SVM modeling of a battery [7] | 53 |
| 2.4 | Flow chart for DT modeling [8] | 54 |
| 2.5 | Schematic of EL Data-level technique with the use of Decision trees [8] | 55 |
| 2.6 | The LiB P2D model from [4] | 58 |

| | | |
|------|--|----|
| 2.7 | Relationships between major Model Order Reduction techniques for the P2D model [9] | 61 |
| 2.8 | State Estimation Techniques | 62 |
| 2.9 | The flowchart of OCV-SOC estimation method [10] | 64 |
| 2.10 | Schematic of a closed-loop feedback estimation algorithm. The output measurement (in this case, voltage) is used as feedback to correct the state or parameter estimation [11]. | 65 |
| 2.11 | Illustration of the state observer based on Adaptive UKF algorithm [12]. . . | 67 |
| 2.12 | The flow diagram of PSO from [13] | 70 |
| 2.13 | Battery model parameters determination using GA [14,15] | 71 |
| 2.14 | Predicting SOC using Neural Networks [16] | 72 |
| 2.15 | Representation of Li-ion battery aging factors and their associated degradation effects, modified version from [17]. | 79 |
| 2.16 | SEI formation in LiBs from [18] | 81 |
| 2.17 | Lithium plating in LiBs from [19] | 82 |
| 2.18 | Schematic showing the basic components of a lithium ion battery cell and the location and consequences of the degradation mechanisms covered in this review, with primary mechanisms labelled in green and secondary mechanisms labelled in dark red [20]. | 82 |
| 3.1 | Schematic representation of the charging process of a Li-ion battery cell. At the top, are the three battery cell domains: negative electrode, separator, and positive electrode; in the middle part and at the bottom, the two phases: the electrolyte phase and the solid phase, respectively. | 89 |
| 3.2 | Simplified form of $i_e(x, t)$ in the SPMe model [21]. | 93 |
| 3.3 | MPMe Model. | 95 |
| 3.4 | MPMe Model fluxes | 96 |
| 3.5 | MPMe Model radial fluxes | 97 |
| 3.6 | MPMe Model: $i_e(x, t)$ | 97 |
| 3.7 | Potentials inside the battery from [5] | 99 |

| | | |
|------|---|-----|
| 3.8 | Total Voltage Comparisons for 2C constant charge | 101 |
| 3.9 | Negative Domain Voltage ($V_{ref}(t)$) Comparisons for 2C constant charge . . . | 102 |
| 3.10 | Positive Domain ($V(t) - V_{ref}(t)$) Voltage Comparisons for 2C constant charge | 102 |
| 3.11 | Total Voltage Comparisons for 4C constant charge | 103 |
| 3.12 | Negative Domain Voltage ($V_{ref}(t)$) Comparisons for 4C constant charge . . . | 103 |
| 3.13 | Positive Domain Voltage ($V(t) - V_{ref}(t)$) Comparisons for 4C constant charge | 103 |
| 3.14 | Heterogeneity in the Electrodes (4C Constant Charge) | 104 |
| 3.15 | Heterogeneity in Electrolyte (4C Constant Charge) | 105 |
| 3.16 | Electric Potential in the negative electrodes (4C Constant Charge) | 106 |
| 3.17 | Electric Potential in the Electrolyte (4C Constant Charge) | 107 |
| 3.18 | Ionic Current (4C Constant Charge) | 107 |
| 3.19 | Total Lithium in Solid Phase (4C Constant Charge) | 108 |
| 3.20 | Total Lithium in Electrolyte Phase (4C Constant Charge) | 109 |
| 3.21 | Total Lithium in individual Solid electrodes (4C Constant Charge) | 109 |
| 3.22 | Total Voltage $V(t)$ Comparisons for 2C constant charge with altered lithium content in the electrolyte | 110 |
| 3.23 | Total Voltage $V(t)$ Comparisons for 2C constant charge with altered lithium content in the solid phase | 111 |
| 3.24 | Concentration in electrolyte in the battery for different temperatures | 113 |
| 3.25 | Solid concentration near the current collector at positive electrode, for differ- ent temperatures for a 1C discharge and after 1000s | 114 |
| 3.26 | Solid concentration near the current collector at the negative electrode, for different temperature for a 1C discharge and after 1000s | 115 |
| 3.27 | Voltage of the battery for different temperature | 115 |
| 4.1 | Observer structure with voltage error injection from [5] | 134 |
| 4.2 | Error in Voltages with the 2C constant discharge | 136 |
| 4.3 | Voltages with the 2C constant discharge | 138 |
| 4.4 | Current profile of the UDDS cycle from [5] | 139 |
| 4.5 | Voltages with the UDDS Cycle from [5] | 141 |

| | | |
|-----|---|-----|
| 4.6 | $c_s^\pm(x, r, t^*)$ and $z^\pm(x, r, t)$ from [5] | 142 |
| 4.7 | Error in estimation of c_{ss}^\pm for the UDDS cycle. | 143 |
| 4.8 | Error in N_{Le} for the UDDS cycle. | 143 |
| 5.1 | Current profile used in BMS predictions from [6]. | 149 |
| 5.2 | Schematic Representation of the Proposed BMS Algorithm from [6] | 150 |
| 5.3 | Error in $N_{Ls}^\pm(t)$ showcasing the accuracy of the BMS Algorithm in SOC estimation from [6]. | 151 |
| 5.4 | SOC estimation | 152 |
| 5.5 | Error in $N_{Ls}(t)$ illustrating the precision of the BMS Algorithm in SOH estimation from [6]. | 154 |
| 5.6 | Lithium Plating Zone from [6] | 155 |
| 5.7 | Lithium Plating Zone over space from [6] | 156 |
| 5.8 | Schematic representation of the SOP estimation algorithm, illustrating the interplay of key parameters and their influence on SOP prediction, adapted from [6]. | 157 |
| 5.9 | SOP prediction from [6]. | 158 |

List of Tables

| | | |
|-----|--|-----|
| 1 | Erreur RMS des tensions de [5] | 29 |
| 2.1 | ECM Table adapted from [22] | 50 |
| 4.1 | RMS error of the voltages for 2C scenario | 135 |
| 4.2 | RMS value of percentage errors in $c_{ss,2C}^{\pm}$ and $N_{Ls,2C}$ | 136 |
| 4.3 | RMS error of the voltages from [5] | 140 |
| 4.4 | RMS value of percentage errors in c_{ss}^{\pm} and N_{Ls} from [5] | 140 |

Nomenclature

Physical Constants and Geometric Parameters

| | |
|------------|--|
| F | Faraday's constant [C/mol] |
| R | Universal gas constant [$J/ (K \text{ kg})$] |
| T | Temperature [K] |
| σ | Conductivity [S/m] |
| l^- | Thickness of positive electrode [m] |
| 0^{sep} | Position at separator/electrode interface [m] |
| l^{sep} | Thickness of separator [m] |
| 0^+ | Position at positive electrode/separator interface [m] |
| l^+ | Thickness of positive electrode [m] |
| L^T | Total thickness of the cell [m] |
| R_s | Solid particle radius [m] |
| ϵ | Volume fraction [-] |
| a^\pm | Specific interfacial surface area [m^2/m^3] |

Electrochemical Parameters

| | |
|---------------|---|
| η_{li}^- | Overpotential [V] |
| j_n^\pm | Molar ionic flux [$mol/m^2 \text{ s}$] |
| ϕ_s^- | Solid phase potential [V] |
| ϕ_e^- | Electrolyte phase potential [V] |
| i_{Li}^- | Current associated with lithium plating [A/m^2] |
| i_0^- | Exchange current density [A/m^2] |

| | |
|----------------------|---|
| i_e^- | Molar current density of lithium in the electrolyte, [A/m^2] |
| α | Charge transfer coefficient |
| $c_{s,\max}$ | Maximum concentration of solid material [mol/m^3] |
| $c_{ss}^\pm(x, t)$ | Concentration of lithium ions on the surface of the solid particles [mol/m^3] |
| $c_s^\pm(x, r, t)$ | Concentration of lithium ions in the solid phase [mol/m^3] |
| $c_e(x, t)$ | Concentration of lithium ions in the electrolyte [mol/m^3] |
| $N_{Ls}^\pm(t)$ | Total amount of cyclable lithium in the individual electrodes [mol] |
| $N_{Le}^\pm(t)$ | Total amount of cyclable lithium in the electrolyte [mol] |
| $N_{Ls}(t)$ | Total amount of cyclable lithium available in the combined electrodes [mol] |
| V_T | Cutoff voltage [V] |
| I | Applied current [A] |
| I_{SOP} | Maximum obtainable current [A] |
| D_e | Diffusion coefficient in the electrolyte [m^2/s] |
| D_s | Diffusion coefficient in the solid phase [m^2/s] |
| κ | Electrolyte conductivity, Siemens per meter |
| σ | Conductivity of the solid [S/m] |
| α_a, α_c | Anodic, cathodic charge transfer coefficient [-] |
| $f_{c/a}$ | Mean molar activity coefficient [-] |
| k^\pm | Kinetic reaction rate [$\text{m}^3/\text{mol}/\text{s}$] |

Acronyms

| | |
|------|--|
| SOC | State of Charge |
| SOH | State of Health |
| SOP | State of Power |
| BMS | Battery Management System |
| MPMe | Multi-Particle Model with Electrolyte dynamics |
| LiB | Lithium-ion Battery |
| EV | Electric Vehicle |

Résumé de la thèse

Contexte

Les batteries au lithium-ion (LiBs) sont devenues une pierre angulaire de la transition mondiale vers les énergies renouvelables, jouant un rôle essentiel dans l'atténuation du changement climatique et des effets du réchauffement global [23]. Leur efficacité et leurs avantages environnementaux en ont fait le choix privilégié pour diverses applications, en particulier dans le secteur des véhicules électriques (VE) [24]. La transition vers les sources d'énergie renouvelable a été accélérée par les avantages des LiBs, tels que la haute densité énergétique et l'impact environnemental réduit par rapport aux batteries traditionnelles [25]. L'électrification du secteur automobile, motivée par les préoccupations concernant les émissions des véhicules, repose fortement sur les LiBs [26]. Cependant, des défis liés à la performance, à la sécurité, à la durée de vie et à la gestion des LiBs subsistent [25]. Aborder ces défis est crucial pour une adoption plus large des VE et pour l'électrification durable du secteur des transports [27].

Le projet INSTABAT, dans le cadre du programme de recherche et d'innovation Horizon 2020 de l'Union européenne, vise à faire progresser la technologie LiB pour les VE en surveillant des paramètres clés en temps réel [28]. Le projet combine des capteurs physiques, des capteurs virtuels et des algorithmes avancés de système de gestion de batterie (BMS) pour atteindre ses objectifs [29].

Cette recherche de doctorat, menée dans le cadre d'INSTABAT, se concentre sur l'avancement de la modélisation LiB et la conception d'observateurs pour les LiBs. Les principaux objectifs comprennent la formulation d'un modèle réduit d'une cellule de batterie tenant compte des profils d'échange de Li inhomogènes, la conception d'un observateur utilisant de nouvelles données de capteurs, l'intégration d'une dépendance physique supplémentaire dans le modèle et l'observateur, et le test de l'efficacité de l'observateur.

Malgré les avantages potentiels, des défis subsistent dans l'évaluation précise de SOX des LiBs en raison de leur comportement complexe dans des conditions variables [30]. Les modèles utilisés sont complexes, avec des variables interdépendantes qui rendent la conception de l'observateur difficile. L'intégration d'une dépendance supplémentaire, telle que la température, ajoute à la complexité et au coût computationnel. Aborder ces défis nécessite

une combinaison de modélisation mathématique, de techniques de contrôle avancées, d’algorithmes d’estimation robustes et de validation expérimentale.

Les principales contributions de cette recherche de doctorat comprennent la formulation d’un modèle multi-particules avec dynamique de l’électrolyte (MPMe), la conception d’un observateur qui intègre les technologies de capteurs potentiels, et l’intégration d’une dépendance physique supplémentaire dans le modèle et l’observateur. Ces contributions ont conduit à la publication d’un article de journal et d’un article de conférence :

- **Asif, Mian Mohammad Arsalan, and Federico Bribiesca-Argomedo. 2023. “Electrochemical State Observer Design for Li-Ion Batteries With Heterogenous Electrode Lithiation.” IEEE Control Systems Letters 7: 3199-3204. <https://doi.org/10.1109/LCSYS.2023.3304248>.**
- **Asif, Mian Mohammad Arsalan, Federico Bribiesca-Argomedo, and Vincent Heiries. 2023. “Real time estimation of electrochemical states in Li-ion batteries and exploitation in BMS algorithms.” Presented at the Battery 2030+ 3rd Annual Conference.**

Globalement, cette recherche vise à améliorer la performance, la sécurité et la fiabilité des LiBs dans les applications VE, avec ses résultats documentés dans des rapports techniques et des articles de recherche pour assurer une diffusion et un impact plus larges.

État de l'art

Modèles de Batterie : La compréhension et la prédiction du comportement des LiBs nécessitent des modèles adaptés. Les modèles principaux abordés sont :

- **Modèles de Circuit Équivalent (ECMs) :** Ces modèles représentent le comportement électrique des LiBs à l'aide de circuits. Bien qu'ils soient efficaces en termes de calcul, ils peuvent ne pas détailler les processus électrochimiques internes [31–34]. La Figure 1 illustre le modèle de Thévenin, un exemple d'ECM, tiré de [1, 2].

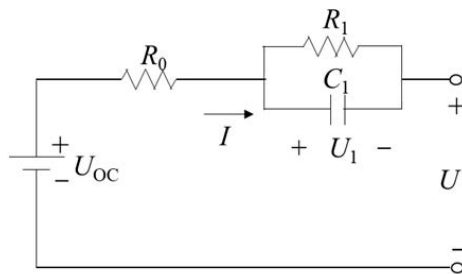


Figure 1: Le modèle de Thévenin, un exemple d'ECM, tiré de [1, 2]

- **Modèles basés sur les données:** Ces modèles, tels que les réseaux neuronaux artificiels (ANNs) [3, 35], les Machines à Vecteurs de Support (SVMs) [36], et autres, peuvent identifier des relations complexes mais nécessitent une grande quantité de données et peuvent être exigeants en ressources [3, 37]. La Figure 2 présente la structure générale des ANNs.
- **Modèles Electrochimiques (EChMs) :** Ces modèles fournissent une vision détaillée des processus électrochimiques internes, mais peuvent être coûteux en calcul [9]. La Figure 3 dépeint le modèle P2D, un type d'EChM.

Techniques d'Estimation d'État : Pour une gestion efficace des LiBs, l'estimation d'état est primordiale. Les techniques principales sont :

- **Méthodes en Boucle Ouverte :** Des méthodes comme le comptage de Coulomb et les techniques basées sur OCV sont simples mais peuvent manquer de précision sur la durée [38–40].

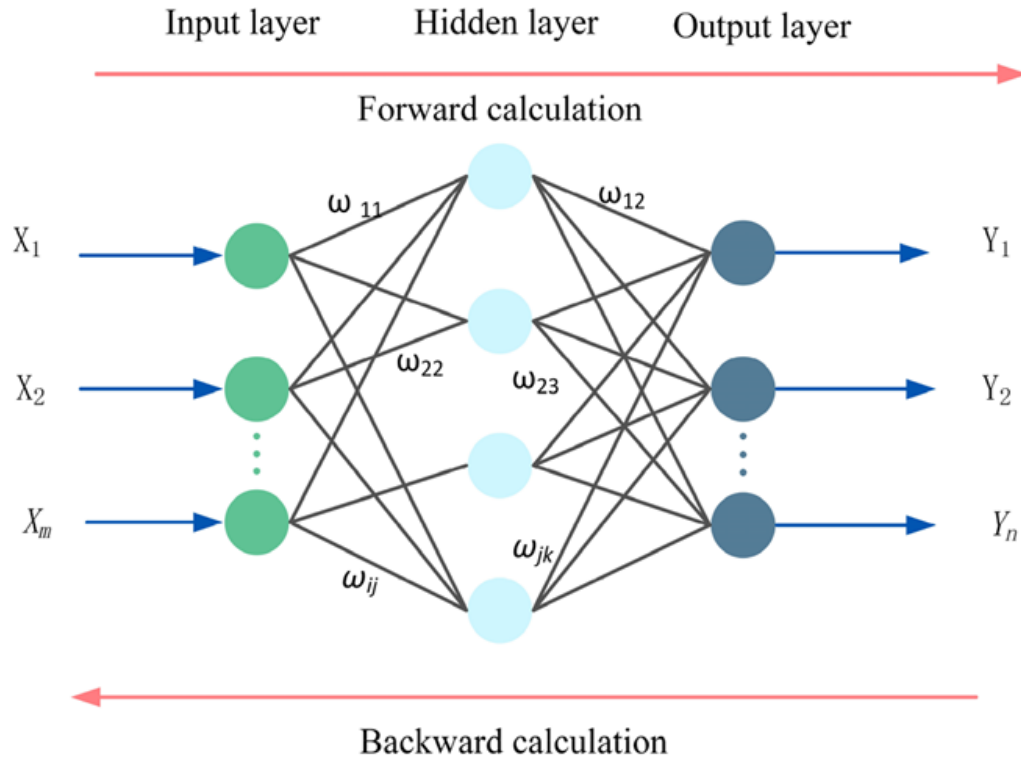


Figure 2: La structure générale des ANNs [3]

- **Méthodologies Adaptatives et Basées sur l'IA** : Des techniques telles que le moindré carré récursif (RLS), les filtres de Kalman, et les approches d'intelligence artificielle peuvent être gourmandes en ressources [14, 41–45].
- **Techniques d'Estimation Basées sur des Modèles et Hybrides** : Ces méthodes combinent des informations détaillées et diverses approches pour une meilleure estimation [33, 34, 46–49].

Modèle de Dégradation du Lithium : La dégradation des LiBs est un aspect crucial à considérer. Elle est classifiée en :

- **Mécanismes** : Transformations internes, tant physiques que chimiques, de la batterie [17, 20].
- **Modes** : Conséquences observables au niveau cellulaire dues aux mécanismes.
- **Effets Opérationnels** : Résultats tels que la réduction de capacité ou de puissance, conséquences des modes [20].

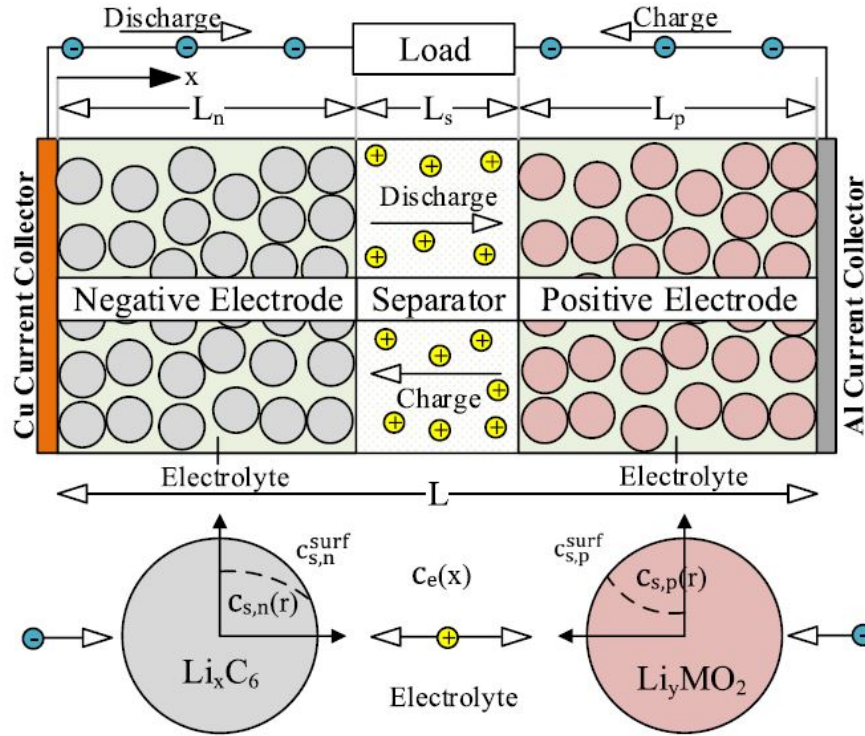


Figure 3: Le modèle P2D, un type d'EChM [4]

En somme, une connaissance approfondie des modèles de batterie, des techniques d'estimation d'état, et des mécanismes de dégradation est vitale pour optimiser la performance et la durabilité des LiBs.

Développement et Analyse du Modèle Multi-Particules avec Dynamique de l'Électrolyte (MPMe)

Ce chapitre se penche sur les subtilités de la modélisation des batteries lithium-ion, soulignant la nécessité d'une représentation plus précise des dynamiques internes de la batterie. Bien que le modèle Doyle Fuller Newman (DFN, de [50]) soit complet, il est gourmand en calculs, le rendant inadapté pour des applications en temps réel. Ce chapitre présente le Modèle Multi-Particules avec Dynamique de l'Électrolyte (MPMe) comme une solution qui fait le lien entre le DFN et le Modèle à Particule Unique avec Électrolyte (SPMe) [21].

Dérivation du Modèle : Le MPMe vise à :

- Reconstituer les hétérogénéités présentes dans les dynamiques internes de la batterie.
- Offrir une efficacité de calcul pour les applications en temps réel.
- Faciliter l'intégration de nouvelles données de capteurs pour la conception d'observateurs.
- Incorporer la dépendance de la température pour divers paramètres électrochimiques.
- Assurer la conservation du lithium dans les deux phases de la batterie.
- Intégrer un modèle de dégradation du lithium pour l'électrode négative.

Le MPMe utilise une représentation multi-particules, formulant des couches à l'intérieur des régions positives, négatives, du séparateur de la batterie. Chaque couche des côtés négatif et positif possède une particule, chaque particule ayant des couches radiales.

Simulation du MPMe : La validation du MPMe est réalisée à travers des simulations MATLAB, en le comparant au modèle DFN à grande échelle et au SPMé. Les résultats du modèle MPMe, notamment en ce qui concerne le comportement de la tension, montrent sa précision supérieure par rapport au SPMé. La Figure 4 montre la comparaison entre le modèle DFN à grande échelle, le SPMé et le MPMe proposé, et la Figure 5 montre l'erreur entre le modèle DFN et ses dérivés (SPMé et MPMe) pour une charge constante de 2C.

Hétérogénéité Spatiale des États Internes : Le modèle MPMe capture les états internes de la batterie, y compris la concentration de lithium dans les électrodes et l'électrolyte,

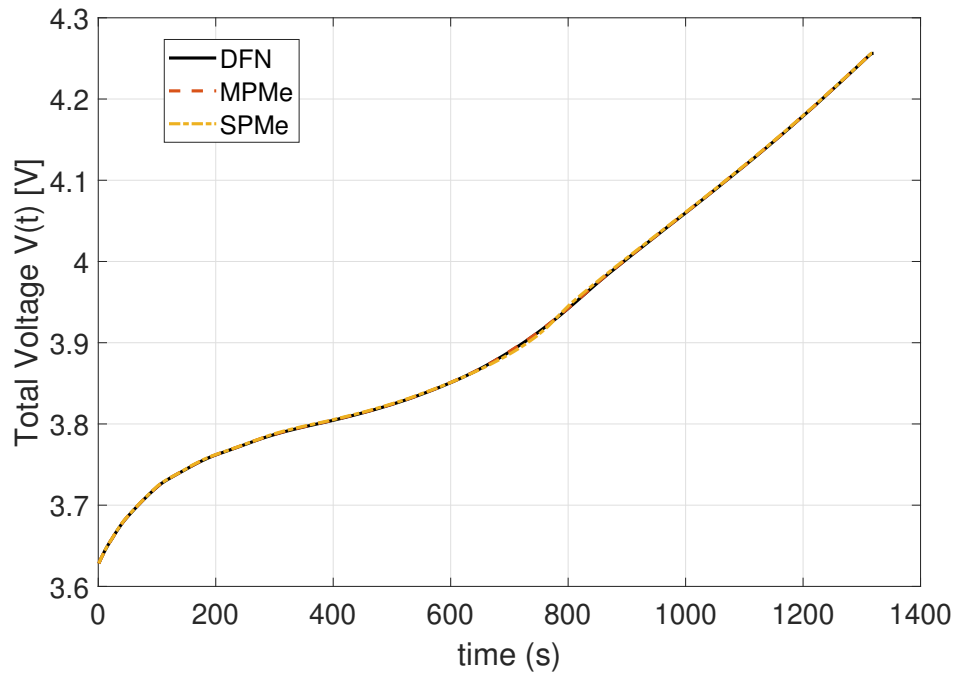


Figure 4: Total Voltage Comparisons for 2C constant charge

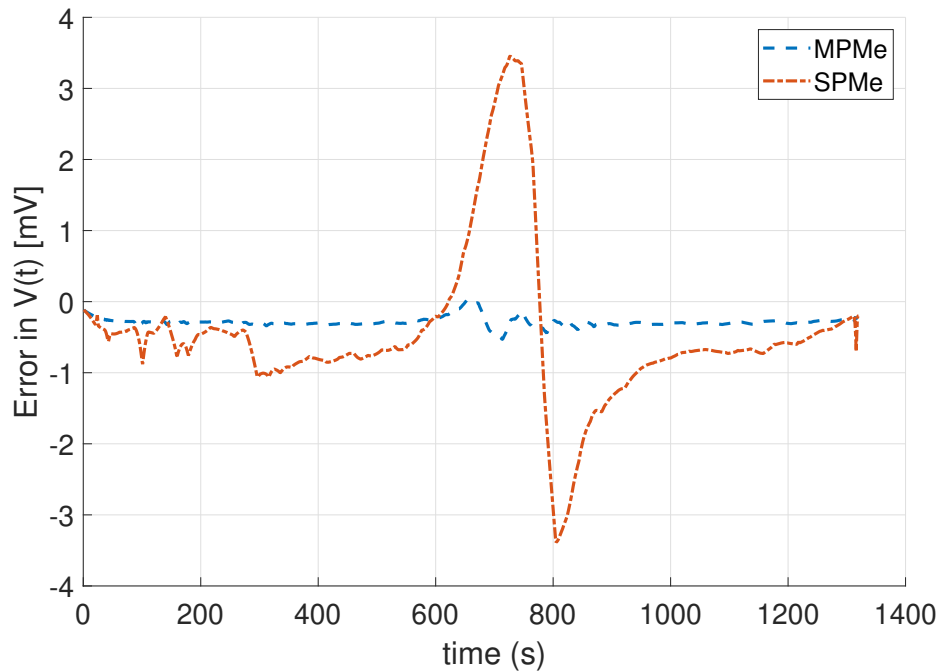


Figure 5: Error in Total Voltage Comparisons 2C constant charge

le potentiel électrique dans les deux phases, la surtension, et d'autres facteurs cruciaux. Le modèle montre l'hétérogénéité présente dans ces états, en particulier sous différents scénarios

de charge. Les figures 6 et 7 montrent l'hétérogénéité des électrodes solides.

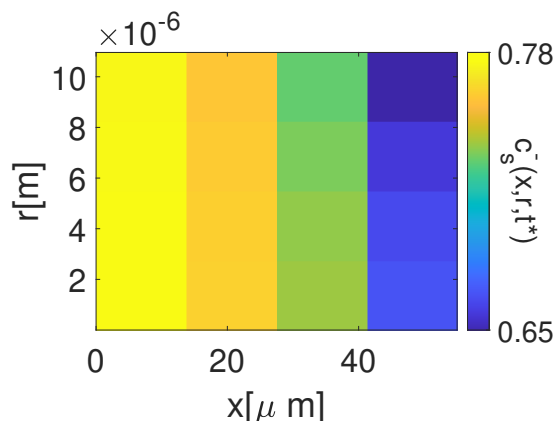


Figure 6: Hétérogénéité dans l'électrode negative (Charge constante à 4C)

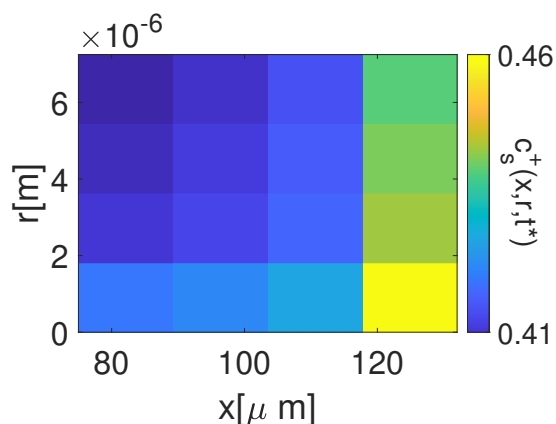


Figure 7: Hétérogénéité dans l'électrode positive (Charge constante à 4C)

Conservation du Lithium dans le Système : Le modèle MPMe assure la conservation du lithium, un aspect crucial pour des simulations précises à long terme. Cette conservation peut être observée à la fois dans les phases solide et électrolytique de la batterie. La Figure 8 montre la conservation du lithium dans la phase solide lors d'une simulation de charge constante à 4C.

Intégration de la Dépendance à la Température dans le Modèle de Batterie : Ce chapitre présente le Modèle à Particule Unique avec Dynamique de l'Électrolyte et Thermique (SPMeT, de [51]) qui prend en compte les variations de température à travers la batterie au lithium-ion. Le modèle SPMéT combine le modèle SPMé avec un modèle thermique, en utilisant la loi d'Arrhenius pour les paramètres dépendant de la température. Le

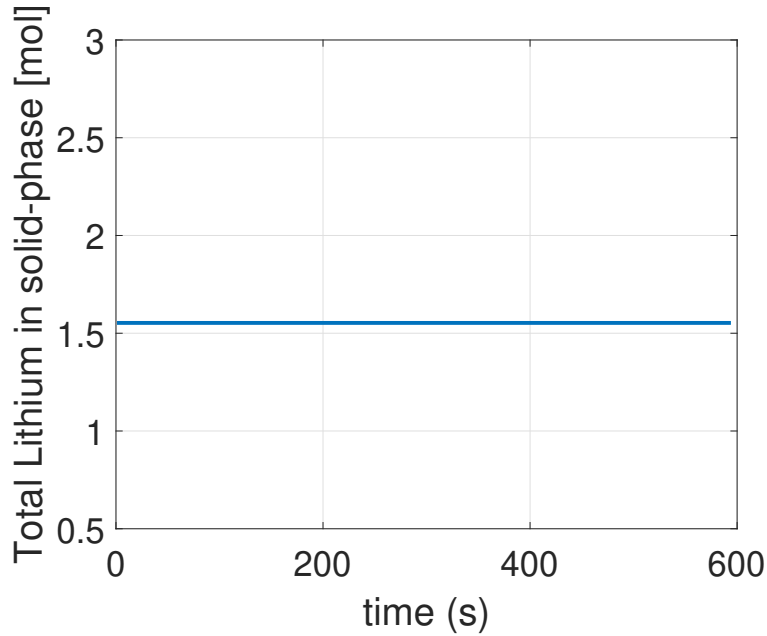


Figure 8: Lithium total dans la phase solide (charge constante à 4C)

chapitre utilise ensuite le principe du SPM_eT dans le cadre du MPMe, démontrant l'impact significatif de la dépendance à la température sur le comportement de la batterie. La Figure 9 montre l'effet de la température sur la tension totale à une charge constante de 1C pour le MPMe.

En conclusion, le Chapitre 3 présente le MPMe comme un modèle robuste et efficace pour capturer les dynamiques internes des batteries lithium-ion, comblant le fossé entre le modèle DFN détaillé et le SPM_e plus simple. Le chapitre souligne l'importance de prendre en compte les variations de température et d'assurer la conservation du lithium pour une modélisation précise de la batterie.

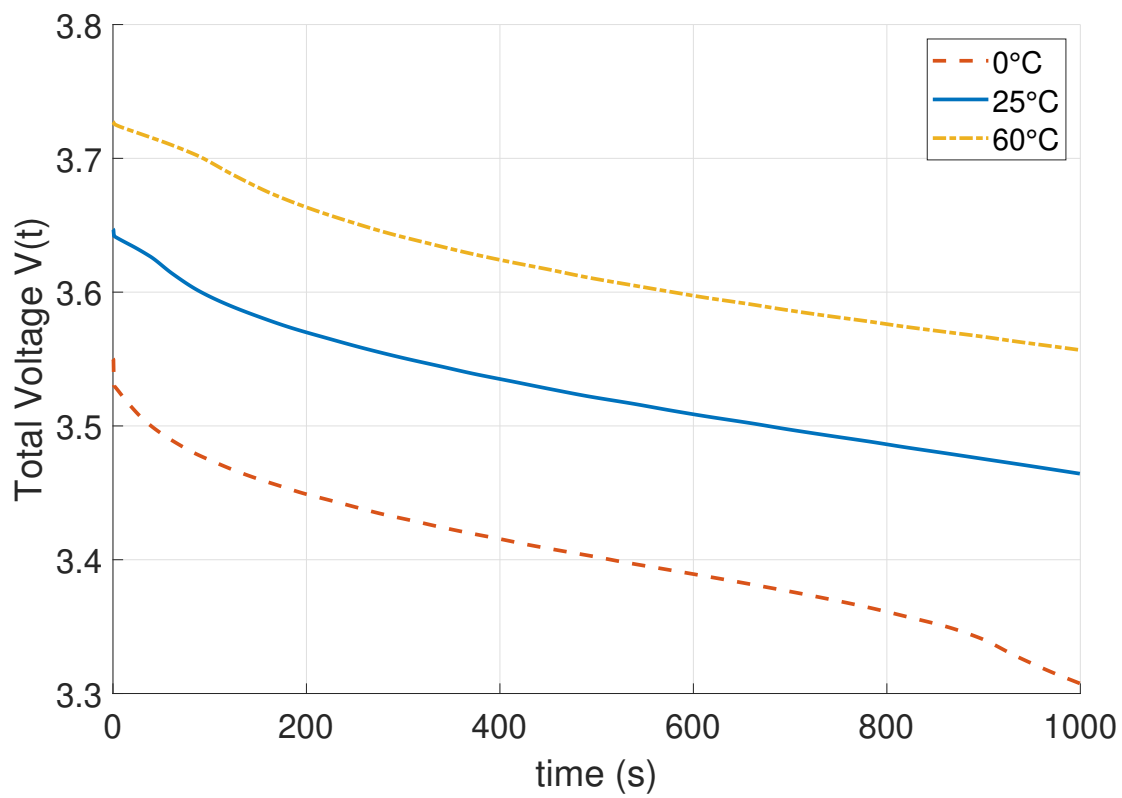


Figure 9: Tension de la batterie pour différentes températures

Observateurs d'État pour le MPMe

Ce chapitre propose une analyse détaillée des observateurs pour les batteries lithium-ion, se concentrant à la fois sur les concentrations d'électrolyte et de lithium solide. L'importance de ces observations est mise en évidence, étant donné leur rôle dans la compréhension du comportement des ions de lithium à l'intérieur de la batterie.

Observateur de Concentration de Lithium dans l'Électrolyte

Cette section approfondit la construction et l'analyse de stabilité de l'observateur d'état pour la concentration de lithium dans l'électrolyte des batteries lithium-ion. Le processus d'observation est essentiel pour comprendre la diffusion des ions lithium à l'intérieur de l'électrolyte.

Hypothèses :

Assumption 1. *Le coefficient de diffusion, noté D_e , est considéré comme constant dans le temps et uniformément borné dans la variable spatiale. Cela signifie qu'il existe une valeur positive minimale, \underline{D}_e , et une valeur maximale, \overline{D}_e , le coefficient de diffusion se situe entre ces deux limites. Dans le reste de la thèse, nous considérerons D_e comme une fonction de la variable spatiale x [5].*

Assumption 2. *Une mesure de la concentration de lithium dans l'électrolyte, notée $c_e(x_r, t)$, est disponible en un point spécifique du séparateur, x_r . Cette hypothèse est cruciale car elle fournit un point de référence pour l'observateur. En ayant une concentration connue à un endroit spécifique, il devient possible d'estimer la concentration dans d'autres parties du système [5].*

Assumption 3. *Le profil spatial des flux ioniques molaires, représenté par $j_n^\pm(x, t)$, est supposé être précisément prédit par le modèle sans nécessité de correction. Cela implique que le profil de courant ionique, $i_e^\pm(x, t)$, est connu. Cette hypothèse découple l'analyse de stabilité de l'observateur d'électrolyte de celle de l'observateur d'électrode. Cependant, il convient de noter que c'est une limitation de la conception actuelle. La stabilité du système*

interconnecté n'est démontrée que dans les résultats de simulation. Cette limitation n'est pas propre à cette approche; d'autres méthodologies dans la littérature, citée comme [21], font également des hypothèses similaires [5].

Simplification du Modèle :

L'équation de diffusion de l'électrolyte du modèle Doyle-Fuller-Newman (DFN) est simplifiée en utilisant la première hypothèse ci-dessus tout en conservant ses caractéristiques essentielles. L'équation simplifiée est :

$$\epsilon_e^j c_{e,t}^j(x, t) = \frac{\partial}{\partial x} \left[D_e(x) c_{e,x}^j(x, t) + \frac{(1 - t_c^0)}{F} i_e^j(x, t) \right]$$

Formulation de l'Observateur de Concentration de l'Électrolyte :

Un observateur est développé sur la base de l'équation de diffusion de l'électrolyte simplifiée. Cet observateur estime la concentration de l'électrolyte en utilisant des mesures à l'électrode de référence. La formulation de l'observateur introduit un terme d'injection d'erreur pour tenir compte des écarts entre les états réels et estimés. En utilisant les hypothèses mentionnées précédemment pour simplifier le modèle, nous pouvons écrire le système observateur comme suit :

$$\begin{aligned} \epsilon_e^j \hat{c}_{e,t}^j(x, t) = & \frac{\partial}{\partial x} \left[D_e(x) \hat{c}_{e,x}^j(x, t) + \frac{1 - t_c^0}{F} i_e^j(x, t) \right] \\ & - P [c_e(x_r, t) - \hat{c}_e(x_r, t)] \end{aligned}$$

où $x_r \in [0^{sep}, l^{sep}]$ désigne la position spatiale de l'électrode de référence.

Analyse de Stabilité :

La stabilité de l'observateur est cruciale. Une proposition établit que le système d'erreur est exponentiellement stable sous certaines conditions. La stabilité est analysée en utilisant une fonction candidate de Lyapunov, et les conditions de stabilité sont dérivées. Pour prouver la stabilité du système, la fonction de Lyapunov suivante est utilisée:

$$\begin{aligned}
V_T &= V_1 + \beta V_2 \\
, V_1(u(\cdot, t)) &\doteq \frac{1}{2} \int_0^{L^T} \epsilon_e u^2(x) dx \geq 0, \\
V_2(u(\cdot, t)) &\doteq \frac{1}{2} \int_0^{L^T} [\epsilon_e D_e(x) u_x^2(x)] dx \geq 0,
\end{aligned}$$

Observateur d'État pour la concentration de lithium solide

Hypothèses

La construction des observateurs d'état pour les électrodes solides est basée sur :

Assumption 4. *Une mesure de tension à une électrode de référence $V_{ref}(t)$ est disponible. Ceci permet des estimations indépendantes des potentiels OCV U^\pm pour chaque électrode [5].*

Assumption 5. *On suppose que la courbe OCV des électrodes U^\pm est uniformément monotone décroissante de telle manière que, en définissant $f(a, b) \doteq U(a) - U(a - b)$, la propriété suivante est satisfaite :*

$$\exists k_1, k_2 < 0 \text{ t.q. } \forall a, b \quad k_1 b^2 \leq f(a, b) b \leq k_2 b^2$$

Notez que les preuves peuvent être adaptées sans problème si la fonction est monotone croissante, nécessitant seulement un changement de signe dans le gain de rétroaction [5].

Formulation de l'Observateur

L'observateur pour la concentration de lithium en phase solide intègre le terme d'erreur de tension, en utilisant la tension de l'électrode de référence. Le système d'erreur contraste les systèmes physique et observateur, avec des coordonnées radiales transformées pour simplifier la notation. L'observateur de la concentration de lithium en phase solide est formulé en

injectant le terme d'erreur de tension [5] :

$$\hat{c}_{s,t}^{\pm}(x, r, t) = \frac{1}{r^2} \frac{\partial}{\partial r} [D_s^{\pm} r^2 \hat{c}_{s,r}^{\pm}]$$

$$\hat{c}_{s,r}^{\pm}(x, 0, t) = 0$$

$$\hat{c}_{s,r}^{\pm}(x, R_s^-, t) = -\frac{j_n^{\pm}(x, t)}{D_s^{\pm}} - g_0^{\pm} [U(c_{ss}^{\pm}(x, t)) - U(\hat{c}_{ss}^{\pm}(x, t))]$$

où $c_{ss}^{\pm}(x, t) \doteq c_s^{\pm}(x, R_s^{\pm}, t)$. La Figure 10 montre la structure globale de l'observateur.

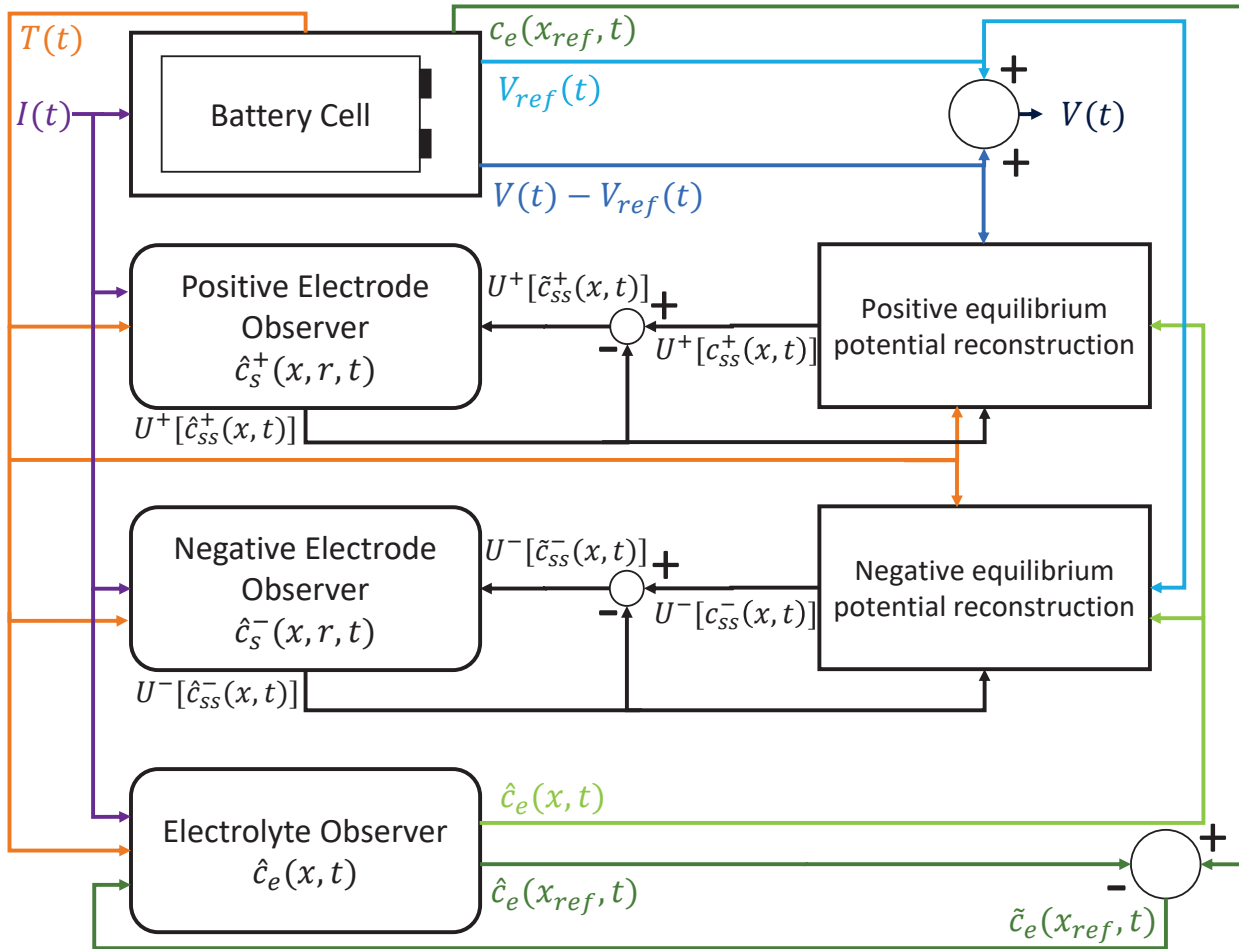


Figure 10: Structure de l'observateur avec injection d'erreur de tension de [5]

Analyse de Stabilité

La stabilité est confirmée en définissant une fonction de Lyapunov et en garantissant la définitude négative de sa dérivée temporelle. Les observateurs proposés, bien qu'ils ne conservent pas le lithium total dans les électrodes, travaillent avec un autre observateur pour corriger les erreurs au fil du temps. Pour prouver la stabilité du système, la fonction de Lyapunov suivante est utilisée:

$$V_s = \frac{1}{2} \int_0^1 \frac{R_s^2}{D_s} r^2 z^2(r, t) dr$$

Validation des observateurs avec les résultats de simulation

Des simulations utilisant un modèle DFN simplifié valident l'efficacité des observateurs. Sous une décharge de 2C, les observateurs, même lorsqu'ils sont initialisés avec des valeurs incorrectes, convergent rapidement vers les vraies valeurs. En utilisant le cycle de conduite UDDS avec un courant de crête de 6C comme on peut le voir sur la Figure 11, les observateurs suivent efficacement les tensions et corrigent les erreurs initiales, prouvant leur robustesse comme on peut le voir sur la Figure 12. Ces résultats montrent la convergence rapide des observateurs proposés avec Injection d'Erreur de Tension (VEI). L'erreur de suivi peut être vue dans le Tableau 1. La Figure 13 montre le $c_s^\pm(x, r, t)$ et $z^\pm(x, r, t)$ normalisés, l'erreur correspondante dans $c_s^\pm(x, r, t)$, à deux instants différents : $t_0 = 0$ et $t^* = 594$ secondes, où le courant atteint son maximum pendant la simulation.

| error (mV) | $V(t)$ | $V_{ref}(t)$ | $V(t) - V_{ref}(t)$ |
|------------------|---------|--------------|---------------------|
| VEI | 5.4502 | 3.0438 | 2.8405 |
| VEI (5mV noise) | 6.9501 | 4.1694 | 4.2133 |
| VEI (10mV noise) | 10.0511 | 6.5705 | 6.7245 |

Table 1: Erreur RMS des tensions de [5]

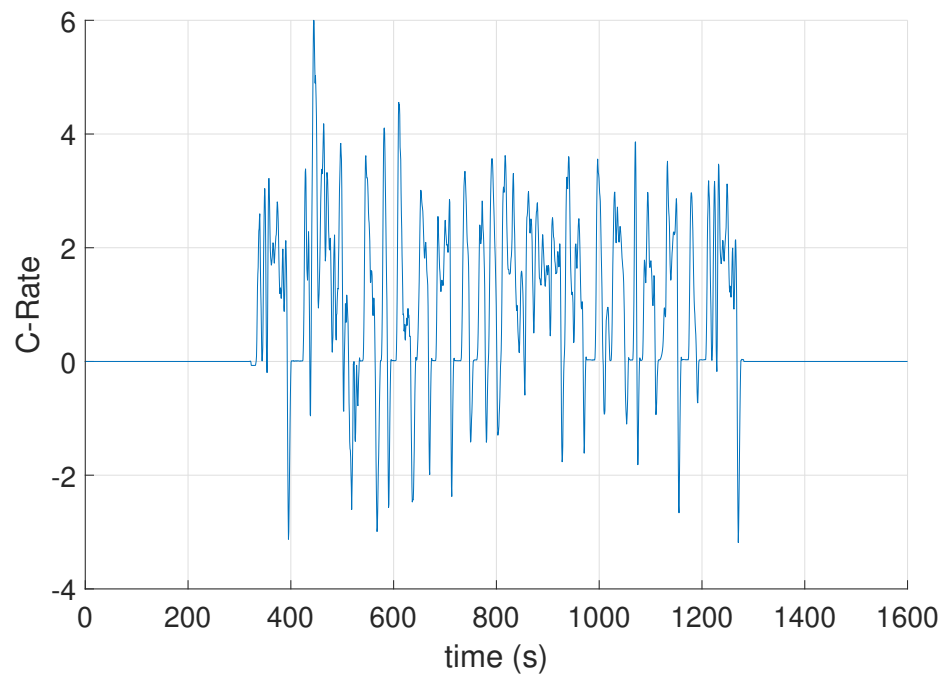
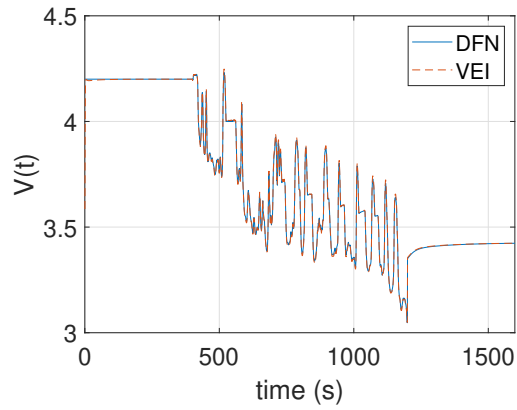
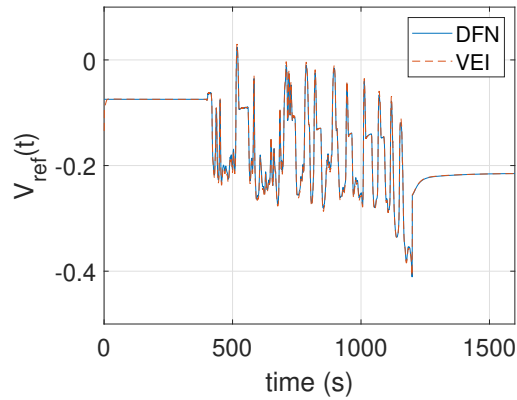


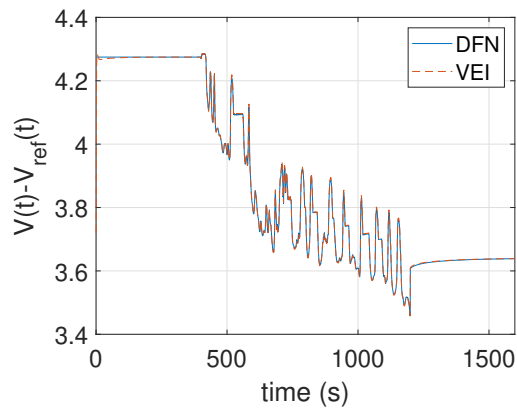
Figure 11: Profil de courant du cycle UDDS de [5]



(a) Total Voltage



(b) $V_{ref}(t)$



(c) $V(t) - V_{ref}(t)$

Figure 12: Tensions avec le cycle UDDS de [5]

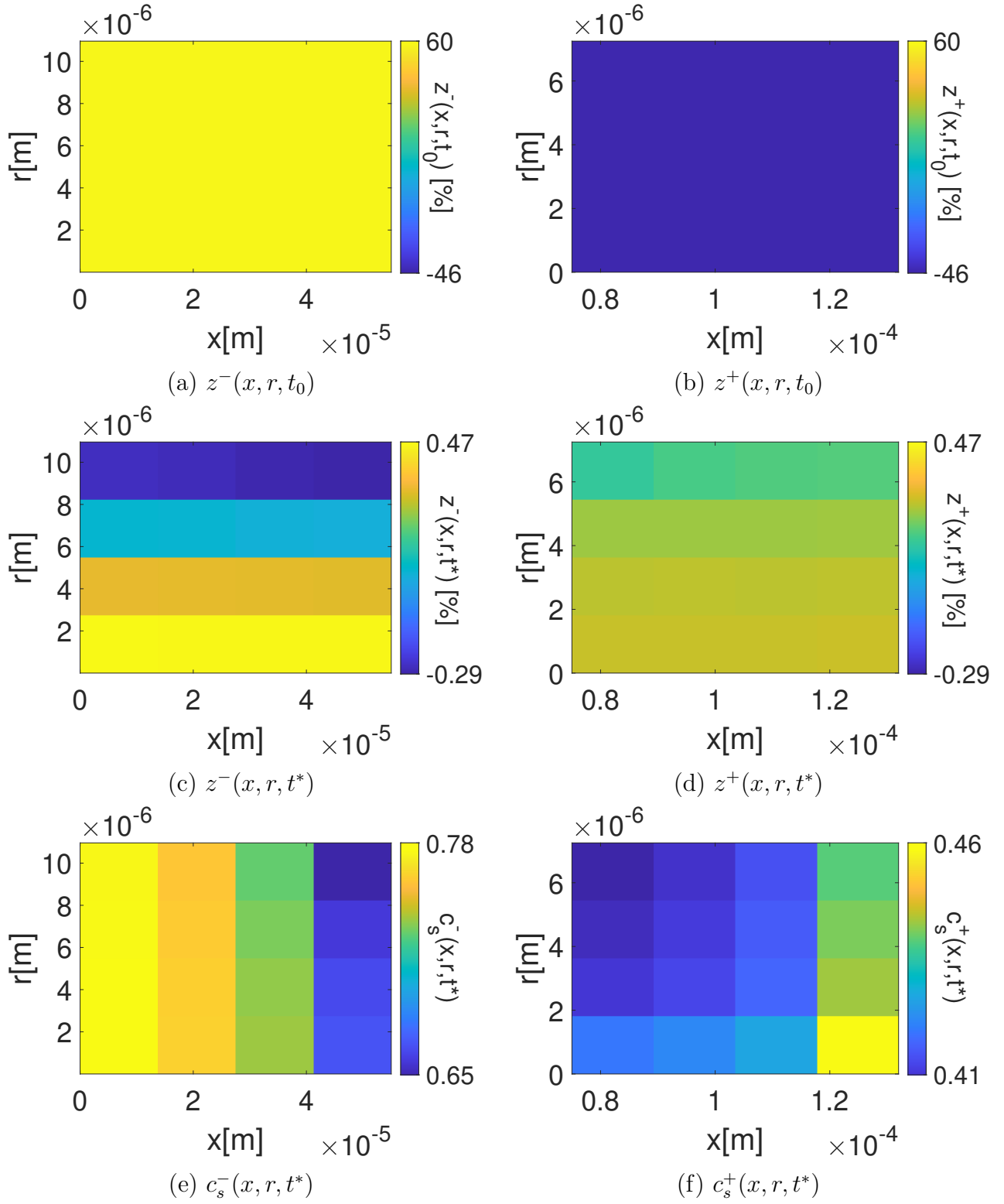


Figure 13: $c_s^\pm(x, r, t^*)$ et $z^\pm(x, r, t)$ de [5]

Prédictions Avancées du BMS - Exploitation de l'Observateur pour les Estimations d'État : Résumé du Chapitre

Ce chapitre se penche sur les prédictions avancées faites par les Systèmes de Gestion de Batterie (BMS) et le rôle de l'observateur dans les estimations d'état. L'accent est principalement mis sur les états clés de la batterie : État de Charge (SOC), État de Santé (SOH), État de Puissance (SOP) et l'identification l'électrocomposition du lithium. La Figure 14 offre un aperçu complet de l'architecture de l'algorithme BMS proposé. Le chapitre éclaire l'intégration du modèle MPMe et des observateurs d'état avec de nouveaux capteurs pour améliorer la précision des prédictions du BMS. L'architecture de l'algorithme BMS proposé est présentée, mettant l'accent sur la synergie entre les différents composants. Des discussions détaillées sur les estimations du SOC et du SOH soulignent leur importance, les méthodologies et la précision de l'algorithme BMS. Le phénomène l'électrocomposition du lithium ses implications et sa gestion sont explorés en profondeur, mettant en évidence ses défis et les stratégies pour une gestion efficace. Enfin, le chapitre présente les subtilités de l'estimation du SOP, son importance et les facteurs influençant sa prédiction. Les Figures 15, et 16 montrent l'estimation en temps réel du SOC, et SOP en utilisant les Algorithmes BMS.

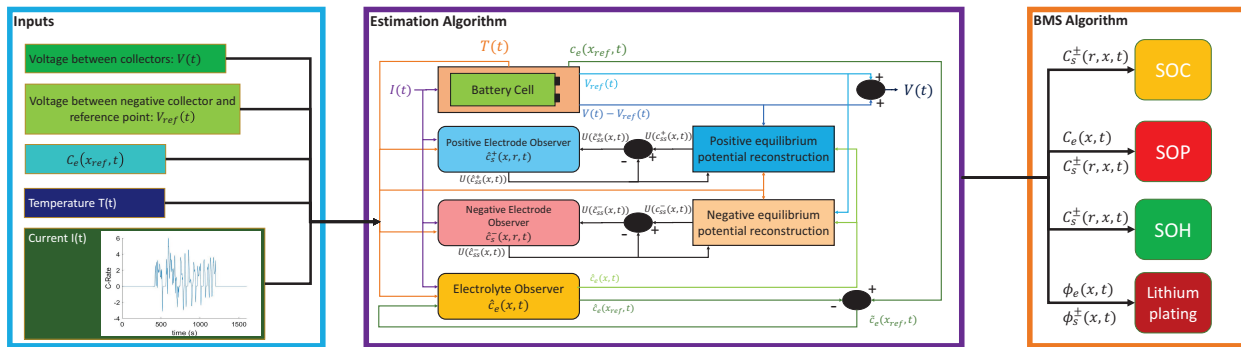


Figure 14: Représentation schématique de l'algorithme BMS proposé de [6]

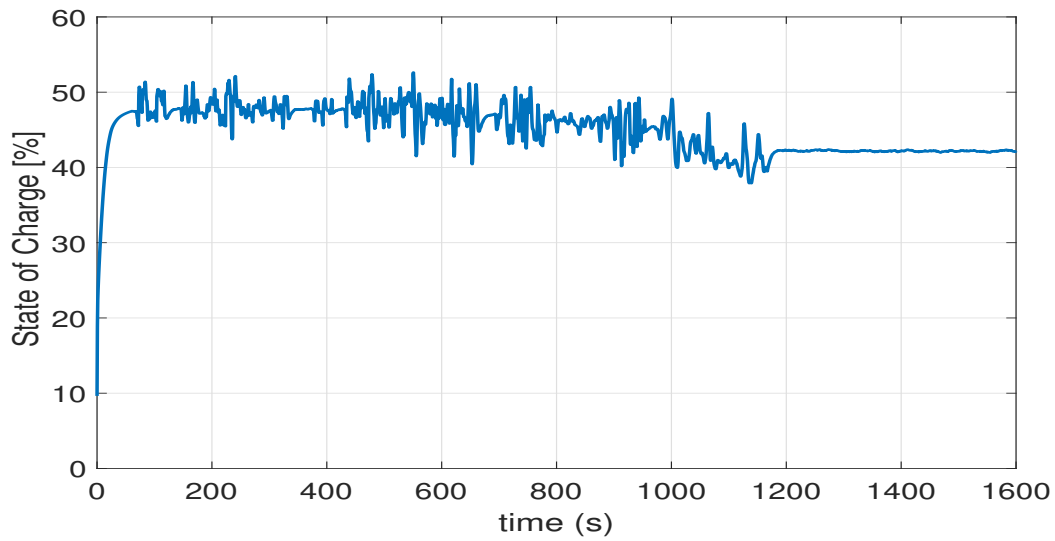


Figure 15: Estimation du SOC

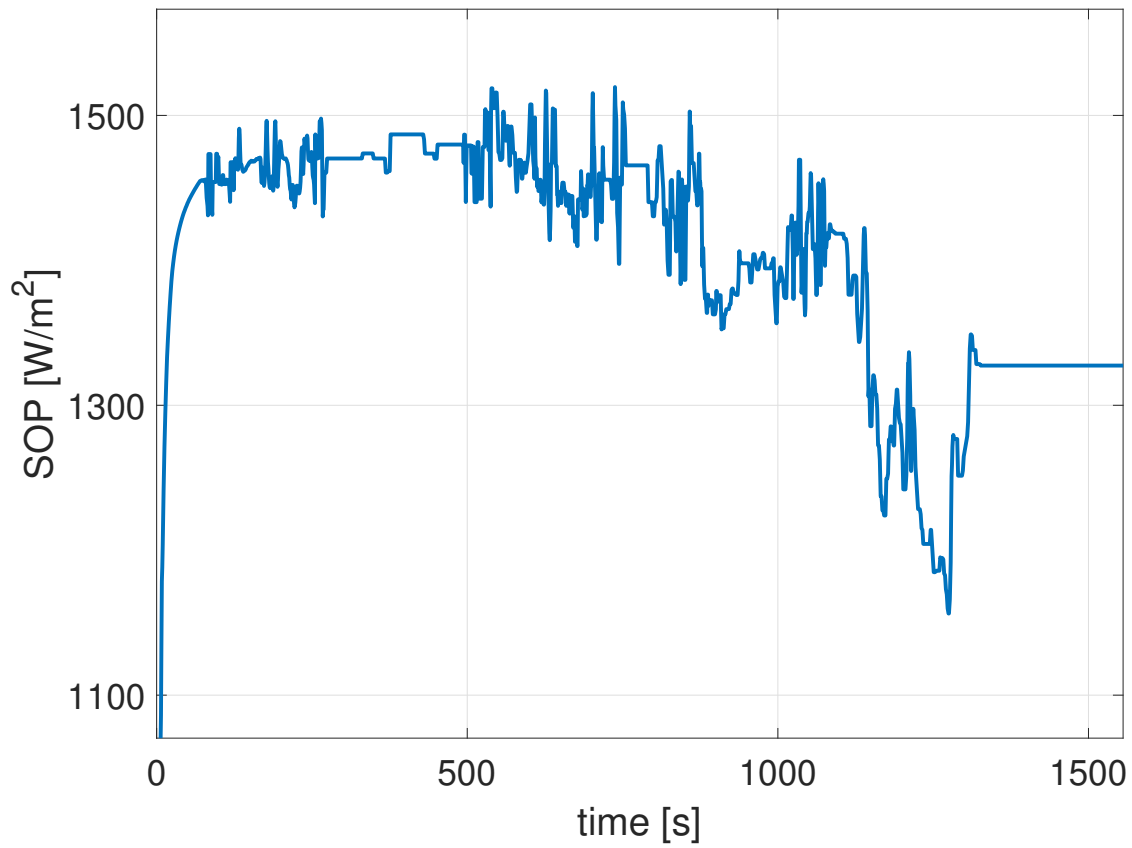


Figure 16: Prédiction du SOP de [6].

Chapter 1

Background

Contents

| | | |
|-----|--|----|
| 1.1 | Motivation | 37 |
| 1.2 | INSTABAT Project | 38 |
| 1.3 | Objectives of the PhD | 40 |
| 1.4 | Challenges and Issues | 41 |
| 1.5 | Summary of the PhD Thesis and Main Contributions | 42 |
| 1.6 | Conclusion of the Chapter | 43 |

Summary of the Chapter

Lithium-ion batteries (LiBs) have become a cornerstone in the global transition away from fossil fuels, playing a pivotal role in mitigating climate change and global warming effects. Their efficiency and environmental benefits have made them the preferred choice for various applications, especially in the electric vehicle (EV) sector. The transition to renewable energy sources has been accelerated by the advantages of LiBs, such as high energy density and reduced environmental impact compared to traditional batteries. The automotive sector's electrification, driven by concerns over vehicular emissions, heavily relies on LiBs. However, challenges related to LiB performance, safety, lifespan, and management remain. Addressing these challenges is crucial for the broader adoption of EVs and the sustainable electrification of the transport sector.

The INSTABAT project, part of the European Union's Horizon 2020 Research and Innovation Program, aims to advance LiB technology for EVs by monitoring key parameters in real-time. The project combines physical sensors, virtual sensors, and advanced battery management system (BMS) algorithms to achieve its objectives.

This PhD research, conducted within the INSTABAT framework, focuses on advancing LiB modeling and observer design for EVs. The primary objectives include formulating a reduced model considering inhomogeneous Li exchange profiles, designing an observer using new sensor data, incorporating additional physical dependence into the model and observer, and testing the observer's effectiveness.

Despite the potential benefits, challenges persist in precise SOX assessment of LiBs due to their complex behavior under varying conditions. The models used are intricate, with interdependent variables that make observer design challenging. Incorporating additional dependence, such as temperature, adds complexity and computational cost. Addressing these challenges requires a combination of mathematical modeling, advanced control techniques, robust estimation algorithms, and experimental validation.

The main contributions of this PhD research include the formulation of a multi-particle model with electrolyte dynamics (MPMe), the design of an observer that integrates potential sensor technologies, and the incorporation of additional physical dependence into the model

and observer. These contributions have led to the publication of a journal paper, and a presentation at a conference:

- **Asif, Mian Mohammad Arsalan, and Federico Bribiesca-Argomedo. 2023. “Electrochemical State Observer Design for Li-Ion Batteries With Heterogenous Electrode Lithiation.” IEEE Control Systems Letters 7: 3199-3204. <https://doi.org/10.1109/LCSYS.2023.3304248>.**
- **Asif, Mian Mohammad Arsalan, Federico Bribiesca-Argomedo, and Vincent Heiries. 2023. “Real time estimation of electrochemical states in Li-ion batteries and exploitation in BMS algorithms.” Presented at the Battery 2030+ 3rd Annual Conference.**

In essence, this research aims to enhance the performance, safety, and reliability of LiBs in EV applications, with its findings documented in technical reports and research papers to ensure wider dissemination and impact.

1.1 Motivation

Lithium-ion batteries (LiBs) have emerged as a pivotal technology in the global pursuit to transition from fossil fuels, combat the escalating crisis of global warming, and mitigate the adverse effects of climate change [23]. The efficiency, and durability of LiBs have rendered them an optimal choice for a wide array of applications. These applications span various sectors, with a particularly prominent role in the field of electric vehicles (EVs), which stand at the forefront of the transport sector’s green revolution [24].

The rampant burning of fossil fuels for transportation and energy production has been a key contributor to greenhouse gas emissions that increase global warming and trigger drastic climate change [52]. The growing environmental crises have prompted a global shift towards renewable energy sources and advanced energy storage technologies. Lithium-ion batteries, owing to their high energy density, long cycle life, and relatively lower environmental impact compared to traditional lead-acid and nickel-cadmium batteries, have emerged as crucial enablers in this transition [25].

In the automotive sector, the vigorous drive towards electrification is fundamentally propelled by increasing environmental concerns over vehicular emissions contributing to air pollution and climate change [26]. LiBs, as the primary energy storage technology in EVs, are central to this transition. These batteries provide a means of efficiently harnessing and utilizing renewable energy, thus reducing the sector's dependence on fossil fuels and the associated greenhouse gas emissions [53].

However, despite the promising role of LiBs in EVs, several challenges related to performance, safety, lifespan, and affordability still need to be addressed. Additionally, the issue of battery management, including State of Charge (SOC), State of Power (SOP), and State of Health (SOH) estimation, pose significant hurdles for the efficient use of LiBs in EVs [25].

This makes it imperative to intensify research efforts focused on LiBs for EV applications. It is through such research that we can refine the design and operation of these batteries, enhance their safety and efficiency, extend their lifespan, and reduce costs. These advancements will facilitate the broader adoption of EVs and contribute significantly to global climate change mitigation efforts by promoting the sustainable electrification of the transport sector [27].

1.2 INSTABAT Project

The INSTABAT project [28] (funded under the European Union's Horizon 2020 Research and Innovation Program Grant 955930) is a significant research endeavor focused on advancing lithium-ion battery technology for EV applications. Its primary objective is to monitor key parameters of Li-ion battery cells in real-time, enabling the development of higher accuracy States of Charge, Health, Power, Energy, and Safety (referred to together as SOX) indicators [28]. By achieving accurate and comprehensive monitoring, the INSTABAT project aims to enhance battery safety, quality, reliability, and overall lifespan.

To fulfill its objectives, the INSTABAT project adopts a multi-faceted approach, combining the integration of physical sensors, the development of virtual sensors, and the design of advanced battery management system (BMS) algorithms. These components work synergistically to provide a comprehensive understanding of battery behavior and enable effective

control strategies.

The project focuses on the development and adaptation of four innovative physical sensors: optical fiber sensors with Fiber Bragg Grating and luminescence probes, reference electrodes, and photo-acoustic gas sensors [29]. At the beginning of the project, these sensors were at different stages of maturity, with some already successfully implemented in laboratory battery cells, while others are still in the concept stage. The sensors are strategically positioned within the battery cells to monitor various key parameters, including temperature, heat flow, pressure, strain, Li concentration, CO₂ concentration, and impedance. Through reliable and operational monitoring of these parameters, the INSTABAT project aims to obtain valuable insights into the physico-chemical degradation phenomena occurring within the battery cell [29].

Complementing the physical sensors, virtual sensors are developed based on electrochemical and thermal reduced models. These virtual sensors leverage the available sensor information and a priori knowledge about the battery system models to estimate the values of variables that are challenging to directly measure. By utilizing advanced algorithms and model-based approaches, the virtual sensors provide real-time estimations of internal battery variables, further enhancing the accuracy of the SOX cell indicators.

The collaborative efforts within the INSTABAT project extend beyond sensor development and integration [29]. The project also focuses on the development of advanced BMS algorithms that incorporate data from both physical and virtual sensors. These algorithms utilize the measured and estimated parameters to improve state prediction, allowing for a more precise estimation of key battery performance metrics, such as SOC, SOH, and SOP. The enhanced BMS algorithms contribute to optimized battery management and control strategies, ultimately improving the overall functionality and safety of Li-ion batteries in EV applications.

1.3 Objectives of the PhD

This PhD research is conducted within the framework of the INSTABAT project [28], focusing on specific tasks that contribute to the advancement of lithium-ion battery modeling and observer design for electric vehicle applications. The primary objectives of this PhD thesis are as follows:

1. Formulate a reduced model that considers inhomogeneous Li exchange profiles between the electrode and electrolyte. The model will capture the spatial variations in Li-ion concentration within the battery, providing a more accurate representation of the electrochemical behavior and performance characteristics.
2. Design an observer that utilizes newly available sensor data in conjunction with the improved model dynamics to accurately represent the battery dynamics. These sensor data, obtained from the INSTABAT project, include measurements such as temperature, current, voltage, and Li concentration. The observer will leverage the additional information to estimate the internal states of the battery system with enhanced accuracy and reliability.
3. Incorporate additional physical dependence of parameters into the model and observer, such as temperature dependence and very limited aging mechanisms of the battery. By considering these dependencies, the model and observer will provide a more comprehensive representation of the battery's behavior, accounting for temperature variations and the degradation processes that occur over the battery's lifetime.
4. Test the effectiveness of the developed observer and confirm the validity of the designed observer on an experimental setup. The performance of the observer will be assessed in terms of estimation accuracy, convergence, and robustness.

By accomplishing these objectives, the PhD research aims to advance the understanding of lithium-ion battery behavior, improve state prediction accuracy, and contribute to the development of more robust battery management and control strategies for electric vehicle

applications. The outcomes of this research will have practical implications for enhancing the performance, safety, and reliability of lithium-ion batteries in real-world EV applications.

1.4 Challenges and Issues

Precise SOX assessment of lithium-ion batteries remains challenging due to their varying characteristics under different working environments [30]. The models used to represent the behavior of lithium-ion batteries are highly complex, with interdependent variables that pose significant challenges in observer design [21]. Developing observers capable of accurately estimating the internal states of the battery requires advanced mathematical techniques and a thorough understanding of the system dynamics. Furthermore, proving the convergence of the designed observers necessitates the use of complex mathematical analysis.

One of the challenges in incorporating additional physical dependence, such as temperature, to improve the accuracy of the models and observers is the increased complexity and computational cost. The already intricate models become even more complex when additional variables are considered. This complexity raises concerns about the computational efficiency and real-time implementation of the models and observers [54]. To ensure practical feasibility, an efficient simulation and model reduction technique must be developed to accurately simulate the models and observers while retaining their essential behavior. The design and proof of convergence for the observers become more intricate as the number of incorporated physical variables increases [55, 56].

In addition to the complexity of the models and observers, another challenge lies in the parametric uncertainty and state dependence of the lithium-ion battery system. The behavior of the batteries can vary due to manufacturing tolerances, aging effects, and operating conditions [57]. Accounting for these uncertainties and variations in the models and observers is crucial for robust and reliable performance. Developing strategies to handle parametric uncertainty and state-dependence, such as sensitivity analysis and adaptive algorithms, is essential for accurate state prediction and estimation [58].

Furthermore, implementing the developed models and observers on an actual experimental setup introduces practical challenges. The models and observers need to be capable

of running in real-time to provide timely and accurate state estimation [21]. Real-time implementation requires efficient algorithms and hardware considerations to ensure the computational demands are met. Additionally, the models and observers must be validated and tested on real battery cells under various operating conditions to ensure their effectiveness and reliability in practical applications [59].

Addressing these challenges requires a comprehensive approach that combines mathematical modeling, advanced control techniques, robust estimation algorithms, and experimental validation. Overcoming these challenges will contribute to the improvement of lithium-ion battery management and control for electric vehicle applications.

1.5 Summary of the PhD Thesis and Main Contributions

This PhD thesis within the context of the INSTABAT project aims to address the challenges associated with lithium-ion battery modeling and observer design for electric vehicle applications. The main contributions of the PhD research, discussed in various sections of the thesis, include:

1. Formulation of a multi-particle model with electrolyte dynamics (MPMe) that considers inhomogeneous Li exchange profiles between the electrode and electrolyte (Section 3).
2. Design of an observer that enables potential sensor technologies (among those studies in the Horizon 2020 INSTABAT project) in conjunction with the MPMe model to accurately estimate battery dynamics (Section 4).
3. Incorporation of additional physical dependencies, such as temperature dependence and limited plating mechanisms, into the model and observer to enhance their accuracy and applicability (Sections 3 and 4).

Based on this, a journal paper has been published, and our has been presented at a conference:

-
- **Asif, Mian Mohammad Arsalan, and Federico Bribiesca-Argomedo. 2023. “Electrochemical State Observer Design for Li-Ion Batteries With Heterogenous Electrode Lithiation.” IEEE Control Systems Letters 7: 3199-3204. <https://doi.org/10.1109/LCSYS.2023.3304248>.**
 - **Asif, Mian Mohammad Arsalan, Federico Bribiesca-Argomedo, and Vincent Heiries. 2023. “Real time estimation of electrochemical states in Li-ion batteries and exploitation in BMS algorithms.” Presented at the Battery 2030+ 3rd Annual Conference.**

The preparation of another journal paper on the experimental validation of the designed observer and battery model is also expected.

The research conducted in this PhD thesis aims to advance the field of lithium-ion battery modeling and observer design, particularly for electric vehicle applications. By providing a comprehensive understanding of the state of the art, developing the MPMe model, designing an observer using newly available sensor data, incorporating additional physical dynamics, and addressing sensitivity analysis, this research contributes to the improvement of battery management and control strategies. The documentation of research findings in technical reports and the publication of research papers ensure the dissemination and wider impact of the research outcomes.

The outcomes of this research have practical implications for enhancing the performance, safety, and reliability of lithium-ion batteries in real-world electric vehicle applications.

1.6 Conclusion of the Chapter

This chapter has provided a comprehensive background and established the foundational knowledge required for the subsequent discussions and analyses throughout this thesis. Lithium-ion batteries (LiBs) have been recognized as a pivotal technology in the transition away from fossil fuels, particularly in the electric vehicle (EV) sector, due to their high energy density and reduced environmental impact. However, the complexity and challenges related to LiB performance, safety, lifespan, and management, particularly in precise State

of Charge, State of Power, State of Health, (SoX) estimation, and observer design, have been highlighted.

The INSTABAT project, under the European Union’s Horizon 2020 Research and Innovation Program, has been introduced as a significant endeavor towards advancing LiB technology for EVs by focusing on real-time monitoring of key parameters. This PhD research, conducted within the INSTABAT framework, has been detailed to focus on advancing LiB modeling and observer design for EVs, with specific objectives including the formulation of a reduced model, designing an observer using new sensor data, incorporating additional physical dependence into the model and observer, and testing the observer’s effectiveness.

The main contributions of this research, including the formulation of a multi-particle model with electrolyte dynamics (MPMe), the design of an observer that integrates potential sensor technologies, the incorporation of additional physical dependence into the model and observer, and BMS algorithms based on the proposed observer and model, have been elucidated. These contributions have been documented through a published journal paper and a conference presentation, with further research underway.

In essence, this research aims to enhance the performance, safety, and reliability of LiBs in EV applications, contributing to the broader adoption of EVs and the sustainable electrification of the transport sector. The subsequent chapters will delve deeper into the specific methodologies, models, and analyses employed in this research, providing a detailed exploration of the developed models, observer design, and experimental validations.

Chapter 2

State of the art

Contents

| | | |
|------------|--|-----------|
| 2.1 | Battery Models | 48 |
| 2.1.1 | Equivalent Circuit Models | 48 |
| 2.1.2 | Machine Learning Models | 51 |
| 2.1.3 | Electrochemical Models | 56 |
| | Comparison of Electrochemical Battery Models | 56 |
| | Pseudo-Two-Dimensional Model (P2D) | 56 |
| | Electrode Average Model (EAM) | 57 |
| | Porous Electrode with Polynomial Model (PPM) | 58 |
| | Single Particle Model (SPM) | 58 |
| | SPM with Electrolyte (SPMe) | 59 |
| 2.2 | State Estimation | 62 |
| 2.2.1 | Open-Loop Methods for state estimation | 62 |
| | Coulomb Counting Estimation | 63 |
| | OCV based method | 63 |
| | Towards Closed-Loop Approaches | 65 |
| 2.2.2 | Adaptive Filter-Based Methodologies for state estimation | 65 |
| | Recursive Least Squares | 66 |
| | Kalman filter-based | 66 |
| 2.2.3 | Adaptive AI-Based Methodologies | 68 |
| | Particle Swarm Optimization | 69 |
| | Genetic Algorithm based Estimation | 71 |
| | Fuzzy-based Neural Networks | 72 |
| | Artificial Neural Networks | 73 |
| 2.2.4 | Model-Based Methodologies for state estimation | 74 |
| | Electrical Circuit Models | 74 |

| | |
|---|-----------|
| Electrochemical Models | 75 |
| 2.2.5 Hybrid estimation techniques for state estimation | 77 |
| 2.3 Lithium Ion Battery Degradation | 78 |
| 2.3.1 Degradation Mechanisms of Lithium-Ion Batteries | 78 |
| Primary Degradation Mechanisms and Their Implications | 80 |
| Key Degradation Mechanisms | 80 |
| Interplay Between Degradation Mechanisms | 81 |
| 2.3.2 Operational Implications of Lithium Degradation | 83 |
| Observable Consequences (Modes) | 83 |
| Operational Effects | 83 |
| 2.4 Conclusion of the Chapter | 84 |

Summary of the Chapter

Battery Models: Battery models are pivotal for understanding and predicting LiB behavior. The main models discussed include:

- **Equivalent Circuit Models (ECMs):** Representing the electrical behavior of LiBs through circuits, ECMs are computationally efficient but may not capture detailed internal electrochemical processes.
- **Machine Learning Models:** These models, including Artificial neural networks (ANNs), Support Vector Machines (SVMs), and others, can learn complex relationships but require extensive data and can be computationally intensive.
- **Electrochemical Models (EChMs):** EChMs provide a comprehensive understanding of internal electrochemical processes, though they can be computationally demanding.

State Estimation Techniques: State estimation is crucial for effective LiB management. The techniques include:

- **Open-Loop Methods:** Direct estimation methods like Coulomb Counting and OCV based methods are simple but may lack long-term accuracy.
- **Adaptive Filter-Based and AI-Based Methodologies:** Methods like Recursive Least Square (RLS), Kalman filters, and Artificial Intelligence (AI) algorithms offer limited state estimation but can be resource-intensive.
- **Model-Based and Hybrid Estimation Techniques:** Model-based methods provide detailed insights, while hybrid methods combine multiple approaches for enhanced estimation.

Lithium Degradation Model: As LiBs expand their applications, understanding their degradation is essential. The degradation is categorized into:

- **Mechanisms:** Physical and chemical transformations within the battery.

-
- **Modes:** Observable consequences at the cell level due to mechanisms.
 - **Operational Effects:** Outcomes like capacity or power fade resulting from the modes.

In essence, a comprehensive understanding of battery models, state estimation techniques, and degradation mechanisms is vital for optimizing LiB performance and longevity in diverse applications.

2.1 Battery Models

In the field of LiB research, various modeling approaches have been developed to understand and predict battery behavior. These models play a crucial role in designing control strategies, optimizing battery performance, and ensuring safe and reliable operation. In this section, we will discuss different battery models, including Equivalent Circuit Models, Machine Learning models, and Electrochemical models, highlighting their characteristics, applications, advantages, and limitations.

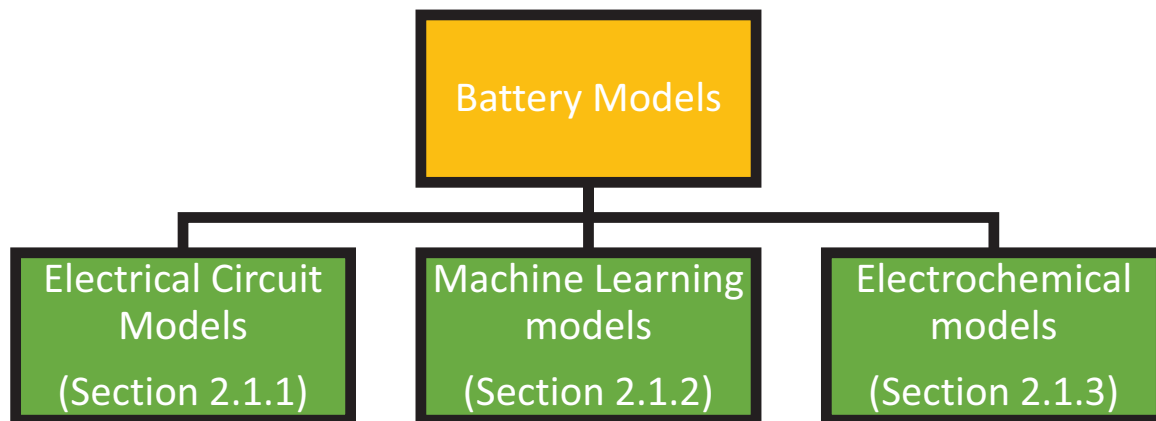


Figure 2.1: Battery Models

2.1.1 Equivalent Circuit Models

Equivalent Circuit Models (ECMs) are widely used in the field of LiB modeling. These models represent the electrical behavior of a LiB through an electrical circuit that approx-

imates the battery's input-output characteristics [31]. ECMs are computationally efficient and provide a relatively simple way to describe battery dynamics. They have been extensively studied and applied in various applications, ranging from battery management systems to electric vehicle design [32]. Most commonly used ECMs are briefly discussed in Table 1.

ECMs typically consist of electrical components such as resistors, capacitors, and current sources, which represent the different electrochemical processes occurring within the battery. These components are interconnected to simulate the complex electrochemical behavior of the LiB. The parameters of the circuit elements are determined through system identification techniques, where experimental data or electrochemical characterization tests are used to estimate the model parameters [60].

Advantages of ECMs include their simplicity, low computational complexity, and good representation of the LiB's overall input-output behavior [54]. They can accurately capture the dynamic response of the battery under different operating conditions, including charge and discharge processes. ECMs are particularly useful for real-time applications where fast estimation of the battery's SOX indicators is required [33].

However, ECMs also have significant limitations. They provide a simplified representation of the complex electrochemical processes occurring within the battery, which limits their accuracy in capturing detailed internal behavior [33, 34]. ECMs lack the ability to capture spatial variations within the battery, such as temperature gradients and concentration gradients. Furthermore, ECMs are highly dependent on accurate parameter estimation, which can be challenging due to variations in cell manufacturing, aging effects, and nonlinear dependencies [15].

Several variants of ECMs have been proposed to improve their accuracy and applicability. These include dynamic ECMs that account for time-varying behavior [61], parameter identification methods that consider aging effects [62], and temperature-dependent models that incorporate thermal dynamics [63]. These advancements aim to enhance the fidelity of ECMs in representing LiB behavior under various operating conditions.

Despite their limitations, ECMs remain popular due to their simplicity, computational efficiency, and reasonable accuracy for many practical applications. They serve as a foundation for more advanced LiB models and are often used as a benchmark for comparison with

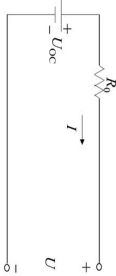
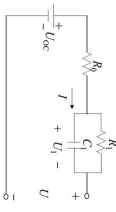
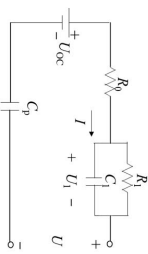
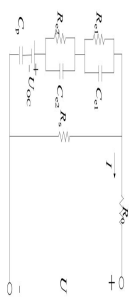
| Classification | Configuration | Description | Advantages | Disadvantages |
|----------------------|---|--|---|---|
| Rint Model [22] |  | A resistor is connected in series with an ideal voltage source. | Simple, easy parameter measurement. | The dynamic characteristics of the battery are not reflected, has low accuracy, and a small range of applications |
| Thevenin Model [1,2] |  | It utilizes a series of n RC circuits connected in series to represent the polarization phenomenon in electrical systems. | The RC loop is commonly used to simulate battery dynamics. Higher-order RC loops enhance the fidelity of battery simulations. | The impact of load current accumulation over time, as well as the change in open-circuit voltage and self-discharge, are not taken into account. Higher number of loops increases computational burden. |
| PNGV model [1] |  | The Thevenin equivalent circuit model incorporates the addition of capacitor C_p to accurately depict the alteration in open-circuit voltage resulting from the accumulation of load current over time. | The calculation burden is reduced in comparison to the 1st order Thevenin equivalent circuit model, while maintaining a higher level of accuracy. | The problem of battery self-discharge is still not addressed. |
| GNL model [1] |  | The utilization of two RC loops in the model serves to represent concentration polarization and electrochemical polarization. This structure closely aligns with the internal characteristics of the cell, contributing to a more accurate representation of its behavior. | Compared to the PNGV model, the proposed approach considers the variation in open circuit voltage caused by load current accumulation over time and incorporates battery self-discharge. This results in higher precision and wider applicability of the model. | Compared to the PNGV model, the proposed model involves more complex calculations and a larger computational burden. |

Table 2.1: ECM Table adapted from [22]

other modeling approaches [34].

In conclusion, ECMs are widely used in LiB modeling due to their simplicity and computational efficiency. While they provide a good approximation of the battery's input-output behavior, they have limitations in capturing detailed internal electrochemical processes and spatially resolved information [33].

2.1.2 Machine Learning Models

Machine learning models have emerged as powerful tools for battery modeling and estimation, leveraging their ability to learn complex relationships from data. Various types of machine learning models have been extensively investigated and applied in battery research. In this section, we discuss some of the prominent types, along with their distinct advantages and limitations.

Artificial Neural Networks: Artificial Neural Networks (ANNs) are computational models inspired by the structure and functioning of biological neural networks [35]. ANNs consist of interconnected artificial neurons, organized in layers, that enable information processing [64]. Figure 2.2 shows the general structure of the general structure of Neural Networks. ANNs excel at capturing intricate nonlinear relationships and can handle both regression and classification tasks effectively. They possess the capability to learn and adapt to diverse data patterns and structures, reducing the reliance on manual feature engineering. However, ANNs typically require a substantial amount of labeled training data to achieve optimal performance. The training process can be computationally intensive, and the risk of overfitting arises when the network is not appropriately regularized or when training data is limited [3, 37, 65–68].

Support Vector Machines : Support Vector Machines (SVM) are supervised learning models that aim to find an optimal hyperplane to separate data points into distinct classes [36]. SVM are widely used in lithium-ion battery modeling due to their ability to capture complex relationships and accurately predict battery behavior [69]. SVM excels at handling high-dimensional data and can detect nonlinear patterns, making it suitable for capturing the intricate dynamics of lithium-ion batteries. SVM's requires careful selection of kernel functions and hyperparameters is crucial for optimal performance. Also, the computational

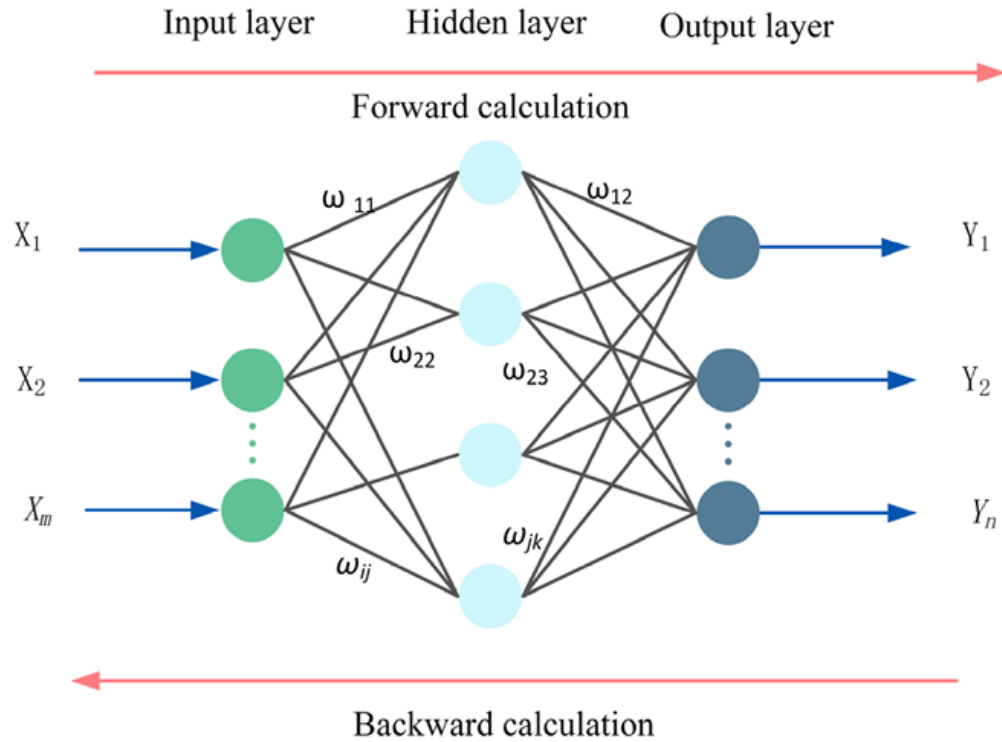


Figure 2.2: General structure of the general structure of Neural Networks [3]

complexity of SVM can be a challenge when dealing with large datasets. Overall, SVM is a valuable tool in lithium-ion battery modeling, offering accurate predictions and insights for battery design and optimization. [69,70]. Figure 2.3 shows the Flow chart for SVM modeling of a battery.

Decision Trees : Decision Trees (DT) are powerful supervised learning models used for classification and regression tasks. They are commonly employed in lithium-ion battery modeling due to their ability to capture complex relationships and accurately predict battery behavior [8]. Decision Trees construct a hierarchical structure of decision rules based on the training data, allowing for interpretable and intuitive representations of battery performance [41,71]. They can handle both numerical and categorical data, making them suitable for various battery parameters. Decision Trees excel at capturing nonlinear patterns and interactions among battery features, enabling accurate predictions. However, they may suffer from overfitting and sensitivity to outliers, which can be mitigated through pruning and ensemble techniques [71]. Figure 2.4 shows the Flow chart for DT modeling of a battery.

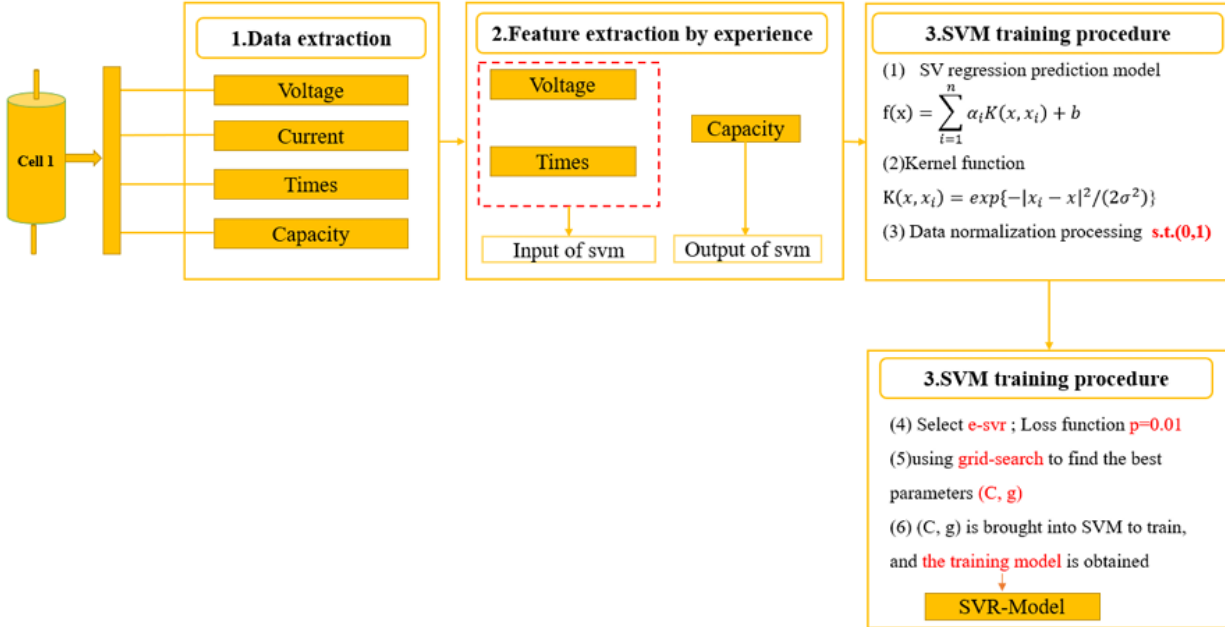


Figure 2.3: Flow chart for SVM modeling of a battery [7]

Deep Learning Models: Deep learning models, such as deep neural networks (DNNs), have gained significant attention in lithium-ion battery modeling due to their ability to extract intricate patterns from complex data [72]. DNNs adopt the adjective “deep” as they consists of multiple layers of interconnected neurons that learn hierarchical representations of the input data. In the context of lithium-ion battery modeling, DNNs are employed to predict battery behavior and performance based on various input parameters. These models excel at capturing nonlinear relationships and can handle high-dimensional data, making them well-suited for the complexities of battery systems [73]. DNNs can learn complex feature representations automatically, enabling them to uncover hidden patterns and correlations in battery data [74]. However, training deep learning models requires a large amount of labeled data and significant computational resources. Overfitting can also be a concern, necessitating regularization techniques and careful model architecture design [75–77].

Ensemble learning Models: Ensemble learning (EL) is a powerful approach in machine learning that combines multiple models to improve overall performance and robustness. In the context of lithium-ion battery modeling, ensemble learning has shown promise in enhancing prediction accuracy and capturing complex battery behavior [78].

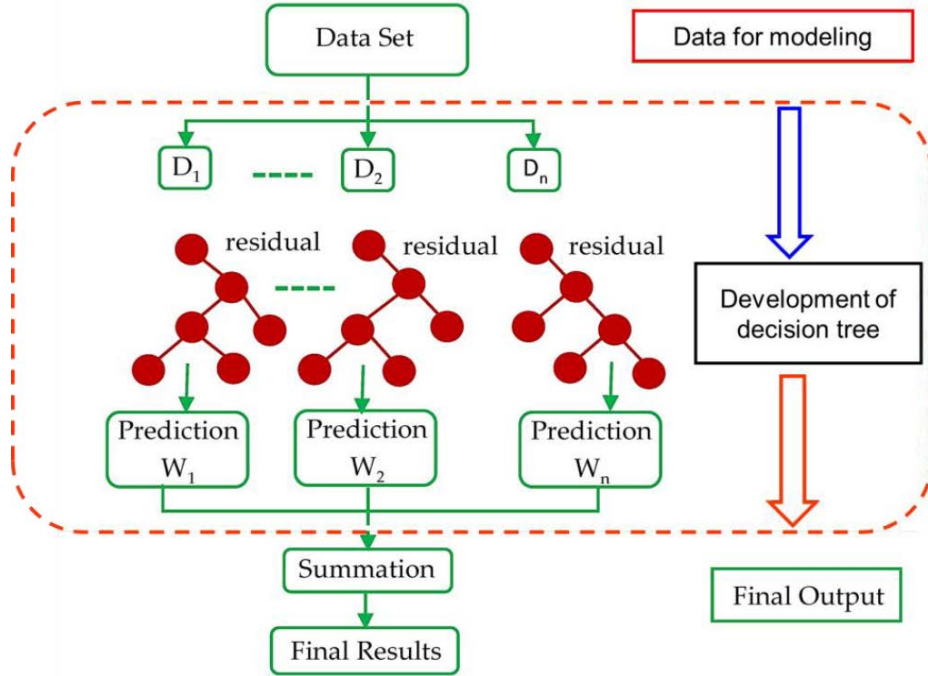


Figure 2.4: Flow chart for DT modeling [8]

There are two main types of ensemble learning: model-level ensemble and data-level ensemble [41,71]. In model-level ensemble, multiple individual models, such as decision trees or support vector machines, are trained independently and their predictions are combined using techniques like majority voting or averaging. This approach leverages the diversity of models to reduce bias and improve generalization capability [79, 80].

Data-level ensemble, on the other hand, focuses on creating diverse training sets to train individual models. This can be achieved through techniques such as bootstrapping, where multiple subsets of the original training data are randomly sampled with replacement. Each subset is then used to train a separate model. By creating diverse training sets, data-level ensemble methods can effectively capture different aspects of the data and enhance the overall predictive performance. Figure 2.5 shows the random forest algorithm which uses multiple decision trees to form a “forest” [81–85].

Ensemble learning offers several advantages in lithium-ion battery modeling. Firstly, it can help mitigate the limitations of individual models and improve overall prediction accuracy. The combination of multiple models or diverse training data can enhance the robustness of the predictions, particularly in scenarios with complex battery behavior and

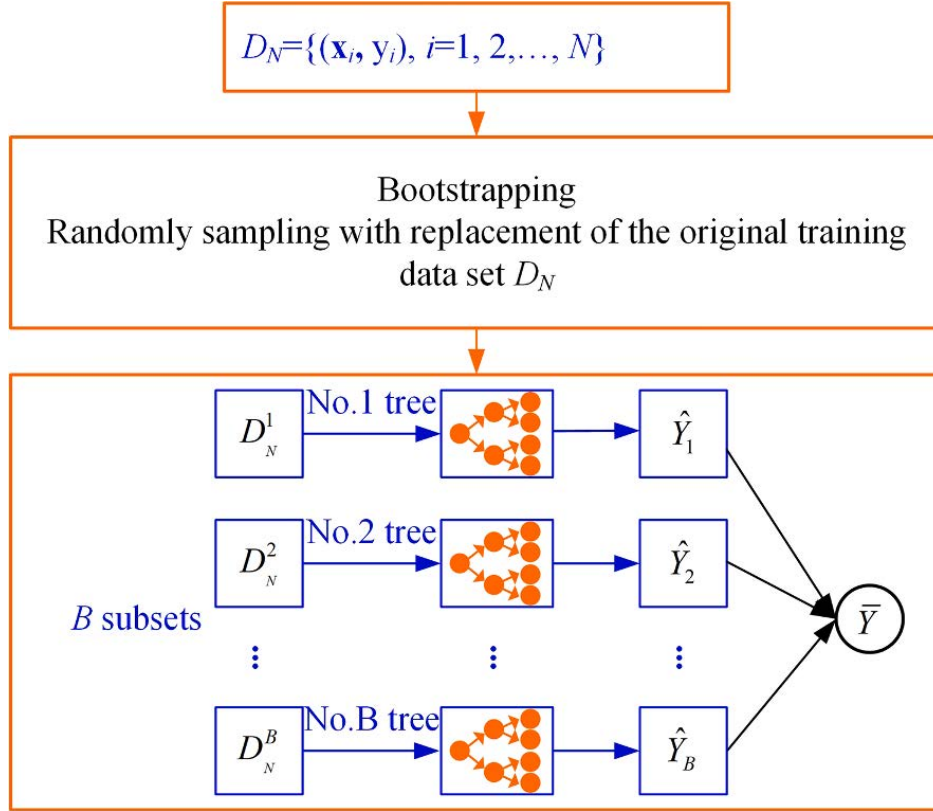


Figure 2.5: Schematic of EL Data-level technique with the use of Decision trees [8]

limited data availability [78].

However, ensemble learning also comes with certain challenges. It requires additional computational resources and can be more complex to implement compared to using a single model. The selection of appropriate ensemble techniques and combination strategies is crucial, as poorly designed ensembles may not yield improved results and can lead to computational overhead [71].

In conclusion, machine learning models offer promising avenues for battery modeling and estimation [8, 35, 36, 72, 78]. Their ability to learn complex relationships from data and adapt to diverse patterns makes them valuable tools in battery research [64, 69, 71, 73]. However, it is important to acknowledge the limitations associated with these models. One of the key challenges is the requirement for a significant amount of labeled training data, which may not always be readily available [3, 37, 65–68]. Additionally, the training process can be computationally intensive, necessitating powerful hardware resources [75–77]. Overfitting is another concern that needs to be carefully addressed to ensure the generalization and

robustness of the models [3, 37, 65]. Interpretability can also be a challenge, particularly for deep learning models, as their complex architectures and learned representations can be difficult to interpret and explain [74]. This means that the internal states of the LiB are not replicable to a large degree, providing little insight into the internal dynamics of the LiB. Overall, while machine learning models offer significant advantages, careful consideration of these limitations should be made when applying them in battery modeling tasks [41, 71].

2.1.3 Electrochemical Models

Electrochemical Models (EChMs) are advanced modeling approaches that aim to capture the detailed electrochemical processes occurring within LiBs. Unlike ECMS, which provide a simplified electrical representation of the battery, EChMs take into account the underlying chemical reactions and transport phenomena that govern battery behavior. EChMs offer a deeper understanding of the internal states and mechanisms of LiBs, making them valuable tools for studying battery performance, degradation, and optimization.

EChMs are typically based on partial differential equations (PDEs) that describe the internal variables of the battery such as lithium-ion concentration, potential distribution, and temperature. EChMs incorporate fundamental principles of electrochemistry, such as Butler-Volmer kinetics for electrode reactions, Nernst diffusion for ion transport, and Ohm's law for electronic conduction.

Comparison of Electrochemical Battery Models

Electrochemical battery models are pivotal in understanding the intricate behaviors of lithium-ion batteries. These models, ranging from empirical to physics-based, offer insights into the battery's operational characteristics and degradation mechanisms. We now detail a comparison of several key electrochemical battery models.

Pseudo-Two-Dimensional Model (P2D) The Pseudo-Two-Dimensional (P2D) model, grounded in the porous electrode theory by John Newman [86, 87], offers a detailed representation of the battery's electrochemical behavior. The model spatially resolves battery dynamics across two primary dimensions: the x direction spanning the collectors and the

r direction within the solid-phase particles, which gives the model its name [88–90]. This model:

- Envisions the cathode and anode as a series of spherical particles submerged in a liquid electrolyte, as depicted in Figure 2.6.
- Captures the spatiotemporal distribution of four states: solid-state lithium concentration (cs), liquid-state lithium concentration (ce), electrode potential (ϕ_s), and electrolyte potential (ϕ_e) [91].
- Uses four partial differential equations (PDEs) to describe processes like spherical diffusion of cs , linear diffusion of ce , and the Ohm’s laws for both ϕ_s and ϕ_e [50].
- Incorporates the Butler–Volmer equation to represent the intercalation reaction current density at the particle surface [92].
- Considers battery aging effects due to electrochemical side reactions, such as solvent reduction and lithium plating [62].

Despite its detailed representation and high accuracy in estimating battery SOH, the P2D model is computationally intensive due to its nonlinearly coupled PDEs. This complexity has limited its direct application in real-time control and estimation. However, recent advancements have applied model reduction and approximation techniques to estimate the model’s states, making it invaluable for in-depth studies on battery behavior, degradation, and control [4, 11].

Electrode Average Model (EAM) The EAM [93] offers a simplified representation. By neglecting the spatial variation of the solid phase concentration and focusing on the electrolyte phase concentration, it:

- Directly links the electrolyte phase concentration with the battery’s State of Charge (SOC).
- Provides a straightforward setup with fewer parameters.
- Ensures high accuracy in estimating battery SOC, especially for real-time applications.

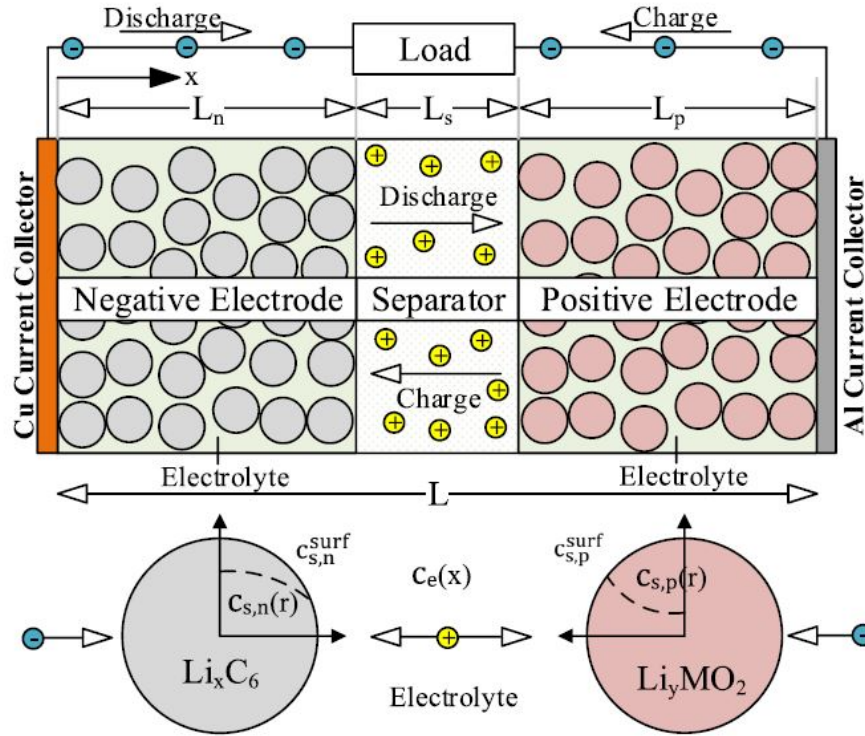


Figure 2.6: The LiB P2D model from [4]

However, the EAM's simplicity comes at the cost of voltage prediction accuracy and potential information loss. Its empirical nature also makes parameter identification challenging [4, 94].

Porous Electrode with Polynomial Model (PPM) The PPM [95] merges the parabolic approximation with the P2D model. By using a parabolic profile to describe each spherical particle, it excels at higher discharge rates ($> 1C$).

Single Particle Model (SPM) The SPM [96–98] simplifies the representation by viewing each electrode as a single spherical particle. This model:

- Simplifies the PDEs of solid phase concentration to ODEs.
- Achieves high accuracy at low discharge rates ($< 1C$).

However, its accuracy diminishes at higher rates, with voltage prediction errors ranging significantly.

SPM with Electrolyte (SPMe) Building upon the SPM, the SPMe [99] incorporates the concentration of the electrolyte phase. While it retains the foundational principles of the SPM, it offers enhanced accuracy at high discharge rates. Yet, this added complexity makes it a more intricate model compared to the traditional SPM.

Note: The SPM stands out as a reliable model, prompting extensive research to enhance its predictive accuracy. This includes considering degradation factors, thermal dynamics, and various conditions like mechanical stress [21, 100, 101]. Additionally, the evolution of battery models, from empirical to physics-based, underscores the industry’s drive to achieve a balance between accuracy and computational efficiency. As battery technologies advance, the need for models that can capture their behaviour becomes paramount, making the study and improvement of these models crucial [95].

EChMs offer several advantages over ML models and ECMs in capturing the detailed electrochemical processes within LiBs which include:

1. **Internal Behavior:** EChMs provide a more comprehensive understanding of the internal behavior of LiBs compared to ML models and ECMs. By incorporating fundamental principles of electrochemistry, EChMs capture the spatiotemporal variations of the key variables aforementioned. This allows for a detailed analysis of phenomena such as concentration polarization, electrode kinetics, and diffusion limitations, which directly impact battery performance.
2. **Mechanism-based:** EChMs are based on physical and chemical principles, making them mechanism-based models. They accurately represent the underlying electrochemical processes occurring within the battery, such as charge transfer reactions, ion transport, and diffusion. In contrast, ML models and ECMs rely on empirical correlations or simplified electrical representations, respectively, which may not fully capture the intricacies of the electrochemical behavior.
3. **Flexibility:** EChMs offer flexibility in incorporating various boundary conditions and operating conditions, making them suitable for studying diverse battery chemistries and designs. They can be adapted to different battery configurations and chemistries by appropriately modifying the model parameters and equations. This flexibility allows

for detailed investigations of specific LiB systems and the optimization of battery performance.

4. **Insight into Aging and Degradation:** EChMs enable the study of complex aging and degradation mechanisms in LiBs. By considering the spatiotemporal variations of variables, EChMs can simulate capacity fade, electrode degradation, and other aging phenomena. This information is crucial for predicting battery lifespan, optimizing battery management strategies, and designing more durable LiBs.

While EChMs offer significant advantages, they also have certain limitations. EChMs are computationally intensive and require sophisticated numerical techniques for solving governing equations. The accurate parameterization of EChMs can be challenging, as it often relies on detailed experimental data and electrochemical characterization. Furthermore, the complexity of EChMs may limit their accessibility to non-experts in electrochemistry and numerical methods.

Efforts are underway to address these limitations and make EChMs more practical and efficient. Simplified versions of EChMs, such as P2D models and reduced-order models, aim to strike a balance between accuracy and computational efficiency [9]. Reduced order models like Single Particle Models (SPMs) offer a less complex alternative to the DFN model, preserving most of its predictive capabilities at a significantly lower computational cost [9]. These models, originally introduced by Atlung et al in 1979 [102], are based on the concept that the behavior of particles within each electrode can be adequately represented by a single representative particle. Various versions of SPMs have been proposed, some incorporating electrolyte dynamics and others not, either derived directly from a list of simplifying assumptions [21, 103–106] or through asymptotic methods used to derive the reduced order models directly from the DFN model [107–111].

All these models fall under the “SPM-type” category and share fundamental characteristics, but they are distinguished into two subcategories: models with electrolyte dynamics (SPMe) and those without (SPM). A key feature of SPM-type models is the decoupling of the spatial variables in the PDEs, which effectively simplifies the problem to a one-dimensional space and significantly reduces the computational complexity compared to the

DFN model [9].

Additionally, model reduction techniques and optimization algorithms are being developed to enhance the efficiency and parameterization of EChMs. Figure 2.7 shows a summary of the techniques used to simplify and reduce the complexity of the P2D EChM. For a more complete detail on these reduction techniques, we refer the reader to [9].

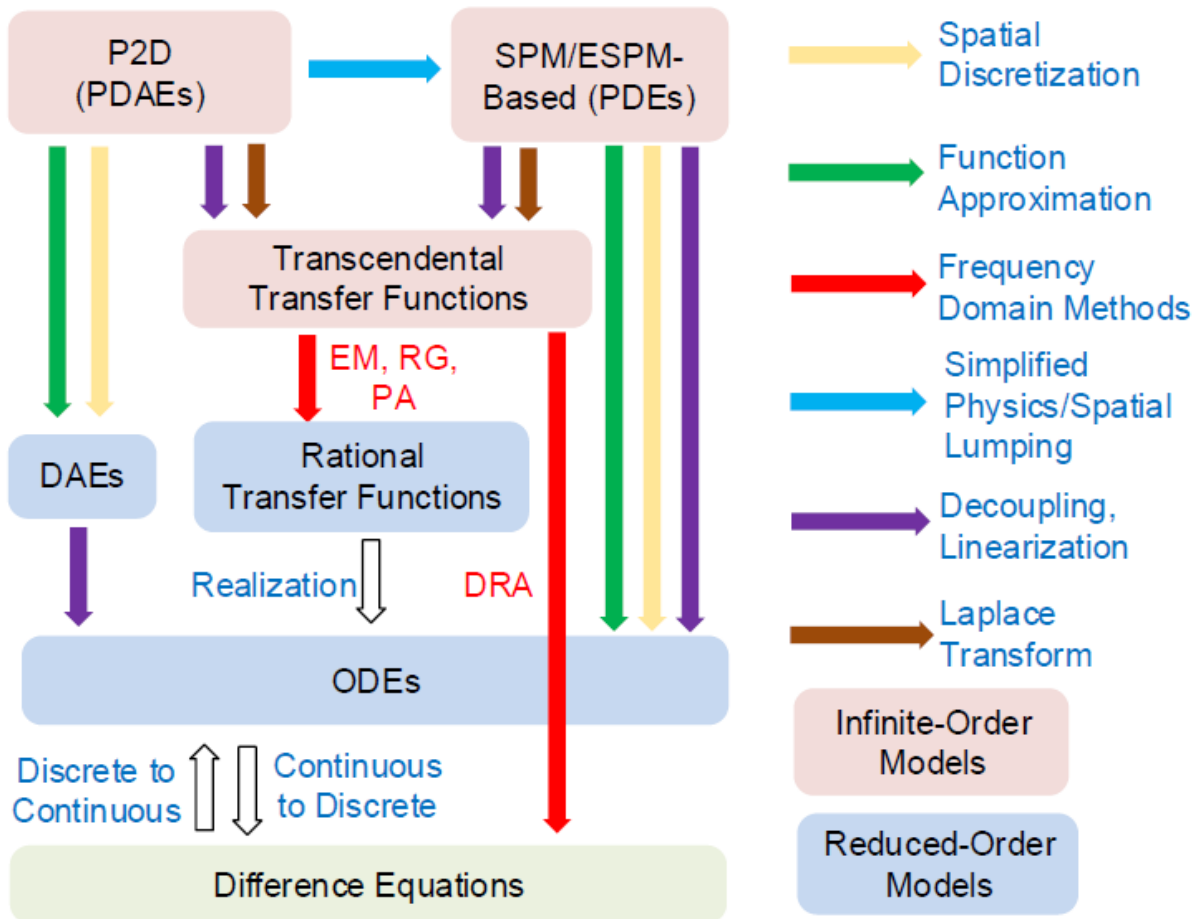


Figure 2.7: Relationships between major Model Order Reduction techniques for the P2D model [9]

In summary, EChMs offer a comprehensive understanding of the internal electrochemical processes within LiBs. They outperform ML models and ECMs by capturing detailed behavior, providing insights into aging and degradation, and offering flexibility in studying diverse battery systems. While EChMs have computational and parameterization challenges, ongoing research aims to overcome these limitations and make EChMs more accessible and

practical for various applications in LiB research and development.

2.2 State Estimation

Accurate estimation of the internal states of a LiB is crucial for effective control and management. State estimation techniques play a vital role in monitoring and predicting the battery's behavior, such as SOX indicators, and other important parameters. In this subsection, we will explore various state estimation methods employed for Li-ion batteries.

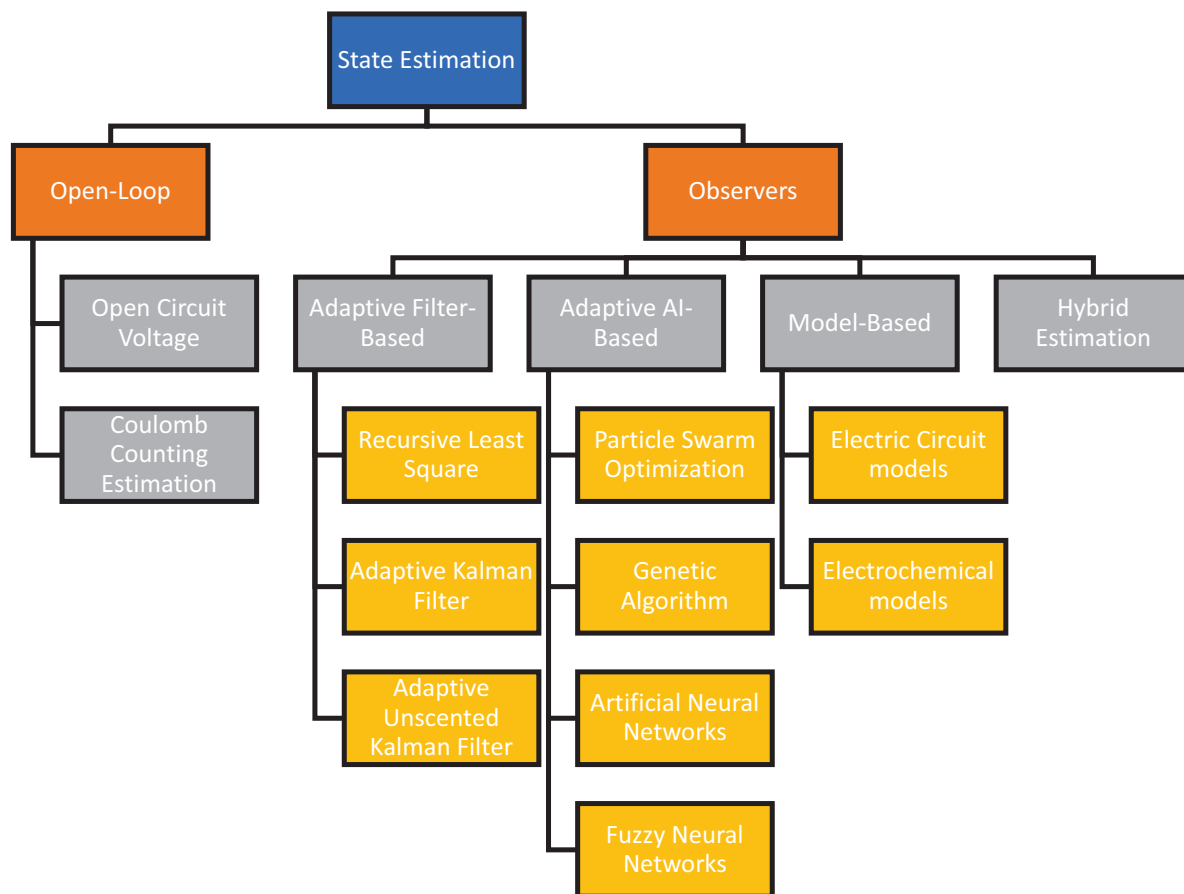


Figure 2.8: State Estimation Techniques

2.2.1 Open-Loop Methods for state estimation

Open-loop methods, also known as direct methods, estimate the battery's internal states based solely on the battery's input and do not use feedback from the output to self-correct.

One widely used open-loop method for Li-ion batteries is the Coulomb Counting Estimation [38–40]. This method calculates the SOC based on the integral of the battery’s charging/discharging current over time, using the initial SOC and nominal capacity.

Coulomb Counting Estimation

Coulomb Counting Estimation is conceptually simple and computationally efficient, making it suitable for real-time applications [38]. It does not require a complex model of the battery system and can provide reasonably accurate SOC estimates under ideal conditions. The method assumes that the battery operates under ideal behavior, without considering the effects of capacity fade, aging, and other factors that can impact the accuracy of the estimation [39].

OCV based method

The OCV based look-up table method utilizes the direct mapping relationship between SOC and external characteristics parameters like OCV and impedance. This approach involves extensive laboratory experiments to characterize battery behavior and establish a relationship between OCV and SOC [112]. The OCV look-up table method is conceptually simple and highly accurate [50]. The SOC estimation based on OCV employs a flowchart shown in Figure 2.9. Initially, the lithium-ion battery (LiB) is fully charged and then discharged using current pulses, followed by a rest period to measure the corresponding OCV. The mapping between OCV and SOC is established, and the instantaneous OCV measurement provides the SOC level. Hysteresis is observed in LiB, with higher voltage during charging compared to discharging, attributed to factors such as ohmic resistance, polarization resistance, and concentration polarization [51]. However, accurate OCV measurement requires sufficient rest time for the battery to reach an equilibrium condition, and OCV measurements are influenced by ambient temperature and battery aging [112, 113].

Advantages of open-loop methods include their simplicity, low computational cost, and real-time performance [38]. They are particularly useful when accurate knowledge of the battery model is not available or when computational resources are limited. Open-loop methods can provide a quick estimate of the battery’s SOC, allowing for basic monitoring

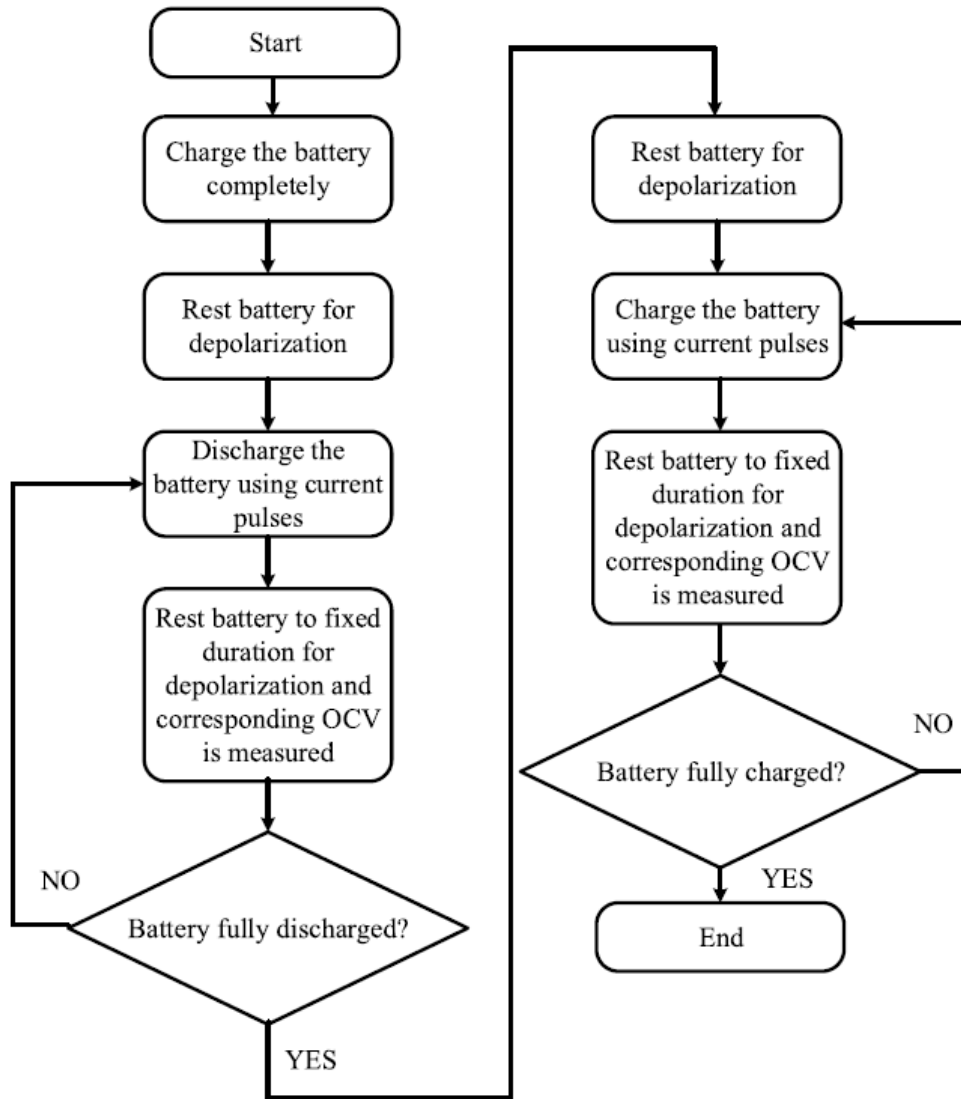


Figure 2.9: The flowchart of OCV-SOC estimation method [10]

and control of the battery system.

However, open-loop methods have certain limitations. They are highly dependent on accurate initial SOC estimation and nominal capacity information [40]. They also cannot be used while charging/discharging the battery and only work at rest [34]. Inaccurate initial SOC estimation and capacity degradation over time can lead to cumulative errors in the SOC estimation. Coulomb Counting Estimation does not account for aging effects, variations in battery behavior, and other factors that can affect the battery's performance. Therefore, open-loop methods may not provide accurate SOC estimates over the long term, especially

in the presence of aging and capacity fade [39]. These factors make Open-loop methods unsuitable as a means to achieve the objectives of this PhD.

Towards Closed-Loop Approaches

It is important to note that open-loop methods are typically used as an initial estimate or as a complement to other more sophisticated state estimation techniques. Combining open-loop methods with feedback-based approaches can improve the accuracy and reliability of the overall state estimation process, especially in the presence of varying operating conditions and aging effects [38]. This is called Closed-loop estimation. Figure 2.10 illustrates a schematic representation of a generic closed-loop estimation approach for Voltage prediction. We now discuss different types of closed-loop observer techniques used in the state estimation of LiBs.

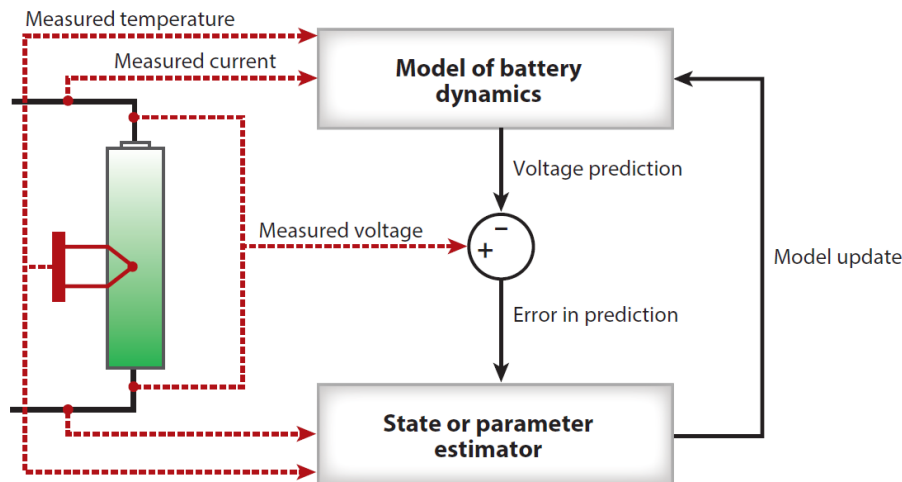


Figure 2.10: Schematic of a closed-loop feedback estimation algorithm. The output measurement (in this case, voltage) is used as feedback to correct the state or parameter estimation [11].

2.2.2 Adaptive Filter-Based Methodologies for state estimation

Adaptive filter-based methodologies are a class of state estimation techniques that utilize adaptive algorithms to continuously update the battery model parameters and improve the accuracy of state estimation [41]. These methods are particularly useful in scenarios where

the battery's characteristics change over time, such as variations in capacity, internal resistance, or other electrochemical parameters.

Recursive Least Squares

One popular adaptive filter-based method is the Recursive Least Squares (RLS) algorithm [41]. The RLS algorithm is an iterative method that estimates the battery model parameters by minimizing the least-squares error between the predicted and measured battery outputs. By adaptively updating the model parameters, the RLS algorithm can account for changes in the battery's behavior and improve the accuracy of state estimation. The RLS algorithm uses a forgetting factor to control the impact of past measurements on the current estimate, allowing it to prioritize recent data while still retaining some memory of previous observations. The advantage of the RLS algorithm is its ability to track time-varying parameters and provide accurate state estimates in dynamic battery systems. Some literature that use RLS in predicting battery states include [114–120]. However, use of RLS identification in a real-time environment raises problems such as the speed of parameter convergence, covariance matrix 'blow up', and biased identification [121].

Kalman filter-based

Kalman filter-based techniques are widely used in lithium-ion battery modeling for state estimation and prediction tasks. The Kalman filter is an optimal recursive estimator that combines measurements and a dynamic system model to estimate the true state of a system. In the context of lithium-ion battery modeling, various Kalman filter-based techniques are employed, including the Extended Kalman Filter (EKF), Unscented Kalman Filter (UKF), and Particle Filter (PF).

The Extended Kalman Filter is commonly used to estimate the state of a nonlinear battery system by linearizing the system dynamics and applying the Kalman filter equations [42, 122–126]. It provides accurate state estimation but relies on the assumption of Gaussian noise and linearity of the system dynamics [43].

The Unscented Kalman Filter, on the other hand, addresses the limitations of the EKF by employing a deterministic sampling technique known as the unscented transformation

[127–130]. It captures the nonlinearities of the battery system more accurately and is more robust to non-Gaussian noise.

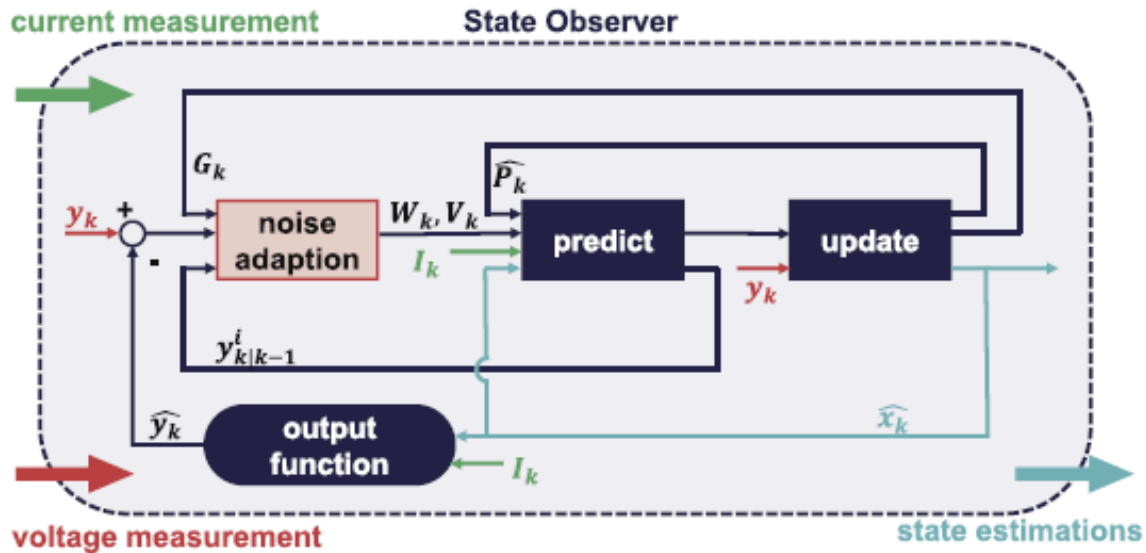


Figure 2.11: Illustration of the state observer based on Adaptive UKF algorithm [12].

Particle Filters are another class of Kalman filter-based techniques that utilize Monte Carlo sampling methods. They represent the probability density function of the battery state using a set of particles, allowing for more flexible and accurate state estimation in nonlinear and non-Gaussian systems [44]. Particle Filters are particularly useful when the battery behavior is highly nonlinear or when the system model is not precisely known.

Kalman filter-based techniques offer several advantages in lithium-ion battery modeling [41]. They provide state estimation that enables accurate tracking of battery dynamics and estimation of battery parameters such as SOC and SOH [131, 132]. These techniques can handle noisy measurements, accommodate nonlinear system dynamics, and provide real-time state estimation, making them suitable for online battery management and control [44].

However, Kalman filter-based techniques also have limitations [41]. They rely on accurate system models and assumptions about noise characteristics, which may not always hold in practical scenarios. Nonlinearities, parameter uncertainties, and model mismatches can lead to suboptimal performance. They also have some convergence issues with the covariance matrices. Additionally, computational complexity can be a concern, particularly with high-

dimensional state spaces or large numbers of particles in Particle Filters [41].

In summary, Kalman filter-based techniques, including the EKF, UKF, and Particle Filters, are valuable tools in lithium-ion battery modeling for state estimation and prediction tasks. They offer accurate and real-time estimation of battery states and parameters. However, consideration should be given to system nonlinearities, noise characteristics, and computational requirements when applying these techniques in practical battery modeling applications.

Adaptive Filter-Based Methodologies, while offering certain advantages, present several challenges in their use for the objectives of this PhD. These methods often demand extensive data-driven adaptations which is challenging when working with the limited and evolving sensor data from the ongoing INSTABAT project. Also, the inherent parameter adaptation characteristic of many adaptive filter-based approaches is not well-suited to this research, as the battery model parameters are expected to undergo changes throughout the PhD. Additionally, the transparency and interpretability limitations of some filter-based techniques can impede their ability to effectively capture the intricate inhomogeneous Li exchange profiles within the battery, which is a key focus of this research.

2.2.3 Adaptive AI-Based Methodologies

State estimation in LiBs is a challenging task due to the complex and nonlinear nature of battery behavior. Adaptive AI-based methodologies have emerged as effective approaches for addressing these challenges and improving the accuracy of state estimation [11, 41]. This subsection explores several adaptive AI-based methodologies, including Particle Swarm Optimization (PSO), Genetic Algorithm (GA) based estimation, Fuzzy-based Neural Networks (FNN), Artificial Neural Networks (ANN), and Fuzzy Logic-based estimation. These methodologies leverage the adaptive capabilities of AI algorithms to enhance the estimation accuracy in LiBs.

Particle Swarm Optimization

Particle Swarm Optimization (PSO) is a population-based optimization algorithm inspired by the social behavior of bird flocking or fish schooling. In PSO, a population of particles moves through the search space, searching for the optimal or near-optimal solution. Each particle adjusts its position and velocity based on its own experience and the best experience of the swarm. PSO has been applied to battery state estimation to optimize battery model parameters and improve the accuracy of state estimation [13, 45, 133, 134]. By adapting the model parameters, PSO can enhance the estimation accuracy, leading to better SOH and SOH estimation in LiBs [135]. The flow diagram of PSO is shown in Figure 2.12.

Advantages of PSO include its ability to handle high-dimensional optimization problems and its simplicity in implementation. It can effectively explore the parameter space and converge to near-optimal solutions. However, PSO may suffer from premature convergence or getting stuck in local optima if not properly tuned. It also requires defining appropriate fitness functions and parameter settings.

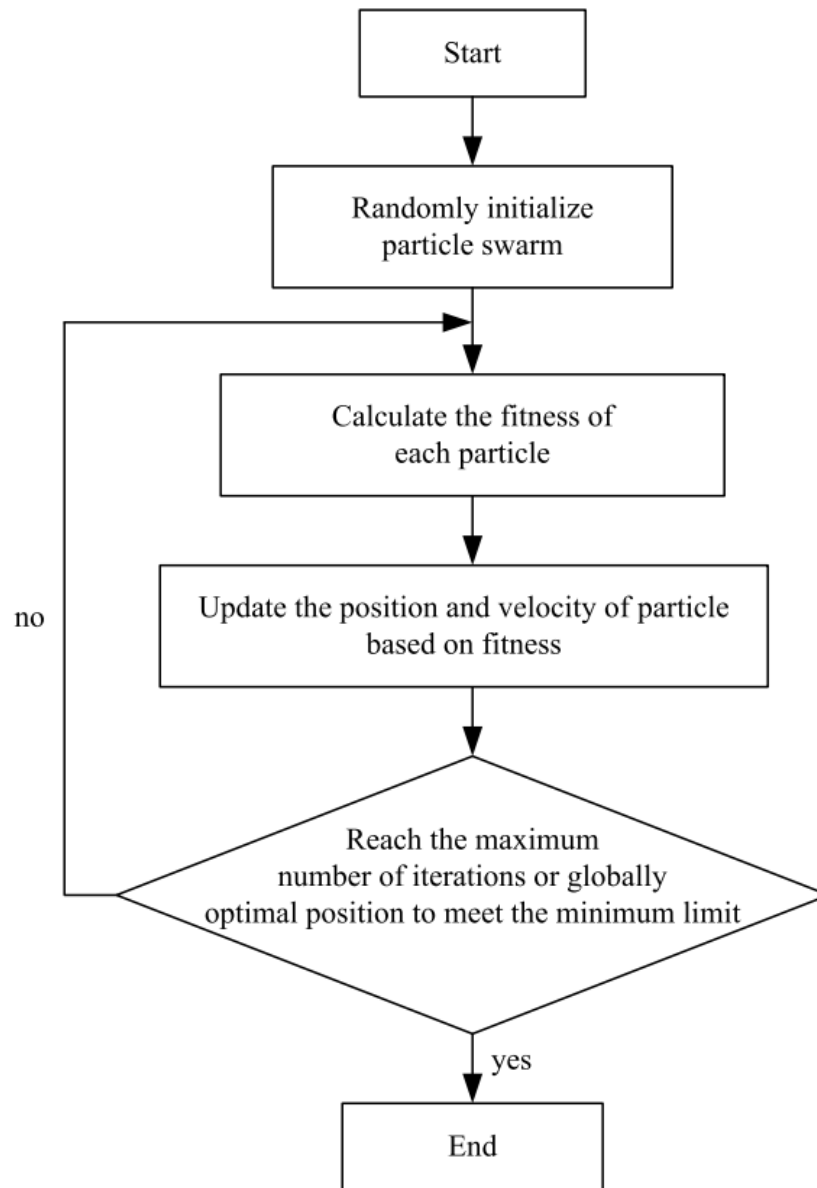


Figure 2.12: The flow diagram of PSO from [13]

Genetic Algorithm based Estimation

Genetic Algorithm (GA) is a search and optimization algorithm inspired by the process of natural selection. It mimics the biological evolution by using mechanisms such as selection, crossover, and mutation to iteratively generate new candidate solutions. GA-based estimation techniques have been employed to optimize battery model parameters and improve state estimation accuracy in LiBs [14,15]. By searching the parameter space, GA can find optimal or near-optimal values that minimize the estimation error. This adaptability improves the accuracy of SOC and SOH estimation in LiBs.

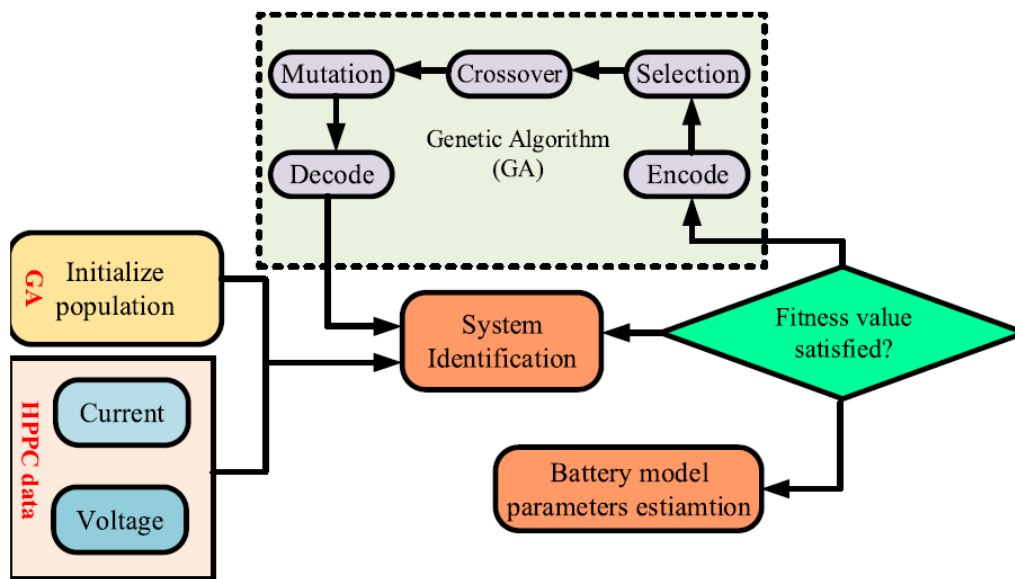


Figure 2.13: Battery model parameters determination using GA [14,15]

The advantages of GA-based estimation include its ability to handle nonlinear and non-convex optimization problems, its global search capabilities, and its ability to handle constraints. GA can explore a wide range of solutions and converge to better estimates. However, GA may require a large population size and a high number of generations to achieve accurate results, making it computationally intensive. It also requires careful selection of genetic operators and parameter settings to ensure effective exploration and exploitation of the search space.

Fuzzy-based Neural Networks

Fuzzy-based Neural Networks (FNN) combine fuzzy logic principles with neural networks to handle the uncertainties and imprecisions inherent in LiB modeling and estimation [41, 136]. Fuzzy logic provides a systematic way to model and reason about imprecise or uncertain information, while neural networks can learn complex relationships between input and state variables. FNN has been applied to LiB state estimation, capturing the nonlinear relationships and adaptively updating the estimation models [41, 137]. Figure 2.14 shows the structure of Neural Networks used in predicting the SOC of a battery.

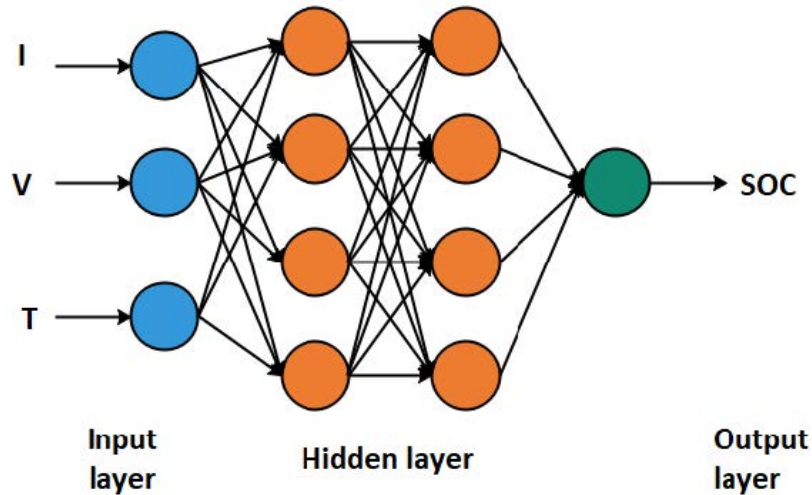


Figure 2.14: Predicting SOC using Neural Networks [16]

The advantages of FNN include their ability to handle nonlinearities, uncertainties, and imprecise information. FNN can effectively capture complex relationships and adapt to varying operating conditions in LiBs [41]. It provides robust estimation results and can handle imprecise input data. However, FNN may require a significant amount of training data to ensure accurate estimation results. The training process for neural networks can also be computationally intensive, requiring appropriate network architectures and training algorithms [11].

Artificial Neural Networks

Artificial Neural Networks (ANN) have been widely used in various fields, including battery state estimation. ANN is a computational model inspired by the structure and function of the human brain. It consists of interconnected nodes (neurons) organized in layers, allowing the network to learn from input-output data and generalize to unseen data. ANN-based estimation techniques have been applied to LiBs, capturing the complex relationships between input variables and battery states [138]. Figure 2.14 shows the structure of Neural Networks used in predicting the SOC of a battery.

The advantages of ANN include their ability to learn from large amounts of data, their capability to handle nonlinear and complex relationships, and their adaptability to varying operating conditions [41]. ANN can effectively capture the dynamic behavior of LiBs and provide accurate state estimation. However, ANN models may lack interpretability, as they are considered black-box models. The training process for ANN can also be computationally demanding, requiring careful selection of network architectures, training algorithms, and hyperparameters [138].

In summary, adaptive AI-based methodologies, including PSO, GA-based estimation, FNN, and ANN, offer promising approaches for state estimation in LiBs. These methodologies leverage the adaptive capabilities of AI algorithms to handle the complexities and uncertainties associated with LiB behavior. They can capture the nonlinear relationships, adapt to varying operating conditions, and provide accurate SOC and SOH estimation. However, considerations should be given to data availability, computational resources, interpretability, and parameter tuning when applying these methodologies in practical LiB applications.

While Adaptive AI-based methodologies offer potential advantages, they are not ideal for this PhD's objectives. These methods rely on data-intensive training, which becomes impractical given the limited availability of sensor data from the evolving INSTABAT project. Also, many of these AI-based approaches necessitate parameter tuning for optimal performance, but the ever-changing nature of the battery model parameters throughout the course of this PhD renders them unfeasible. Additionally, the lack of interpretability in ANN mod-

els conflicts with the goal of accurately capturing inhomogeneous Li exchange profiles within the battery.

2.2.4 Model-Based Methodologies for state estimation

Model-based methodologies for state estimation in LiBs utilize mathematical models that describe the electrochemical and electrical behavior of batteries. These methodologies include ECMs and EChMs. By incorporating detailed physics-based models, model-based methodologies aim to provide accurate and interpretable state estimation in LiBs.

Electrical Circuit Models

ECMs are widely used for battery state estimation due to their simplicity and computational efficiency. ECMs represent the LiB as an equivalent circuit, where the electrical components of the circuit correspond to different electrochemical processes and phenomena occurring within the battery. These models relate the terminal voltage of the battery to its internal states, such as SOC and SOH [33,34].

One example of an ECM commonly used for LiB state estimation is the Thevenin model [1,2]. The Thevenin model represents the battery as an ideal voltage source in series with an internal resistance. The voltage source represents the OCV of the battery, which is a function of the SOC. The internal resistance accounts for the voltage drop across the battery due to its internal resistance and polarization effects.

Advantages of ECMs include their simplicity, fast computation, and ease of implementation [33]. They provide a good trade-off between accuracy and computational complexity, making them suitable for real-time applications. ECMs are widely used in practical LiB applications, such as electric vehicles and portable electronics, where real-time estimation is crucial for battery management and control [34].

In electric vehicle applications, ECMs can be used to estimate the SOC and SOH of the battery in real-time. By measuring the terminal voltage and using the ECM, the SOC can be estimated based on the relationship between the terminal voltage and the battery's OCV [33]. The SOH estimation can also be performed by monitoring the internal resistance

of the battery, which can indicate the degradation or aging of the battery [60].

However, ECMs have limitations in capturing the complex electrochemical processes occurring inside the battery. They provide limited information about the internal behavior of the battery, making them less suitable for applications that require detailed insights into the electrochemical phenomena [33]. The accuracy of ECMs may also be affected by variations in temperature, current rate, and aging effects, as these models do not explicitly consider these factors. Despite these limitations, ECMs remain a practical and efficient choice for battery state estimation in many applications [34].

In summary, ECMs offer a simple and computationally efficient approach for LiB state estimation. They are widely used in practical applications and provide a good trade-off between accuracy and computational complexity. While ECMs may lack the detailed insights provided by more complex models, they are suitable for real-time estimation and can be effectively employed for SOC and SOH estimation in LiBs.

This PhD aims to formulate a battery model that captures inhomogeneous Li exchange profiles and incorporates physical dependencies, such as temperature dependence and plating mechanisms. ECMs, with their simplified equivalent circuit representations, cannot adequately account for these complex electrochemical processes and dependencies on a spatial level inside the battery, limiting their ability to provide detailed insights into the battery's behavior.

Electrochemical Models

EChMs, including the DFN model, are complex systems composed of interconnected PDEs and algebraic equations. The PDEs primarily depict transport phenomena within the cell, such as diffusion and advection, while the algebraic equations represent relative potentials and reaction rates driven by these potentials. This intricate combination presents a challenging problem for observer design [46].

Recent efforts have focused on reducing DFN-like models to create manageable observation problems. Some studies have directly addressed the observation problem of a discretized version of the DFN model [139], but the resulting algorithms are often difficult to tune, and their convergence frequently depends on the selection of non-trivial parameters.

Numerous studies have centered around a specific reduced, yet still infinite-dimensional, model known as the SPM [140–155]. This model and its variants primarily overlook the electrolyte behavior in the cell and concentrate on solid diffusion in the electrodes. However, for fast-charging applications, the fidelity of the SPM and similar reductions are limited due to high electrolyte polarization and potential lithium depletion.

To enhance accuracy at high C rates, more advanced extensions of the SPM model have been developed [156–163]. Based on these extended models, a first batch of observer designs has been proposed [159, 160, 164–168]. However, these approaches often lack convergence and stability guarantees, lose spatially distributed information, or do not ensure lithium conservation due to the model reduction methods employed or the feedback designs.

A significant approach to achieving provably stable estimation algorithms for extended SPM models was presented in a study where a Single-Particle Model with electrolyte dynamics (SPMe) was developed [21]. This model was used to extend a previous observer design [143] while maintaining convergent error estimates. Importantly, the reduced model retains the fundamental electrochemical sense of the variables and the infinite-dimensional (i.e., PDE) structure of the DFN model. The use of a PDE model allows for the physical significance of equations and feedback laws to be retained independently of the discretization method used for the algorithm implementation. This decouples the problem of observer design from that of optimizing the model reduction for practical implementation.

However, EChMs are computationally expensive and require detailed knowledge of material properties, kinetic parameters, and other battery-specific parameters [55]. Obtaining accurate parameter values for EChMs can be challenging, as these parameters can vary with operating conditions and battery aging [56]. Additionally, EChMs often require complex numerical methods, such as finite element methods or finite difference methods, for solving the coupled partial differential equations, which adds to the computational complexity [57, 58].

Despite these challenges, EChMs are valuable tools for research and development in LiB technology [59]. They provide a detailed understanding of battery behavior and can be used for optimizing battery performance, design, and control strategies [55, 56]. However, their high computational requirements and parameter sensitivity make them less suitable for real-time applications compared to simpler models like equivalent circuit models [55–57].

For the objectives of this PhD, EChMs emerge as the most suitable choice. They excel in capturing intricate electrochemical phenomena occurring within the battery, offering a detailed understanding of internal states and behaviors critical for formulating a battery model with inhomogeneous Li exchange profiles and incorporating physical dependencies. EChMs accurately simulate complex processes, including lithium-ion diffusion and interfacial reactions, which are fundamental for comprehending battery performance and degradation. Importantly, EChMs can retain the electrochemical sense of variables and the infinite-dimensional structure of the DFN model, allowing for the development of provably stable estimation algorithms. This unique advantage decouples observer design from model reduction challenges encountered during practical implementation, aligning perfectly with the research goals. While EChMs are computationally demanding and require precise parameterization, their ability to provide in-depth insights into battery behavior makes them indispensable for achieving the objectives of this PhD research.

2.2.5 Hybrid estimation techniques for state estimation

Accurate SOC and SOH estimation of LiBs is pivotal for optimal EV performance. Hybrid state estimation methods, combining model-based and machine-learning approaches, offer a promising solution to address the limitations of each individual method. We perform a review of some of these methods in the existing literature.

The PSO algorithm has been frequently employed with model-based methods for SOC estimation of LiBs [47]. Key parameters of the ECM, such as voltage, capacity, resistance, and temperature, are optimized using PSO as a search algorithm [169, 170]. PSO was also used to search for optimal SVM parameters for SOC estimation [171]. A NN algorithm-based SOC estimation model was developed for LiB batteries used in EV application with the PSO algorithm used to search for the best values of network parameters [172].

GA has been effectively used for optimizing the ECM model parameters for precise SOC estimation [48], for OCV methods [173], and in combination with the coulomb counting method [174]. Further applications of GA with Fuzzy NN methods have demonstrated satisfactory SOC tracking precision and superior performance [175, 176].

An increasing interest exists in hybrid physics-ML modeling for LiBs, combining the

benefits of both approaches. One study [45] integrates a one-dimensional electrochemical model with various types of NNs. Another study [46] employs recurrent NNs to learn the differences between LiB terminal voltage and SPM output voltage. Additionally, in [47], an NN is combined with a simplified SPM and lumped thermal model to predict terminal voltage. Recently, [49] expands ML to conduct aging-aware hybrid modeling with EChM models, leading to the design of a hybrid model conscious of the SOH.

Hybrid state estimation techniques hold immense promise in achieving the goal of accurate state estimation for LiBs. Nevertheless, they also bring forth significant challenges, encompassing complexities, data dependencies, and computational resource demands. In the context of this PhD research, we have made the decision to use of EChMs in developing both the model and observer. This decision is grounded in the practical constraints of available sensor data. While acknowledging the potential of hybrid techniques, we view them as a promising perspective once we have access to complete experimental results from these novel sensors.

2.3 Lithium Ion Battery Degradation

2.3.1 Degradation Mechanisms of Lithium-Ion Batteries

Lithium-ion batteries (LiBs) have transitioned from their nascent applications in consumer electronics to more demanding roles in transport and large-scale energy storage systems. As their prominence in these sectors grows, a comprehensive understanding of the underlying degradation mechanisms becomes paramount. This review delves into these mechanisms, elucidating the intricate relationships between various degradation processes and their observable outcomes.

Degradation in LiBs is multifaceted and can be systematically classified into three distinct levels [177]:

1. **Mechanisms:** These refer to the actual physical and chemical transformations taking place within the battery [178]. They are the foundational causes of degradation and often remain elusive to direct observation during battery operation [179].

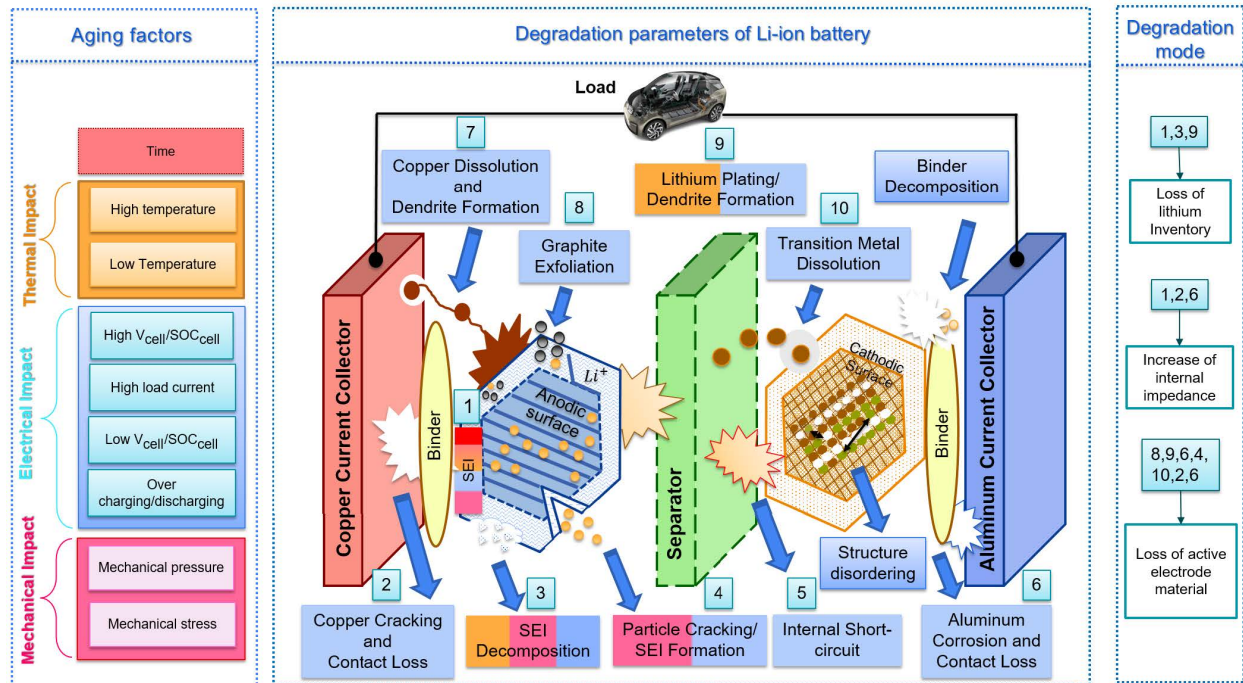


Figure 2.15: Representation of Li-ion battery aging factors and their associated degradation effects, modified version from [17].

2. **Modes:** Representing a mid-level perspective, modes encapsulate the observable consequences at the cell level that arise due to the underlying mechanisms [180]. They offer a more tangible insight into the degradation process [181,182].
3. **Operational Effects:** At the highest level, operational effects, such as capacity or power fade, manifest as the direct outcomes of the degradation modes [183]. These effects are readily measurable and are often the primary indicators of battery health [184].

The degradation process is structured into these three levels for clarity and systematic understanding. Within the realm of mechanisms, five primary and thirteen secondary processes have been identified that contribute to degradation during standard operation. These mechanisms culminate in five discernible modes [177].

Primary Degradation Mechanisms and Their Implications

The primary mechanisms play a pivotal role in shaping battery performance. Let's delve into some of the prominent lithium degradation mechanisms, offering insights into their consequences and adverse impacts on battery operation.

Key Degradation Mechanisms

- 1. Solid-Electrolyte Interphase (SEI) Growth:** The SEI is a crucial passivation layer that forms on most negative electrode (NE) surfaces when the liquid electrolyte interacts with the electron-conductive surface of the NE, especially when operating at voltages below the electrochemical stability window of the electrolyte [185]. This layer initially forms during the first cycle, leading to a capacity reduction. As the cell ages, the SEI layer thickens, predominantly on graphite NEs, due to various reasons such as diffusion of solvent molecules through the existing SEI, exposure of new electrode surfaces from cracking, and deposition of side reaction products [177]. The growth of the SEI layer can be influenced by factors like high temperatures and high currents [186]. The SEI layer, while serving as a protective barrier, also consumes the electrolyte solvent, leading to reduced conductivity and increased impedance in cells. SEI formation can be seen as illustrated in Figure 2.16 from [18].
- 2. Lithium Plating:** Lithium plating is a side reaction where metallic lithium forms on the NE surface instead of intercalating into it [187]. This phenomenon can be triggered by various factors including low temperatures, high state of charge (SOC), high charge currents, and insufficient NE mass. The plated lithium can undergo further side reactions with the electrolyte, leading to SEI growth. Over time, this can result in the formation of "dead lithium" that cannot be recovered, leading to loss of lithium inventory and increased impedance. Lithium plating is observable on the physical battery as seen in Figure 2.17 from [19].
- 3. Positive Electrode Structural Change and Decomposition:** The degradation of the positive electrode (PE) is highly dependent on its chemistry [188]. For layered oxides like NMC ($\text{LiNi}_x\text{Mn}_y\text{Co}_z\text{O}_2$), the main degradation mechanisms include

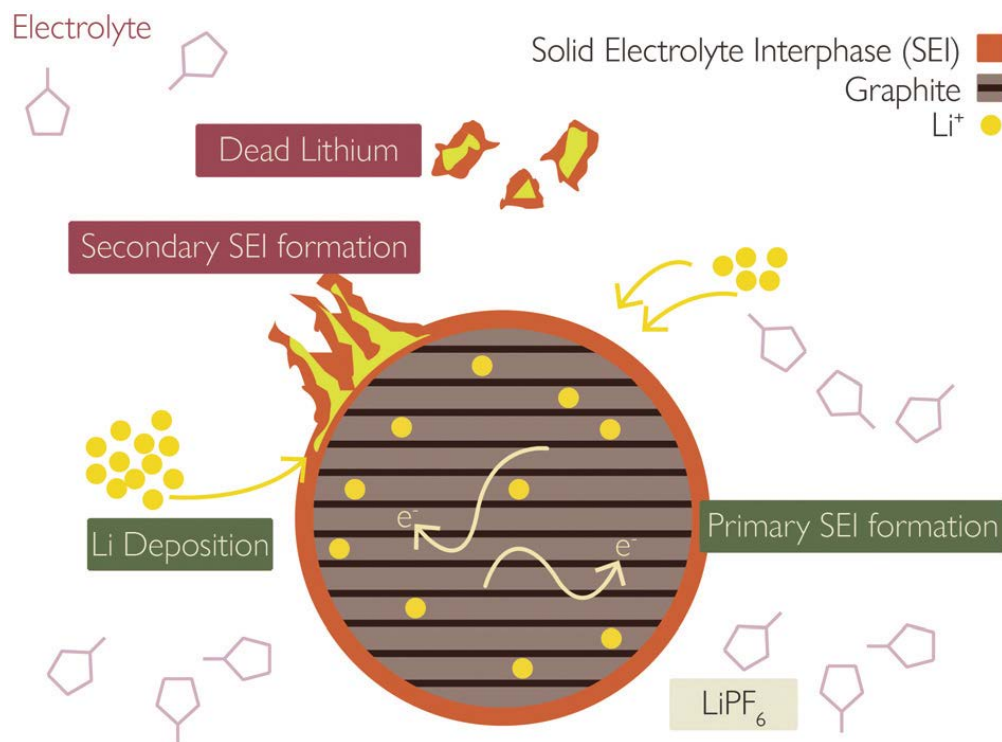


Figure 2.16: SEI formation in LiBs from [18]

phase change, oxidation of lattice oxygen, electrolyte decomposition, and TM/Li⁺ site exchange. These processes can lead to the release of lattice oxygen, formation of gaseous products, and electrolyte decomposition. The similar ionic radii of Li⁺ and Ni²⁺ can also lead to site switching in the PE crystal lattice, affecting the diffusion of Li [189, 190].

Interplay Between Degradation Mechanisms

The degradation mechanisms in LiBs are not isolated events. They often interact, leading to a cascade of effects [177]. For example, lithium plating can induce further SEI growth, consuming more electrolyte in the process. Similarly, the dissolution of transition metals from the positive electrode can accelerate SEI formation on the NE [19, 191–193].

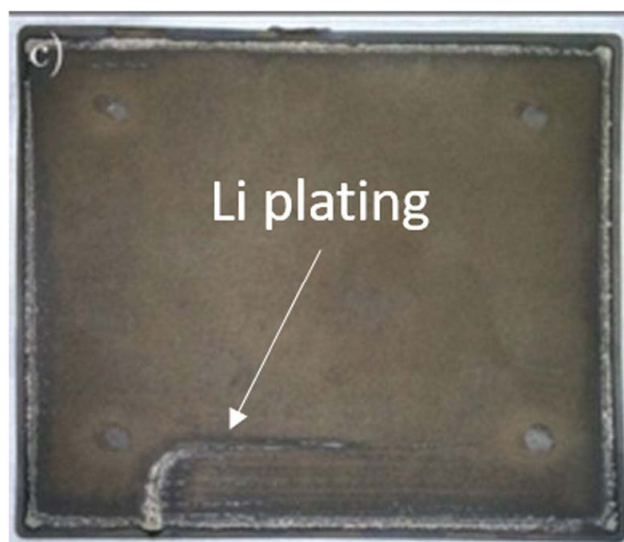


Figure 2.17: Lithium plating in LiBs from [19]

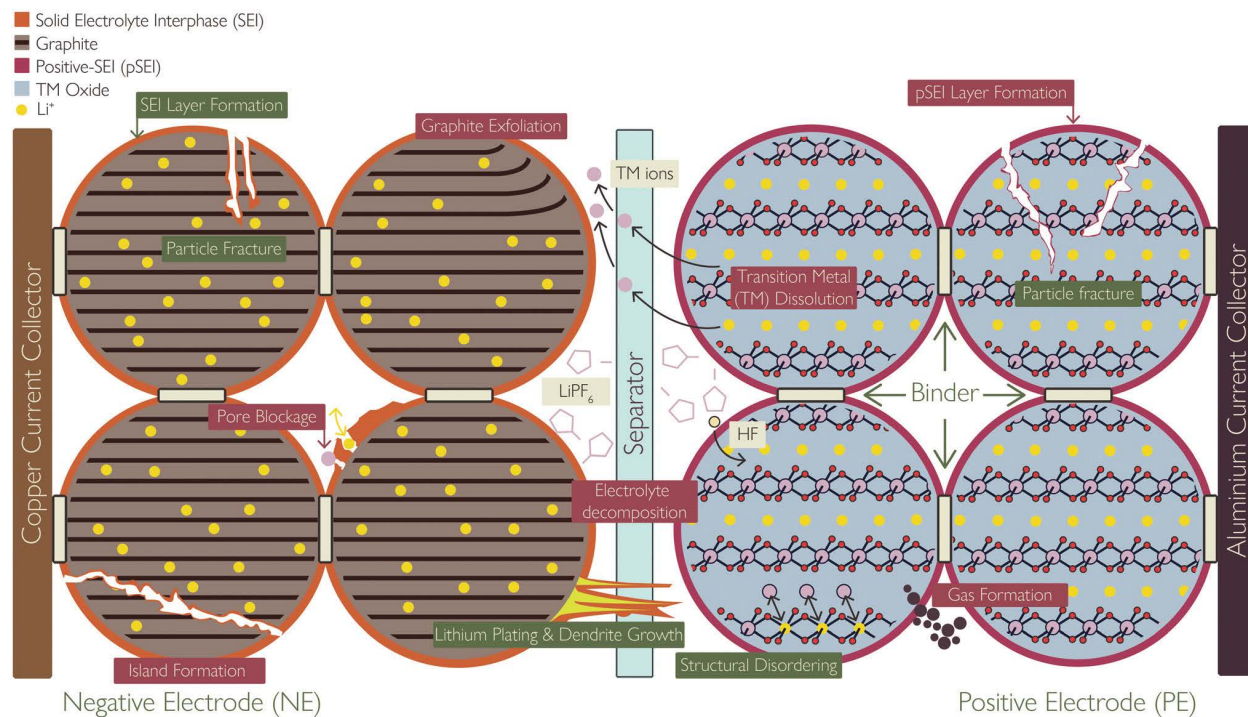


Figure 2.18: Schematic showing the basic components of a lithium ion battery cell and the location and consequences of the degradation mechanisms covered in this review, with primary mechanisms labelled in green and secondary mechanisms labelled in dark red [20].

2.3.2 Operational Implications of Lithium Degradation

From an operational standpoint, the culmination of these mechanisms and modes manifests as capacity and power fade [177]. Capacity fade refers to the reduction in the usable capacity of the battery, while power fade denotes a decrease in the deliverable power post-degradation [194,195]. These operational effects are the primary metrics used in assessing battery health and predicting end-of-life scenarios [177].

Observable Consequences (Modes)

The degradation mechanisms lead to observable modes, which include [177]:

1. **Loss of Active Material (LAM):** Active mass of the negative electrode that is no longer available for the insertion of lithium due to particle cracking and loss of electrical contact or blocking of active sites by resistive surface layers. Similarly, the active mass of the positive that is no longer available for the insertion of lithium due to structural disordering, particle cracking, or loss of electrical contact. [177,196–200].
2. **Loss of Lithium Inventory (LLI):** Lithium ions that are consumed by parasitic reactions, such as surface film formation (e.g. SEI growth), decomposition reactions, and lithium plating, and are no longer available for cycling between the positive and negative electrode, leading to capacity fade [196].
3. **Stoichiometric Drift:** Associated with LLI, this mode refers to the imbalance between the electrodes in terms of their lithium content, which can affect the overall performance and efficiency of the battery [201].
4. **Impedance Change:** This mode groups mechanisms that affect the kinetic behavior of the cell, leading to increased resistance [202]. Factors like SEI growth, pore blockage, and loss of electrolyte can contribute to this mode [203].

Operational Effects

The culmination of degradation mechanisms and modes results in operational effects, the most prominent being:

-
1. **Capacity Fade:** This refers to a reduction in the usable capacity of the cell, which can be due to loss of active material, loss of lithium inventory, or other degradation mechanisms that reduce the cell's ability to store energy [194].
 2. **Power Fade:** A reduction in the deliverable power of the cell post-degradation, often linked to increased impedance and reduced efficiency of the cell [195, 204].

In conclusion, understanding the intricate web of degradation mechanisms, modes, and their operational implications is crucial for enhancing the longevity and reliability of LiBs, especially as they find applications in more demanding sectors. In this PhD, we will concentrate our efforts on integrating lithium plating into our proposed models and BMS algorithms, aligning with the available electrochemical data and adhering to the stringent timelines set by the INSTABAT project.

2.4 Conclusion of the Chapter

This chapter embarked on an exploration of battery modeling, state estimation methodologies, and degradation mechanisms in lithium-ion batteries (LiBs), laying a robust foundation for the subsequent research endeavors in this PhD thesis.

Initially, battery modeling was discussed, emphasizing the significance of capturing inhomogeneous Li exchange profiles and incorporating physical dependencies like temperature and plating mechanisms. State estimation methodologies like Adaptive Filter-based techniques, which despite their adaptability and robustness, are constrained by their dependency on accurate initial parameter values and their susceptibility to inaccuracies amidst system nonlinearities [3, 11, 71]. Adaptive AI-based methodologies, while potent in managing complex, nonlinear systems and possessing the capability to learn and adapt from data, are deemed suboptimal due to their intensive data requirements, challenges in parameter tuning, and a lack of interpretability, especially in the context of the evolving INSTABAT project [41, 205].

We then moved towards Model-Based Methodologies, with a focus on Electrical Circuit Models (ECMs) and Electrochemical Models (EChMs). ECMs, despite their computational

efficiency and widespread application in practical scenarios, were found to be limited in capturing complex electrochemical processes and dependencies within the battery, thus restricting their capability to provide detailed insights into the battery's internal behavior [33, 34]. EChMs, on the other hand, emerged as the methodology of choice for this research, owing to their unparalleled ability to capture intricate electrochemical phenomena and provide a detailed understanding of internal states and behaviors, which are pivotal for formulating a battery model that encapsulates inhomogeneous Li exchange profiles and incorporates physical dependencies [55–59].

Hybrid methodologies, which amalgamate model-based and machine-learning approaches, were acknowledged for their potential to address the limitations of individual methods by optimizing key parameters and enhancing SOC estimation. However, due to the complexities, data dependencies, and computational resource demands they introduce, and considering the practical constraints of available sensor data in this research, their application is viewed as a promising future perspective [47, 48, 169–176].

The latter part of the chapter delved into the degradation mechanisms of LiBs, providing a systematic understanding of the degradation process, from mechanisms to modes and their operational effects, such as capacity and power fade [177, 194, 195]. The degradation mechanisms, including pivotal ones like Solid-Electrolyte Interphase (SEI) Growth and Lithium Plating, were elucidated, offering insights into their consequences and adverse impacts on battery operation [19, 185, 187]. Within the strict INSTABAT project timeline, this PhD research prioritizes integrating lithium plating into proposed models and BMS algorithms.

In conclusion, the detailed exploration and critical analysis of various state estimation methodologies and degradation mechanisms have informed the decision to utilize EChMs for developing both the model and observer in this PhD research. The subsequent chapters will delve deeper into the development of the proposed model and observer, guided by the foundational knowledge established in this chapter, and will explore the implications of the developed models in the context of LiBs.

Chapter 3

Development and Analysis of the Multi-Particle Model with Electrolyte Dynamics

Contents

| | | |
|------------|--|------------|
| 3.1 | Doyle-Fuller-Newman Model | 88 |
| 3.2 | Single Particle Model with Electrolyte Dynamics (SPMe) . . . | 92 |
| 3.3 | Derivation of the Multi-Particle Model with Electrolyte Dynamics (MPMe) | 94 |
| 3.4 | Simulation of the MPMe | 100 |
| 3.4.1 | Validation of the Model | 100 |
| 3.4.2 | Spatial Heterogeneity of Internal States | 104 |
| 3.4.3 | Lithium Conservation in the System | 108 |
| 3.4.4 | Simulation Analysis: Effects of Incorrect Lithium Amounts | 110 |
| | Deviation in Lithium Content within the Electrolyte Phase | 110 |
| | Deviation in Lithium Content within the Solid Phase | 110 |
| 3.5 | Integration of Temperature dependence in the Battery model parameters | 111 |
| 3.5.1 | Single Particle Model with Electrolyte and Thermal Dynamics . . | 111 |
| 3.5.2 | Thermal dependence of parameters | 112 |
| 3.5.3 | Effect of Temperature on battery behaviour | 113 |
| 3.6 | Conclusion of the Chapter | 116 |

Summary of the Chapter

This chapter delves into the intricacies of lithium-ion battery modeling, emphasizing the need for a more accurate representation of the battery's internal dynamics. The Doyle Fuller Newman (DFN) model, while comprehensive, is computationally intensive, making it unsuitable for real-time applications. This chapter introduces the Multi-Particle Model with Electrolyte dynamics (MPMe) as a solution that bridges the gap between the DFN and the Single Particle Model with Electrolyte (SPMe).

Derivation of the Model: The MPMe aims to:

- Reconstruct the heterogeneities present in internal battery dynamics.
- Offer computational efficiency for real-time applications.
- Facilitate the integration of new sensor data for observer designs.
- Incorporate spatial temperature dependence for various electrochemical parameters.
- Ensure lithium conservation in both battery phases.
- Integrate a lithium degradation model for the negative electrode.

The MPMe uses a multi-particle representation, formulating layers within the battery's positive, negative, and separator regions. Each layer in the negative and positive sides has one particle, with each particle having radial layers.

Simulation of the MPMe: The MPMe's validation is conducted through MATLAB simulations, comparing it with the full-scale DFN model and the SPM. The MPMe model's results, especially in voltage behavior, demonstrate its higher accuracy compared to the SPM.

Spatial Heterogeneity of Internal States: The MPMe model captures the battery's internal states, including lithium concentration within the electrodes and electrolyte, electric potential across both phases, overpotential, and other crucial factors. The model showcases the heterogeneity present in these states, especially under different charging scenarios.

Lithium Conservation in the System: The MPMe model ensures the conservation of lithium, a crucial aspect for accurate long-term simulations. The conservation can be seen in both the solid and electrolyte phases of the battery.

Integration of Temperature Dependence in the Battery Model: The chapter introduces the Single Particle Model with Electrolyte and Thermal Dynamics (SPMeT) that considers temperature variations across the Li-ion battery. The SPMeT model combines the SPMe model with a thermal model, using the Arrhenius law for temperature-dependent parameters. The chapter further utilises the principle of the SPMeT in the MPMe framework, demonstrating the significant impact of temperature dependence on battery behavior.

In conclusion, Chapter 3 presents the MPMe as a robust and efficient model for capturing the internal dynamics of lithium-ion batteries, bridging the gap between the detailed DFN model and the simpler SPMe. The chapter underscores the importance of considering temperature variations and ensuring lithium conservation for accurate battery modeling and simulations.

3.1 Doyle-Fuller-Newman Model

In this chapter, we will focus on the development of an electrochemical PDE-based model that is derived from the full-scale (Doyle-Fuller-Newman) DFN model [50]. To do this, we start by providing a complete account of the DFN model.

The DFN model divides the cells into three regions: anode, separator, and cathode. It considers two phases in the Li-ion battery: the electrolyte with states evolving over the x dimension, and the solid with states evolving in the x as well as the r dimension [21]. Figure 3.1 shows the schematic of the DFN model during the charging of the battery.

The solid concentration $c_s^\pm(x, r, t)$ and electrolyte concentration $c_e^j(x, t)$ evolve over time t through the diffusion equations [21]:

$$\frac{\partial c_s^\pm(x, r, t)}{\partial t} = \frac{1}{r^2} \frac{\partial}{\partial r} \left[D_s^\pm r^2 \frac{\partial c_s^\pm}{\partial r} \right] \quad (3.1)$$

$$\epsilon_e^j \frac{\partial c_e^j(x, t)}{\partial t} = \frac{\partial}{\partial x} \left[D_e^{eff}(c_e^j) \frac{\partial c_e^j}{\partial x} + \frac{(1 - t_c^0)}{F} i_e^j(x, t) \right] \quad (3.2)$$

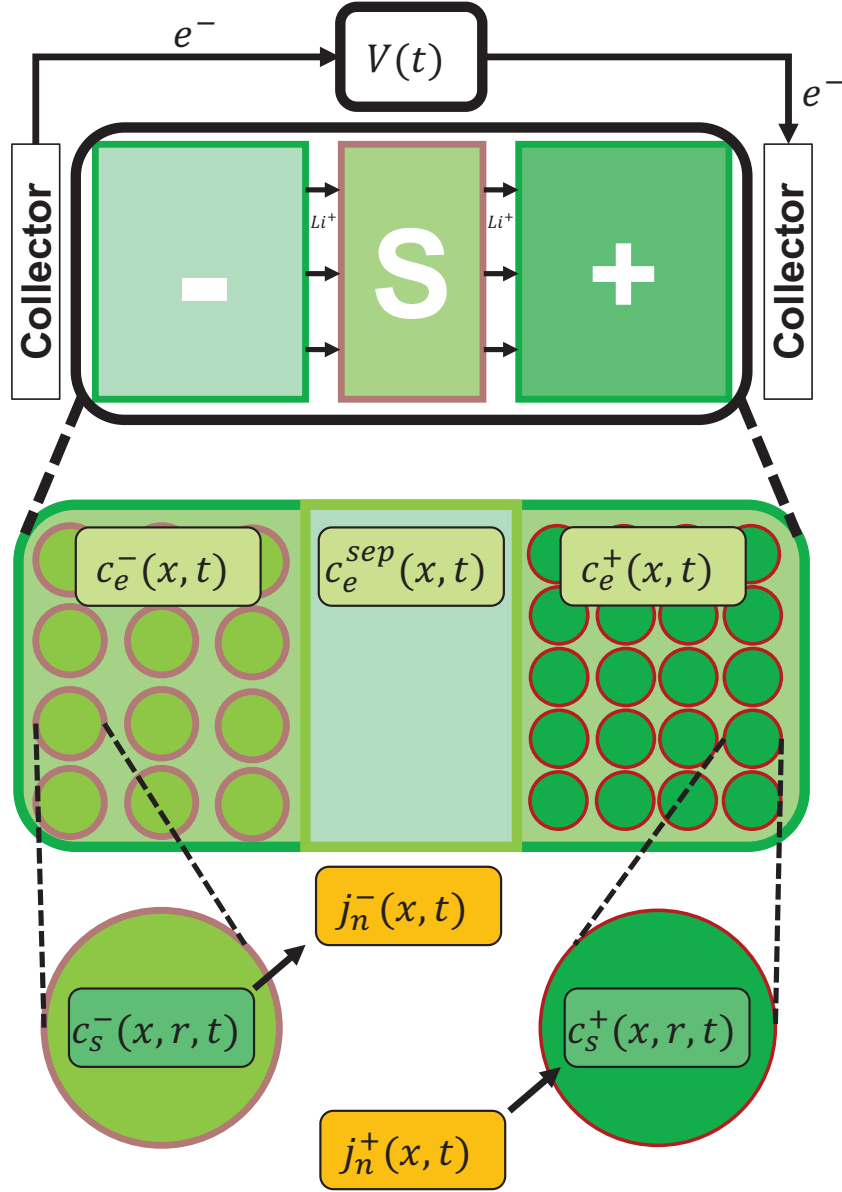


Figure 3.1: Schematic representation of the charging process of a Li-ion battery cell. At the top, are the three battery cell domains: negative electrode, separator, and positive electrode; in the middle part and at the bottom, the two phases: the electrolyte phase and the solid phase, respectively.

for $j \in \{-, sep, +\}$. These are dependent upon the electrolyte electric potential $\phi_e(x, t)$, solid electric potential $\phi_s^\pm(x, t)$, ionic current $i_e^\pm(x, t)$, and molar ionic fluxes $j_n^\pm(x, t)$ [50]:

$$\sigma^{eff, \pm} \frac{\partial \phi_s^\pm}{\partial x}(x, t) = i_e^\pm(x, t) - I(t) \quad (3.3)$$

$$\kappa^{eff} \frac{\partial \phi_e}{\partial x}(x, t) = -i_e^\pm(x, t) + \kappa^{eff}(c_e) \frac{2RT}{F} (1 - t_c^0) \left(1 + \frac{d \ln(f_{c/a})}{d \ln c_e} \right) \frac{\partial \ln c_e}{\partial x}(x, t) \quad (3.4)$$

$$\frac{\partial i_e^\pm}{\partial x}(x, t) = a^\pm F j_n^\pm(x, t) \quad (3.5)$$

$$j_n^\pm(x, t) = \frac{1}{F} i_0^\pm(x, t) \left[e^{\frac{\alpha_a F}{RT} \eta^\pm(x, t)} - e^{-\frac{\alpha_a F}{RT} \eta^\pm(x, t)} \right] \quad (3.6)$$

$$i_0^\pm(x, t) = k^\pm [c_{ss}^\pm(x, t)]^{\alpha_c} [c_e(x, t) (c_{s,max}^\pm - c_{ss}^\pm(x, t))]^{\alpha_a} \quad (3.7)$$

$$\eta^\pm(x, t) = \phi_s^\pm(x, t) - \phi_e(x, t) - U^\pm(c_{ss}^\pm(x, t)) - F R_f^\pm j_n^\pm(x, t) \quad (3.8)$$

$$c_{ss}^\pm(x, t) = c_s^\pm(x, R_s^\pm, t) \quad (3.9)$$

where $D_e^{eff} = D_e(c_e) \cdot (\epsilon_e^j)^{brug}$, $\sigma^{eff} = \sigma \cdot (\epsilon_s^j + \epsilon_f^j)^{brug}$, and $\kappa^{eff} = \kappa(c_e) \cdot (\epsilon_e^j)^{brug}$ are effective electrolyte diffusivity, effective solid conductivity, and effective electrolyte conductivity given by the Bruggeman relationship [21].

The solid-phase diffusion boundary conditions are:

$$\frac{\partial c_s^\pm}{\partial r}(x, 0, t) = 0 \quad (3.10)$$

$$\frac{\partial c_s^\pm}{\partial r}(x, R_s^\pm, t) = -\frac{1}{D_s^\pm} j_n^\pm(x, t) \quad (3.11)$$

Equation (3.10) shows that there is no lithium flux on average at the center of the solid particles since the model averages over angular variables while Equation (3.11) states that the solid-phase lithium flux at the surface of the particles is equal to the molar ionic flux j_n .

The electrolyte-phase diffusion boundary conditions are:

$$\frac{\partial c_e^-}{\partial x}(0^-, t) = \frac{\partial c_e^+}{\partial x}(0^+, t) = 0 \quad (3.12)$$

$$D_e^{-,eff}(c_e(L^-)) \frac{\partial c_e^-}{\partial x}(L^-, t) = D_e^{sep,eff}(c_e(0^{sep})) \frac{\partial c_e^{sep}}{\partial x}(0^{sep}, t) \quad (3.13)$$

$$D_e^{sep,eff}(c_e(L^{sep})) \frac{\partial c_e^{sep}}{\partial x}(L^{sep}, t) = D_e^{+,eff}(c_e(L^+)) \frac{\partial c_e^+}{\partial x}(L^+, t) \quad (3.14)$$

$$c_e(L^-, t) = c_e(0^{sep}, t) \quad (3.15)$$

$$c_e(L^{sep}, t) = c_e(L^+, t) \quad (3.16)$$

Equation (3.12) states that there is zero Lithium flux at both edges of the battery as Lithium

cannot flow out of it. Equations (3.13) and (3.14) state that between two regions of the battery, there is a Lithium flux continuity. Equations (3.15) and (3.16) state that there is a continuity in the value of the concentrations between different regions.

The boundary conditions for the electrolyte-phase potentials are:

$$\phi_e(0^-, t) = 0 \quad (3.17)$$

$$\phi_e(L^-, t) = \phi_e(0^{sep}, t) \quad (3.18)$$

$$\phi_e(L^{sep}, t) = \phi_e(L^+, t) \quad (3.19)$$

The ionic current boundary conditions are given by:

$$i_e^-(0^-, t) = i_e^+(0^+, t) = 0 \quad (3.20)$$

Note that $i_e(x, t) = I(t)$ for $x \in [0_{sep}, L^{sep}]$. The input to the model is the applied current density $I(t)[A/m^2]$ and the output voltage measured across the current collectors is given by

$$V(t) = \phi_s^+(0^+, t) - \phi_s^-(0^-, t) \quad (3.21)$$

More complete detail of the model is given in [50, 91, 206, 207]. The DFN model exhibits a mathematical structure comprising linear partial differential equations (PDEs), quasi-linear PDEs, ordinary differential equations (ODEs) in space, and nonlinear algebraic constraints. This intricate structure poses a significant challenge for model-based state estimation. Although solving the equations in their full form guarantees high accuracy and precision, it incurs substantial computational costs.

In an endeavor to alleviate the computational burden, researchers have devised simplified versions of the DFN model, such as the Single Particle Model (SPM) [208]. Subsequently, efforts were made to incorporate electrolyte dynamics into the simplified model, leading to the development of the Single Particle Model with Electrolyte dynamics (SPMe) [21].

3.2 Single Particle Model with Electrolyte Dynamics (SPMe)

We now detail the SPMe [21] which offers a simplified solution to the DFN model, enabled by the following assumptions:

1. The concentration of lithium in the solid phase of each electrode remains constant along the spatial coordinate x and uniformly across time. Mathematically, $c_s^\pm(x, r, t)$ and $j_n^\pm(x, t)$ are constant in the x -direction.
2. The exchange current density term $i_0^\pm(x, t)$ can be approximated as a constant over x and represented by its averaged value $\hat{i}_0^\pm(t)$.
3. The total moles of lithium in both the solid and electrolyte phases are conserved. Combining this assumption with the first one, j_n^\pm can be proportionally related to the input current $I(t)$.
4. The constants $\alpha_a = \alpha_c = \alpha$ are approximately equal, which holds true in most practical scenarios.

With the first assumption in conjunction with (3.5), we can express the molar ion flux as proportional to the input current:

$$\bar{j}_n^+ = \frac{I(t)}{F a^+ L^+}, \quad \bar{j}_n^- = \frac{I(t)}{F a^- L^-} \quad (3.22)$$

The ionic current $i_e(x, t)$ exhibits a trapezoidal shape as depicted in Figure 3.2 from [21].

Subsequently, we can derive the equations for solid-phase diffusion and electrolyte diffusion:

$$\frac{\partial c_s^\pm(r, t)}{\partial t} = \frac{1}{r^2} \frac{\partial}{\partial r} \left[D_s^\pm r^2 \frac{\partial c_s^\pm}{\partial r} \right] \quad (3.23)$$

$$\frac{\partial \bar{c}_s^\pm(0, t)}{\partial r} = 0, \quad \frac{\partial \bar{c}_s^\pm(R_s^\pm, t)}{\partial r} = \pm \frac{1}{D_s^\pm F a^\pm L^\pm} I(t) \quad (3.24)$$

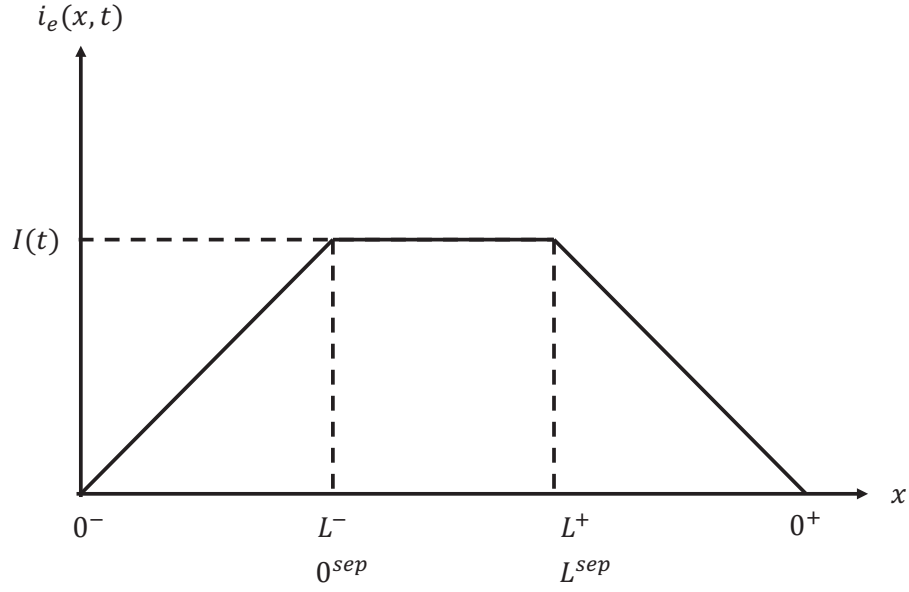


Figure 3.2: Simplified form of $i_e(x, t)$ in the SPMe model [21].

$$\frac{\partial c_e^-(x, t)}{\partial t} = \frac{\partial}{\partial x} \left[\frac{D_e^{eff}(c_e^-)}{\epsilon_e^-} \frac{\partial c_e^-}{\partial x} + \frac{(1 - t_c^0)}{\epsilon_e^- FL^-} I(t) \right] \quad (3.25)$$

$$\frac{\partial c_e^{sep}(x, t)}{\partial t} = \frac{\partial}{\partial x} \left[\frac{D_e^{eff}(c_e^{sep})}{\epsilon_e^{sep}} \frac{\partial c_e^{sep}}{\partial x} \right] \quad (3.26)$$

$$\frac{\partial c_e^+(x, t)}{\partial t} = \frac{\partial}{\partial x} \left[\frac{D_e^{eff}(c_e^+)}{\epsilon_e^+} \frac{\partial c_e^+}{\partial x} + \frac{(1 - t_c^0)}{\epsilon_e^+ FL^+} I(t) \right] \quad (3.27)$$

The simplified overpotential is determined using the Butler-Volmer equation [209], taking into account the aforementioned assumptions and substitutions [210]:

$$\bar{\eta}^\pm(t) = \frac{RT}{aF} \sinh^{-1} \left(\frac{\mp I(t)}{2a^\pm L^\pm \bar{i}_0^\pm(t)} \right) \quad (3.28)$$

The electrolyte potential is obtained by integrating across x across the entire cell, yielding the expression:

$$\begin{aligned} & \bar{\phi}_e^+(0^+, t) - \bar{\phi}_e^-(0^-, t) \\ &= \frac{L^+ + 2L^{sep} + L^-}{2\bar{\kappa}} I(t) + \frac{2RT}{F} (1 - t_c^0) k_f(t) [\ln c_e(0^+, t) - \ln c_e(0^-, t)]. \end{aligned} \quad (3.29)$$

By combining (3.22), (3.28), and (3.29), the expression for the output voltage can be derived:

$$\begin{aligned}
V(t) = & \frac{RT}{aF} \sinh^{-1} \left(\frac{-I(t)}{2a^+L^+i_0^+(t)} \right) \\
& - \frac{RT}{aF} \sinh^{-1} \left(\frac{I(t)}{2a^-L^-i_0^-(t)} \right) \\
& + U^+(\bar{c}_{ss}^+(t)) - U^-(\bar{c}_{ss}^-(t)) \\
& - \left(\frac{R_f^+}{a^+L^+} + \frac{R_f^-}{a^-L^-} \right) I(t) \\
& + \frac{L^+ + 2L^{sep} + L^-}{2\bar{\kappa}} I(t) \\
& + \frac{2RT}{F} (1 - t_c^0) k_f(t) [\ln c_e(0^+, t) - \ln c_e(0^-, t)] \\
V(t) = & h(\bar{c}_{ss}^+, \bar{c}_{ss}^-, c_e(0^+, t), c_e(0^-, t), I(t))
\end{aligned} \tag{3.30}$$

3.3 Derivation of the Multi-Particle Model with Electrolyte Dynamics (MPMe)

In this section, we present one of the main contributions of this PhD Thesis. In order to increase the fidelity of this model at higher C-rates, we set to develop a model with the following characteristics:

- Able to reconstruct the heterogeneities present in the internal battery dynamics.
- Simple and computationally cheap to run in real-time applications.
- Can easily cater to the implementation of new sensor data for observer designs.
- Incorporates Temperature dependence on a spatial level for different electrochemical parameters.
- Lithium conservation in both phases of the battery.
- Integrates a lithium degradation model for the negative electrode.

In the SPMe, the solid-phase dynamics are represented using a single particle in both, the cathode and the anode. In order to have a more accurate representation of the DFN model with the ability to reproduce the heterogeneities present inside a real battery, we propose a Multi-Particle Model with electrolyte dynamics (MPMe) to better represent the dynamics of the battery. The MPMe uses a multi-particle representation by formulating layers within the positive, negative, and separator regions of the battery. The representation of the MPMe can be seen in Figure 3.3. We can see in the figure that each layer of the negative and positive side has one particle. As seen, each particle has radial layers. The lengths are also denoted in the figure for each region and individual layer within them. In Figure 3.4 shows the fluxes

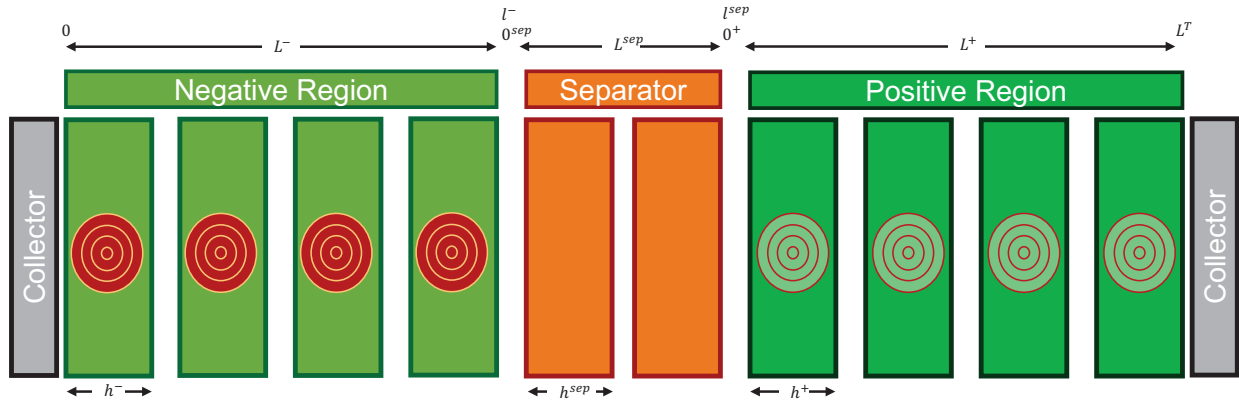


Figure 3.3: MPMe Model.

in individual layers for each respective region of the battery. Note that in the separator, there will be interaction between the electrolyte and the solid electrode layers. As we can see from the figure, each layer has several parameters. This includes:

- The Overpotential $\eta^\pm(x, t)$
- The Open-Circuit Voltage $U^\pm(x, t)$
- the electrolyte electric potential $\phi_e^\pm(x, t)$
- The concentration of lithium in the electrolyte $c_e(x, t)$
- The electrolyte diffusivity $D_e^\pm(c_e, t)$
- The molar ionic fluxes $j_n^\pm(x, t)$ and hence also the ionic current $i_e^\pm(x, t)$

- The concentration of the lithium in the solid phase $c_s^\pm(x, r, t)$ and hence also the solid surface concentration $c_{ss}^\pm(x, t)$

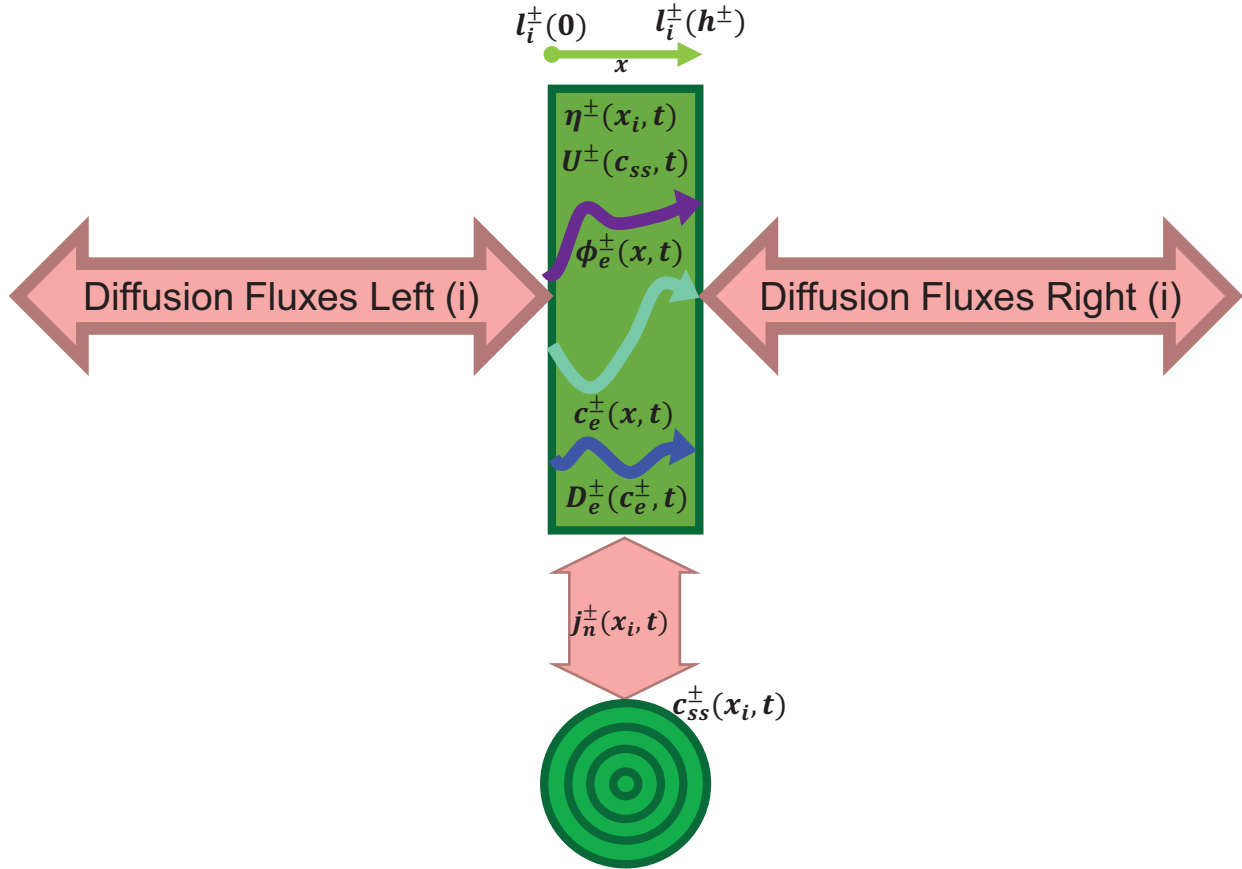


Figure 3.4: MPMe Model fluxes

Each layer has its own single-particle to represent the solid-dynamics within the cathode and anode regions. Figure 3.5 shows detail on the construction of the radial layers in each particle of a single finite volume. We can see that each radial layer has its own:

- concentration of lithium in the solid phase $c_s^\pm(x, r, t)$
- solid diffusivity coefficient $D_s^\pm(r, t)$
- Volume of the sphere $V(j)$
- Radius of the sphere $h_s * N^j$
- The outermost shell interacts with the electrolyte phase through a relationship with the molar ionic fluxes $j_n^\pm(x, t)$

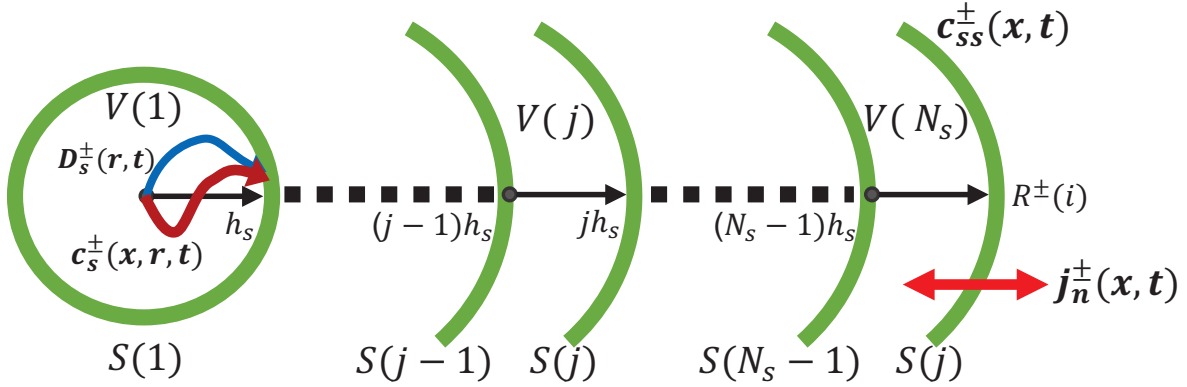


Figure 3.5: MPMe Model radial fluxes

For every layer, this leads to different solid surface concentration $c_{ss,i}^j(x, t)$, leading to a different molar ion flux $j_{n,i}^j(x, t)$, and therefore different ionic current $i_{e,i}^j(x, t)$. Unlike the SPMe where the $i_e(x, t)$ is trapezoid-shaped, it now has a constant slope for every individual layer that varies between layers. Figure 3.6 shows the shape of the $i_{e,i}^j(x, t)$ for the MPMe.

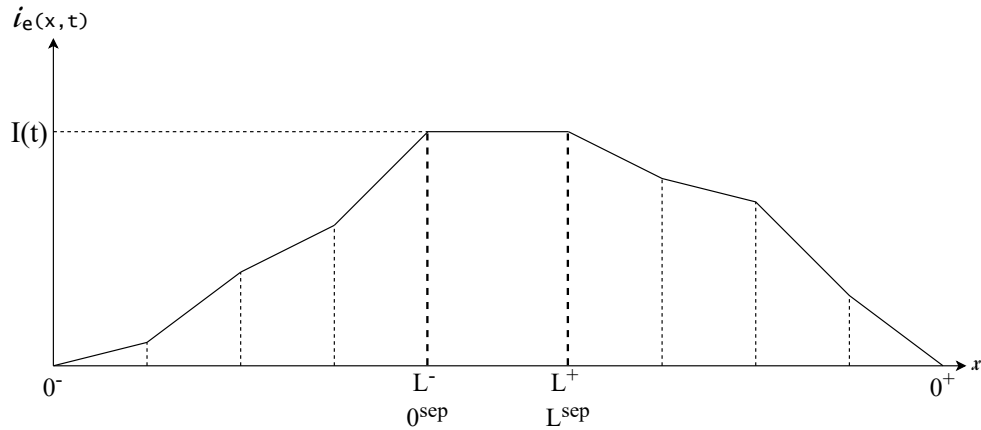


Figure 3.6: MPMe Model: $i_e(x, t)$

The anode, separator, and cathode regions are all denoted through $j \in \{-, +, sep\}$ with each region having variable total number of layers denoted by N^j . Note that if we reduce $N^j = \{1, 1, 1\}$, the system transforms to the regular DFN model but with a single particle representation of the solid phase. For layers within the same region, with constant j , the boundary conditions are given as:

$$c_{e,i}^j(h^j, t) = c_{e,i+1}^j(0, t) \quad (3.31)$$

$$\frac{\partial c_{e,i}^j}{\partial x}(h^j, t) = \frac{\partial c_{e,i+1}^j}{\partial x}(0, t) \quad (3.32)$$

where $i \in \{1, \dots, N^j - 1\}$ and requires $N^j \geq 2$. (3.31) dictates that there is continuity of value between two layers of the same region while Equation (3.32) dictates that there is continuity of fluxes between two layers of the same region of the electrolyte. Inter-regional boundary conditions are similar to the DFN model and can be denoted as:

$$c_{e,N^-}^-(h^-, t) = c_{e,1}^{sep}(0, t) \quad (3.33)$$

$$c_{e,N^{sep}}^{sep}(h^{sep}, t) = c_{e,1}^+(0, t) \quad (3.34)$$

Equation (3.34) dictates that there is continuity of value of concentrations of lithium between the last layer of the anode and the first layer of the separator. Equation (3.33) dictates that there is continuity of value of concentrations of lithium between the last layer of the separator and the first layer of the cathode. These are similar to Equations (3.15) and (3.16) conditions defined earlier in the DFN model.

$$\frac{\partial c_{e,1}^-}{\partial x}(0, t) = \frac{\partial c_{e,N^+}^+}{\partial x}(h^+, t) = 0 \quad (3.35)$$

$$D_e^{-,eff}(c_{e,N^-}^-(h^-)) \frac{\partial c_{e,N^-}^-}{\partial x}(h^-, t) = D_e^{sep,eff}(c_{e,1}(0)) \frac{\partial c_{e,1}^{sep}}{\partial x}(0, t) \quad (3.36)$$

$$D_e^{sep,eff}(c_{e,N^{sep}}^{sep}(h^{sep})) \frac{\partial c_{e,N^{sep}}^{sep}}{\partial x}(h^{sep}, t) = D_e^{+,eff}(c_{e,1}^+(0)) \frac{\partial c_{e,1}^+}{\partial x}(0, t) \quad (3.37)$$

Equation (3.35) is similar to Equation (3.12) and states that there is no flux leaving the sides of the battery. Equations (3.36) and (3.37) are synonymous to Equations (3.13) and (3.14), stating that flux entering one region is equal to the flux leaving the adjacent region.

Figure 3.7 shows the potentials inside the battery for the MPMe. The positive domain is now defined as $x \in (x^r, L^T)$ and the negative domain as $x \in (0, x^r)$. Here, x^r denotes

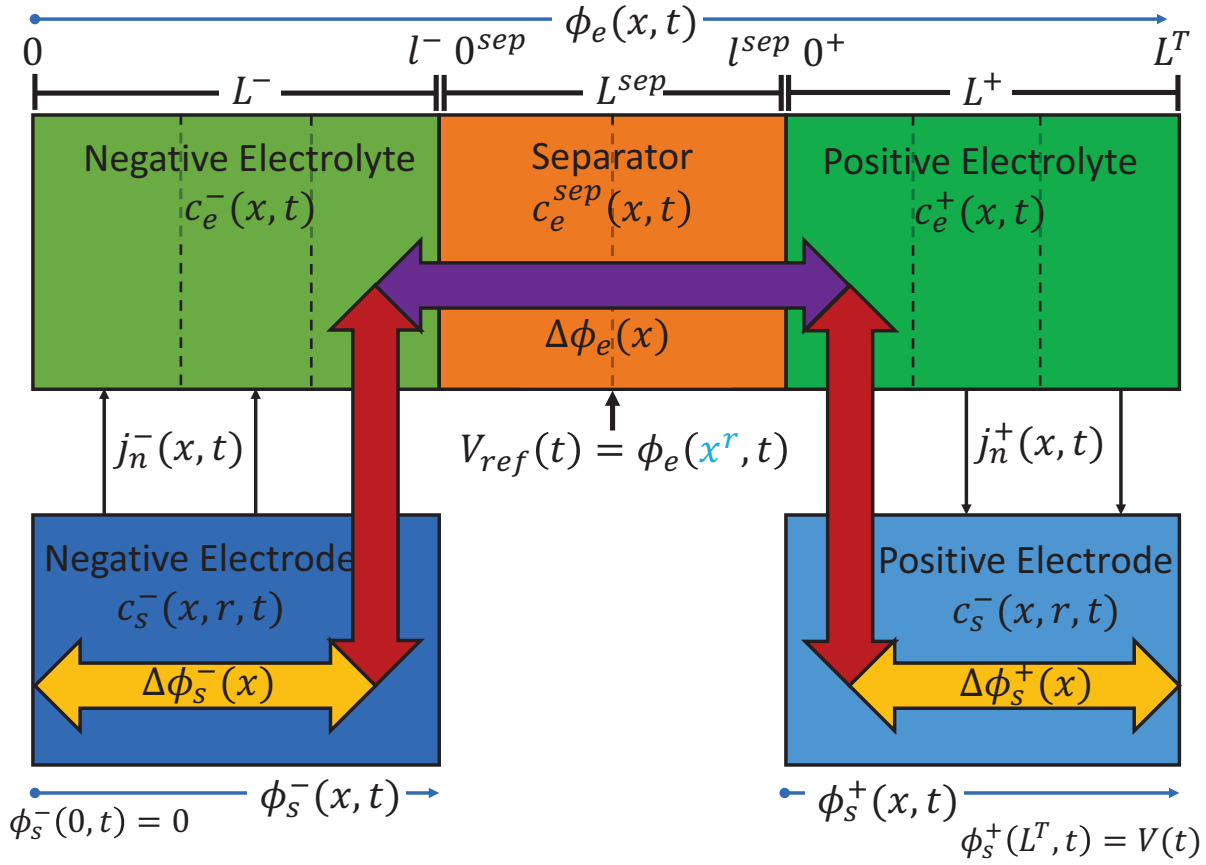


Figure 3.7: Potentials inside the battery from [5]

the location within the separator where the reference electrode is positioned, associated with the voltage $V_{ref}(t)$. Using 3.7 and the governing equations in (3.1-3.9), we can write the following relationships for the positive and negative domain voltages:

$$\begin{aligned}
 V_{ref}(t) &= \Delta\phi_e^-(x^-) + (\phi_e(x^-) - \phi_s(x^-)) + \Delta\phi_s(x^-) \\
 V_{ref}(t) &= \phi_e(x^r, t) - \phi_e(x^-, t) - U(c_{ss}^-(x^-, t)) \\
 &\quad - FR_f^- j_n^-(x^-, t) - \eta^-(x^-, t) + \phi_s^-(x^-, t),
 \end{aligned} \tag{3.38}$$

$$\begin{aligned}
 V(t) - V_{ref}(t) &= \Delta\phi_e^+(x^+) + (\phi_s(x^+) - \phi_e(x^+)) + \Delta\phi_s(x^+) \\
 V(t) - V_{ref}(t) &= \phi_e(x^+, t) - \phi_e(x^r, t) + \phi_s^+(L^T, t) \\
 &\quad - \phi_s^+(x^+, t) - FR_f^+ j_n^+(x^+, t) - \eta^+(x^+, t) + U(c_{ss}^+(x^+, t))
 \end{aligned}$$

where x^+ and x^- represent specific points within the positive and negative domains of the battery, respectively.

The total voltage of the battery, $V(t)$, is determined by the sum of the voltages across the positive and negative domains. Essentially, it represents the difference in the solid electric potential between the collectors:

$$V(t) = \phi_s^+(L^T, t) - \phi_s^-(0, t) \quad (3.39)$$

3.4 Simulation of the MPMe

The validation of the proposed MPMe model is conducted through simulations on the MATLAB coding platform. Initially, the model is simulated and subsequently compared with the full-scale DFN model in MATLAB to ensure its accuracy.

3.4.1 Validation of the Model

To assess the accuracy of the proposed DFN against existing techniques, the PDE-based model was simulated using MATLAB. For this purpose, the finite volume-based MPMe model was temporally discretized. This can be achieved through various techniques, including explicit, implicit, and Crank-Nicolson schemes.

In this PhD, we have decided to use the implicit scheme for the simulation of the MPMe, DFN, and SPMe models. This choice is attributed to the increased computational efficiency, as it enables us to use sufficiently large time steps for practical applications. This is a necessary objective in the final implementation of the developed virtual electrochemical sensors.

We now proceed to conduct a comparative analysis to emphasize the accuracy and viability of the MPMe model. In the conducted simulations, the DFN model was implemented with a highly granular finite volume-based approach, with a time step of 0.1 seconds and spatial layers defined as $N^j = [20, 8, 20]$, ensuring a detailed representation of the electrochemical phenomena. In contrast, the proposed MPMe model, with the same underlying

equations as that of the DFN, was configured with a coarser time step of 1 second and a spatial discretization of $N^j = [4, 2, 4]$, providing a balance between computational efficiency and model accuracy. Lastly, the SPMe model was employed with a time discretization of 1 second and a simplified spatial representation using single layers. These spatial and temporal discretizations apply to all subsequent simulations of these models unless otherwise stated and align with those in [5].

Figure 3.8 displays the total voltage of the battery between the collectors, obtained from simulations of a full-scale DFN model, the previously derived MPMe model, and the SPMe model for the purpose of comparison. Here, the full-scale DFN model is a very finely discretized (in both spatial and temporal dimensions) finite volume simulation, and it serves as the reference for comparing the MPMe and SPMe models. All three simulations start with the same SOC, total amount of lithium, and an identical current profile. The simulation results are shown for a constant charging scenario of 2C current.

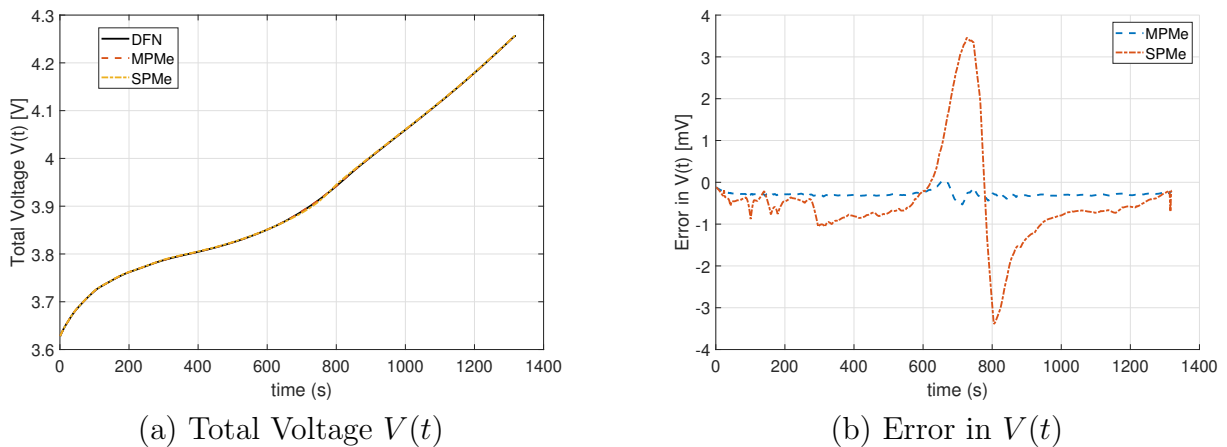
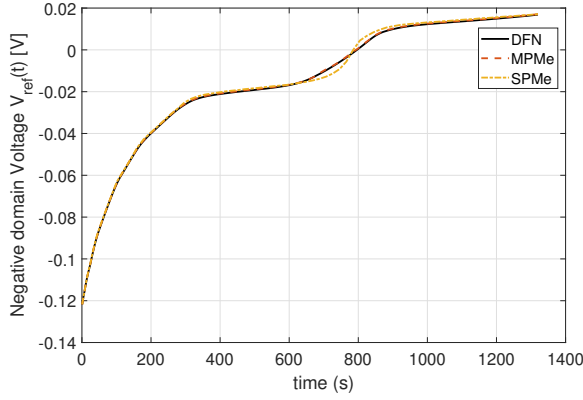


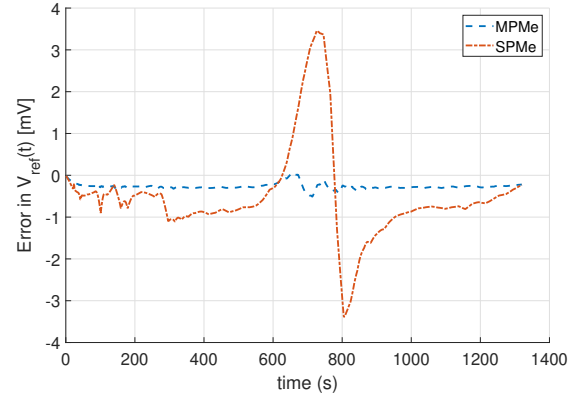
Figure 3.8: Total Voltage Comparisons for 2C constant charge

It can be observed from Figure 3.8(a) that the voltage obtained from the MPMe simulation is closer to the reference DFN simulation, when compared to the SPMe simulation. The discrepancy between the DFN and its derivatives is illustrated in Figure 3.8 (b). Figures 3.9 and 3.10 show the Voltages and corresponding errors for the negative and positive domain for the 2C constant charge scenario, respectively.

Similarly, the simulations are compared for a C-rate of 4C constant charge current profile, and the corresponding voltage and error curves are depicted in Figures 3.11(a) and 3.11(b),

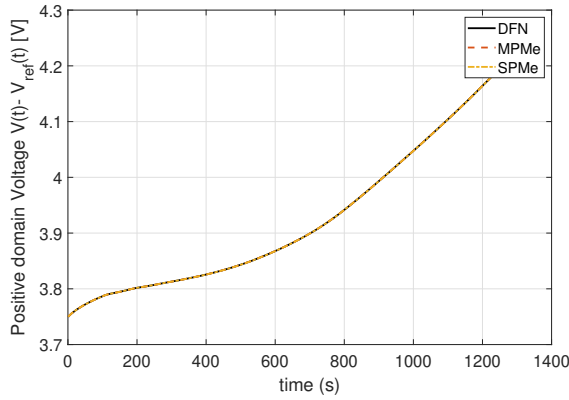


(a) Negative Domain Voltage $V_{ref}(t)$

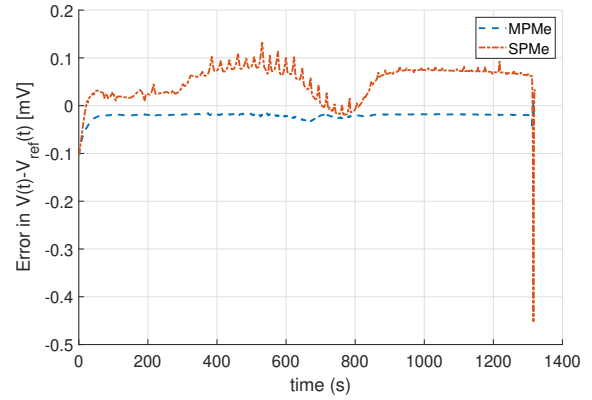


(b) Error in $V_{ref}(t)$

Figure 3.9: Negative Domain Voltage ($V_{ref}(t)$) Comparisons for 2C constant charge



(a) Positive Domain Voltage $V(t) - V_{ref}(t)$

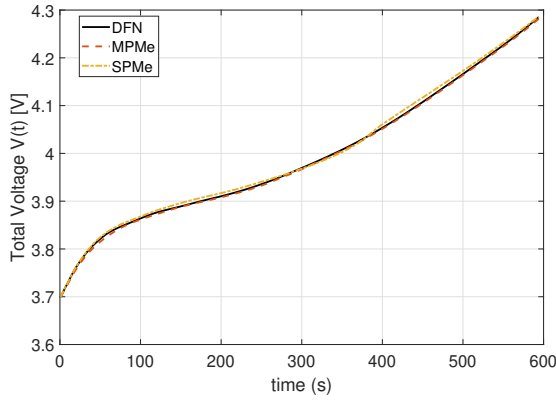


(b) Error in $V(t) - V_{ref}(t)$

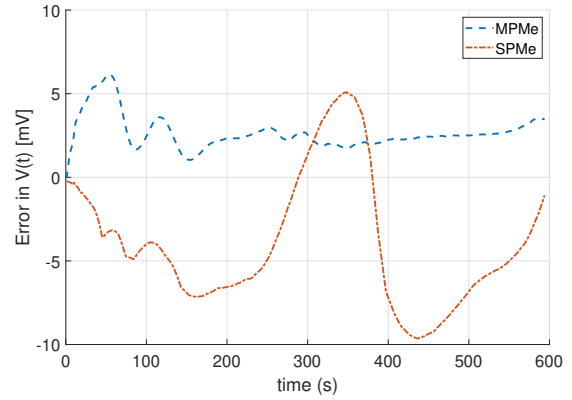
Figure 3.10: Positive Domain ($V(t) - V_{ref}(t)$) Voltage Comparisons for 2C constant charge

respectively. Figures 3.12 and 3.13 show the Voltages and corresponding errors for the negative and positive domain for the 4C constant charge scenario, respectively.

The results clearly demonstrate that the MPMe simulation exhibits higher accuracy compared to the existing SPMe derivatives. This confirms the validity of the MPMe model in better replicating the system's voltage behavior.

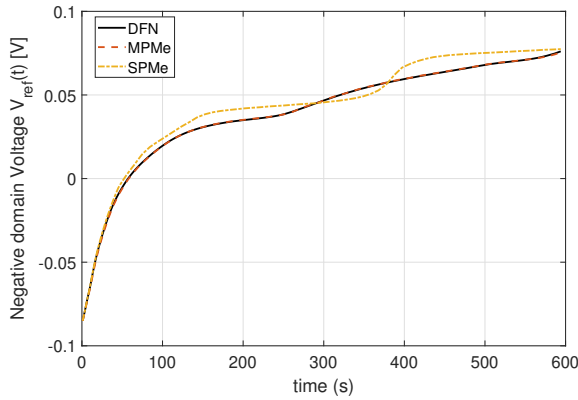


(a) Total Voltage $V(t)$

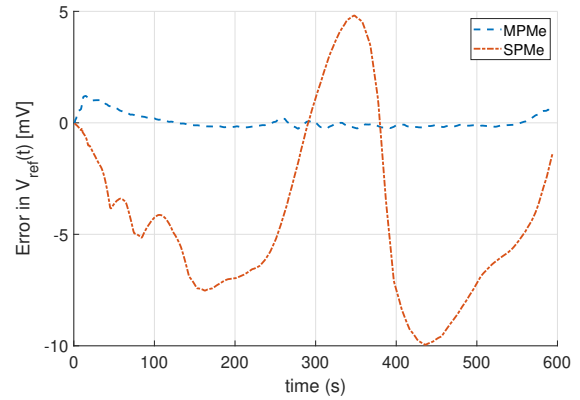


(b) Error in $V(t)$

Figure 3.11: Total Voltage Comparisons for 4C constant charge

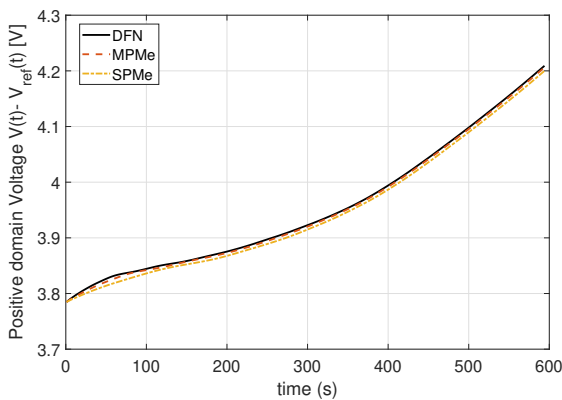


(a) Negative Domain Voltage $V_{ref}(t)$

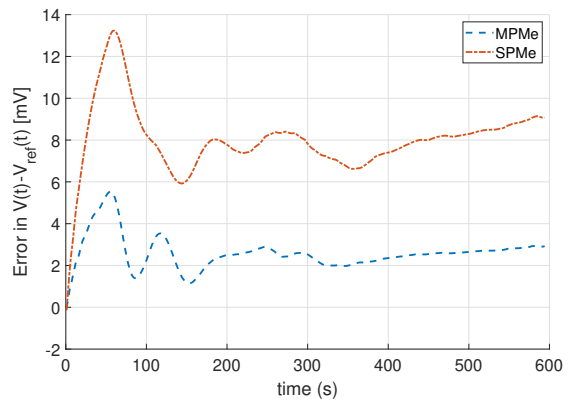


(b) Error in $V_{ref}(t)$

Figure 3.12: Negative Domain Voltage ($V_{ref}(t)$) Comparisons for 4C constant charge



(a) Positive Domain Voltage $V(t) - V_{ref}(t)$



(b) Error in $V(t) - V_{ref}(t)$

Figure 3.13: Positive Domain Voltage ($V(t) - V_{ref}(t)$) Comparisons for 4C constant charge

3.4.2 Spatial Heterogeneity of Internal States

While accurately reproducing the input-output behavior of a battery is undeniably important, the true value of the EChM models lies in their capacity to faithfully replicate the battery's internal electrochemical parameters. This encompasses the internal variations within the battery that influence its dynamics. Unlike the SPM_e approach, which was discussed earlier and linearizes the internal states, the MPME model comprehensively captures these internal states. These states include the concentration of lithium within the electrodes and electrolyte, the electric potential across both phases, the overpotential, and other crucial factors.

Figures 3.14(a) and 3.14(b) illustrate the heterogeneity present in both the positive and negative solid electrodes of the battery, as observed in the simulation conducted at 4C constant charge.

Similarly, the concentration of lithium in the electrolyte can also be viewed spatially through the battery for a constant 4C charge as seen in Figure 3.15. The polarity of the concentration depends on the diffusion coefficient, current density, and temperature. Higher current and lower electrolyte diffusion coefficient leads to an increased polarity in the concentration of the electrolyte. The effect of temperature will be discussed in more detail in a subsequent section.

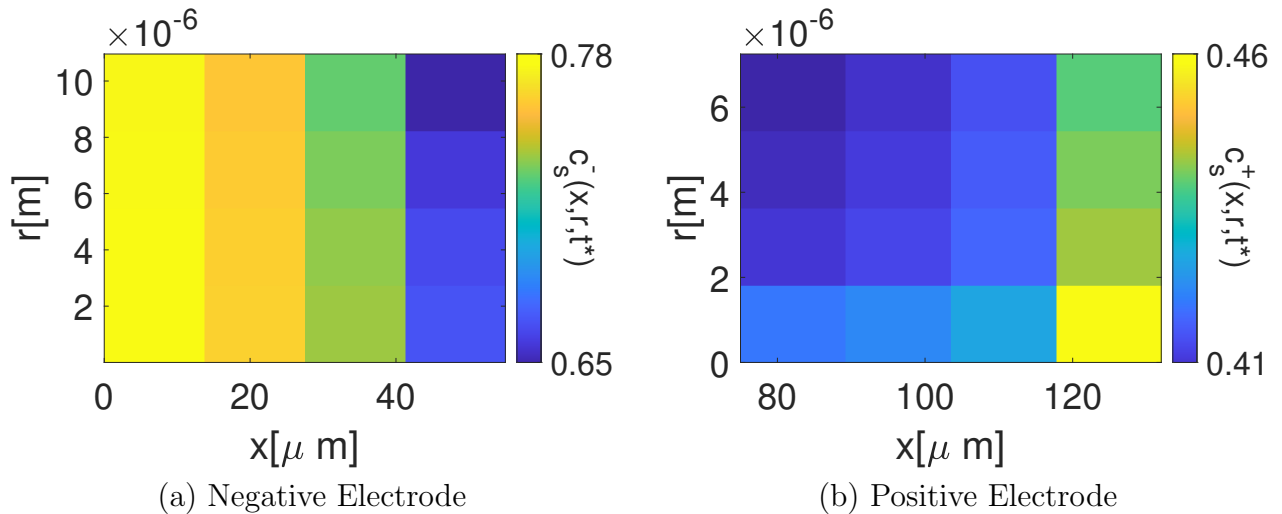


Figure 3.14: Heterogeneity in the Electrodes (4C Constant Charge)

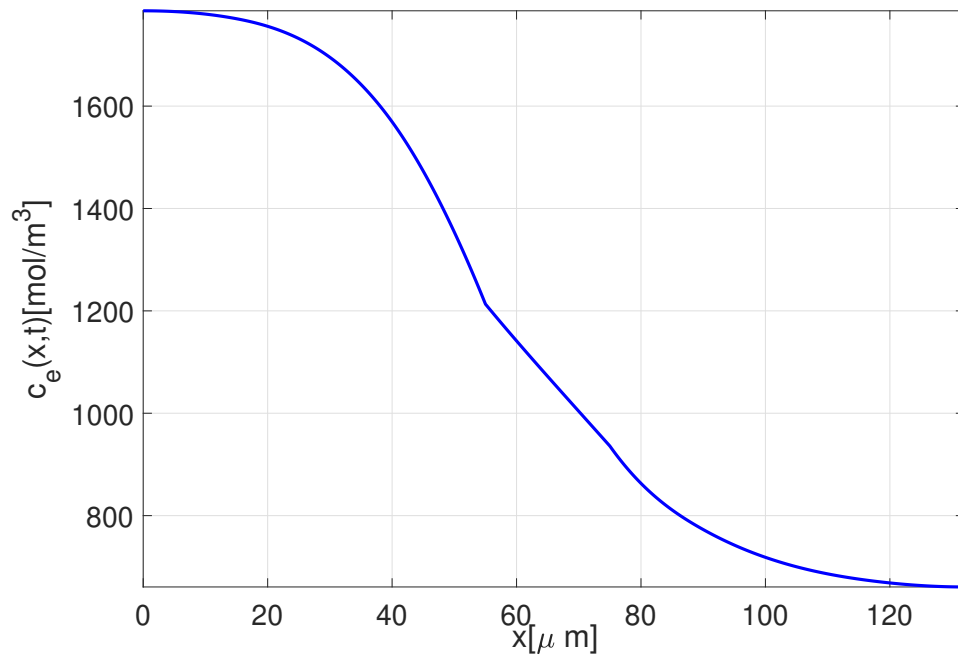
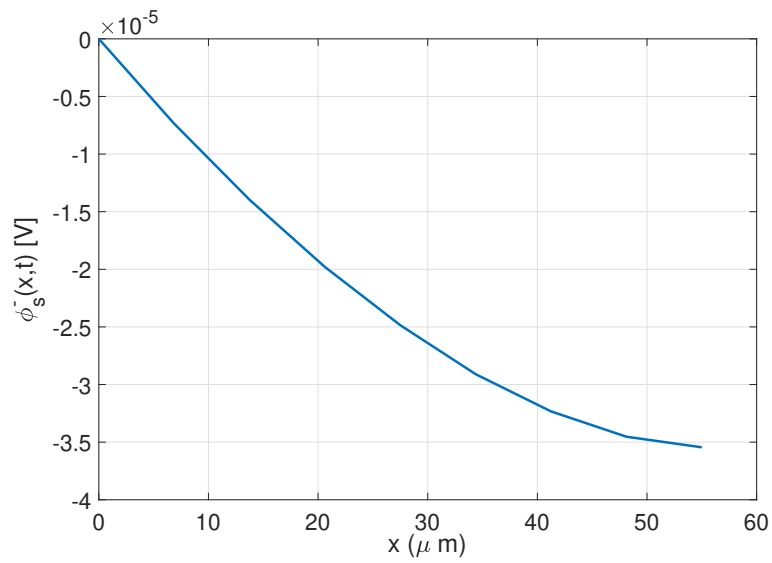
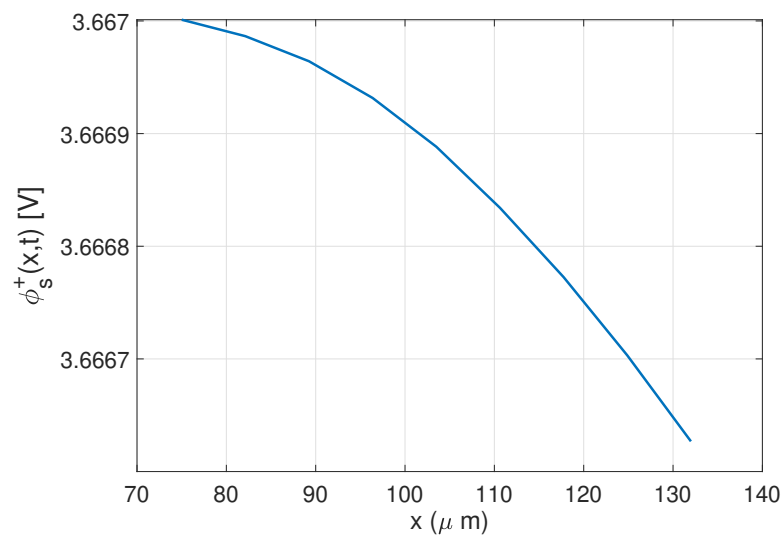


Figure 3.15: Heterogeneity in Electrolyte (4C Constant Charge)

With the heterogeneity of the lithium concentration in both phases now highlighted, we can illustrate its impact on the prediction of other significant electrochemical parameters that play a crucial role in monitoring and optimizing the performance of LiBs. These parameters include the electric potential in both phases, and the ionic current. Figures 3.16(a), 3.16(b), 3.17, and 3.18 depict the reconstruction of and heterogeneity present in these aforementioned electrochemical variables.



(a) Negative Electrode



(b) Positive Electrode

Figure 3.16: Electric Potential in the negative electrodes (4C Constant Charge)

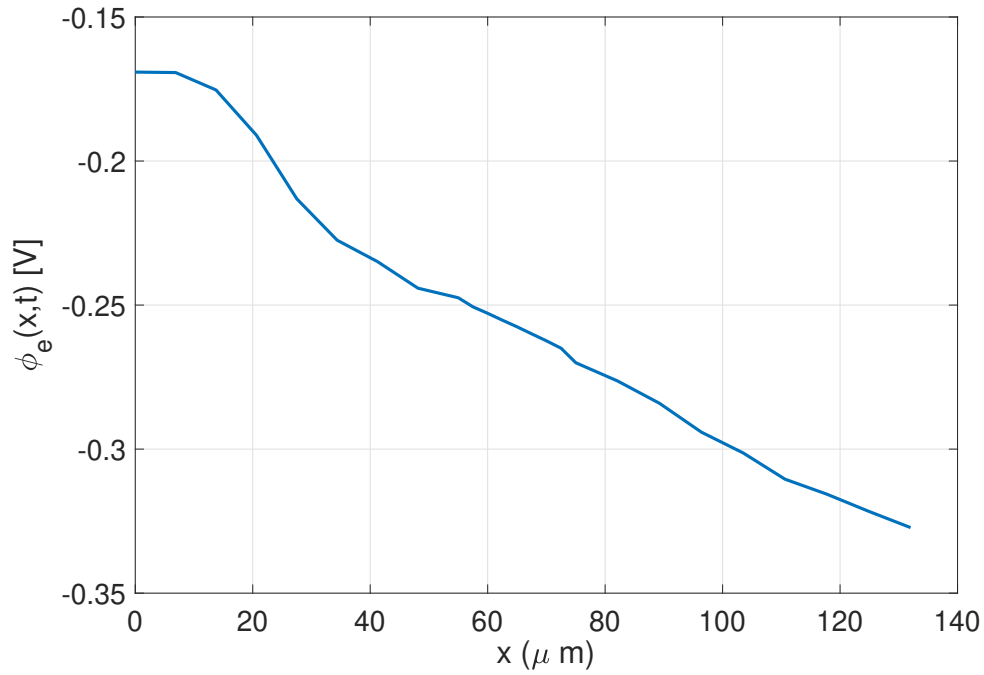


Figure 3.17: Electric Potential in the Electrolyte (4C Constant Charge)

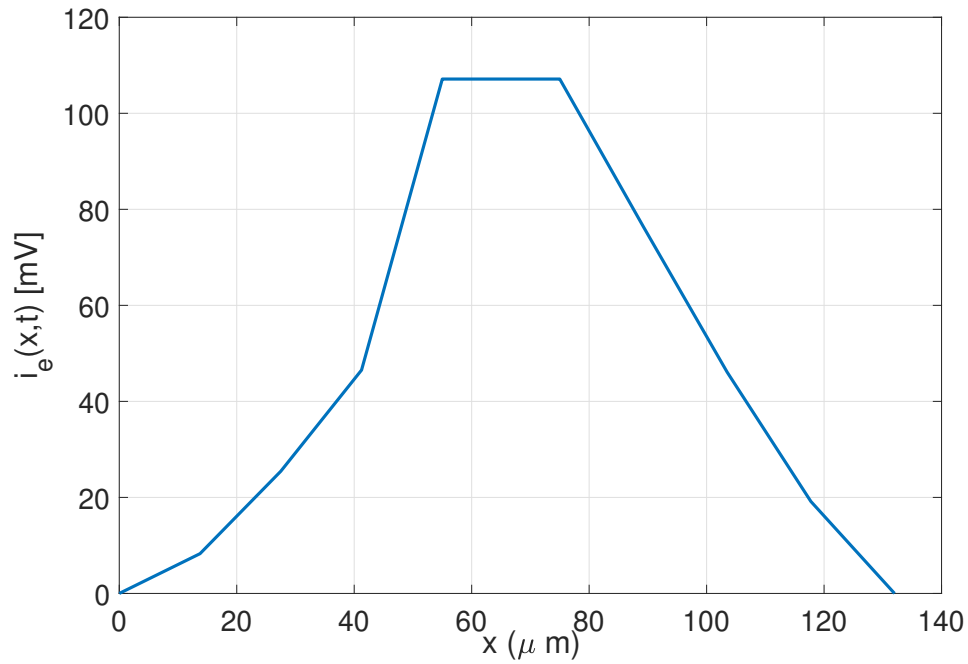


Figure 3.18: Ionic Current (4C Constant Charge)

3.4.3 Lithium Conservation in the System

Another crucial aspect of the MPMe model is its inherent conservation of lithium, owing to its finite volume-based approach. Figure 3.19 illustrates the total amount of lithium present in the solid phase of the battery. It can be seen that the total lithium remains constant as the simulation progresses, affirming its conservation.

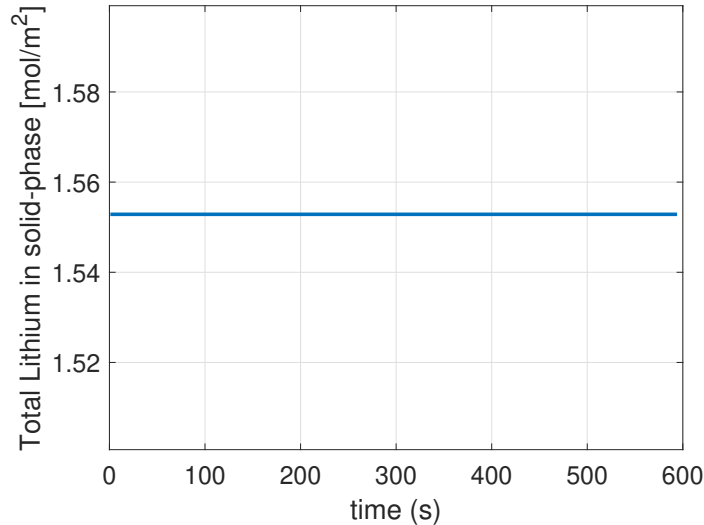


Figure 3.19: Total Lithium in Solid Phase (4C Constant Charge)

A similar assessment can be conducted for the electrolyte phase of the battery. In Figure 3.20, the total amount of lithium in the electrolyte is presented. The minimal variation implies that lithium is conserved within the electrolyte.

Based on these observations, we conclude that the total amount of lithium is conserved in both phases. However, it's important to note that this conservation doesn't apply to individual electrodes. Figure 3.21 demonstrates the variations in the total moles of cyclable lithium within the negative and positive electrodes, respectively. This parameter holds significance as it contributes to determining the state-of-charge (SoX) parameters in subsequent discussions. Additionally, it's worth noting that the sum of cyclable lithium in the negative and positive electrodes equates to the amount shown in Figure 3.19, which remains nearly constant.

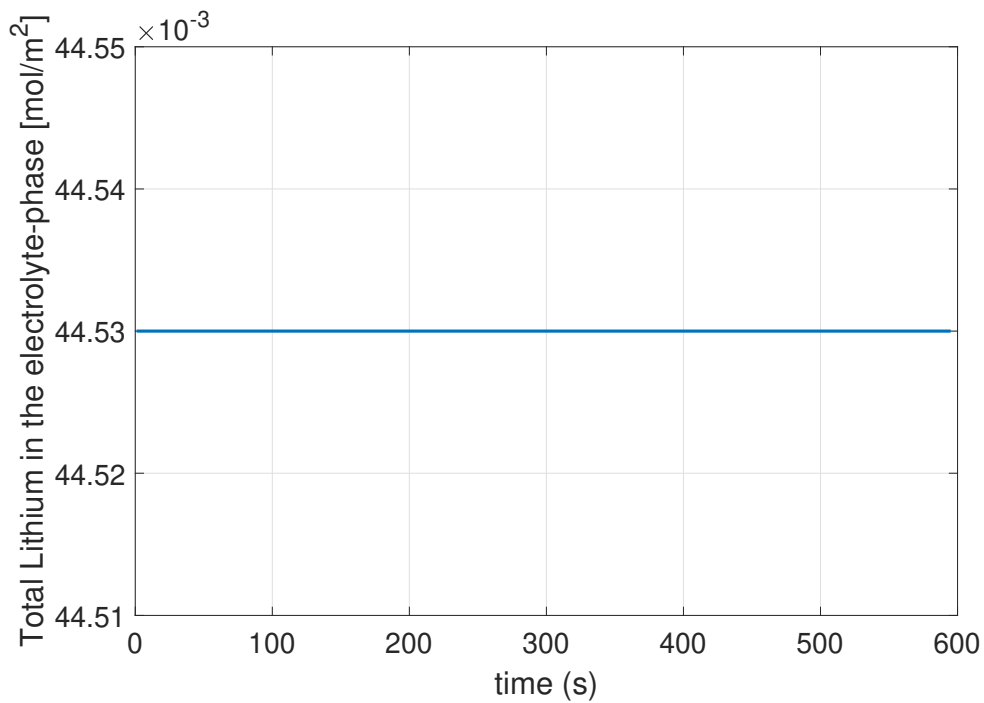


Figure 3.20: Total Lithium in Electrolyte Phase (4C Constant Charge)

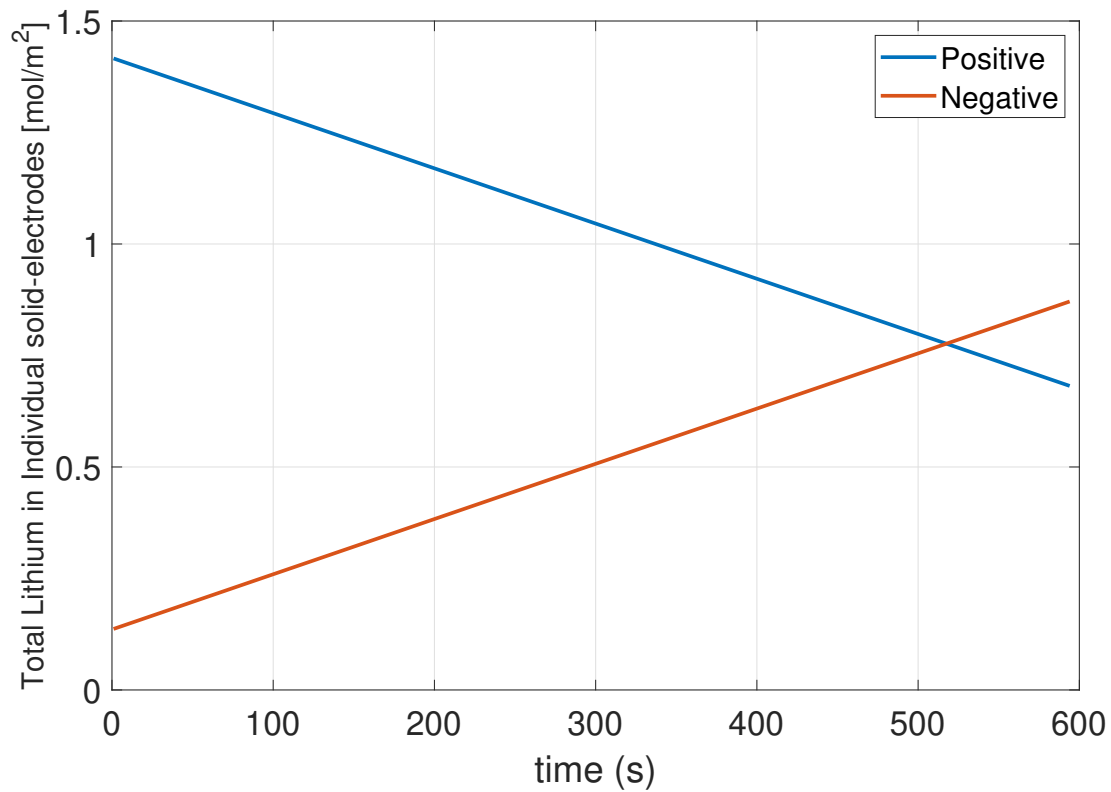


Figure 3.21: Total Lithium in individual Solid electrodes (4C Constant Charge)

3.4.4 Simulation Analysis: Effects of Incorrect Lithium Amounts

In this section, we delve into a detailed analysis of the implications arising from deviations in the total lithium content within the solid and electrolyte phases of the LiB.

Revisiting the previously discussed 2C constant charge simulation, we introduce deviations in the total lithium content. Initially, we focus on the electrolyte phase and subsequently shift our attention to the solid phase.

Deviation in Lithium Content within the Electrolyte Phase

We executed the simulation for the MPMe and SPMe models, introducing a 10% reduction in the lithium content of the electrolyte phase. Figure 3.22(a) presents the resultant voltage, while Figure 3.22(b) delineates the associated voltage error. The results indicate a notable discrepancy in the voltage when comparing the full-scale DFN model, which maintains the correct lithium content, with its derivatives (MPMe and SPMe).

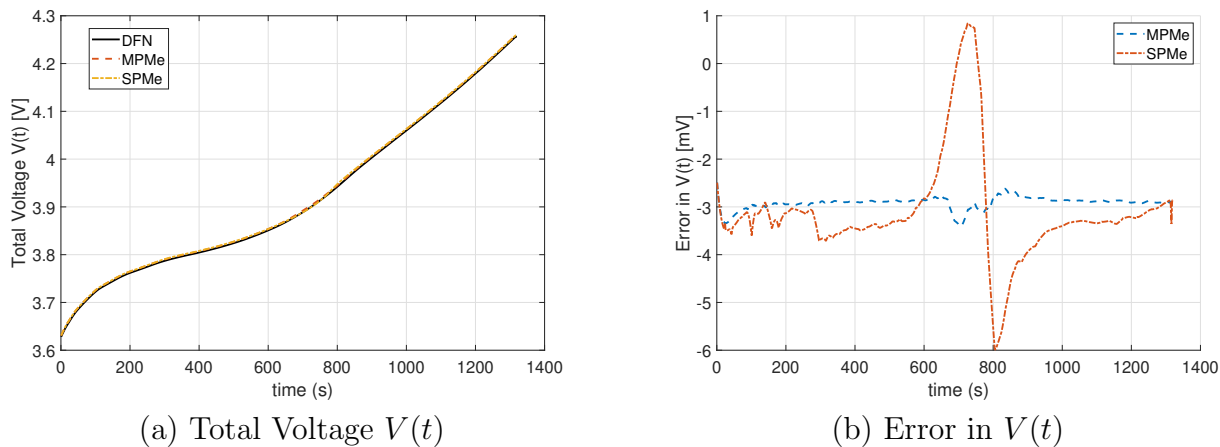


Figure 3.22: Total Voltage $V(t)$ Comparisons for 2C constant charge with altered lithium content in the electrolyte

Deviation in Lithium Content within the Solid Phase

Similarly, we conducted the simulation with a 10% reduction in the lithium content of the battery's solid phase. Figure 3.23(a) presents the total voltage curve, and Figure 3.23(b) provides insights into the associated voltage errors. The results underscore that even minor deviations in the lithium content can lead to significant errors in voltage predictions.

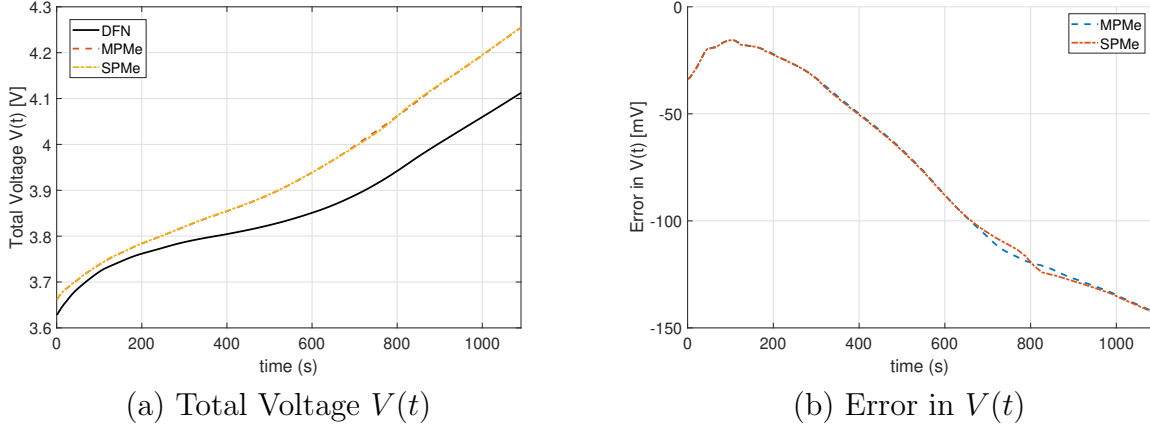


Figure 3.23: Total Voltage $V(t)$ Comparisons for 2C constant charge with altered lithium content in the solid phase

These findings emphasize the importance of accurate lithium content measurements. Addressing this challenge is a significant contribution of this research. In the next chapter of this PhD thesis, we will present a non-conservative observer that helps correct this deviation in total lithium with the individual electrodes of the battery [5].

3.5 Integration of Temperature dependence in the Battery model parameters

3.5.1 Single Particle Model with Electrolyte and Thermal Dynamics

In the previous subsection, we discussed the SPMe model which does not consider temperature variations across the Li-ion battery in many of its variables. To address this limitation, the Single Particle Model with Electrolyte and Thermal Dynamics (SPMeT) [51] was developed. The SPMeT model combines the SPMe model with a thermal model derived from [211]. In SPMeT, temperature-dependent parameters follow the Arrhenius law:

$$P(T_{avg}) = P_{ref} \exp\left(\frac{E_{\alpha P}}{R} \left(\frac{1}{T_{ref}} - \frac{1}{T_{avg}}\right)\right) \quad (3.40)$$

When conducting real-time simulations of Li-ion batteries, a judicious balance must be

struck between model complexity and accuracy. Furthermore, ensuring the numerical conservation of total lithium over time is crucial, as seemingly minor errors in lithium transfer between the solid and electrolyte phases can accumulate and lead to inaccurate simulations over extended time frames.

3.5.2 Thermal dependence of parameters

The battery behavior is dependent on the thermal conditions of the battery, particularly when operating in a wide temperature range (INSTABAT specifications [28, 29]). We now extend the principle of the SPM_eT for the dependence of transport and kinetic parameters on the temperature into our approach, the MPM_e framework.

An Arrhenius law is used for the solid diffusion coefficient relating the transport of lithium with the concentration gradient in the solid phase of the electrodes. In this case, the diffusivity coefficient will take the following form:

$$D_s^\pm = D_{s,0}^\pm \exp \left[\frac{-E_{a,d}^\pm}{R} \left(\frac{1}{T} - \frac{1}{T_0} \right) \right] \quad (3.41)$$

The conductivity of the electrolyte is another important parameter in determining the ohmic potential drop through the electrolyte. The relationship between the conductivity of the electrolyte κ , and the temperature and concentration is expressed from [212] as:

$$\sqrt{\frac{\kappa}{c_e}} = \int_{i=0}^2 \int_{j=0}^2 \kappa_{i,j} \cdot c_e^i \cdot T^j \quad (3.42)$$

The electrolyte diffusion coefficient is considered as depending on the temperature and concentrations based on relationship (from [213] which requires the previously computed value of conductivity) :

$$D_e = \frac{\kappa k_B T}{e^2 N_a c_e} \quad (3.43)$$

The reference current density is used to determine the ionic current using Butler-Volmer kinetics. An Arrhenius law is used to model its thermal dependence, with $T_0 = 298.15K$:

$$i_{o,ref}^{\pm} = i_{o,ref,0}^{\pm} \exp \left[\frac{-E_{a,k}^{\pm}}{R} \left(\frac{1}{T} - \frac{1}{T_0} \right) \right] \quad (3.44)$$

3.5.3 Effect of Temperature on battery behaviour

We now demonstrate the effect of change in operating temperature in the values of the internal electrochemical variables predicted by our reduced model. The simulation used to demonstrate the temperature variation uses a 1-C constant discharge of the battery from near 100% SOC. The three temperatures compared are 0°C, 25°C and 60°C.

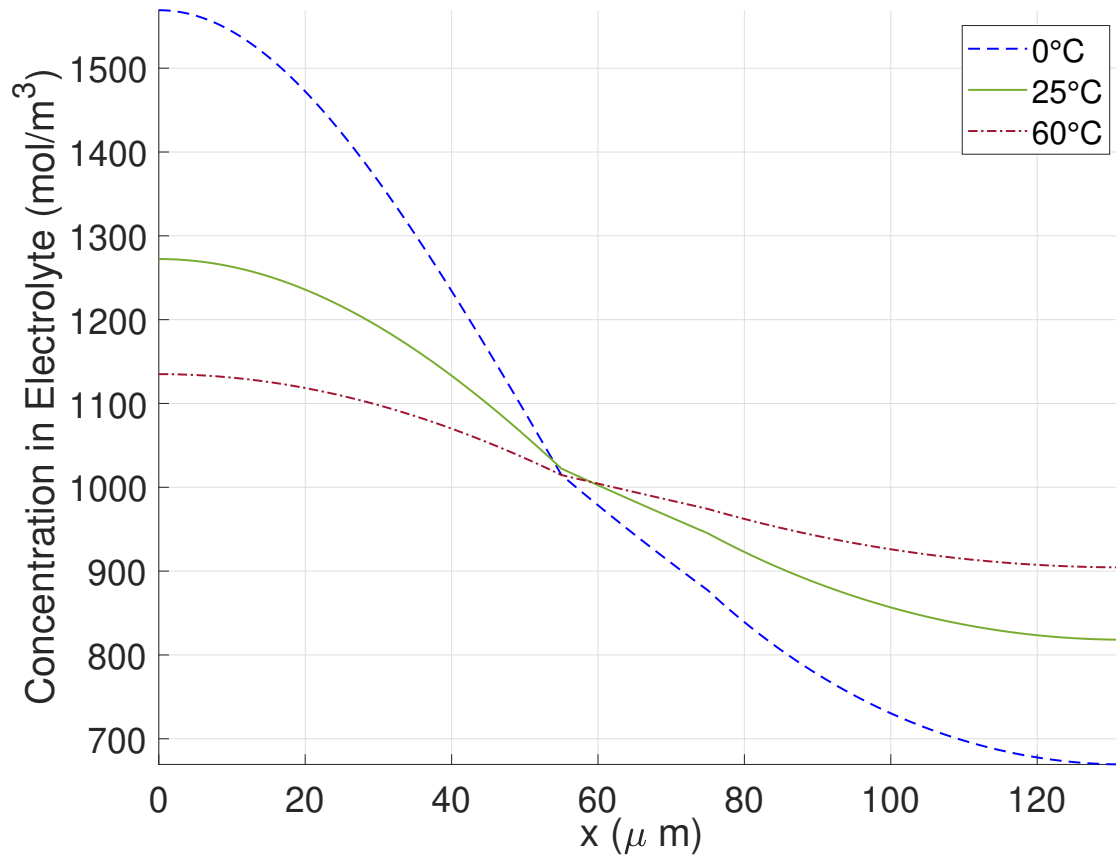


Figure 3.24: Concentration in electrolyte in the battery for different temperatures

Figure 3.24 shows the different values of electrolyte concentration through the battery

for a constant 1C discharge at different temperatures. It can be seen that the concentration profile is significantly dependent on temperature.

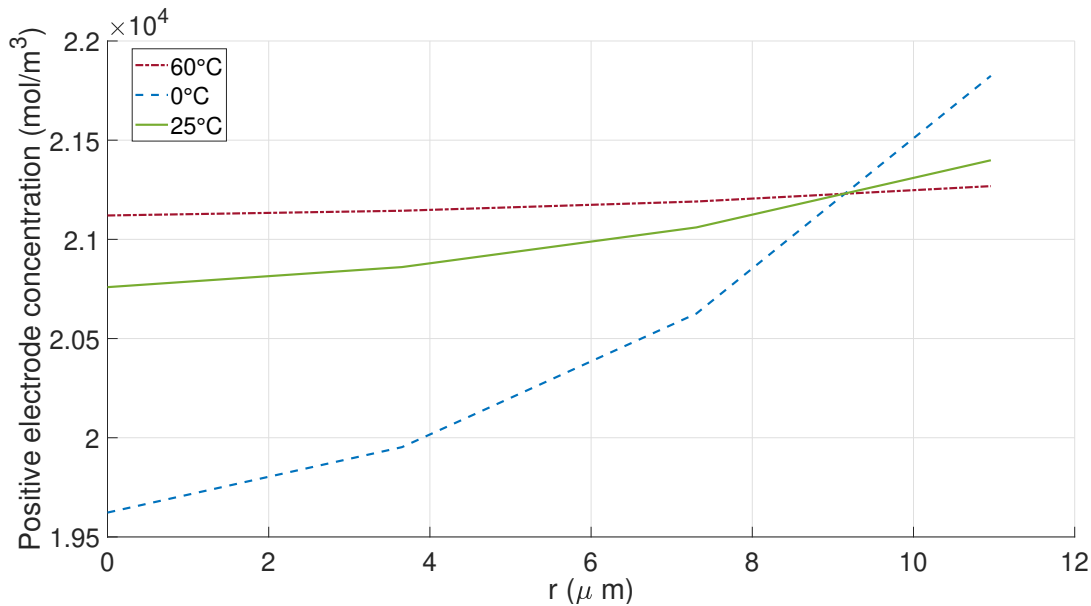


Figure 3.25: Solid concentration near the current collector at positive electrode, for different temperatures for a 1C discharge and after 1000s

Figure 3.25 shows the solid concentration of the positive electrode for different temperatures for a particle located near the positive collector. There is a positive relationship between the diffusivity of the positive electrode concentration and temperature. The simulation is taken at a 1-C constant discharge from 100% SOC at time $t=1000s$.

Figure 3.26 shows the solid concentration of the negative electrode for different temperatures for a particle located near the negative collector. There is a positive relationship between the diffusivity of the positive electrode concentration and temperature.

Figure 3.27 shows the corresponding overall voltage curves for the surface concentrations shown in Figure 3.25 and Figure 3.26 with a constant current profile of 1-C discharge. The shape of the electrolyte is similar to that in Figure 3.24 for the corresponding temperatures. This shows the effect of temperature on the overall voltage from the parameters discussed previously.

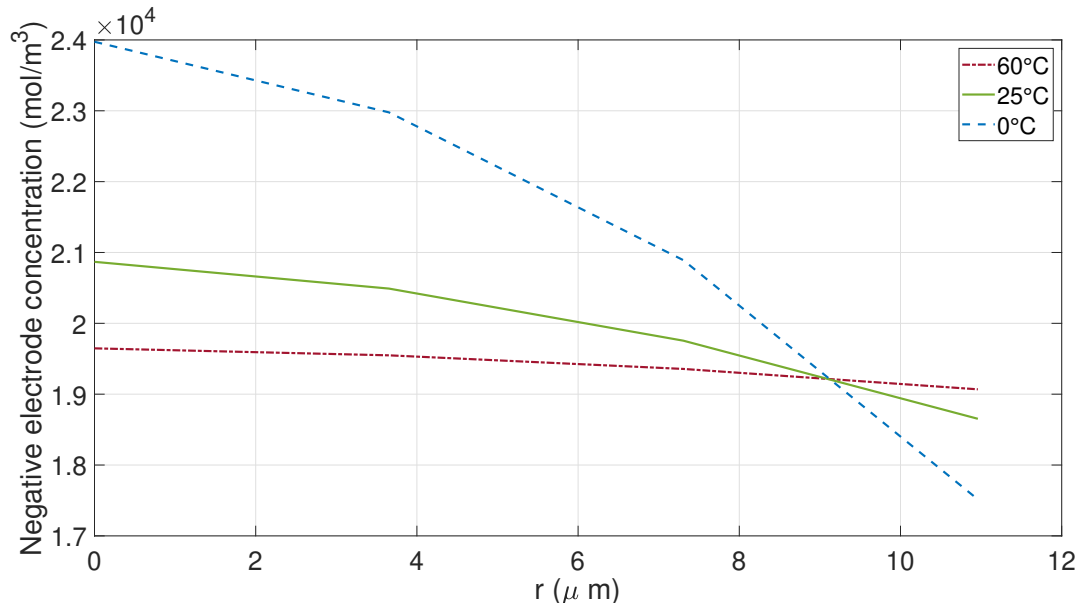


Figure 3.26: Solid concentration near the current collector at the negative electrode, for different temperature for a 1C discharge and after 1000s

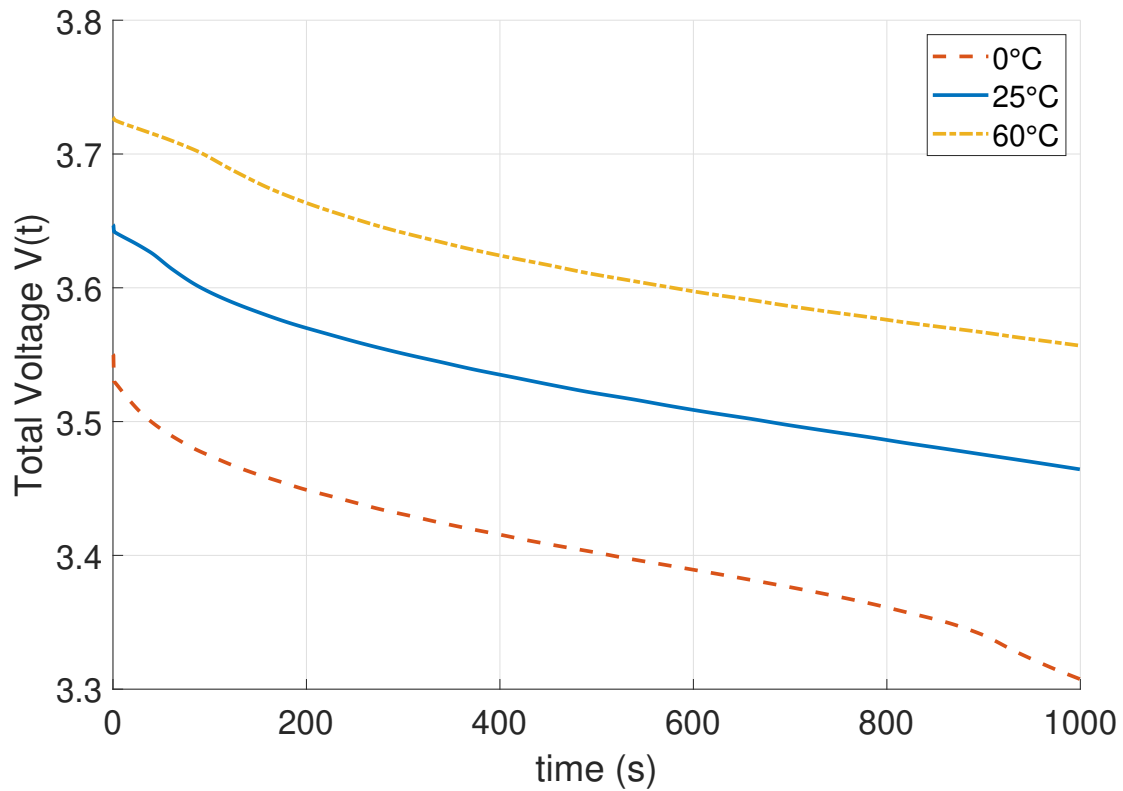


Figure 3.27: Voltage of the battery for different temperature

3.6 Conclusion of the Chapter

This chapter has elucidated the development and capabilities of the Multi-Particle Model with Electrolyte (MPMe), showcasing its pivotal role in simulating and understanding Li-ion battery dynamics with a keen focus on maintaining a balance between computational efficiency and physical accuracy.

The MPMe has an intrinsic ability to conserve lithium across various domains of the battery, ensuring the stability and reliability of its predictions. Its adeptness in accurately replicating the system's voltage behavior, while minimizing computational complexity, underscores its potential applicability in real-time scenarios and advanced Battery Management Systems (BMS).

Moreover, the model's capability to capture the spatial heterogeneity of internal states and to conserve lithium in the system, even under varied operational scenarios, has been distinctly highlighted through simulations under different C-rates and temperature conditions.

The incorporation of temperature dependencies into the model enhances its accuracy under varied thermal conditions, providing crucial insights for optimizing and managing battery operations across different thermal environments.

In summary, the MPMe model emerges as a robust, reliable, and computationally efficient tool for simulating and analyzing Li-ion battery dynamics. The subsequent chapters delve deeper into the applicability of the MPMe model in the development of state observers and Battery Management System algorithms, leveraging the principles and findings discussed in this chapter.

Chapter 4

State Observers for the MPM_e

Contents

| | | |
|------------|---|------------|
| 4.1 | State Observer for the Electrolyte Lithium Concentration . . . | 120 |
| 4.1.1 | Assumptions | 121 |
| 4.1.2 | Model Simplification | 122 |
| 4.1.3 | Formulation of the Electrolyte Concentration Observer | 122 |
| 4.1.4 | Stability Analysis | 124 |
| 4.2 | State observer for the solid lithium concentration using voltage error injection | 129 |
| 4.2.1 | Assumptions | 129 |
| 4.2.2 | Observer Formulation | 129 |
| 4.2.3 | Stability Analysis | 131 |
| 4.3 | Validation of the observers with simulation results | 135 |
| 4.3.1 | Constant Discharge Scenario at 2C Current | 135 |
| 4.3.2 | Electric Vehicle charge/discharge cycle | 139 |
| 4.4 | Conclusion of the Chapter | 144 |

Summary of the Chapter

This chapter offers a detailed analysis of observers for lithium-ion batteries, focusing on both the electrolyte and solid lithium concentrations. The importance of these observations is highlighted, given their role in understanding lithium ion behavior within the battery.

Electrolyte Lithium Concentration Observer

This section delves into the construction and stability analysis of the state observer for the electrolyte lithium concentration in lithium-ion batteries. The observation process is pivotal for understanding the diffusion of lithium ions within the electrolyte.

Assumptions:

To simplify the formulation of the electrolyte observer, we take some assumptions. These include the diffusion coefficient, D_e , now being uniformly bounded, allowing the decoupling of its dependencies. A measurement of the lithium concentration, $c_e(x_r, t)$, is assumed to be available at a specific point in the separator, x_r . The spatial profile of molar ionic fluxes, $j_n^\pm(x, t)$, is assumed to be accurately predicted by the model. These assumptions will be rigorously discussed in the chapter.

Model Simplification: The Doyle-Fuller-Newman (DFN) model's electrolyte diffusion equation is simplified using the first assumption above while retaining its essential characteristics. The simplified equation is:

$$\epsilon_e^j c_{e,t}^j(x, t) = \frac{\partial}{\partial x} \left[D_e(x) c_{e,x}^j(x, t) + \frac{(1 - t_c^0)}{F} i_e^j(x, t) \right]$$

Formulation of the Electrolyte Concentration Observer: An observer is developed based on the simplified electrolyte diffusion equation. This observer estimates the electrolyte concentration using measurements at the reference electrode. The observer's formulation introduces an error injection term to account for discrepancies between actual and estimated states.

Stability Analysis: The stability of the observer is crucial. A proposition establishes that the error system is exponentially stable under certain conditions. The stability is

analyzed using a candidate Lyapunov function, and conditions for stability are derived.

State Observer for the solid lithium concentration

Assumptions Similar to the electrolyte observer, the solid observer also requires some assumptions for its formulation. The construction of state observers for solid electrodes is based on the assumed availability of a voltage measurement at a reference electrode $V_{\text{ref}}(t)$, and the assumption that the OCV curve of the electrodes U^\pm is monotonically decreasing. These assumptions will also be rigorously discussed in the chapter.

Observer Formulation The observer for the solid-phase lithium concentration integrates the voltage error term, using the reference electrode's voltage. The error system contrasts the physical and observer systems, with radial coordinates transformed for notation simplicity.

Stability Analysis Stability is confirmed by defining a Lyapunov function and ensuring its time derivative's negative definiteness. The proposed observers, while not conserving total lithium in electrodes, work with another observer to correct errors over time.

Validation of the observers with simulation results

Simulations using a simplified DFN model validate the observers' efficacy. Under a 2C discharge, the observers, even when initialized with incorrect values, converge rapidly to true values. Using the UDDS drive cycle with a peak current of 6C, the observers effectively track voltages and correct initial errors, proving their robustness.

4.1 State Observer for the Electrolyte Lithium Concentration

This chapter is based on our journal publication:

Asif, Mian Mohammad Arsalan, and Federico Bribiesca-Argomedo. 2023. “Electrochemical State Observer Design for Li-Ion Batteries With Heterogenous Electrode Lithiation.” IEEE Control Systems Letters 7: 3199-3204.

<https://doi.org/10.1109/LCSYS.2023.3304248>.

In the aforementioned publication, we emphasized the significance of real-time reconstruction of electrochemical state information for achieving high-fidelity monitoring and optimal performance in advanced battery management systems. We introduced a Partial Differential Equation (PDE) based observer tailored for a simplified Doyle-Fuller-Newman electrochemical model of a Li-ion battery. This observer is designed to reconstruct the internal states of the battery using current and voltage measurements. Furthermore, we explored the potential benefits of integrating new sensor technologies within the battery cell, with a specific focus on the utilization of reference electrode and fiber-optic sensors. The stability of the observer components was rigorously analyzed using Lyapunov techniques. Through simulation results, we demonstrated the observer’s capability in spatially tracking the electrochemical states of the original system. Additionally, we assessed the robustness of the observer in the presence of noise in input measurements.

In this chapter, we delve deeper into the derivation of the observer and provide a more comprehensive discussion of its contributions and implications. Note that from henceforth, for the sake of notational simplicity and to streamline subsequent analyses, we represent De^{eff} as D_e .

In this section, we will discuss the construction and stability analysis of the state observer for 1) c_e in the electrolyte, and 2) c_s^\pm in the electrode domains, including new measurements available from a reference electrode and a potential Li concentration sensor [5].

The process of observing the state of the electrolyte lithium concentration is a crucial aspect in understanding the behavior of lithium-ion batteries. This observation is particularly significant when considering the diffusion of lithium ions within the electrolyte. To derive

the observer for the electrolyte concentration, certain assumptions are made to simplify the complex nature of the system.

4.1.1 Assumptions

Assumption 6. *The diffusion coefficient, denoted as D_e , is considered to be constant in time and uniformly bounded in the spatial variable x . This means that there exists a minimum positive value, \underline{D}_e , and a maximum value, \overline{D}_e , such that for any concentration c_e^j , the diffusion coefficient lies between these two bounds. In the remainder of the Chapter, we will consider D_e as a function of spatial variable x [5].*

Assumption 7. *A measurement of the lithium concentration in the electrolyte, denoted as $c_e(x_r, t)$, is available at a specific point in the separator, x_r . This assumption is crucial as it provides a reference point for the observer. By having a known concentration at a specific location, it becomes feasible to estimate the concentration in other parts of the system [5].*

Assumption 8. *The spatial profile of molar ionic fluxes, represented by $j_n^\pm(x, t)$, is assumed to be accurately predicted by the model without any need for correction. This implies that the ionic current profile, $i_e^\pm(x, t)$, is known. This assumption decouples the stability analysis of the electrolyte observer from that of the electrode observer. However, it's worth noting that this is a limitation of the current design. The stability of the interconnected system is only demonstrated in simulation results. This limitation is not unique to this approach; other methodologies in the literature, such as the one cited as [21], also make similar assumptions [5].*

While these sensors may not be commonly found in current Li-ion cells, they are actively researched. In particular, this work is part of the ongoing European INSTABAT project [28, 205], which focuses on the development of new sensor technologies, including these two specific sensors. The choice of these assumptions was driven by the sensors expected to be developed in the course of this project (and integrated into a Proof-of-Concept platform). The main objective of the current work is to prepare adequate algorithms to exploit signals coming from these sensors and integrate them into the BMS system. This is a necessary step for any techno-economic feasibility study of the sensors. Several works demonstrate

the existing research of these sensors [214–218]. This helps substantiate the feasibility of Assumption 7 and the upcoming Assumption 9. More precisely, one of the newest sensing technologies currently under development uses optical sensors to reconstruct the lithium concentration [214].

4.1.2 Model Simplification

In the context of the Doyle-Fuller-Newman (DFN) model, the electrolyte diffusion equation plays a pivotal role in characterizing the behavior of lithium-ion batteries. To facilitate a more tractable analysis and further investigations, it is often beneficial to derive a simplified representation of this equation [5].

Given the equation (3.2) and under the constraints imposed by Assumption 6, we can derive a more concise expression for the electrolyte diffusion. This derivation aims to retain the essential characteristics of the system while reducing its complexity for analytical purposes.

$$\epsilon_e^j c_{e,t}^j(x, t) = \frac{\partial}{\partial x} \left[D_e(x) c_{e,x}^j(x, t) + \frac{(1 - t_c^0)}{F} i_e^j(x, t) \right] \quad (4.1)$$

It is worth noting that the boundary conditions corresponding to this equation remain analogous to those of the original model.

It is crucial to understand that while simplifications are made for analytical convenience, care is taken to ensure that the essence and critical dynamics of the original system are preserved. This refined model serves as a foundation for further studies and investigations into the intricate behaviors of lithium-ion batteries.

4.1.3 Formulation of the Electrolyte Concentration Observer

The study of lithium-ion batteries, especially in the context of the Doyle-Fuller-Newman (DFN) model, necessitates the development of tools and methodologies to monitor and predict their behavior. One such tool is the observer, which allows for the estimation of system states based on available measurements and a mathematical model of the system.

Building upon the foundation laid by the simplified electrolyte diffusion equation, as articulated in Equation (4.1), we endeavor to design an observer that capitalizes on the electrolyte concentration measurements at the reference electrode. This approach is motivated by the potential benefits of having real-time estimates of the electrolyte concentration, which can be instrumental in optimizing battery performance and longevity.

Incorporating Assumption 7, the formulation of the electrolyte concentration observer is enriched by introducing an error injection term ($P[c_e(x_r, t) - \hat{c}_e(x_r, t)]$) into the diffusion equation. This term serves to account for discrepancies between the actual and estimated states, thereby enhancing the accuracy of the observer.

$$\begin{aligned} \epsilon_e^j \hat{c}_{e,t}^j(x, t) = & \frac{\partial}{\partial x} \left[D_e(x) \hat{c}_{e,x}^j(x, t) + \frac{1 - t_c^0}{F} i_e^j(x, t) \right] \\ & - P [c_e(x_r, t) - \hat{c}_e(x_r, t)] \end{aligned} \quad (4.2)$$

where $x_r \in [0^{sep}, l^{sep}]$ denotes the spatial location of the reference electrode.

To further elucidate the performance of the observer, we define the error system as the disparity between the physical system, represented by (3.2), and the observer system depicted in (4.2). Let $u(x) \doteq c_e(x, t) - \hat{c}_e(x, t)$ be the error in the electrolyte concentration estimation. Under Assumptions 6 and 7, the diffusion equation governing the dynamics of this error system can be articulated as:

$$\epsilon_e^j u_t(x) = [D_e(x) u_x(x)]_x + P u(x_r) \quad (4.3)$$

This equation is accompanied by boundary conditions that mirror those of the original system, as delineated in Section 3.3.

For the sake of analytical tractability and notational brevity, we have opted to suppress the explicit time-dependence of the variables $u(x)$. However, it is imperative to recognize that these variables, along with their derivatives, are intrinsically time-dependent, and this temporal aspect plays a significant role in the dynamics of the system.

4.1.4 Stability Analysis

A critical aspect of any observer design is ensuring its stability. For the given system, a proposition is presented that establishes the conditions under which the error system is stable [5].

Proposition 1. $\forall P < 0$, the origin of the error system in (4.3) is exponentially stable in the $H_1(0, L^T)$ norm if Assumptions 6 - 8 hold [5].

Proof. Let us define a candidate Lyapunov function $V_T = V_1 + \beta V_2$ where

$$\begin{aligned} V_1(u(\cdot, t)) &\doteq \frac{1}{2} \int_0^{L^T} \epsilon_e u^2(x) dx, \\ V_2(u(\cdot, t)) &\doteq \frac{1}{2} \int_0^{L^T} [\epsilon_e D_e(x) u_x^2(x)] dx, \end{aligned} \tag{4.4}$$

$\epsilon_e > 0$ varies with regions $j \in \{-, sep, +\}$, and $\beta > 0$ is chosen later. Also, from Assumption 6, $D_e \geq \underline{D}_e \geq 0$ and, therefore there exists a positive constant α_V such that $V_T \geq \alpha_V \|u\|_{H_1(0, L^T)}^2$. By differentiating V_1 with respect to time and using the error system equations, the time derivative is obtained:

$$\dot{V}_1 = \int_0^{L^T} \epsilon_e u_t(x) u(x) dx$$

By substituting Equation (4.3) into the integral on the right-hand side of the equation, we obtain:

$$\dot{V}_1 = \int_0^{L^T} \frac{\partial}{\partial x} [D_e(x) u_x(x)] u(x) dx + \int_0^{L^T} P u(x_r) u(x) dx \tag{4.5}$$

Integration by parts on the first term on the right-hand side can be performed to give:

$$\begin{aligned} \dot{V}_1 &= - \int_0^{L^T} D_e(x) u_x^2(x) dx + \int_0^{L^T} P u(x_r) u(x) dx \\ &\leq -\underline{D}_e \left[\int_0^{x_r} u_x^2(x) dx + \int_{x_r}^{L^T} u_x^2(x) dx \right] + \int_0^{L^T} P u(x_r) u(x) dx \end{aligned}$$

Lets us now define for the negative domain, the following relationship through integration

by parts:

$$\int_0^{x_r} u^2(x)dx = u^2(x_r)x_r - 2 \int_0^{x_r} xu(x)u_x(x)dx$$

Using Young's Inequality, the right-hand side of the equation becomes:

$$\begin{aligned} \int_0^{x_r} u^2(x)dx &\leq u^2(x_r)x_r + A_1 \int_0^{x_r} xu^2(x)dx + \frac{1}{A_1} \int_0^{x_r} xu_x^2(x)dx \\ &\leq x_r \left[u^2(x_r) + A_1 \int_0^{x_r} u^2(x)dx + \frac{1}{A_1} \int_0^{x_r} u_x^2(x)dx \right] \end{aligned}$$

for any $A_1 > 0$. Rearranging the above inequality and writing $x_r \leq M_A$ where $M_A = \max\{x_r, L^T - x_r\}$ yields:

$$- \int_0^{x_r} u_x^2(x)dx \leq A_1 u^2(x_r) + \frac{A_1^2 M_A - A_1}{M_A} \int_0^{x_r} u^2(x)dx \quad (4.6)$$

Following a similar process on the positive domain yields:

$$- \int_{x_r}^{L^T} u_x^2 dx \leq A_2 u^2(x_r) + \frac{A_2^2 (M_A) - A_2}{M_A} \int_{x_r}^{L^T} u^2 dx \quad (4.7)$$

for any $A_2 > 0$. Now adding (4.6) and (4.7), defining $A \doteq A_1 = A_2 > 0$, and then rearranging the inequality yields

$$- \int_0^{L^T} u_x^2 dx \leq - \left[\frac{A - A^2 M_A}{M_A} \right] \int_0^{L^T} u^2 dx + 2A u^2(x_r) \quad (4.8)$$

We choose $A \in (0, 1/M_A)$ to ensure that $(A - A^2 M_A) > 0$. By utilizing equation (4.8) with $V_1(t) \leq (\bar{\epsilon}_e/2) \int_0^{L^T} u^2(x)dx$, the resulting expression for \dot{V}_1 is:

$$\begin{aligned} \dot{V}_1 &\leq - \underline{D}_e \kappa_A \int_0^{L^T} u^2(x)dx + 2\underline{D}_e A u^2(x_r) + \int_0^{L^T} P u(x_r) u(x) dx \\ &\leq - \frac{2\underline{D}_e}{\bar{\epsilon}_e} \kappa_A V_1 + 2\underline{D}_e A u^2(x_r) + \int_0^{L^T} P u(x_r) u(x) dx \end{aligned}$$

where $\kappa_A = (A - A^2 M_A)/M_A$, and $\bar{\epsilon}_e$ is the maximum value of ϵ_e . Using the following

relationships:

$$\begin{aligned}\int_{x_r}^{L^T} Pu(x_r)u(x)dx &= Pu(x_r) \left[[L^T - x_r]u(x_r) + \int_{x_r}^{L^T} \int_{x_r}^x u_x(s)dsdx \right] \\ \int_0^{x_r} Pu(x_r)u(x)dx &= Pu(x_r) \left[x_ru(x_r) + \int_0^{x_r} \int_{x_r}^x u_x(s)dsdx \right]\end{aligned}$$

on the last term on the right-hand side of the inequality, the candidate Lyapunov function V_1 can be expressed as

$$\begin{aligned}\dot{V}_1 &\leq -\frac{2\underline{D}_e}{\bar{\epsilon}_e}\kappa_A V_1 + 2\underline{D}_e Au^2(x_r) + Pu^2(x_r)(L^T) \\ &\quad + \int_0^{L^T} Pu(x_r) \int_{x_r}^x u_x(s)dsdx\end{aligned}$$

By employing Young's and Cauchy-Schwarz Inequalities on the fourth term of the right-hand side of the above inequality, we obtain

$$\begin{aligned}\dot{V}_1 &\leq -\frac{2\underline{D}_e}{\bar{\epsilon}_e}\kappa_B V_1(t) + \frac{L^T}{2\gamma}|x - x_r| \int_{\min\{x_r, x\}}^{\max\{x_r, x\}} u_x^2(s)ds \\ &\quad + u^2(x_r) \left[2\underline{D}_e A + PL^T + \frac{P^2 L^T}{2}\gamma \right]\end{aligned}$$

where $\gamma > 0$. We now bound the integral and absolute coefficient of the second term on the right-hand side with the interval $[0, L^T]$ to obtain

$$\begin{aligned}\dot{V}_1 &\leq -\frac{2\underline{D}_e}{\bar{\epsilon}_e}\kappa_B V_1(t) + \frac{(L^T)^2}{2\gamma} \int_0^{L^T} u_x^2(x)dx \\ &\quad + u^2(x_r) \left[2\underline{D}_e A + PL^T + \frac{P^2 L^T}{2}\gamma \right]\end{aligned}$$

We now differentiate V_2 with respect to time and utilize the expression in (4.3) to obtain:

$$\dot{V}_2 = \int_0^{L^T} (D_e(x)u_x(x) [D_e(x)u_x(x)]_{xx}) dx$$

Integration by parts on the right-hand side can be performed to yield:

$$\dot{V}_2 = - \int_0^{L^T} \frac{\partial}{\partial x} [D_e(x)u_x(x)]^2 dx$$

Utilizing Poincare's Inequality, writing the term on the right-hand side of the inequality as the sum of two elements, and introducing the inequality $V_2(t) \leq (\bar{\epsilon}_e/2) \int_0^{L^T} D_e(x)u_x^2 dx$, allows us to rewrite the above inequality as

$$\begin{aligned} \dot{V}_2 &\leq -\frac{\alpha}{4L^{T^2}} \underline{D}_e^2 \int_0^{L^T} u_x^2(x) dx - \frac{1-\alpha}{4L^{T^2}} \underline{D}_e \int_0^{L^T} D_e(x)u_x^2(x) dx \\ &\leq -\frac{\alpha}{4L^{T^2}} \underline{D}_e^2 \int_0^{L^T} u_x^2(x) dx - \frac{1-\alpha}{2\bar{\epsilon}_e L^{T^2}} \underline{D}_e V_2 \end{aligned}$$

where $0 < \alpha < 1$. We can now write the Lyapunov function V_T and its time derivative as

$$\begin{aligned} V_T(t) &= V_1(t) + \beta V_2(t) \\ \dot{V}_T(t) &= \dot{V}_1(t) + \beta \dot{V}_2(t) \\ &\leq -\frac{2\underline{D}_e}{\bar{\epsilon}_e} \kappa_A V_1(t) + \left[\frac{L^{T^2}}{2\gamma} - \frac{\alpha \underline{D}_e^2}{4L^{T^2}} \beta \right] \int_0^{L^T} u_x^2(x) dx \\ &\quad - \frac{1-\alpha}{2\bar{\epsilon}_e L^{T^2}} \beta \underline{D}_e V_2(t) + u^2(x_r) \left[2\underline{D}_e A + PL^T \left(1 + \frac{P}{2} \gamma \right) \right] \\ &\leq -\frac{\underline{D}_e}{\bar{\epsilon}_e} \min \left\{ 2\kappa_A, \frac{1-\alpha}{2L^{T^2}} \right\} V_T(t) + \left[\frac{L^{T^2}}{2\gamma} - \frac{\alpha \underline{D}_e^2}{4L^{T^2}} \beta \right] \\ &\quad \times \int_0^{L^T} u_x^2(x) dx + u^2(x_r) \left[2\underline{D}_e A + PL^T + \frac{P^2 L^T}{2} \gamma \right] \end{aligned}$$

In order to guarantee the exponential stability of the solution, it is necessary to satisfy the following constraints:

$$\begin{aligned} 2L^{T^4} - \alpha \underline{D}_e^2 \beta \gamma &\leq 0, \\ 4\underline{D}_e A + 2PL^T + P^2 L^T \gamma &\leq 0. \end{aligned} \tag{4.9}$$

With the choice of parameters:

$$\gamma = -\frac{1}{P},$$

$$0 < A \leq \min \left\{ \frac{L^T}{4\gamma \underline{D}_e}, \frac{1}{M_A} \right\},$$

$$\beta \geq \frac{2(L^T)^4}{\gamma \alpha \underline{D}_e^2},$$

the constraints in (4.9) are satisfied. This proves the exponential stability of the electrolyte state observer system. □

4.2 State observer for the solid lithium concentration using voltage error injection

4.2.1 Assumptions

In this subsection, we delve into the intricacies of constructing state observers for solid electrodes, leveraging the voltage available at the reference electrode [5]. The foundation of this construction is built upon the following assumptions:

Assumption 9. *A voltage measurement at a reference electrode $V_{ref}(t)$ is available. This allows for independent estimations of OCV potentials U^\pm for each electrode [5].*

Assumption 10. *The OCV curve of the electrodes U^\pm is assumed to be uniformly monotonically decreasing in such a way that, defining $f(a, b) \doteq U(a) - U(a - b)$, the following property is satisfied:*

$$\exists k_1, k_2 < 0 \text{ s.t. } \forall a, b \quad k_1 b^2 \leq f(a, b)b \leq k_2 b^2 \quad (4.10)$$

Note that the proofs can be adapted without problem if the function is monotonically increasing, requiring only a change of sign in the feedback gain [5].

4.2.2 Observer Formulation

Using Assumption 9, the solid-phase lithium concentration observer is formulated by injecting the voltage error term [5]:

$$\begin{aligned} \hat{c}_{s,t}^\pm(x, r, t) &= \frac{1}{r^2} \frac{\partial}{\partial r} [D_s^\pm r^2 \hat{c}_{s,r}^\pm] \\ \hat{c}_{s,r}^\pm(x, 0, t) &= 0 \\ \hat{c}_{s,r}^\pm(x, R_s^-, t) &= -\frac{j_n^\pm(x, t)}{D_s^\pm} \\ &\quad - g_0^\pm [U(c_{ss}^\pm(x, t)) - U(\hat{c}_{ss}^\pm(x, t))] \end{aligned} \quad (4.11)$$

where $c_{ss}^\pm(x, t) \doteq c_s^\pm(x, R_s^\pm, t)$. Let us define the error system as the physical system represented by (3.1) and (3.11) minus the observer system (4.11), once again using Assumption

8 to decouple the stability analysis of both observers:

$$z_t(r, t) = \frac{1}{r^2} \frac{\partial}{\partial r} [D_s r^2 z_r(r, t)]$$

$$z_r(R_s^\pm, t) = g_0 [U(\bar{z}(R_s^\pm, t)) - U(\hat{z}(R_s^\pm, t))], \quad z_r(0, t) = 0.$$

where $z(r, t) \doteq c_s^\pm(x, r, t) - \hat{c}_s^\pm(x, r, t)$, $\hat{z} \doteq \hat{c}_s^\pm(x, r, t)$, $\bar{z} \doteq c_s^\pm(x, r, t)$, and the dependence on x has been suppressed [5]. To arrive at this error injection term, at particular points x^\pm , the voltage equations in (3.38) are used to write [5]:

$$U(\hat{c}_{ss}^-(x^-, t)) = -\hat{V}_{ref}(t) + \hat{\phi}_e(x^r, t) - \hat{\phi}_e(x^-, t)$$

$$- FR_f^- \hat{j}_n^-(x^-, t) - \hat{\eta}^-(x^-, t) + \hat{\phi}_s^-(x^-, t)$$

$$U(\hat{c}_{ss}^+(x^+, t)) = \hat{V}(t) - \hat{V}_{ref}(t) - \hat{\phi}_e(x^+, t) + \hat{\phi}_e(x^r, t) - \hat{\phi}_s^+(L^T, t)$$

$$+ \hat{\phi}_s^+(x^+, t) + FR_f^+ \hat{j}_n^+(x^+, t) + \hat{\eta}^+(x^+, t)$$
(4.12)

Assumption 8 implies in particular that ϕ_s^\pm and j_n^\pm are identical in both the estimated and real systems, and since the electrolyte subsystem observer converges exponentially to the actual value, we approximate the terms necessary for the error injection term using the measured voltages as follows [5]:

$$U(c_{ss}^-(x^-, t)) - U(\hat{c}_{ss}^-(x^-, t)) \approx V_{ref}(t) - \hat{V}_{ref}(t)$$

$$U(c_{ss}^+(x^+, t)) - U(\hat{c}_{ss}^+(x^+, t)) \approx [V(t) - V_{ref}(t)] - [\hat{V}(t) - \hat{V}_{ref}(t)]$$
(4.13)

Using Assumption 10, we can express the error system in a compact form as:

$$z_t(r, t) = \frac{1}{r^2} \frac{\partial}{\partial r} [D_s r^2 z_r(r, t)]$$

$$z_r(R_s^\pm, t) = g_0 f(\bar{z}(R_s^\pm, t), z(R_s^\pm, t)), \quad z_r(0, t) = 0$$

The radial coordinates are now transformed via normalization with the scaled value of R_s^\pm such that $\bar{r} = r/R_s^\pm$. This simplifies the notation by allowing us to drop the bars over the

radial coordinates, resulting in the final expression for the error system [5]:

$$z_t(r, t) = \frac{1}{R_s^2 r^2} \frac{\partial}{\partial r} [D_s r^2 z_r(r, t)] \quad (4.14)$$

$$z_r(1, t) = R_s g_0 f(\bar{z}(1, t), z(1, t)), \quad z_r(0, t) = 0 \quad (4.15)$$

4.2.3 Stability Analysis

The proof commences with the definition of a candidate Lyapunov function. The time derivative of this function is computed, and by employing integration by parts and substituting appropriate expressions, we derive certain inequalities [5]. Utilizing the properties from Assumption 10, we further refine these inequalities. The choice of boundary gain ensures the negative definiteness of the time derivative of the Lyapunov function, thereby establishing the exponential stability of the electrode observers. The detailed mathematical manipulations and transformations are presented in the proposition and its proof below .

Proposition 2. *For $\alpha \in (0, 1)$, let g_0 be chosen such that $0 < g_0 \leq -3/[2k_2\alpha R_s]$ with k_2 defined in Assumption 10, then the origin of the error system given by Equations (4.14)-(4.15) is exponentially stable in the $L^2(S)$ norm, where $S = \{r \in \mathbb{R}^3 \mid \|r\| \leq 1\}$ if Assumptions 8 - 10 hold [5].*

Proof. Let us define a candidate Lyapunov function [5]:

$$V_s = \frac{1}{2} \int_0^1 \frac{R_s^2}{D_s} r^2 z^2(r, t) dr$$

There exists some positive constant $\alpha_{V_s} > 0$ such that $V_s \geq \alpha_{V_s} \|z\|_{L^2(S)}^2$. We now compute the time derivative

$$\dot{V}_s = \int_0^1 \frac{\partial}{\partial r} [r^2 z_r(r, t)] z(r, t) dr$$

By expanding the right-hand side of the equation, utilizing the method of integration by

parts, and substituting $z_r(1, t)$ with the expression in Equation (4.15), we obtain:

$$\dot{V}_s = z(1, t)R_s g_0 f(\bar{z}(1, t), z(1, t)) - \int_0^1 r^2 z_r^2(r, t) dr$$

Using the properties defined in Assumption 10, we are able to write:

$$\dot{V}_s \leq k_2 R_s g_0 z^2(1, t) - \int_0^1 r^2 z_r^2(r, t) dr$$

Since k_2 is negative, we define a strictly positive constant $k_s = -k_2 R_s g_0$ such that $g_0 > 0$.

We then split the first term on the right-hand side of the inequality into two parts to obtain:

$$\dot{V}_s \leq k_s [-\alpha z^2(1, t) - (1 - \alpha)z^2(1, t)] - \int_0^1 r^2 z_r^2(r, t) dr. \quad (4.16)$$

where $0 < \alpha < 1$. Let us now manipulate the term $-k_s \alpha z^2(1, t)$ through a change of variables:

$$\begin{aligned} w(r, t) &= z(r, t)r \\ w_r(r, t) &= z(r, t) + rz_r(r, t) \end{aligned}$$

which allows us to write $-z^2(1, t) = -w^2(1, t)$. We can now use Poincaré's Inequality to write

$$\begin{aligned} -z^2(1, t) &\leq -\frac{1}{2} \int_0^1 w^2(r, t) dr + 2 \int_0^1 w_r^2(r, t) dr \\ &\leq -\frac{D_s V_s}{R_s^2} + 2 \int_0^1 (z(r, t) + rz_r(r, t))^2 dr \end{aligned}$$

Through integration by parts, $\int_0^1 (2rz(r, t)z_r(r, t)) dr = z^2(1, t) - \int_0^1 z^2(r, t) dr$, which allows us to write

$$-z^2(1, t) \leq -\frac{D_s V_s}{3R_s^2} + \frac{2}{3} \int_0^1 r^2 z_r^2(r, t) dr \quad (4.17)$$

As the coefficient $k_s \alpha$ is strictly positive, we substitute the result of the inequality (4.17)

into the main Lyapunov inequality (4.16), and combine common terms to write:

$$\dot{V}_s \leq -k_s \frac{\alpha D_s}{3R_s^2} V_s + \left[\frac{2k_s \alpha}{3} - 1 \right] \int_0^1 r^2 z_r^2(r, t) dr - (1 - \alpha) k_s z^2(1, t)$$

With the choice of boundary gain $0 < g_0 \leq -3/[2k_2 \alpha R_s]$, the time derivative of the candidate Lyapunov function is negative definite which proves the exponential stability of the electrode observers. Using the maximum value of g_0 , we can further simplify the inequality to:

$$\dot{V}_s \leq -\frac{D_s}{2R_s^2} V_s - \frac{3(1 - \alpha)}{2\alpha} z^2(1, t)$$

□

The proposed electrode observers are non-conservative; they do not conserve the total amount of lithium in the electrodes. They are used in conjunction with the conservative observer proposed in [21] at a larger time scale. This enables the observer system to gradually correct an error in solid-phase lithium over time. The overall structure of the combined PDE-based observers for the electrolyte and electrode lithium concentrations is illustrated in Figure 4.1.

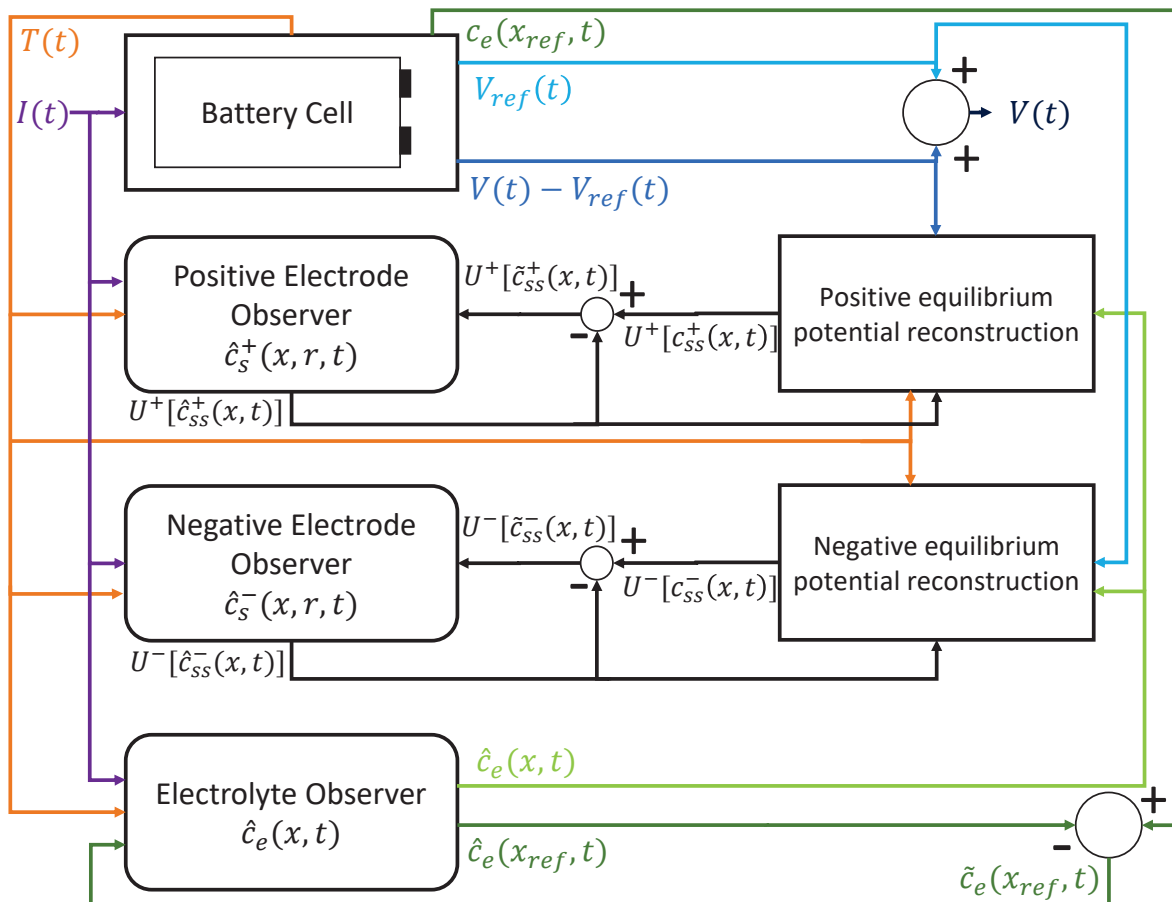


Figure 4.1: Observer structure with voltage error injection from [5]

4.3 Validation of the observers with simulation results

In this section, a comprehensive simulation analysis using a finite volume based simplified DFN model is conducted to evaluate the efficacy of the proposed observers for the electrolyte and electrodes.

Note that, for observer validation, an initial configuration is employed wherein the observer gain is set to a high value. This deliberate choice is made with the objective of facilitating rapid convergence of the system to its actual states, with a specific focus on $c_{ss}(x, t)$, a key determinant of output voltages. Following the initialization phase, characterized by the time until application of current in the simulation, the observer gains are reduced by a magnitude of 10. This strategic adjustment is intended to diminish the influence of observer injection on the intricate internal diffusion processes within the solid particle layers, thereby promoting a more ‘natural’ emulation of the system.

4.3.1 Constant Discharge Scenario at 2C Current

To assess the efficacy of the two observers under a constant current scenario, a 2C discharge is employed. The data provided to the observers encompass voltage measurements at the reference electrode and the collectors, current, and temperature. The observers are initialized with incorrect values of SOC and total moles of lithium in the solid and electrolyte phases, 5% and 25%, respectively. It’s worth noting that a time step of one second was used in the computation of these results, and higher precision can be achieved with finer discretizations.

A constant current profile for the 2C discharge cycle is used with a step at $t = 100$ seconds. The constant 2C current is a typical scenario for many applications, and it serves as a benchmark for evaluating the observer’s performance.

Figure 4.3(a) and 4.3(b) showcase that the Voltage Error Injection (VEI) observer rapidly converges to the true voltages of the positive and negative domains, with the RMS of the error presented in Table 4.1. The overall voltage is the summation of the two plots.

| error (mV) | $V_{2C}(t)$ | $V_{ref,2C}(t)$ | $V_{2C}(t) - V_{ref,2C}(t)$ |
|------------|-------------|-----------------|-----------------------------|
| VEI | 0.344 | 0.1149 | 0.4149 |

Table 4.1: RMS error of the voltages for 2C scenario

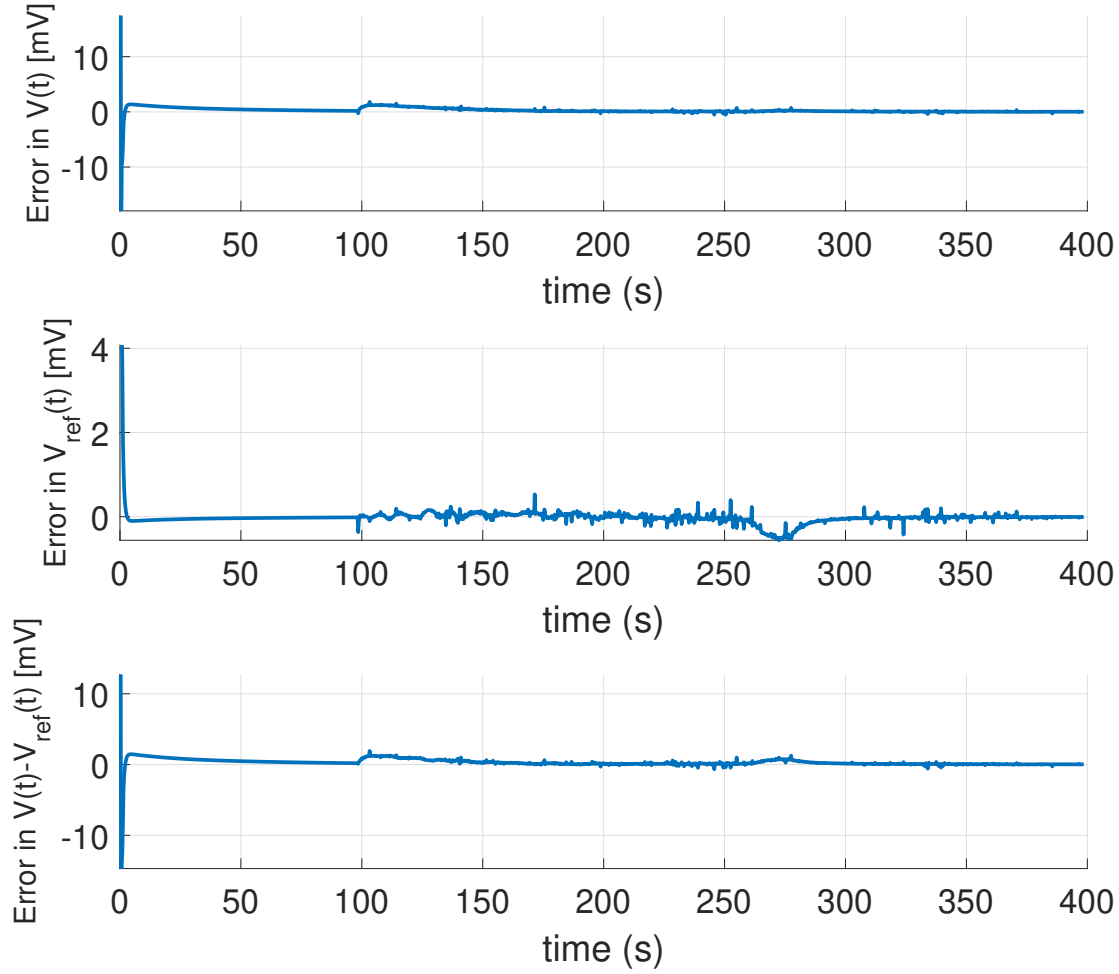


Figure 4.2: Error in Voltages with the 2C constant discharge

The observer promptly tracks $c_{ss,2C}^{\pm}(x, t)$ and rectifies the initial error in total moles of lithium in the solid phase $N_{Ls,2C}$, as indicated in Table 4.2. The error in $c_{ss,2C}^{\pm}(x, t)$ is spatially averaged.

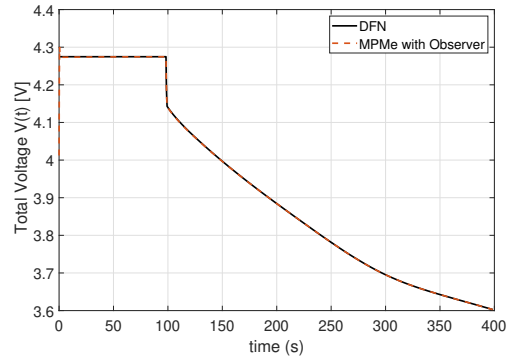
| error (%) | $c_{ss,2C}^{-}$ | $c_{ss,2C}^{+}$ | $N_{Ls,2C}$ |
|-----------|-----------------|-----------------|-------------|
| VEI | 0.3010 | 0.2340 | 0.0041 |

Table 4.2: RMS value of percentage errors in $c_{ss,2C}^{\pm}$ and $N_{Ls,2C}$

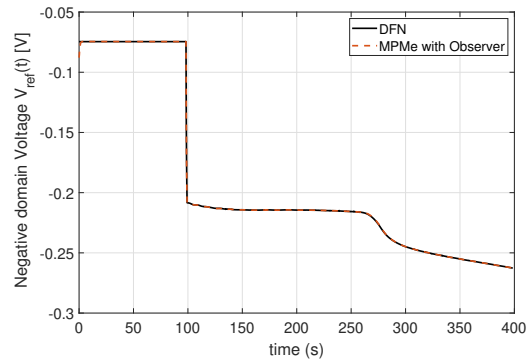
The convergence of the electrolyte observer under the 2C scenario is also noteworthy. After an initialization period of 100 seconds, the observer rapidly converges to the actual value and total moles of lithium in the electrolyte ($N_{Le,2C}$), with an RMS percentage error

of only 0.0265 and 0.0366, respectively. This further underscores the reliability and precision of the proposed electrolyte observer in tracking the system's state under a constant current scenario.

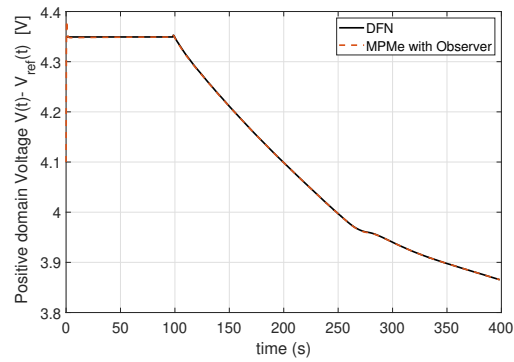
Note that the reasons for the overshoot of the observers include the initial higher gain and the time discretization. A finer temporal discretization would result in reduced overshoots and increased accuracy of results at the exchange of computational cost.



(a) $V(t)$



(a) $V_{ref.2C}(t)$



(b) $V_{2C}(t) - V_{ref.2C}(t)$

Figure 4.3: Voltages with the 2C constant discharge

4.3.2 Electric Vehicle charge/discharge cycle

To evaluate the performance of the two observers under varying operating conditions, the UDDS drive cycle which features a peak current of 6C is utilized [5]. The data provided to the observers include the voltage readings at the reference electrode and the collectors, current, and temperature. The observers are initialized with incorrect values of SOC and total moles of lithium in the solid and electrolyte phases, 5% and 25%, respectively. Note that a time step of one second was used in the computation of these results and higher accuracy can be achieved with smaller discretizations.

Figure 4.4 depicts the current profile of the UDDS drive cycle. The peak of 6-C is higher than those reported in previous studies, which demonstrates the performance of the observer in extreme conditions. Figure 4.5(b) and 4.5(c) demonstrate that the Voltage Error Injection

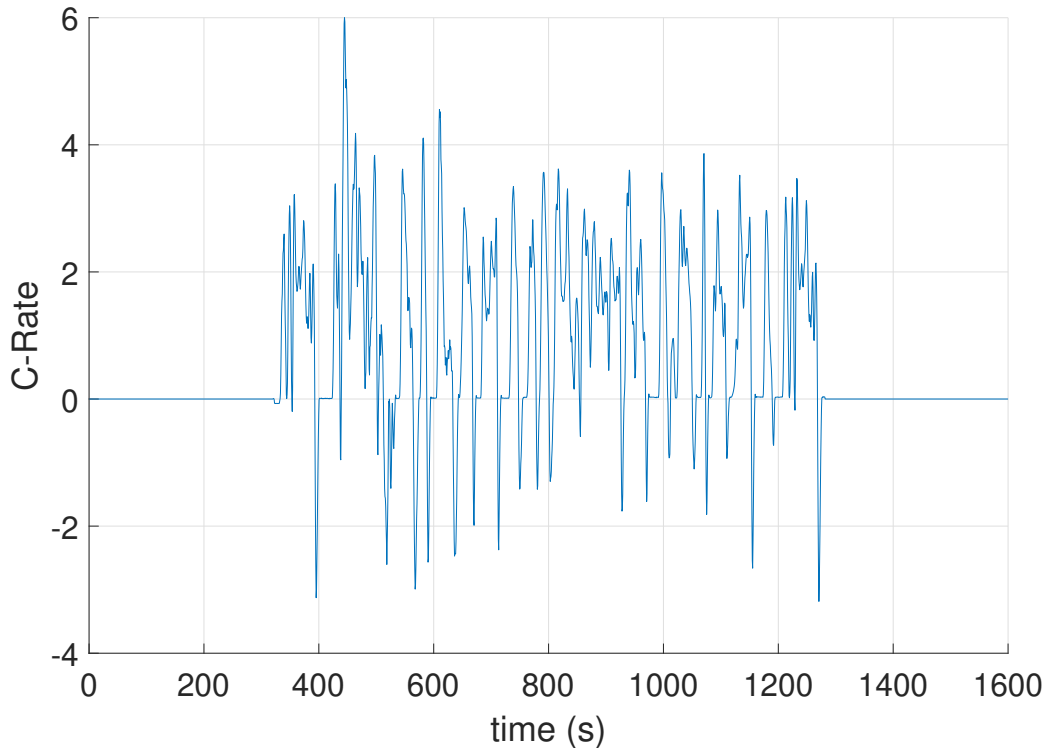


Figure 4.4: Current profile of the UDDS cycle from [5]

(VEI) observer quickly converges to the true voltages of the positive and negative domains with RMS of the error shown in Table 4.3. The total voltage is the sum of the two plots. This result is an improvement of the result in [21], wherein the utilization of a 4C UDDS current

yielded an RMS error of 7.4 mV. The observer quickly tracks $c_{ss}^{\pm}(x, t)$ and corrects the initial

| error (mV) | $V(t)$ | $V_{ref}(t)$ | $V(t) - V_{ref}(t)$ |
|------------------|---------|--------------|---------------------|
| VEI | 5.4502 | 3.0438 | 2.8405 |
| VEI (5mV noise) | 6.9501 | 4.1694 | 4.2133 |
| VEI (10mV noise) | 10.0511 | 6.5705 | 6.7245 |

Table 4.3: RMS error of the voltages from [5]

error in total moles of lithium in the solid phase N_{L_s} as shown in Table 4.4. Note that the error in $c_{ss}^{\pm}(x, t)$ is spatially averaged [5]. Figure 4.6 displays the normalised $c_s^{\pm}(x, r, t)$ and $z^{\pm}(x, r, t)$, the corresponding error in $c_s^{\pm}(x, r, t)$, at two different time instances: $t_0 = 0$ and $t^* = 594$ seconds, where the current reaches its maximum during the simulation. This figure shows that the observer system is able to estimate the original system on a spatial level [5].

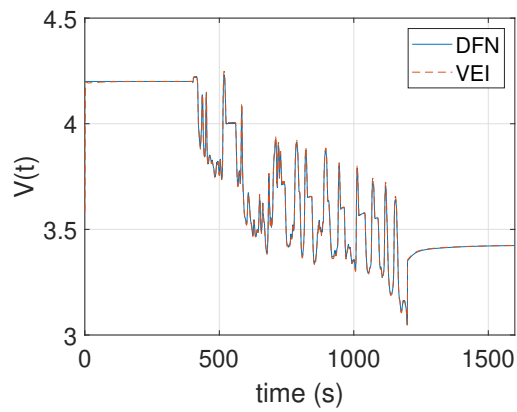
Under the same initial conditions, the robustness of the observer is now tested against voltage noise at the three measurement points of measurement: both collectors and the reference electrode. VEI (5mV noise) signifies a cumulative voltage noise level of 15mV. The RMS values of the voltage and spatially averaged error in $c_{ss}^{\pm}(x, t)$ are presented in Tables 4.3 and 4.4, respectively. The observer is able to handle large noise in measurement with little loss in accuracy.

| error (%) | c_{ss}^- | c_{ss}^+ | N_{L_s} |
|------------------|------------|------------|-----------|
| VEI | 0.4717 | 0.3346 | 0.0089 |
| VEI (5mV noise) | 0.4673 | 0.3424 | 0.1657 |
| VEI (10mV noise) | 0.5275 | 0.3791 | 0.2067 |

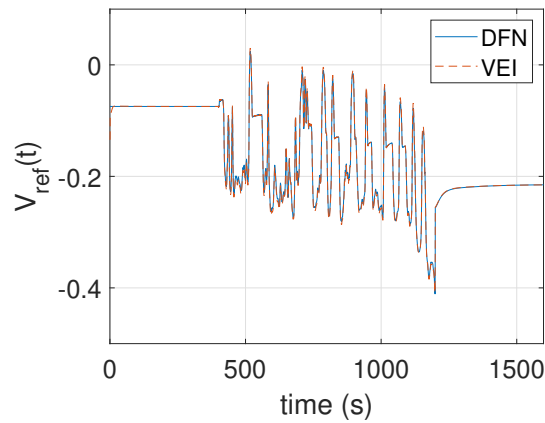
Table 4.4: RMS value of percentage errors in c_{ss}^{\pm} and N_{L_s} from [5]

The convergence of the electrolyte observer is now discussed. Simulation results show that after initialization of 200 seconds, the observer quickly converges to the actual value and total moles of lithium in the electrolyte (N_{L_e}) as shown in Figure 4.8, with an RMS percentage error of only 0.0269 and 0.0370, respectively. These results confirm the proposed electrolyte observer's reliability and accuracy in tracking the system's state [5].

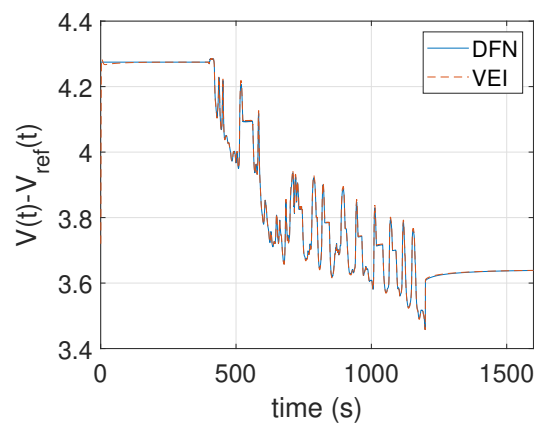
Again, note that the reasons for the overshoot of the observers include the initial higher gain and the time discretization. Hence, a finer temporal discretization would result in reduced overshoots and increased accuracy of results at the exchange of computational cost.



(a) Total Voltage



(b) $V_{ref}(t)$



(c) $V(t) - V_{ref}(t)$

Figure 4.5: Voltages with the UDDS Cycle from [5]

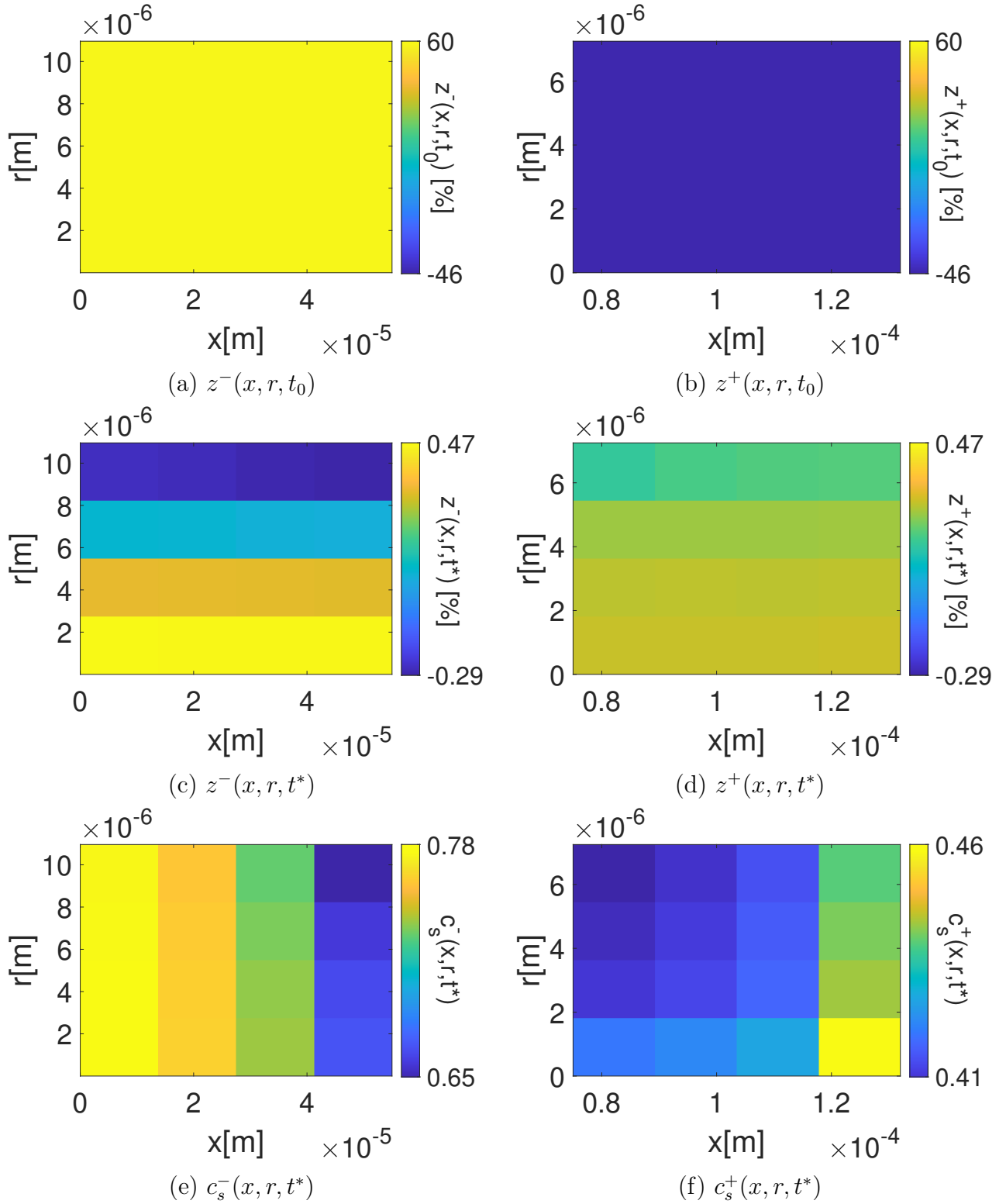


Figure 4.6: $c_s^\pm(x, r, t^*)$ and $z^\pm(x, r, t)$ from [5]

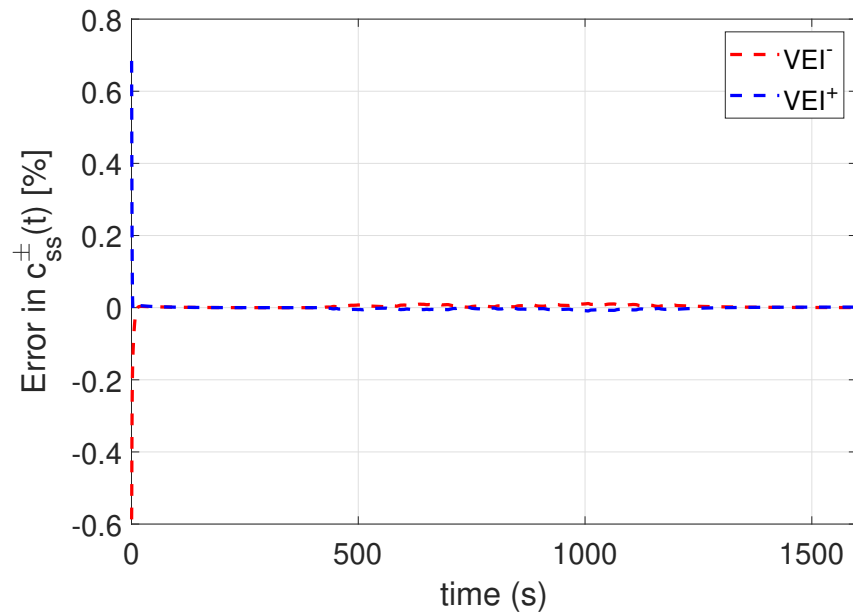


Figure 4.7: Error in estimation of c_{ss}^{\pm} for the UDDS cycle.

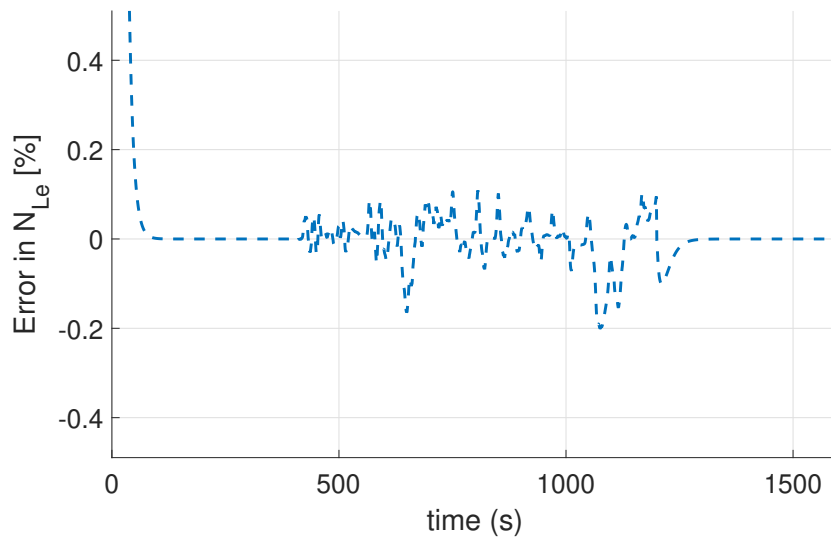


Figure 4.8: Error in N_{Le} for the UDDS cycle.

4.4 Conclusion of the Chapter

This chapter has delved into the development and validation of state observers for both electrolyte and solid lithium concentrations in battery systems, each with its unique formulation, assumptions, and stability analysis.

The observer for the electrolyte lithium concentration was formulated under certain assumptions and model simplifications. The stability analysis was conducted through the definition of a candidate Lyapunov function, and by employing integration by parts and substituting appropriate expressions, certain inequalities were derived. The choice of boundary gain ensured the negative definiteness of the time derivative of the Lyapunov function, establishing the exponential stability of the electrode observers.

The observer for the solid lithium concentration was developed with a focus on utilizing Voltage Error Injection (VEI) as a mechanism to enhance convergence to the true voltages of the positive and negative domains. Assumptions and model simplification were crucial in ensuring the negative definiteness of the time derivative of the Lyapunov function, thereby proving the exponential stability of the electrode observers [5]. The overall structure of the dual observers was proposed which showed the solid and electrolyte observers working in unison to track the internal states of the battery.

The observers were validated under various scenarios, including a 2C discharge and a UDDS profile, to evaluate their performance under different operating conditions. In the 2C discharge scenario, the observers were initialized with incorrect values of SOC and total moles of lithium in the solid and electrolyte phases, and yet, they demonstrated rapid convergence to the true voltages of the positive and negative domains, with minimal RMS error [5]. Under the UDDS profile, even with a peak current of 6C, the observers showcased robust performance, effectively tracking the system state and correcting initial errors in the total moles of lithium in both the solid and electrolyte phases. The observer system was able to estimate the original system on a spatial level, even under varying conditions, affirming its reliability and accuracy in tracking the system's state [5].

In summary, the developed observers have demonstrated robust and reliable performance in estimating the states of lithium concentrations in both the electrolyte and solid phases of

battery systems under various conditions and scenarios. This chapter has provided a solid foundation for further exploration and development of state observers in battery management systems, contributing to the overarching goal of enhancing the safety, reliability, and performance of battery systems in practical applications.

Chapter 5

Advanced BMS Predictions: Leveraging the Observer for State Estimations

Contents

| | | |
|------------|--|------------|
| 5.1 | Battery Management System Predictions | 148 |
| 5.2 | State of Charge Estimation | 151 |
| 5.3 | State of Health Estimation | 153 |
| 5.3.1 | Lithium Plating Management | 154 |
| 5.4 | State of Power | 156 |
| 5.5 | Conclusion of the Chapter | 158 |

Summary of the Chapter

This chapter delves into the advanced predictions made by Battery Management Systems (BMS) and the role of the observer in state estimations. The primary focus is on the key battery states: State of Charge (SOC), State of Health (SOH), State of Power (SOP), and the identification of Lithium Plating. The chapter elucidates the integration of the MPMe model and state observers with novel sensors to enhance the accuracy of BMS predictions. The proposed BMS algorithm's architecture is presented, emphasizing the synergy between various components. Detailed discussions on SOC and SOH estimations highlight their significance, methodologies, and the precision of the BMS algorithm. The phenomenon of lithium plating, its mechanism, implications, and management are explored in-depth, emphasizing its challenges and strategies for effective management. Lastly, the chapter presents the intricacies of SOP estimation, its importance, and the factors influencing its prediction.

5.1 Battery Management System Predictions

This chapter is derived from our work presented at the Battery 2030+ 3rd Annual Conference:

Asif, Mian Mohammad Arsalan, Federico Bribiesca-Argomedo, and Vincent Heiries. 2023. “Real time estimation of electrochemical states in Li-ion batteries and exploitation in BMS algorithms.” Presented at the Battery 2030+ 3rd Annual Conference.

In the referenced work [6], we introduced an electrochemical observer, drawing inspiration from [21], and juxtaposed it with a higher order discretization of the Doyle–Fuller–Newman Model as detailed in [50]. We further explored innovative approaches on how this observer can be harnessed by the latest BMS SOX indicators. Moving beyond the realm of enhanced SOC estimation, we integrated the physics-based model into an estimation algorithm specifically designed to determine the power capability of the battery cell. This integration is pivotal in ensuring that the battery operates within its safe regions, thereby preventing any potential deviations from its safe operating area. The estimation of the battery’s maximum available power is achieved by formulating and subsequently solving a constrained nonlinear optimization problem.

In this chapter, we will delve deeper into Battery Management Systems, provide a more comprehensive discussion on SOX predictors, and elucidate the broader implications of our findings.

Battery Management Systems (BMS) play a pivotal role in ensuring the optimal performance, safety, and longevity of lithium-ion batteries. A cornerstone of an effective BMS is its ability to accurately predict key battery states, which are instrumental in making real-time decisions that influence battery operation and health. In this section, we delve into the intricacies of using the observer to derive these critical state predictions for the BMS.

The primary states of interest, which serve as the bedrock of our BMS predictive framework, encompass:

1. State of Charge (SOC): A measure of the current battery capacity relative to its maximum capacity.

-
2. State of Health (SOH): An indicator of the overall condition and health of the battery, reflecting its current state compared to a fresh, undegraded battery.
 3. State of Power (SOP): A metric that quantifies the battery’s ability to deliver or accept power under specific conditions.
 4. Identification of Lithium Plating: Recognizing the onset and progression of lithium plating within the battery, which can have significant implications for battery performance and safety.

Building upon the foundation laid by the previously introduced MPMe model and the state observers tailored for novel sensors, this section elucidates how spatially heterogeneous information, gleaned from these tools, can be harnessed to refine the accuracy of the aforementioned BMS predictors. Such an approach not only enhances the precision of state estimations but also offers deeper insights into the battery’s internal dynamics, facilitating more informed BMS decision-making.

Figure 5.1 shows the input current for the BMS simulations. Figure 5.2 provides a comprehensive overview of the proposed BMS algorithm’s architecture. It delineates the interplay between the inputs, the underlying battery model, the state observer, and the resultant BMS predictors. This holistic framework underscores the synergy between various components, emphasizing the importance of each element in achieving accurate and reliable BMS predictions.

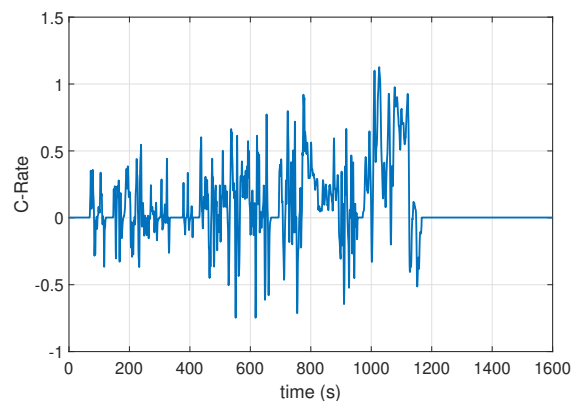


Figure 5.1: Current profile used in BMS predictions from [6].

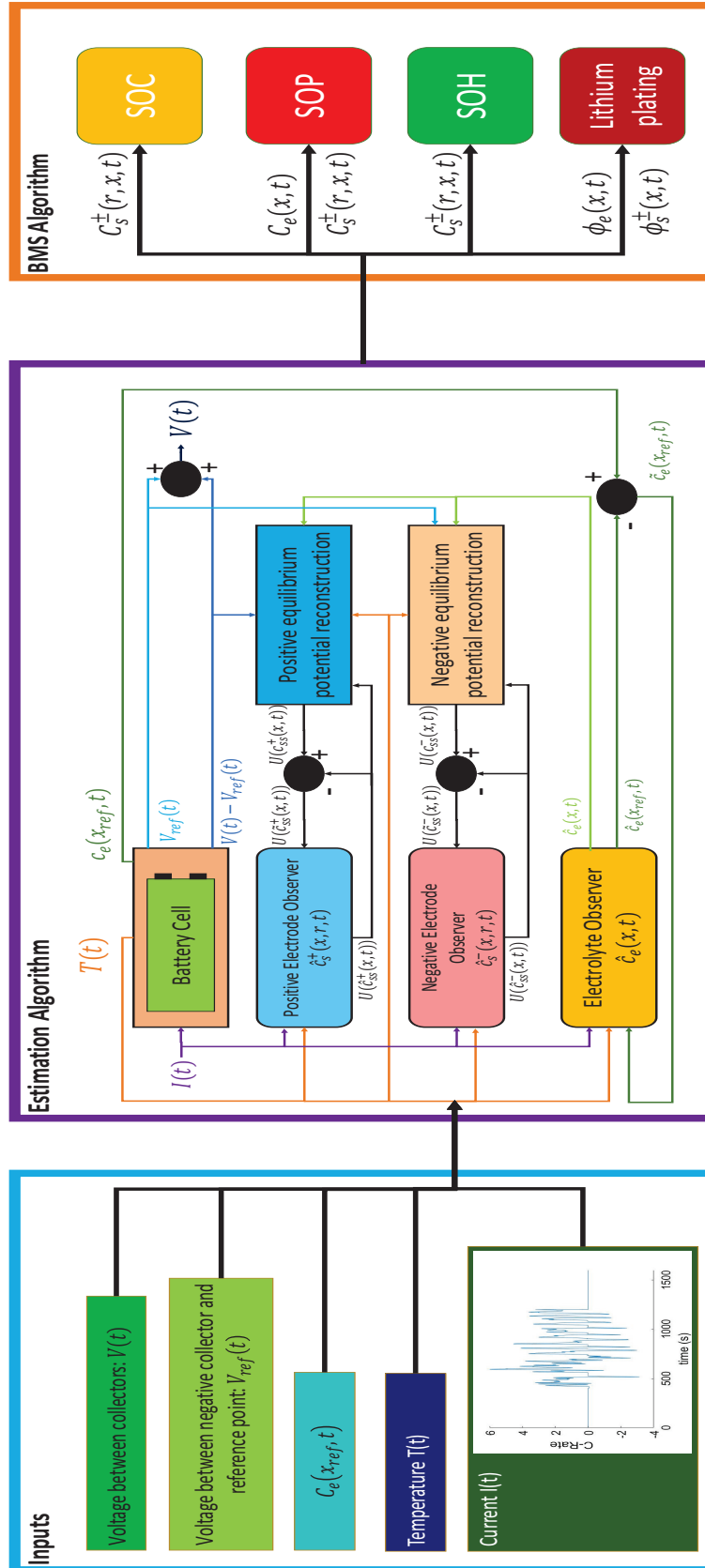


Figure 5.2: Schematic Representation of the Proposed BMS Algorithm from [6]

5.2 State of Charge Estimation

The State of Charge (SOC) is a pivotal parameter in battery management, representing the current charge level of a battery in relation to its maximum capacity. In essence, it provides a quantifiable measure of the remaining energy in a battery, expressed as a percentage of the battery's total capacity.

A more technical approach to predicting the SOC involves the evaluation of $N_{L_s}^{\pm}(t)$, which denotes the total cyclable lithium present inside the individual cells of the battery. This metric serves as a reliable indicator of the battery's state, offering insights into its charge status and overall health.

To ensure precision in SOC estimation, the Battery Management System (BMS) Algorithm is employed. Notably, the viability of this algorithm is shown by its accuracy; the root mean square (RMS) error in the estimation of $N_{L_s}^{\pm}(t)$ is remarkably low, registering at less than 0.04%. Such a minimal error margin underscores the robustness and reliability of the BMS Algorithm in SOC prediction.

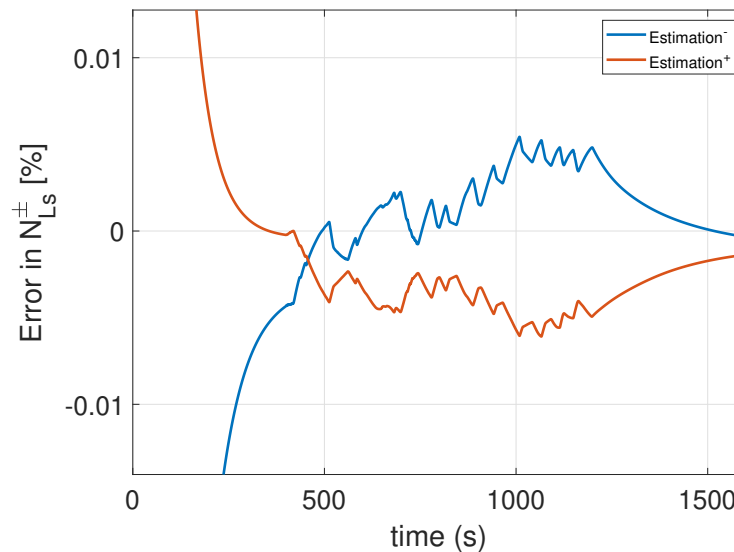


Figure 5.3: Error in $N_{L_s}^{\pm}(t)$ showcasing the accuracy of the BMS Algorithm in SOC estimation from [6].

The accompanying Figure 5.3 provides a visual representation of the error in $N_{L_s}^{\pm}(t)$, further emphasizing the precision of the BMS Algorithm in estimating the SOC.

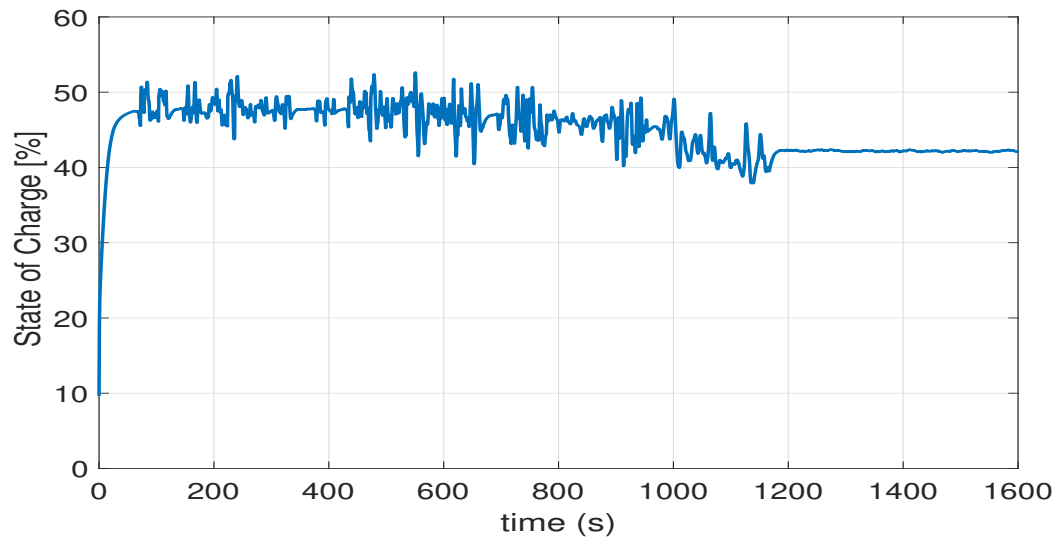


Figure 5.4: SOC estimation

It's important to note that the presented results stem from a comparison between two simulations. The full-scale DFN simulation is more finely discretized in both space and time, offering a detailed representation. However, when compared with experimental results, the errors are expected to be higher. Factors that would affect the accuracy of SOC prediction would include the accuracy of the estimated parameters like diffusion coefficients, conductivities, and the OCV curve. Also, the sensor noise is a key factor that needs to be taken into account.

5.3 State of Health Estimation

The State of Health (SOH) is a fundamental metric in battery management systems, offering insights into the overall condition and longevity of a battery. It quantifies the level of degradation a battery has undergone since its inception, providing a clear indication of its remaining useful life. In essence, the SOH serves as a health index, enabling users and systems to make informed decisions regarding battery usage, maintenance, and replacement.

The BMS Algorithm approach to predicting the SOH involves the evaluation of $N_{Ls}(t)$, which represents the total amount of cyclable lithium available in the battery's electrodes. Initially, the algorithm establishes a baseline, setting the SOH to 100%, which corresponds to a new battery. As the battery undergoes charge and discharge cycles, the BMS Algorithm tracks changes in $N_{Ls}(t)$, reflecting the battery's evolving state.

The prediction of SOH is further refined using $c_s^\pm(x, r, t)$, a parameter that accounts for the concentration of lithium ions across the electrodes. However, it's crucial to ensure the correct initialization of the total amount of lithium in the system, as an incorrect initialization can lead to deviations in the SOH estimation.

The robustness and precision of the BMS Algorithm in SOH estimation are underscored by its accuracy metrics. Specifically, the RMS error in the estimation of $N_{Ls}(t)$ is remarkably low, registering at less than $2e-4\%$. Such a minimal error margin emphasizes the algorithm's capability to provide reliable and consistent SOH predictions. However, it is important to note that this is again a comparison between two simulations, and actual experimental results would vary. Experimental validation of these methods remains a perspective in the short term, based on the advancement of the INSTABAT project [28, 29].

Figure 5.5 offers a visual representation of the error in $N_{Ls}(t)$, further emphasizing the BMS Algorithm's reliability in estimating the SOH. Such accurate estimations are pivotal for ensuring the safe and efficient operation of batteries, especially in critical applications where battery reliability is paramount.

In conclusion, the SOH serves as a vital metric, encapsulating the health and degradation status of batteries. Accurate SOH estimations, facilitated by advanced algorithms, pave the way for optimized battery usage, extended battery life, and enhanced safety protocols.

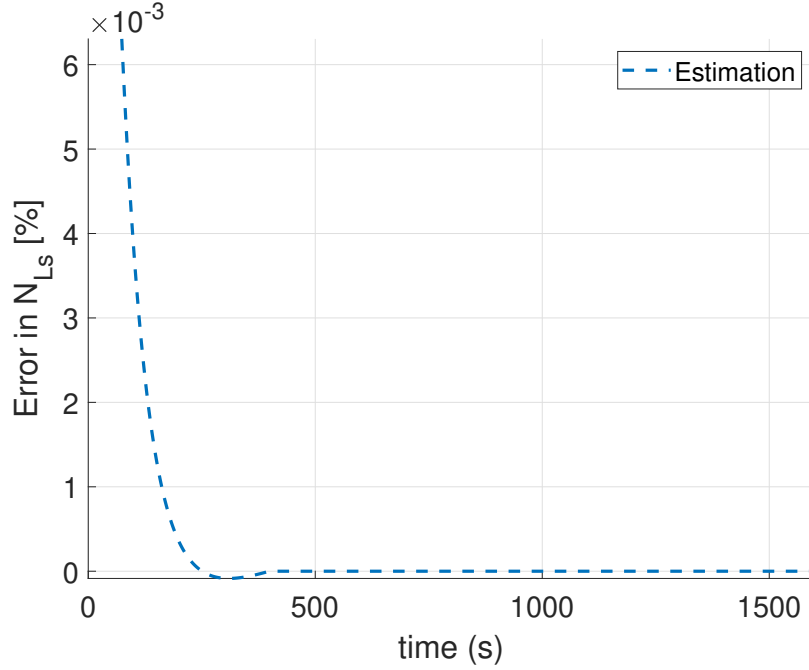


Figure 5.5: Error in $N_{Ls}(t)$ illustrating the precision of the BMS Algorithm in SOH estimation from [6].

5.3.1 Lithium Plating Management

Lithium plating, a phenomenon that has garnered significant attention in the realm of lithium-ion battery research, poses challenges to both the performance and safety of these energy storage systems [177]. This phenomenon is characterized by the deposition of metallic lithium on the anode surface, a process that deviates from the conventional intercalation of lithium ions into the anode's crystal structure [19].

1. **Governing Equations:** The phenomenon of lithium plating can be mathematically represented through a set of equations that capture the electrochemical dynamics at play:

$$\begin{aligned}
 \eta_{Li}^-(x, t) &= \phi_s^-(x, t) - \phi_e^-(x, t) \\
 i_{Li}^-(x, t) &= i_0^- \left[e^{\frac{\alpha \eta^- F}{RT}} - e^{\frac{-(1-\alpha) \eta^- F}{RT}} \right], \text{ for } \eta^- < 0 \\
 i_{t,e}^-(x, t) &= i_e^-(x, t) + i_{Li}^-(x, t)
 \end{aligned} \tag{5.1}$$

These equations, derived from fundamental electrochemical principles, offer insights

into the conditions under which lithium plating occurs and its subsequent effects on the battery's performance [177, 187, 219].

2. **Role of the BMS:** With a comprehensive understanding of the lithium plating mechanism and its associated reactions, the BMS can make informed decisions to optimize various facets of battery performance. Specifically, the BMS can:

- (a) Enhance the accuracy of SOH and SOC estimations, thereby providing a more realistic assessment of the battery's operational state [55, 177].
- (b) Improve fast charging capabilities by monitoring and mitigating conditions conducive to lithium plating [177, 220].
- (c) Bolster safety measures by preemptively identifying and managing scenarios that might lead to lithium plating and its associated risks [220].

Figure 5.6 shows the spatially averaged $\eta_{li}^-(x, t)$ over time from Equation (5.1). This shows that when $\eta_{li}^-(x, t)$ is negative, lithium plating occurs in those areas. It is important to note that these are areas where there is fast charging occurring.

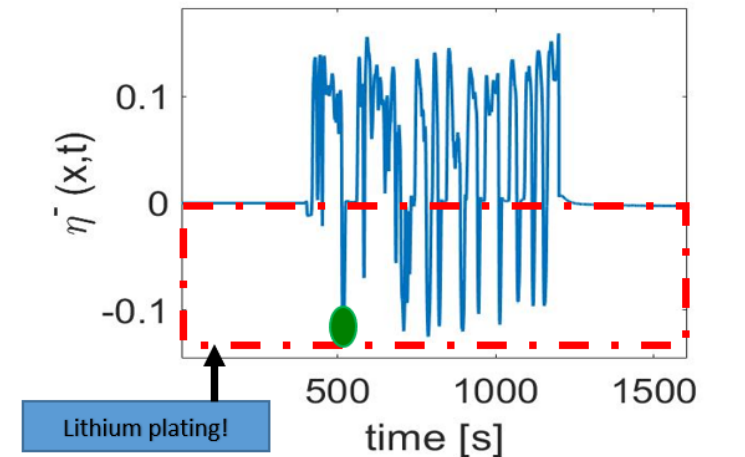


Figure 5.6: Lithium Plating Zone from [6]

Figure 5.7 illustrates $\eta_{li}^-(x, t)$ over space x , at a specific time instance when the charging is at its peak. A notable observation from the figure is the heightened occurrence of lithium plating near the collectors compared to regions closer to the separator. This spatial varia-

tion in lithium plating can be attributed to various factors, including current distribution, electrode morphology, and electrolyte concentration gradients [6].

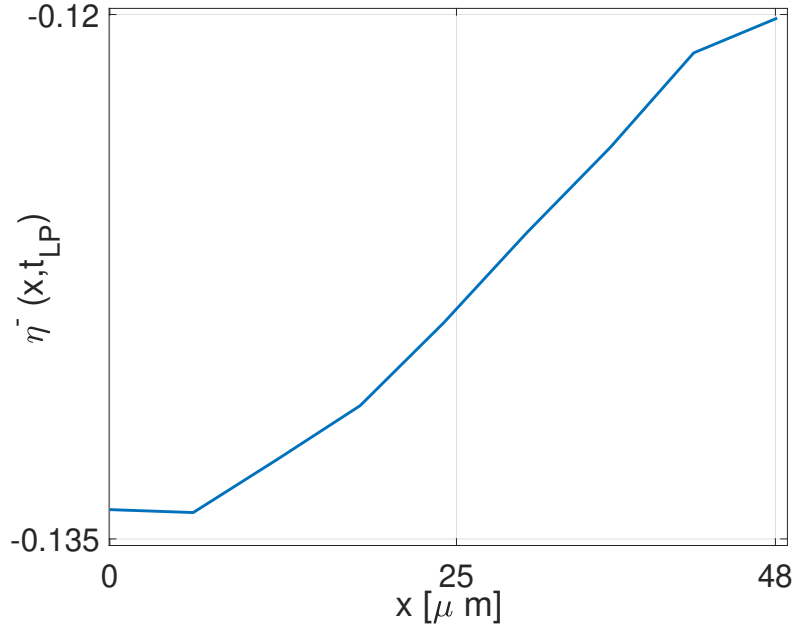


Figure 5.7: Lithium Plating Zone over space from [6]

In conclusion, lithium plating, while posing challenges to lithium-ion battery performance and safety, can be effectively managed through a combination of fundamental understanding, mathematical modeling, and proactive battery management strategies [6].

5.4 State of Power

The State of Power (SOP) is a pivotal metric in battery management, offering insights into the instantaneous power that a battery can deliver or absorb under given conditions. Accurate SOP estimation is paramount for optimizing battery performance, ensuring safety, and extending battery life [6, 220].

In the context of the BMS presented in this work, the SOP and the maximum obtainable current, denoted as I_{SOP} , are predicted leveraging a set of key parameters. Specifically, the cutoff voltage, represented as V_T , and the lithium-ion concentrations in the solid phase, $c_s^\pm(x, r, t)$, and in the electrolyte, $c_e(x, t)$, serve as the foundational inputs for the SOP

estimation algorithm.

With a comprehensive understanding of these internal states, the BMS can furnish a more nuanced and accurate prediction of the SOP. Furthermore, the integration of the lithium plating model augments the SOP estimation process. Lithium plating, a phenomenon that can significantly impact battery performance and safety, plays a crucial role in determining the power capabilities of the battery, especially during high-demand scenarios like fast charging. By accounting for the effects of lithium plating, the BMS can optimize the power extracted from the battery, thereby enhancing its lifecycle and ensuring efficient energy utilization [6].

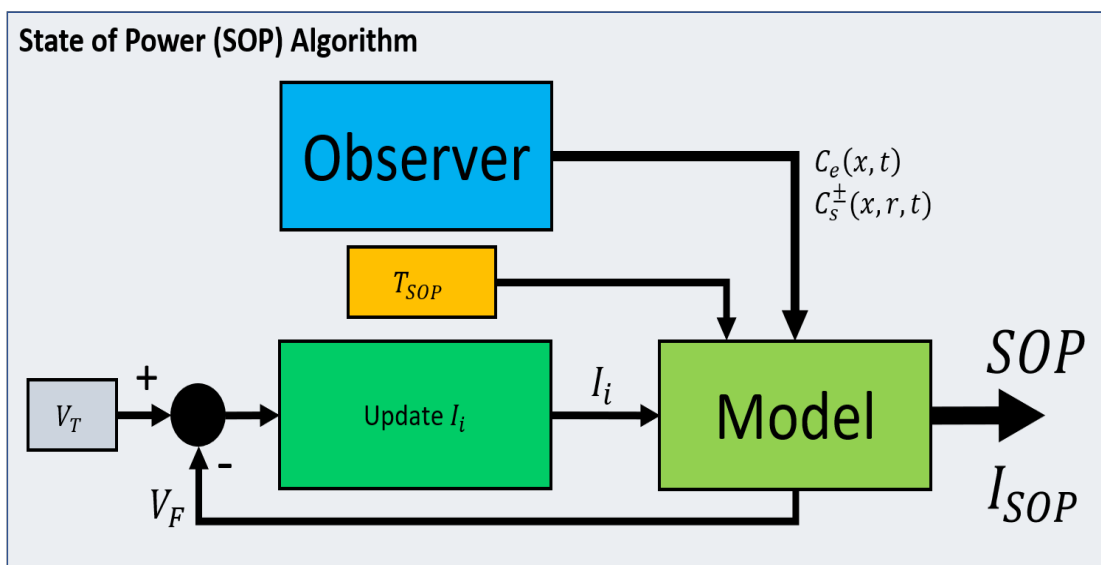


Figure 5.8: Schematic representation of the SOP estimation algorithm, illustrating the interplay of key parameters and their influence on SOP prediction, adapted from [6].

Simulating the SOP Algorithm on every time step can have significant computational expenses, posing challenges for real-time applications. This issue can be addressed by simulating it over an extended time scale or by employing coarser discretizations of the model inside the SOP Algorithm. These adjustments can enhance computational efficiency and alleviate the constraints associated with real-time processing.

In summation, the SOP estimation methodology delineated herein offers a comprehensive approach to predicting the power capabilities of lithium-ion batteries. By integrating key internal states and accounting for phenomena like lithium plating, the BMS ensures that the battery operates optimally, safely, and efficiently across diverse operational scenarios [6].

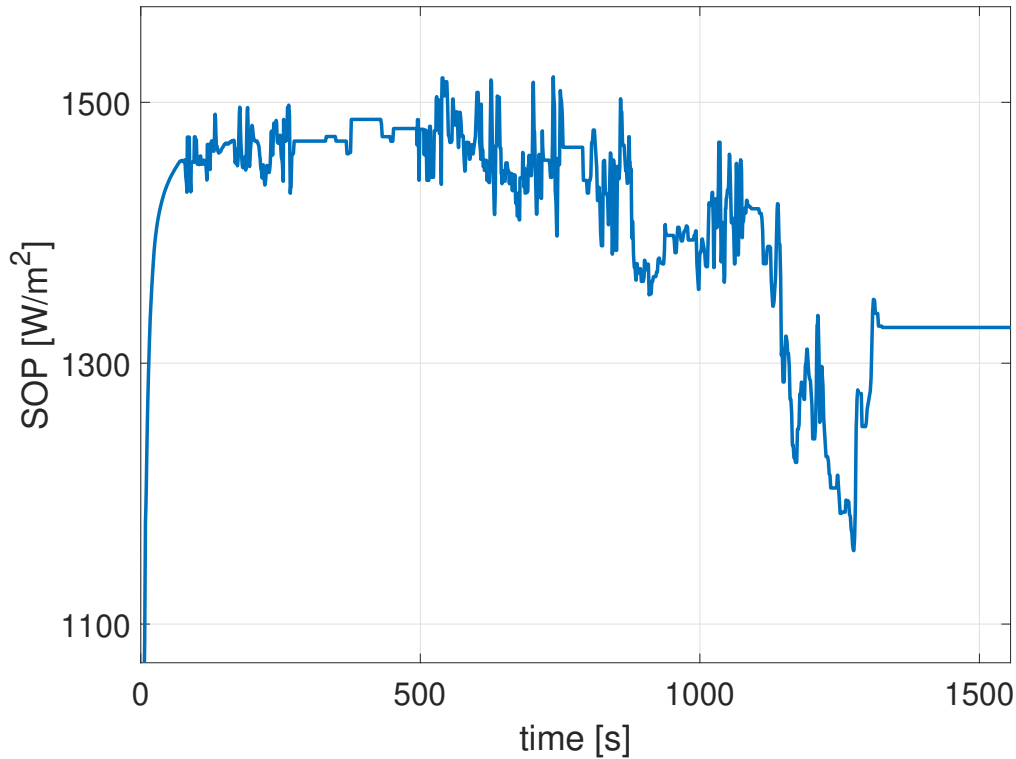


Figure 5.9: SOP prediction from [6].

5.5 Conclusion of the Chapter

This chapter has provided an in-depth exploration into the advanced predictions made by Battery Management Systems (BMS) and the pivotal role of the observer in state estimations, focusing on key battery states: State of Charge (SOC), State of Health (SOH), State of Power (SOP), and the identification of Lithium Plating.

The integration of the MPMe model and state observers with novel sensors has been discussed, enhancing the accuracy of BMS predictions and ensuring the battery operates within its safe regions [6]. The proposed BMS algorithm’s architecture has been presented, emphasizing the synergy between various components and enhancing the precision of state estimations, which not only offers deeper insights into the battery’s internal dynamics but also facilitates more informed BMS decision-making.

SOC, representing the current charge level of a battery in relation to its maximum capacity, has been discussed in detail, with a focus on the evaluation of $N_{L_s}^{\pm}(t)$, which denotes the

total cyclable lithium present inside the individual cells of the battery. The BMS Algorithm has been employed to ensure precision in SOC estimation, demonstrating a remarkably low RMS error in the estimation of $N_{Ls}^{\pm}(t)$ [6].

SOH, providing a clear indication of a battery's remaining useful life, has been explored, with the BMS Algorithm approach to predicting the SOH involving the evaluation of $N_{Ls}(t)$. The robustness and precision of the BMS Algorithm in SOH estimation have been demonstrated by its accuracy metrics, with the RMS error in the estimation of $N_{Ls}(t)$ being remarkably low [6].

The phenomenon of lithium plating has been explored in-depth, emphasizing its challenges and strategies for effective management. Lithium plating, characterized by the deposition of metallic lithium on the anode surface, has been discussed, with a focus on the governing equations and the role of the BMS in enhancing the accuracy of SOH and SOC estimations, improving fast charging capabilities, and bolstering safety measures [19, 55, 177, 187, 219, 220].

SOP, offering insights into the instantaneous power that a battery can deliver or absorb under given conditions, has been discussed. The SOP and the maximum obtainable current, denoted as I_{SOP} , are predicted leveraging a set of key parameters, with the integration of the lithium plating model augmenting the SOP estimation process [6].

In summary, the chapter has provided a comprehensive exploration of the advanced predictions made by BMS, with a focus on key battery states and the role of the observer in state estimations. The insights and methodologies discussed herein pave the way for further research and development in the realm of BMS and battery technology.

Chapter 6

Conclusion of the Thesis

Contents

| | | |
|------------|--|------------|
| 6.1 | Main Contributions of this PhD: | 161 |
| 6.2 | Future Perspectives | 162 |

This PhD research has delved deeply into the intricacies of Lithium-ion batteries (LiBs), their modeling, state estimation, and management, especially in the context of electric vehicles (EVs).

- **Chapter 1** provided a comprehensive background on the significance of LiBs in the global transition away from fossil fuels, emphasizing their pivotal role in the EV sector. The chapter also introduced the INSTABAT project and set the objectives of this research within its framework [23, 24, 28].
- **Chapter 2** offered a detailed review of battery models and state estimation techniques and their relevance to the objectives of this PhD. From Equivalent Circuit Models to Machine Learning Models and Electrochemical Models, the chapter highlighted the strengths and limitations of each approach [3, 31–33, 35].
- **Chapter 3** introduced the Multi-Particle Model with Electrolyte dynamics (MPMe), a novel model bridging the gap between the detailed DFN model and the simpler SPMe. The chapter emphasized the model’s ability to capture internal battery dynamics on a spatial level, incorporate temperature dependence, and ensure lithium conservation.
- **Chapter 4** delved into the development of state observers for both the electrolyte and solid lithium concentrations. The chapter discussed the formulation, assumptions, and stability analysis of these observers, validating their efficacy through simulations [5].
- **Chapter 5** explored the integration of the MPMe model and state observers into an advanced Battery Management System (BMS) algorithm. The chapter discussed the predictions of key battery states which include SOC, SOH, and SOP, emphasizing the role of the observer in enhancing the accuracy of these predictions.

6.1 Main Contributions of this PhD:

1. Formulation of the Multi-Particle Model with Electrolyte dynamics (MPMe) that captures the heterogeneities present in internal battery dynamics on a spatial level, offers

computational efficiency for real-time applications, includes temperature dependence of variables, and actively conserves lithium.

2. Development of state observers for both the electrolyte and solid lithium concentrations, providing a robust mechanism for tracking and estimating key battery states including their respective concentrations, the total amount of cyclable lithium in the battery, and voltages of individual electrodes.
3. Integration of the MPMe model and state observers with novel sensors to enhance the accuracy of Battery Management System (BMS) predictions.
4. Presentation of an advanced BMS algorithm architecture that synergizes various components for precise estimations of SOC, SOH, SOP, and identification of Lithium Plating.

In essence, this research has made significant strides in advancing LiB technology for EVs, offering novel methodologies and tools that address the challenges faced by LiBs and pave the way for their broader adoption in the EV sector. The findings of this research, documented in technical reports and research papers [29], are poised to significantly enhance the performance, safety, and reliability of LiBs in the future.

6.2 Future Perspectives

The advancements made in this research provide a solid foundation for future explorations in the realm of LiB technology. As we look ahead, several promising avenues emerge:

1. **Experimental Validation:** A pivotal next step within the INSTABAT Project is to subject the developed observer system to rigorous experimental validation. The plan is to first assess the observers using experimental datasets, followed by laboratory tests to ascertain their real-time performance and reliability.
2. **Use of hybrid state estimation techniques:** When access to experimental data from the INSTABAT is available, we can enhance our current model (MPMe) and

proposed state observers using hybrid state estimation techniques, such as combining them with ML or AI.

3. **Spatial Thermal Dynamics Integration:** Enhancing the MPMe model with spatial thermal dynamics presents a promising direction. While the current model acknowledges temperature dependence, it doesn't account for spatial temperature variations. Addressing this would refine the model's accuracy, aligning it more closely with real-world conditions.
4. **Exploring Different Chemistries:** Broadening the scope of the observers to accommodate various battery chemistries could significantly expand their applicability. This extension would bolster the versatility of the observers, amplifying the research's impact across diverse battery applications.
5. **Advancements in Lithium Degradation Management:** Managing lithium degradation remains a complex challenge. While the current MPMe model provides some insights into lithium plating, there's ample room for further exploration. Future endeavors should focus on integrating the other types of lithium degradation phenomena and enhancing the precision of the model, observer, and associated algorithms.
6. **Exploration of Sensor Technologies:** This research underscores the transformative potential of integrating additional sensors into observer formulation. A logical progression would be to investigate other sensor technologies, assessing their potential applicability, and contributions, to battery modeling and control strategies.

In essence, the future of energy storage is bright, and the contributions of this research will undoubtedly play a pivotal role in shaping it. The above perspectives provide a roadmap for continued exploration and innovation in the field of LiB technology.

Bibliography

- [1] J. Li and Y. Xiao, “Overview of modeling status of lithium ion battery,” Energy Storage Sci. Technol., vol. 11, pp. 697–703, 2022.
- [2] X. Wu and X. Zhang, “Parameter identification of second order rc equivalent circuit model of lithium battery,” J. Nanjing Univ., vol. 56, pp. 754–761, 2020.
- [3] Z. Cui, L. Wang, Q. Li, and K. Wang, “A comprehensive review on the state of charge estimation for lithium-ion battery based on neural network,” International Journal of Energy Research, vol. 46, no. 5, pp. 5423–5440, 2022.
- [4] A. Jokar, B. Rajabloo, M. Désilets, and M. Lacroix, “Review of simplified pseudo-two-dimensional models of lithium-ion batteries,” Journal of Power Sources, vol. 327, pp. 44–55, 2016. [Online]. Available: <https://www.sciencedirect.com/science/article/pii/S0378775316308916>
- [5] M. M. A. Asif and F. Bribiesca-Argomedo, “Electrochemical state observer design for li-ion batteries with heterogenous electrode lithiation,” IEEE Control Systems Letters, vol. 7, pp. 3199–3204, 2023.
- [6] M. M. A. Asif, F. Bribiesca-Argomedo, and V. Heiries, “Real time estimation of electrochemical states in li-ion batteries and exploitation in bms algorithms,” in Battery 2030+ 3rd Annual Conference, Uppsala, Sweden, 2023. [Online]. Available: <https://meetbattery2030.eu/>

-
- [7] T. Sun, R. Wu, Y. Cui, and Y. Zheng, “Sequent extended kalman filter capacity estimation method for lithium-ion batteries based on discrete battery aging model and support vector machine,” Journal of Energy Storage, vol. 39, p. 102594, 2021.
- [8] P. Sharma and B. J. Bora, “A review of modern machine learning techniques in the prediction of remaining useful life of lithium-ion batteries,” Batteries, vol. 9, no. 1, p. 13, 2022.
- [9] Y. Li, D. Karunathilake, D. M. Vilathgamuwa, Y. Mishra, T. W. Farrell, C. Zou, et al., “Model order reduction techniques for physics-based lithium-ion battery management: A survey,” IEEE Industrial Electronics Magazine, vol. 16, no. 3, pp. 36–51, 2021.
- [10] M. U. Ali, A. Zafar, S. H. Nengroo, S. Hussain, M. Junaid Alvi, and H.-J. Kim, “Towards a smarter battery management system for electric vehicle applications: A critical review of lithium-ion battery state of charge estimation,” Energies, vol. 12, no. 3, p. 446, 2019.
- [11] X. Lin, Y. Kim, S. Mohan, J. B. Siegel, and A. G. Stefanopoulou, “Modeling and estimation for advanced battery management,” Annual Review of Control, Robotics, and Autonomous Systems, vol. 2, pp. 393–426, 2019.
- [12] W. Li, Y. Fan, F. Ringbeck, D. Jöst, X. Han, M. Ouyang, and D. U. Sauer, “Electrochemical model-based state estimation for lithium-ion batteries with adaptive unscented kalman filter,” Journal of Power Sources, vol. 476, p. 228534, 2020. [Online]. Available: <https://www.sciencedirect.com/science/article/pii/S03787775320308387>
- [13] X. Yang, Y. Chen, B. Li, and D. Luo, “Battery states online estimation based on exponential decay particle swarm optimization and proportional-integral observer with a hybrid battery model,” Energy, vol. 191, p. 116509, 2020.
- [14] Z. Chen, X. Li, J. Shen, W. Yan, and R. Xiao, “A novel state of charge estimation algorithm for lithium-ion battery packs of electric vehicles,” Energies, vol. 9, no. 9, p. 710, 2016.

-
- [15] D. N. How, M. Hannan, M. H. Lipu, and P. J. Ker, "State of charge estimation for lithium-ion batteries using model-based and data-driven methods: A review," Ieee Access, vol. 7, pp. 136 116–136 136, 2019.
- [16] M. Charkhgard and M. Farrokhi, "State-of-charge estimation for lithium-ion batteries using neural networks and ekf," IEEE transactions on industrial electronics, vol. 57, no. 12, pp. 4178–4187, 2010.
- [17] C. R. Birkl, M. R. Roberts, E. McTurk, P. G. Bruce, and D. A. Howey, "Degradation diagnostics for lithium ion cells," Journal of Power Sources, vol. 341, pp. 373–386, 2017.
- [18] X. Zhao, Y. Yin, Y. Hu, and S. Y. Choe, "Electrochemical-thermal modeling of lithium plating/stripping of $\text{Li}(\text{Ni}_{0.6}\text{Mn}_{0.2}\text{Co}_{0.2})\text{O}_2/\text{carbon}$ lithium-ion batteries at subzero ambient temperatures," J. Power Sources, vol. 418, pp. 61–73, 2019.
- [19] I. D. Campbell, M. Marzook, M. Marinescu, and G. J. Offer, "How observable is lithium plating? differential voltage analysis to identify and quantify lithium plating following fast charging of cold lithium-ion batteries," J. Electrochem. Soc., vol. 166, pp. A725–A739, 2019.
- [20] X.-G. Yang, Y. Leng, G. Zhang, S. Ge, and C.-Y. Wang, "Modeling of lithium plating induced aging of lithium-ion batteries: Transition from linear to nonlinear aging," Journal of Power Sources, vol. 360, pp. 28–40, 2017.
- [21] S. J. Moura, F. B. Argomedo, R. Klein, A. Mirtabatabaei, and M. Krstic, "Battery state estimation for a single particle model with electrolyte dynamics," IEEE Transactions on Control Systems Technology, vol. 25, no. 2, pp. 453–468, 2016.
- [22] J. Zhao, Y. Zhu, B. Zhang, M. Liu, J. Wang, C. Liu, and X. Hao, "Review of state estimation and remaining useful life prediction methods for lithium-ion batteries," Sustainability, vol. 15, no. 6, p. 5014, 2023.
- [23] B. Lin and W. Wu, "Why people want to buy electric vehicle: An empirical study in first-tier cities of china," Energy Policy, vol. 112, pp. 233–241, 2018.

-
- [24] X. Hu, C. Zou, C. Zhang, and Y. Li, “Technological developments in batteries: a survey of principal roles, types, and management needs,” IEEE Power and Energy Magazine, vol. 15, no. 5, pp. 20–31, 2017.
- [25] Y. Xing, E. W. Ma, K. L. Tsui, and M. Pecht, “Battery management systems in electric and hybrid vehicles,” Energies, vol. 4, no. 11, pp. 1840–1857, 2011.
- [26] G. Berckmans, M. Messagie, J. Smekens, N. Omar, L. Vanhaverbeke, and J. Van Mierlo, “Cost projection of state of the art lithium-ion batteries for electric vehicles up to 2030,” Energies, vol. 10, no. 9, p. 1314, 2017.
- [27] B. Gundogdu, D. T. Gladwin, M. P. Foster, and D. A. Stone, “A forecasting battery state of charge management strategy for frequency response in the uk system,” in 2018 IEEE International Conference on Industrial Technology (ICIT). IEEE, 2018, pp. 1726–1731.
- [28] INSTABAT Project, “Instabat project - battery 2030+ group,” Web page, CEA - INSTABAT Project, 2023, accessed: 2023-06-12. [Online]. Available: <https://www.instabat.eu/>
- [29] —, “Public deliverables - instabat,” Web page, CEA - INSTABAT Project, 2023, accessed: 2023-06-12. [Online]. Available: <https://www.instabat.eu/public-deliverables-library-instabat/>
- [30] M. A. Hannan, M. H. Lipu, A. Hussain, P. J. Ker, T. I. Mahlia, M. Mansor, A. Ayob, M. H. Saad, and Z. Dong, “Toward enhanced state of charge estimation of lithium-ion batteries using optimized machine learning techniques,” Scientific reports, vol. 10, no. 1, pp. 1–15, 2020.
- [31] J. P. Rivera-Barrera, N. Muñoz-Galeano, and H. O. Sarmiento-Maldonado, “Soc estimation for lithium-ion batteries: Review and future challenges,” Electronics, vol. 6, no. 4, p. 102, 2017.

-
- [32] L. Zhang, H. Peng, Z. Ning, Z. Mu, and C. Sun, "Comparative research on rc equivalent circuit models for lithium-ion batteries of electric vehicles," Applied Sciences, vol. 7, no. 10, p. 1002, 2017.
- [33] M.-K. Tran, A. DaCosta, A. Mevawalla, S. Panchal, and M. Fowler, "Comparative study of equivalent circuit models performance in four common lithium-ion batteries: LFP, NMC, LMO, NCA," Batteries, vol. 7, no. 3, p. 51, 2021.
- [34] R. Guo and W. Shen, "A review of equivalent circuit model based online state of power estimation for lithium-ion batteries in electric vehicles," Vehicles, vol. 4, no. 1, pp. 1–29, 2022.
- [35] A. K. Jain, J. Mao, and K. M. Mohiuddin, "Artificial neural networks: A tutorial," Computers in Mathematics with Applications, vol. 29, no. 3, pp. 31–44, Mar. 1996.
- [36] Q. Wang, M. Ye, M. Wei, G. Lian, and C. Wu, "Co-estimation of state of charge and capacity for lithium-ion battery based on recurrent neural network and support vector machine," Energy Reports, vol. 7, pp. 7323–7332, 2021.
- [37] Q. Yang, J. Xu, X. Li, D. Xu, and B. Cao, "State-of-health estimation of lithium-ion battery based on fractional impedance model and interval capacity," International Journal of Electrical Power & Energy Systems, vol. 119, p. 105883, July 2020.
- [38] C. R. Lashway and O. A. Mohammed, "Adaptive battery management and parameter estimation through physics-based modeling and experimental verification," IEEE Transactions on Transportation Electrification, vol. 2, no. 4, pp. 454–464, 2016.
- [39] C. Truchot, M. Dubarry, and B. Y. Liaw, "State-of-charge estimation and uncertainty for lithium-ion battery strings," Applied Energy, vol. 119, pp. 218–227, 2014. [Online]. Available: <https://www.sciencedirect.com/science/article/pii/S0306261913010556>
- [40] D. Ali, S. Mukhopadhyay, and H. Rehman, "A novel adaptive technique for li-ion battery model parameters estimation," in 2016 IEEE National Aerospace and Electronics Conference (NAECON) and Ohio Innovation Summit (OIS). IEEE, 2016, pp. 23–26.

-
- [41] Y. Liu, Q. Zhou, and G. Cui, “Machine learning boosting the development of advanced lithium batteries,” Small Methods, vol. 5, no. 8, p. 2100442, 2021.
- [42] Y. Liang, S. Wang, Y. Fan, X. Yang, Y. Xie, and C. Fernandez, “Joint state of charge and state of health estimation of lithium-ion battery using improved adaptive dual extended kalman filter based on piecewise forgetting factor recursive least squares,” in 2022 4th International Conference on Smart Power Internet Energy Systems (SPIES), 2022, pp. 1923–1927.
- [43] S. Jafari and Y.-C. Byun, “Xgboost-based remaining useful life estimation model with extended kalman particle filter for lithium-ion batteries,” Sensors, vol. 22, no. 23, 2022. [Online]. Available: <https://www.mdpi.com/1424-8220/22/23/9522>
- [44] E. Walker, S. Rayman, and R. E. White, “Comparison of a particle filter and other state estimation methods for prognostics of lithium-ion batteries,” Journal of Power Sources, vol. 287, pp. 1–12, 2015.
- [45] R. Li, S. Xu, S. Li, Y. Zhou, K. Zhou, X. Liu, and J. Yao, “State of charge prediction algorithm of lithium-ion battery based on pso-svr cross validation,” Ieee Access, vol. 8, pp. 10 234–10 242, 2020.
- [46] J. P. Rivera-Barrera, N. Muñoz-Galeano, and H. O. Sarmiento-Maldonado, “Soc estimation for lithium-ion batteries: Review and future challenges,” Electronics, vol. 6, no. 4, 2017.
- [47] M.-H. Golbon-Haghighi, H. Saeidi-Manesh, G. Zhang, and Y. Zhang, “Pattern synthesis for the cylindrical polarimetric phased array radar (cpar),” Prog. Electromagn. Res. M, vol. 66, pp. 87–98, Mar 2018.
- [48] Z. Chen, X. Li, J. Shen, W. Yan, and R. Xiao, “A novel state of charge estimation algorithm for lithium-ion battery packs of electric vehicles,” Energies, vol. 9, no. 9, p. 710, 2016.
- [49] H. Tu, S. Moura, Y. Wang, and H. Fang, “Integrating physics-based modeling with machine learning for lithium-ion batteries,” Applied Energy, vol. 329, p. 120289, 2023.

-
- [50] M. Doyle, T. F. Fuller, and J. Newman, "Modeling of galvanostatic charge and discharge of the lithium/polymer/insertion cell," Journal of the Electrochemical society, vol. 140, no. 6, p. 1526, 1993.
- [51] H. Perez, S. Dey, X. Hu, and S. Moura, "Optimal charging of li-ion batteries via a single particle model with electrolyte and thermal dynamics," Journal of The Electrochemical Society, vol. 164, no. 7, p. A1679, 2017.
- [52] IPCC, "Climate change 2023: Synthesis report. contribution of working groups i, ii and iii to the sixth assessment report of the intergovernmental panel on climate change," Intergovernmental Panel on Climate Change, Geneva, Switzerland, Tech. Rep., 2023.
- [53] X.-H. Sun, T. Yamamoto, and T. Morikawa, "Fast-charging station choice behavior among battery electric vehicle users," Transportation Research Part D: Transport and Environment, vol. 46, pp. 26–39, 2016.
- [54] N. K. M'Sirdi, A. Belhani, and A. Naamane, "Battery models for estimation of state of charge by sliding mode observer," in Sustainability in Energy and Buildings: Proceedings of the 3rd International Conference in Sustainability in Energy and Buildings (SEB'11). Springer, 2012, pp. 133–149.
- [55] M. Adaikkappan and N. Sathiyamoorthy, "Modeling, state of charge estimation, and charging of lithium-ion battery in electric vehicle: A review," International Journal of Energy Research, vol. 46, no. 3, pp. 2141–2165, 2022.
- [56] X. Wang, X. Wei, J. Zhu, H. Dai, Y. Zheng, X. Xu, and Q. Chen, "A review of modeling, acquisition, and application of lithium-ion battery impedance for onboard battery management," ETransportation, vol. 7, p. 100093, 2021.
- [57] Y. Zhao, P. Stein, Y. Bai, M. Al-Siraj, Y. Yang, and B.-X. Xu, "A review on modeling of electro-chemo-mechanics in lithium-ion batteries," Journal of Power Sources, vol. 413, pp. 259–283, 2019.

-
- [58] S. Tamilselvi, S. Gunasundari, N. Karuppiah, A. Razak RK, S. Madhusudan, V. M. Nagarajan, T. Sathish, M. Z. M. Shamim, C. A. Saleel, and A. Afzal, “A review on battery modelling techniques,” Sustainability, vol. 13, no. 18, p. 10042, 2021.
- [59] W. Chen, J. Liang, Z. Yang, and G. Li, “A review of lithium-ion battery for electric vehicle applications and beyond,” Energy Procedia, vol. 158, pp. 4363–4368, 2019.
- [60] N. K. M’Sirdi, A. Belhani, and A. Naamane, “Battery models for estimation of state of charge by sliding mode observer,” in Sustainability in Energy and Buildings: Proceedings of the 3rd International Conference in Sustainability in Energy and Buildings (SEB’11). Springer, 2012, pp. 133–149.
- [61] Y. Song, M. Park, M. Seo, and S. W. Kim, “Online state-of-charge estimation for lithium-ion batteries considering model inaccuracies under time-varying current conditions,” IEEE Access, vol. 8, pp. 192 419–192 434, 2020.
- [62] F. An, J. Huang, C. Wang, Z. Li, J. Zhang, S. Wang, and P. Li, “Cell sorting for parallel lithium-ion battery systems: Evaluation based on an electric circuit model,” Journal of Energy Storage, vol. 6, pp. 195–203, 2016.
- [63] X. Lin, H. E. Perez, S. Mohan, J. B. Siegel, A. G. Stefanopoulou, Y. Ding, and M. P. Castanier, “A lumped-parameter electro-thermal model for cylindrical batteries,” Journal of Power Sources, vol. 257, pp. 1–11, 2014.
- [64] M. H. Hassoun, Fundamentals of artificial neural networks. MIT Press, 1995.
- [65] H. Dai, G. Zhao, M. Lin, J. Wu, and G. Zheng, “A novel estimation method for the state of health of lithium-ion battery using prior knowledge-based neural network and markov chain,” IEEE Transactions on Industrial Electronics, vol. 66, no. 10, pp. 7706–7716, Oct. 2019.
- [66] H. Chaoui and C. C. Ibe-Ekeocha, “State of charge and state of health estimation for lithium batteries using recurrent neural networks,” IEEE Transactions on Vehicular Technology, vol. 66, no. 10, pp. 8773–8783, Oct. 2017.
-

-
- [67] A. Eddahech, O. Briat, N. Bertrand, J. Y. Deletage, and J. M. Vinassa, "Behavior and state-of-health monitoring of li-ion batteries using impedance spectroscopy and recurrent neural networks," International Journal of Electrical Power & Energy Systems, vol. 42, no. 1, pp. 487–494, Nov. 2012.
- [68] Y. Wu, Q. Xue, J. Shen, Z. Lei, Z. Chen, and Y. Liu, "State of health estimation for lithium-ion batteries based on healthy features and long short-term memory," IEEE Access, vol. 8, pp. 28 533–28 547, Feb. 2020.
- [69] L. Xuan, L. Qian, J. Chen, X. Bai, and B. Wu, "State-of-charge prediction of battery management system based on principal component analysis and improved support vector machine for regression," IEEE Access, vol. 8, pp. 164 693–164 704, 2020.
- [70] X. Li, Y. Ma, and J. Zhu, "An online dual filters rul prediction method of lithium-ion battery based on unscented particle filter and least squares support vector machine," Measurement, vol. 184, p. 109935, 2021.
- [71] X. Sui, S. He, S. B. Vilsen, J. Meng, R. Teodorescu, and D.-I. Stroe, "A review of non-probabilistic machine learning-based state of health estimation techniques for lithium-ion battery," Applied Energy, vol. 300, p. 117346, 2021.
- [72] P. Khumprom and N. Yodo, "A data-driven predictive prognostic model for lithium-ion batteries based on a deep learning algorithm," Energies, vol. 12, no. 4, p. 660, Feb 2019.
- [73] M. Park, M. Seo, Y. Song, and S. W. Kim, "Capacity estimation of li-ion batteries using constant current charging voltage with multilayer perceptron," IEEE Access, vol. 8, pp. 180 762–72, Oct 2020.
- [74] A. G. Ivakhnenko, "Polynomial theory of complex systems," IEEE Trans Syst Man, Cybern, vol. SMC-1, no. 4, pp. 364–378, Oct 1971.
- [75] J. Kim, J. Yu, M. Kim, K. Kim, and S. Han, "Estimation of li-ion battery state of health based on multilayer perceptron: as an ev application," IFAC-PapersOnLine, vol. 51, no. 28, pp. 392–7, 2018.

-
- [76] J. Wu, Y. Wang, X. Zhang, and Z. Chen, “A novel state of health estimation method of li-ion battery using group method of data handling,” J Power Sources, vol. 327, pp. 457–64, Sep 2016.
- [77] L. Song, K. Zhang, T. Liang, X. Han, and Y. Zhang, “Intelligent state of health estimation for lithium-ion battery pack based on big data analysis,” J Energy Storage, vol. 32, p. 101836, Dec 2020.
- [78] B. Gou, Y. Xu, and X. Feng, “An ensemble learning-based data-driven method for online state-of-health estimation of lithium-ion batteries,” IEEE Trans Transp, Oct 2020.
- [79] S. Shen, M. Sadoughi, M. Li, Z. Wang, and C. Hu, “Deep convolutional neural networks with ensemble learning and transfer learning for capacity estimation of lithium-ion batteries,” Appl Energy, vol. 260, p. 114296, Feb 2020.
- [80] J. Meng, L. Cai, D. I. Stroe, J. Ma, G. Luo, and R. Teodorescu, “An optimized ensemble learning framework for lithium-ion battery state of health estimation in energy storage system,” Energy, vol. 206, p. 118140, Sep 2020.
- [81] K. Liu, X. Hu, H. Zhou, L. Tong, D. Widanalage, and J. Macro, “Feature analyses and modelling of lithium-ion batteries manufacturing based on random forest classification,” IEEE/ASME Trans Mechatron, pp. 1–1, Jan 2021.
- [82] Y. Li, D. I. Stroe, Y. Cheng, H. Sheng, X. Sui, and R. Teodorescu, “On the feature selection for battery state of health estimation based on charging–discharging profiles,” J Energy Storage, vol. 33, p. 102122, Jan 2021.
- [83] X. Sui, S. He, D. Stroe, and R. Teodorescu, “Lithium-ion battery state of health estimation using empirical mode decomposition sample entropy and support vector machine,” in IEEE Applied Power Electronics Conference and Exposition (APEC), Mar 2020, pp. 3424–3429.
-

-
- [84] A. Lamprecht, M. Riesterer, and S. Steinhorst, “Random forest regression of charge balancing data: A state of health estimation method for electric vehicle batteries,” in International Conference on Omni-layer Intelligent Systems (COINS), 2020.
- [85] X. Hu, Y. Che, X. Lin, and S. Onori, “Battery health prediction using fusion-based feature selection and machine learning,” IEEE Transactions on Transp, Aug 2020.
- [86] M. Doyle, T. Fuller, and J. Newman, “Modeling of galvanostatic charge and discharge of the lithium/polymer/insertion cell,” J. Electrochem. Soc., vol. 140, pp. 1526–1533, 1993.
- [87] K. Smith and C. Wang, “Power and thermal characterization of a lithium-ion battery pack for hybrid-electric vehicles,” J. Power Sources, vol. 160, pp. 662–673, 2006.
- [88] D. Zhang, S. Dey, H. E. Perez, and S. J. Moura, “Remaining useful life estimation of lithium-ion batteries based on thermal dynamics,” in Proc. Amer. Control Conf. (ACC), May 2017, pp. 4042–4047.
- [89] M. Doyle and J. Newman, “The use of mathematical modeling in the design of lithium/polymer battery systems,” Electrochim. Acta, vol. 40, no. 13-14, pp. 2191–2196, Oct 1995.
- [90] P. Ramadass, B. Haran, P. M. Gomadam, R. White, and B. N. Popov, “Development of first principles capacity fade model for li-ion cells,” J. Electrochem. Soc., vol. 151, no. 2, p. A196, 2004.
- [91] R. Darling and J. Newman, “Modeling a porous intercalation electrode with two characteristic particle sizes,” Journal of The Electrochemical Society, vol. 144, no. 12, p. 4201, 1997.
- [92] J. C. Forman, S. Bashash, J. L. Stein, and H. K. Fathy, “Reduction of an electrochemistry-based li-ion battery model via quasi-linearization and pade approximation,” Journal of the Electrochemical Society, vol. 158, no. 2, p. A93, 2010.

-
- [93] D. Di Domenico, G. Fiengo, and A. Stefanopoulou, "Lithium-ion battery state of charge estimation with a kalman filter based on a electrochemical model," in Proc. IEEE Int. Conf. Control Appl., Sep 2008, pp. 702–707.
- [94] K. A. Smith, C. D. Rahn, and C.-Y. Wang, "Model order reduction of 1d diffusion systems via residue grouping," 2008.
- [95] M. Elmahallawy, T. Elfouly, A. Alouani, and A. Massoud, "A comprehensive review of lithium-ion batteries modeling, and state of health and remaining useful lifetime prediction," IEEE Access, 2022.
- [96] B. S. Haran, B. N. Popov, and R. E. White, "Determination of the hydrogen diffusion coefficient in metal hydrides by impedance spectroscopy," J. Power Sources, vol. 75, no. 1, pp. 56–63, Sep 1998.
- [97] G. Ning and B. N. Popov, "Cycle life modeling of lithium-ion batteries," J. Electrochem. Soc., vol. 151, no. 10, p. A1584, 2004.
- [98] S. Santhanagopalan, Q. Guo, P. Ramadass, and R. E. White, "Review of models for predicting the cycling performance of lithium ion batteries," J. Power Sources, vol. 156, no. 2, pp. 620–628, 2006.
- [99] S. J. Moura, F. B. Argomedo, R. Klein, A. Mirtabatabaei, and M. Krstic, "Battery state estimation for a single particle model with electrolyte dynamics," IEEE Trans. Control Syst. Technol., vol. 25, no. 2, pp. 453–468, Mar 2017.
- [100] D. Zhang, S. Dey, L. D. Couto, and S. J. Moura, "Battery adaptive observer for a single-particle model with intercalation-induced stress," IEEE Trans. Control Syst. Technol., vol. 28, no. 4, pp. 1363–1377, Jul 2020.
- [101] J. Li, K. Adewuyi, N. Lotf, R. G. Landers, and J. Park, "A single particle model with chemical/mechanical degradation physics for lithium ion battery state of health (soh) estimation," Appl. Energy, vol. 212, pp. 1178–1190, Feb 2018.

-
- [102] S. Atlung, K. West, and T. Jacobsen, “Dynamic aspects of solid solution cathodes for electrochemical power sources,” J. Electrochem. Soc., vol. 126, pp. 1311–1321, 1979.
- [103] A. M. Bizeray, J. H. Kim, S. R. Duncan, and D. A. Howey, “Identifiability and parameter estimation of the single particle lithium-ion battery model,” IEEE Trans. Control Syst. Technol., vol. 27, pp. 1–16, 2018.
- [104] X. Han, M. Ouyang, L. Lu, and J. Li, “Simplification of physics-based electrochemical model for lithium ion battery on electric vehicle. part i: diffusion simplification and single particle model,” J. Power Sources, vol. 278, pp. 802–813, 2015.
- [105] —, “Simplification of physics-based electrochemical model for lithium ion battery on electric vehicle. part ii: pseudo-two-dimensional model simplification and state of charge estimation,” J. Power Sources, vol. 278, pp. 814–822, 2015.
- [106] P. Kemper and D. Kum, “Extended single particle model of li-ion batteries towards high current applications,” in 2013 9th IEEE Vehicle Power and Propulsion Conf. (IEEE VPPC 2013). IEEE, 2013, pp. 158–163.
- [107] F. Brosa Planella, M. Sheikh, and W. Widanage, “Systematic derivation and validation of a reduced thermal-electrochemical model for lithium-ion batteries using asymptotic methods,” Electrochim. Acta, vol. 388, p. 138524, 2021.
- [108] S. G. Marquis, V. Sulzer, R. Timms, C. P. Please, and S. J. Chapman, “An asymptotic derivation of a single particle model with electrolyte,” J. Electrochem. Soc., vol. 166.
- [109] I. R. Moyles, M. G. Hennessy, T. G. Myers, and B. R. Wetton, “Asymptotic reduction of a porous electrode model for lithium-ion batteries,” SIAM J. Appl. Math., vol. 79, pp. 1528–1549, 2019.
- [110] G. Richardson, G. Denuault, and C. P. Please, “Multiscale modelling and analysis of lithium-ion battery charge and discharge,” J. Eng. Math., vol. 72, pp. 41–72, 2012.
- [111] G. Richardson, I. Korotkin, R. Ranom, M. Castle, and J. Foster, “Generalised single particle models for high-rate operation of graded lithium-ion electrodes: systematic derivation and validation,” Electrochim. Acta, vol. 339, p. 135862, 2020.
-

-
- [112] J. Kim, G.-S. Seo, C. Chun, B.-H. Cho, and S. Lee, "Ocv hysteresis effect-based soc estimation in extended kalman filter algorithm for a lifepo 4/c cell," in 2012 IEEE International Electric Vehicle Conference. IEEE, 2012, pp. 1–5.
- [113] H. He, X. Zhang, R. Xiong, Y. Xu, and H. Guo, "Online model-based estimation of state-of-charge and open-circuit voltage of lithium-ion batteries in electric vehicles," Energy, vol. 39, no. 1, pp. 310–318, 2012.
- [114] B. Xiao, B. Xiao, and L. Liu, "State of health estimation for lithium-ion batteries based on the constant current–constant voltage charging curve," Electron, vol. 9, no. 8, p. 1279, Aug. 2020.
- [115] W. Pan, Q. Chen, M. Zhu, J. Tang, and J. Wang, "A data-driven fuzzy information granulation approach for battery state of health forecasting," Journal of Power Sources, vol. 475, p. 228716, Nov. 2020.
- [116] Z. Deng, L. Yang, Y. Cai, H. Deng, and L. Sun, "Online available capacity prediction and state of charge estimation based on advanced data-driven algorithms for lithium iron phosphate battery," Energy, vol. 112, pp. 469–480, Oct. 2016.
- [117] D. Liu, Y. Song, L. Li, H. Liao, and Y. Peng, "On-line life cycle health assessment for lithium-ion battery in electric vehicles," Journal of Cleaner Production, vol. 199, pp. 1050–1065, Oct. 2018.
- [118] D. Yang, Y. Wang, R. Pan, R. Chen, and Z. Chen, "State-of-health estimation for the lithium-ion battery based on support vector regression," Applied Energy, vol. 227, pp. 273–283, Oct. 2018.
- [119] K. De Brabanter, J. De Brabanter, J. A. K. Suykens, and B. De Moor, "Approximate confidence and prediction intervals for least squares support vector regression," IEEE Transactions on Neural Networks, vol. 22, no. 1, pp. 110–120, Jan. 2011.
- [120] Y. Deng, H. Ying, E. Jiaqiang, H. Zhu, K. Wei, and J. Chen, "Feature parameter extraction and intelligent estimation of the state-of-health of lithium-ion batteries," Energy, vol. 176, pp. 91–102, June 2019.

-
- [121] G. S. H. O. P. MALIK and S. J. CHENG, “Some issues on the practical use of recursive least squares identification in self-tuning control,” International Journal of Control, vol. 53, no. 5, pp. 1021–1033, 1991. [Online]. Available: <https://doi.org/10.1080/00207179108953663>
- [122] H. Dai, X. Wei, Z. Sun, J. Wang, and W. Gu, “Online cell SoC estimation of Li-ion battery packs using a dual time-scale Kalman filtering for EV applications,” Applied Energy, vol. 95, pp. 227–237, Jul. 2012.
- [123] Y. Li, C. Wang, and J. Gong, “A combination Kalman filter approach for state of charge estimation of lithium-ion battery considering model uncertainty,” Energy, vol. 109, pp. 933–946, Aug. 2016.
- [124] W. Wang and J. Mu, “State of charge estimation for lithium-ion battery in electric vehicle based on Kalman filter considering model error,” IEEE Access, vol. 7, pp. 29 223–29 235, 2019.
- [125] Z. Zeng, J. Tian, D. Li, and Y. Tian, “An online state of charge estimation algorithm for lithium-ion batteries using an improved adaptive Cubature Kalman filter,” Energies, vol. 11, no. 1, p. 59, Jan. 2018.
- [126] Q. Yu, R. Xiong, and C. Lin, “Online estimation of state-of-charge based on the H infinity and unscented Kalman filters for lithium-ion batteries,” Energy Procedia, vol. 105, pp. 2791–2796, May 2017.
- [127] B. Fridholm, M. Nilsson, and T. Wik, “Robustness comparison of battery state of charge observers for automotive applications,” IFAC Proceedings Volumes, vol. 47, no. 3, pp. 2138–2146, 2014, 19th IFAC World Congress. [Online]. Available: <https://www.sciencedirect.com/science/article/pii/S1474667016419294>
- [128] Y. Tian, B. Xia, W. Sun, Z. Xu, and W. Zheng, “A modified model based state of charge estimation of power lithium-ion batteries using unscented kalman filter,” Journal of Power Sources, vol. 270, pp. 619–626, 2014. [Online]. Available: <https://www.sciencedirect.com/science/article/pii/S0378775314011975>

-
- [129] Q. Yu, R. Xiong, and C. Lin, “Online estimation of state-of-charge based on the h infinity and unscented kalman filters for lithium ion batteries,” Energy Procedia, vol. 105, pp. 2791–2796, 2017, 8th International Conference on Applied Energy, ICAE2016, 8-11 October 2016, Beijing, China. [Online]. Available: <https://www.sciencedirect.com/science/article/pii/S1876610217306525>
- [130] J. Guo, S. Liu, and R. Zhu, “An unscented kalman filtering method for estimation of state-of-charge of lithium-ion battery,” Frontiers in Energy Research, vol. 10, p. 998002, 2023.
- [131] K. S. Ng, C. S. Moo, Y. P. Chen, and Y. C. Hsieh, “Enhanced coulomb counting method for estimating state-of-charge and state-of-health of lithium-ion batteries,” Appl Energy, vol. 86, no. 9, pp. 1506–1511, Sep 2009.
- [132] C. Zou, C. Manzie, D. Nešić, and A. G. Kallapur, “Multi-time-scale observer design for state-of-charge and state-of-health of a lithium-ion battery,” J Power Sources, vol. 335, pp. 121–130, 2016.
- [133] M. Wei, M. Ye, J. B. Li, Q. Wang, and X. Xu, “State of charge estimation of lithium-ion batteries using lstm and narx neural networks,” Ieee Access, vol. 8, pp. 189 236–189 245, 2020.
- [134] X. Ren, S. Liu, X. Yu, and X. Dong, “A method for state-of-charge estimation of lithium-ion batteries based on pso-lstm,” Energy, vol. 234, p. 121236, 2021.
- [135] —, “A method for state-of-charge estimation of lithium-ion batteries based on pso-lstm,” Energy, vol. 234, p. 121236, 2021. [Online]. Available: <https://www.sciencedirect.com/science/article/pii/S0360544221014845>
- [136] X. Sui, S. He, J. Meng, R. Teodorescu, and D. I. Stroe, “Fuzzy entropy-based state of health estimation for li-ion batteries,” IEEE Transactions on Emerging Topics in Power Electronics, Dec. 2020, early access.
-

-
- [137] —, “Fuzzy entropy-based state of health estimation of lifepo4 batteries considering temperature variation,” in IEEE Energy Conversion Congress and Exposition (ECCE), Detroit, MI, USA, 2020, pp. 4401–4406.
- [138] T. Weigert, Q. Tian, and K. Lian, “State-of-charge prediction of batteries and battery–supercapacitor hybrids using artificial neural networks,” Journal of Power Sources, vol. 196, no. 8, pp. 4061–4066, 2011. [Online]. Available: <https://www.sciencedirect.com/science/article/pii/S0378775310018756>
- [139] A. M. Bizeray, S. Zhao, S. R. Duncan, and D. A. Howey, “Lithium-ion battery thermal-electrochemical model-based state estimation using orthogonal collocation and a modified extended kalman filter,” Journal of Power Sources, vol. 296, pp. 400–412, 2015.
- [140] D. Di Domenico, A. Stefanopoulou, and G. Fiengo, “Lithium-ion battery state of charge and critical surface charge estimation using an electrochemical model-based extended kalman filter,” Journal of Dynamic Systems, Measurement and Control, vol. 132, no. 6, p. 061302, 2010.
- [141] S. Santhanagopalan and R. E. White, “Online estimation of the state of charge of a lithium ion cell,” Journal of Power Sources, vol. 161, no. 2, pp. 1346–1355, 2006.
- [142] —, “State of charge estimation using an unscented filter for high power lithium ion cells,” International Journal of Energy Research, vol. 34, no. 2, pp. 152–163, 2009.
- [143] S. J. Moura, M. Krstic, and N. Chaturvedi, “Adaptive pde observer for battery soc/soh estimation via an electrochemical model,” ASME Journal of Dynamic Systems, Measurement, and Control, vol. 136, p. 011015, 2014.
- [144] S. Dey and B. Ayalew, “Nonlinear observer designs for state-of-charge estimation of lithium-ion batteries,” in American Control Conference (ACC), Portland, OR, USA, 2014.
- [145] S. Dey, B. Ayalew, and P. Pisu, “Nonlinear robust observers for state-of-charge estimation of lithium-ion cells based on a reduced electrochemical model,” IEEE Transactions on Control Systems Technology, vol. 23, no. 5, pp. 1935–1942, 2015.
-

-
- [146] Y. Wang, H. Fang, Z. Sahinoglu, T. Wada, and S. Hara, “Adaptive estimation of the state of charge for lithium-ion batteries,” IEEE Transactions on Control Systems Technology, vol. 23, no. 3, pp. 948–962, 2015.
- [147] P. Ascencio, A. Astolfi, and T. Parisini, “Backstepping pde-based adaptive observer for a single particle model of lithium-ion batteries,” in IEEE Conference on Decision and Control (CDC), Las Vegas, NV, USA, 2016.
- [148] P. Blondel, R. Postoyan, S. Raël, S. Benjamin, and P. Desprez, “Nonlinear circle-criterion observer design for an electrochemical battery model,” IEEE Transactions on Control Systems Technology, vol. 27, no. 2, pp. 889–897, 2019.
- [149] B. Jenkins, A. Krupadanam, and A. M. Annaswamy, “Fast adaptive observers for battery management systems,” IEEE Transactions on Control Systems Technology, vol. In Press, 2019.
- [150] S.-X. Tang, L. Camacho-Solorio, Y. Wang, and M. Krstic, “State-of-charge estimation from a thermal-electrochemical model of lithium-ion batteries,” Automatica, vol. 83, pp. 206–219, 2017.
- [151] M. Guo, G. Sikha, and R. E. White, “Single-particle model for a lithium-ion cell: Thermal behavior,” Journal of the Electrochemical Society, vol. 158, no. 2, pp. A122–A132, 2011.
- [152] D. Zhang, S. Dey, and S. J. Moura, “Lithium-ion battery state estimation for a single particle model with intercalation-induced stress,” IEEE Transactions on Control Systems Technology, vol. In Press, 2019.
- [153] D. Zhang, S. Dey, L. D. Couto, and S. J. Moura, “Battery adaptive observer for a single particle model with intercalation-induced stress,” IEEE Transactions on Control Systems Technology, vol. In Press, 2019.
- [154] S. Koga, L. Camacho-Solorio, and M. Krstic, “State estimation for lithium ion batteries with phase transition materials,” in Dynamic Systems and Control Conference, 2017.
-

-
- [155] R. Drummond and S. Duncan, “Observer design for the doyle-fuller-newman li-ion battery model without electrolyte dynamics,” Journal of Energy Storage, vol. 23, pp. 250–257, 2019.
- [156] E. Prada, D. Di Domenico, Y. Creff, J. Bernard, V. Sauvant-Moynot, and F. Huet, “Simplified electrochemical and thermal model of lifepo4-graphite li-ion batteries for fast charge applications,” Journal of the Electrochemical Society, vol. 159, no. 9, pp. A1508–A1519, 2012.
- [157] H. He, R. Xiong, and J. Fan, “Online estimation of internal resistance and open-circuit voltage of lithium-ion batteries in electric vehicles,” Journal of Power Sources, vol. 196, no. 8, pp. 3921–3932, 2011.
- [158] L. Zhou, J. Zhang, C. Yang, L. Qi, and C. Liu, “Lithium-ion battery thermal-electrochemical model-based state estimation using orthogonal collocation and a modified extended kalman filter,” arXiv, 2023.
- [159] V. Doyen, C. Turpin, G. Dauphin-Tanguy, and S. Genies, “Lithium-ion battery state of charge and critical surface charge estimation using an electrochemical model-based extended kalman filter,” Journal of Dynamic Systems, Measurement, and Control, vol. 141, no. 12, 2019.
- [160] S. Santhanagopalan, Q. Guo, P. Ramadass, and R. E. White, “Online estimation of the state of charge of a lithium ion cell,” Journal of Power Sources, vol. 195, no. 12, pp. 3921–3932, 2010.
- [161] S. Duncan, S. Moura, R. Singh, and H. K. Fathy, “Adaptive partial differential equation observer for battery state-of-charge/state-of-health estimation via an electrochemical model,” Journal of Dynamic Systems, Measurement, and Control, vol. 138, no. 12, 2016.
- [162] H. E. Perez, X. Hu, and S. J. Moura, “Optimal charging of batteries via a single particle model with electrolyte and thermal dynamics,” in American Control Conference (ACC), Boston, MA, USA, 2016.

-
- [163] H. E. Perez, S. Dey, X. Hu, and S. J. Moura, “Optimal charging of li-ion batteries via a single particle model with electrolyte and thermal dynamics,” Journal of the Electrochemical Society, vol. 164, no. 7, pp. A1679–A1687, 2017.
- [164] R. Klein, N. A. Chaturvedi, J. Christensen, J. Ahmen, R. Findeisen, and A. Kojic, “Electrochemical model based observer design for a lithium-ion battery,” IEEE Transactions on Control Systems Technology, vol. 21, no. 2, pp. 289–301, 2013.
- [165] K. A. Smith, C. D. Rahn, and C.-Y. Wang, “Model-based electrochemical estimation and constraint management for pulse operation of lithium ion batteries,” IEEE Transactions on Control Systems Technology, vol. 18, no. 3, pp. 654–663, 2010.
- [166] M. Corno, N. Bhatt, S. M. Savaresi, and M. Verhaegen, “Electrochemical model-based state of charge estimation for li-ion cells,” IEEE Transactions on Control Systems Technology, vol. 23, no. 1, pp. 117–127, 2015.
- [167] K. D. Stetzel, L. L. Aldrich, M. S. Trimboli, and G. L. Plett, “Electrochemical state and internal variables estimation using a reduced-order physics-based model of a lithium-ion cell and an extended kalman filter,” Journal of Power Sources, vol. 278, pp. 490–505, 2015.
- [168] A. Bartlett, S. Marcicki, S. Onori, G. Rizzoni, X. G. Yang, and T. Miller, “Model-based state of charge estimation and observability analysis of a composite electrode lithium-ion battery,” in IEEE Conference on Decision and Control (CDC), Florence, Italy, 2013.
- [169] Q. Sun, H. Lv, S. Wang, S. Jing, J. Chen, and R. Fang, “Hv battery soc estimation algorithm based on pso,” in Proc. 3rd Int. Conf. Electromech. Control Technol. Transp., 2018, pp. 667–670.
- [170] L. Rozaqi, E. Rijanto, and S. Kanarachos, “Comparison between rlsga and rls-pso for li-ion battery soc and soh estimation: A simulation study,” J. Mechatron., Elect. Power, Veh. Technol., vol. 8, no. 1, pp. 40–49, Jul 2017.
-

-
- [171] G. F. Guo, L. Shui, X. L. Wu, and B. G. Cao, “Soc estimation for li-ion battery using svm based on particle swarm optimization,” Adv. Mater. Res., vol. 1051, pp. 1004–1008, Oct 2014.
- [172] M. S. H. Lipu, M. A. Hannan, A. Hussain, and M. H. M. Saad, “Optimal bp neural network algorithm for state of charge estimation of lithium-ion battery using pso with pca feature selection,” J. Renew. Sustain. Energy, vol. 9, no. 6, Nov 2017, art. no. 064102.
- [173] Y. Zheng, L. Lu, X. Han, J. Li, and M. Ouyang, “Lifepo4 battery pack capacity estimation for electric vehicles based on charging cell voltage curve transformation,” J. Power Sources, vol. 226, pp. 33–41, Mar 2013.
- [174] J. Xu, B. Cao, Z. Chen, and Z. Zou, “An online state of charge estimation method with reduced prior battery testing information,” Int. J. Elect. Power Energy Syst., vol. 63, pp. 178–184, Dec 2014.
- [175] X. Hu, S. E. Li, and Y. Yang, “Advanced machine learning approach for lithium-ion battery state estimation in electric vehicles,” IEEE Trans. Transport. Electri., vol. 2, no. 2, pp. 140–149, Jun 2016.
- [176] W.-Y. Chang, “Estimation of the state of charge for a lfp battery using a hybrid method that combines a rbf neural network, an ols algorithm and aga,” Int. J. Elect. Power Energy Syst., vol. 53, pp. 603–611, May 2013.
- [177] J. S. Edge, S. O’Kane, R. Prosser, N. D. Kirkaldy, A. N. Patel, A. Hales, A. Ghosh, W. Ai, J. Chen, J. Yang, et al., “Lithium ion battery degradation: what you need to know,” Physical Chemistry Chemical Physics, vol. 23, no. 14, pp. 8200–8221, 2021.
- [178] X. Lin, J. Park, L. Liu, Y. Lee, W. Lu, and A. M. Sastry, “A comprehensive capacity fade model and analysis for li-ion batteries,” J. Electrochem. Soc., vol. 160, pp. A1701–A1710, 2013.
- [179] J. Li, R. G. Landers, and J. Park, “A comprehensive single-particle-degradation model for battery state-of-health prediction,” J. Power Sources, vol. 456, p. 227950, 2020.

-
- [180] M. Dubarry, C. Truchot, and B. Y. Liaw, “Synthesize battery degradation modes via a diagnostic and prognostic model,” J. Power Sources, vol. 219, pp. 204–216, 2012.
- [181] Y. Zhang, Q. Tang, Y. Zhang, J. Wang, U. Stimming, and A. A. Lee, “Identifying degradation patterns of lithium ion batteries from impedance spectroscopy using machine learning,” Nat. Commun., vol. 11, pp. 6–11, 2020.
- [182] A. Torayev, P. C. M. M. Magusin, C. P. Grey, C. Merlet, and A. A. Franco, “Text mining assisted review of the literature on li-o2 batteries,” J. Phys.: Mater., vol. 2, p. 044004, 2019.
- [183] C. Hendricks, N. Williard, S. Mathew, and M. Pecht, “A failure modes, mechanisms, and effects analysis (fmmea) of lithium-ion batteries,” J. Power Sources, vol. 297, pp. 113–120, 2015.
- [184] D. Klotz, D. S. Ellis, H. Dotan, and A. Rothschild, “Empirical: In operando analysis of the charge carrier dynamics in hematite photoanodes by peis,imps and invs,” Phys. Chem. Chem. Phys., vol. 18, pp. 23 438–23 457, 2016.
- [185] X. Jin, A. Vora, V. Hoshing, T. Saha, G. Shaver, O. Wasynczuk, and S. Varigonda, “Applicability of available li-ion battery degradation models for system and control algorithm design,” Control Eng. Pract., vol. 71, pp. 1–9, 2018.
- [186] J. M. Reniers, G. Mulder, and D. A. Howey, “Review and performance comparison of mechanical-chemical degradation models for lithium-ion batteries,” J. Electrochem. Soc., vol. 166, pp. A3189–A3200, 2019.
- [187] X. G. Yang, S. Ge, T. Liu, Y. Leng, and C. Y. Wang, “A look into the voltage plateau signal for detection and quantification of lithium plating in lithium-ion cells,” J. Power Sources, vol. 395, pp. 251–261, 2018.
- [188] J. Cho and M. M. Thackeray, “Structural changes of LiMn_2O_4 spinel electrodes during electrochemical cycling,” J. Electrochem. Soc., vol. 146, pp. 3577–3581, 1999.
-

-
- [189] R. Jung, M. Metzger, F. Maglia, C. Stinner, and H. A. Gasteiger, "Oxygen release and its effect on the cycling stability of linix mnycozo2 (nmc) cathode materials for li-ion batteries," J. Electrochem. Soc., vol. 164, pp. A1361–A1377, 2017.
- [190] D. Li, H. Li, D. Danilov, L. Gao, J. Zhou, R. A. Eichel, Y. Yang, and P. H. L. Notten, "Temperature-dependent cycling performance and ageing mechanisms of c6/lini1/3mn1/3co1/3o2 batteries," J. Power Sources, vol. 396, pp. 444–452, 2018.
- [191] Q. Liu, C. Du, B. Shen, P. Zuo, X. Cheng, Y. Ma, G. Yin, and Y. Gao, "Understanding undesirable anode lithium plating issues in lithium-ion batteries," RSC Adv., vol. 6, pp. 88 683–88 700, 2016.
- [192] X. M. Liu and C. B. Arnold, "Effects of current density on defect-induced capacity fade through localized plating in lithium-ion batteries," J. Electrochem. Soc., vol. 167, p. 130519, 2020.
- [193] T. C. Bach, S. F. Schuster, E. Fleder, J. Müller, M. J. Brand, H. Lormann, A. Jossen, and G. Sextl, "Nonlinear aging of cylindrical lithium-ion cells linked to heterogeneous compression," J. Energy Storage, vol. 5, pp. 212–223, 2016.
- [194] I. Laresgoiti, S. Kaßbitz, M. Ecker, and D. U. Sauer, "Modeling mechanical degradation in lithium ion batteries during cycling: Solid electrolyte interphase fracture," J. Power Sources, vol. 300, pp. 112–122, 2015.
- [195] A. Jana, G. M. Shaver, and R. E. García, "Physical, on the fly, capacity degradation prediction of linimncoo2-graphite cells," J. Power Sources, vol. 422, pp. 185–195, 2019.
- [196] C. R. Birkl, M. R. Roberts, E. McTurk, P. G. Bruce, and D. A. Howey, "Degradation diagnostics for lithium ion cells," Journal of Power Sources, vol. 341, pp. 373–386, 2017. [Online]. Available: <https://www.sciencedirect.com/science/article/pii/S0378775316316998>
- [197] J. A. Gilbert, I. A. Shkrob, and D. P. Abraham, "Transition metal dissolution, ion migration, electrocatalytic reduction and capacity loss in lithium-ion full cells," J. Electrochem. Soc., vol. 164, pp. A389–A399, 2017.
-

-
- [198] C. Zhan, T. Wu, J. Lu, and K. Amine, "Dissolution, migration, and deposition of transition metal ions in li-ion batteries exemplified by mn-based cathodes – a critical review," Energy Environ. Sci., vol. 11, pp. 243–257, 2018.
- [199] S. Komaba, B. Kaplan, T. Ohtsuka, Y. Kataoka, N. Kumagai, and H. Groult, "Inorganic electrolyte additives to suppress the degradation of graphite anodes by dissolved mn(ii) for lithium-ion batteries," J. Power Sources, vol. 119–121, pp. 378–382, 2003.
- [200] A. Blyr, C. Sigala, G. Amatuc, D. Guyonard, Y. Chabre, and J.-M. Tarascon, "Self-discharge of $\text{LiMn}_2\text{O}_4/\text{C}$ li-ion cells in their discharged state: Understanding by means of three-electrode measurements cells in their discharged state," J. Electrochem. Soc., vol. 145, pp. 194–209, 1998.
- [201] Y. Merla, B. Wu, V. Yufit, N. P. Brandon, R. F. Martinez-Botas, and G. J. Offer, "Novel application of differential thermal voltammetry as an in-depth state-of-health diagnosis method for lithium-ion batteries," J. Power Sources, vol. 307, pp. 308–319, 2016.
- [202] X. Han, L. Lu, Y. Zheng, X. Feng, Z. Li, J. Li, and M. Ouyang, "A review on the key issues of the lithium ion battery degradation among the whole life cycle," Transportation, vol. 1, p. 100005, 2019.
- [203] J. Vetter, P. Novák, M. R. Wagner, C. Veit, K.-C. Moller, J. O. Besenhard, M. Winter, M. Wohlfahrt-Mehrens, C. Vogler, and A. Hammouche, "Ageing mechanisms in lithium-ion batteries," J. Power Sources, vol. 147, pp. 269–281, 2005.
- [204] A. Ghosh, J. M. Foster, G. J. Offer, and A. Marinescu, "Shrinking-core model for the degradation of high-nickel cathodes (nmc811) in li-ion batteries: Passivation layer growth and oxygen evolution," J. Electrochem. Soc., vol. 168, p. 020509, 2021.
- [205] "Innovative physical/virtual sensor platform for battery cell," <https://cordis.europa.eu/project/id/955930>.
- [206] K. E. Thomas, J. Newman, and R. M. Darling, Mathematical modeling of lithium batteries. Springer, 2002.
-

-
- [207] R. Romagnoli, L. D. Couto, A. Goldar, M. Kinnaert, and E. Garone, “A feedback charge strategy for li-ion battery cells based on reference governor,” Journal of process control, vol. 83, pp. 164–176, 2019.
- [208] S. Santhanagopalan, Q. Guo, P. Ramadass, and R. E. White, “Review of models for predicting the cycling performance of lithium ion batteries,” Journal of Power Sources, vol. 156, no. 2, pp. 620–628, 2006. [Online]. Available: <https://www.sciencedirect.com/science/article/pii/S0378775305007810>
- [209] G. L. Plett, “Extended kalman filtering for battery management systems of lipb-based hev battery packs: Part 3. state and parameter estimation,” Journal of Power sources, vol. 134, no. 2, pp. 277–292, 2004.
- [210] X. Han, M. Ouyang, L. Lu, and J. Li, “Simplification of physics-based electrochemical model for lithium ion battery on electric vehicle. part i: Diffusion simplification and single particle model,” Journal of Power Sources, vol. 278, pp. 802–813, 2015.
- [211] H. E. Perez, J. B. Siegel, X. Lin, A. G. Stefanopoulou, Y. Ding, and M. P. Castanier, “Parameterization and validation of an integrated electro-thermal cylindrical lfp battery model,” in Dynamic Systems and Control Conference, vol. 45318. American Society of Mechanical Engineers, 2012, pp. 41–50.
- [212] D. M. Bernardi and J.-Y. Go, “Analysis of pulse and relaxation behavior in lithium-ion batteries,” Journal of Power Sources, vol. 196, pp. 412–427, 2011.
- [213] M. Ecker, T. K. D. Tran, P. Dechent, S. Katz, A. Warnecke, and D. U. Sauer, “Parameterization of a physico-chemical model of a lithium-ion battery: I. determination of parameters,” Journal of The Electrochemical Society, vol. 162, pp. A1836–A1848, 2015.
- [214] E. Villemin and O. Raccurt, “Optical lithium sensors,” Coordination Chemistry Reviews, vol. 435, p. 213801, 2021.
-

-
- [215] T. Amietszajew, E. McTurk, D. Greenwood, and R. Bhagat, “Development and evaluation of in-situ instrumentation for cylindrical li-ion cells using fibre optic sensors,” HardwareX, vol. 3, pp. 100–109, 2018.
- [216] J. Schwartz et al., “Embedded fiber optic sensors for in situ and in-operando monitoring of advanced batteries,” MRS Online Proceedings Library, vol. 1740, pp. 7–12, 2014.
- [217] P. P. R. M. L. Harks, F. M. Mulder, and P. H. L. Notten, “In situ methods for li-ion battery research: A review of recent developments,” Journal of Power Sources, vol. 288, pp. 92–105, 2015.
- [218] L. Meyer, N. Saqib, and J. Porter, “Operando optical spectroscopy studies of batteries,” Journal of The Electrochemical Society, vol. 168, no. 9, p. 090561, 2021.
- [219] X. G. Yang, Y. Leng, G. Zhang, S. Ge, and C. Y. Wang, “Modeling of lithium plating induced aging of lithium-ion batteries: Transition from linear to nonlinear aging,” J. Power Sources, vol. 360, pp. 28–40, 2017.
- [220] G. Vennam, A. Sahoo, and S. Ahmed, “A survey on lithium-ion battery internal and external degradation modeling and state of health estimation,” Journal of Energy Storage, vol. 52, p. 104720, 2022.

FOLIO ADMINISTRATIF

THESE DE L'INSA LYON, MEMBRE DE L'UNIVERSITE DE LYON

NOM :ASIF

DATE de SOUTENANCE : 19/12/2023

Prénoms : Mian Mohammad Arsalan

TITRE : Electrochemical Virtual Sensor Development for Lithium-ion Batteries

NATURE : Doctorat

Numéro d'ordre : 2023ISAL0117

Ecole doctorale : Electronique, Electrotechnique, Automatique (ED 160)

Spécialité : Automatique

RESUME :

Dans cette thèse de doctorat, l'auteur se concentre sur l'avancement de la modélisation et de la conception d'observateurs pour les batteries lithium-ion (LiBs). Les LiB jouent un rôle essentiel dans la transition vers les énergies renouvelables et l'électrification des véhicules, mais elles présentent encore des défis en termes de performance, de sécurité et de gestion. L'auteur développe un modèle multi-particules avec dynamique de l'électrolyte (MPMe) pour mieux représenter le comportement des LiBs. De plus, des observateurs d'état sont conçus pour estimer la concentration de lithium dans l'électrolyte et la concentration de lithium solide. Ces observateurs sont validés à l'aide de simulations, démontrant leur efficacité dans la surveillance en temps réel des LiBs. Cette recherche vise à améliorer la performance, la sécurité et la fiabilité des LiBs, contribuant ainsi à une adoption plus large des véhicules électriques et à une électrification durable du secteur des transports.

MOTS-CLÉS : batterie Li-ion, systèmes de contrôle, observateurs d'état

Laboratoire (s) de recherche : Ampère

Directeur de thèse : Eric BIDEAUX

Président de jury :

Composition du jury :

VAZQUEZ VALENZUELA, Rafael, DI MEGLIO, Florent, CADET, Catherine, SENAME, Olivier, BIDEAUX, Eric, BRIBIESCA ARGOMEDO, Federico